

ION-EXCHANGE MEMBRANES

GUEST EDITORS: YOSHINOBU TANAKA, SEUNG-HYEON MOON, VICTOR V. NIKONENKO,
AND TONGWEN XU





Ion-Exchange Membranes

International Journal of Chemical Engineering

Ion-Exchange Membranes

Guest Editors: Yoshinobu Tanaka, Seung-Hyeon Moon,
Victor V. Nikonenko, and Tongwen Xu



Copyright © 2012 Hindawi Publishing Corporation. All rights reserved.

This is a special issue published in "International Journal of Chemical Engineering." All articles are open access articles distributed under the Creative Commons Attribution License, which permits unrestricted use, distribution, and reproduction in any medium, provided the original work is properly cited.

Editorial Board

Muthanna Al-Dahhan, USA
Miguel J. Bagajewicz, USA
Alfons Baiker, Switzerland
Jerzy Bądyga, Poland
Mostafa Barigou, UK
Gino Baron, Belgium
Hans-Jörg Bart, Germany
Raghunath V. Chaudhari, USA
Jean-Pierre Corriou, France
Donald L. Feke, USA
James J. Feng, Canada
Rafiqul Gani, Denmark
Jinlong Gong, China
Thomas R. Hanley, USA
Michael Harris, USA

Kus Hidajat, Singapore
Vladimir Hlavacek, USA
Xijun Hu, Hong Kong
M. G. Ierapetritou, USA
Dilhan M. Kalyon, USA
Kyung Aih Kang, USA
Iftekhhar A. Karimi, Singapore
B. D. Kulkarni, India
Deepak Kunzru, India
Janez Levec, Slovenia
Jose C. Merchuk, Israel
Badie I. Morsi, USA
S. Murad, USA
Dmitry Murzin, Finland
Ahmet N. Palazoglu, USA

Fernando T. Pinho, Portugal
Peter N. Pintauro, USA
Doraiswami Ramkrishna, USA
Alírio Rodrigues, Portugal
Jose Alberto Romagnoli, USA
Adrian Schumpe, Germany
Moshe Sheintuch, Israel
Katsumi Tochigi, Japan
Evangelos Tsotsas, Germany
Toshinori Tsuru, Japan
Tapio Westerlund, Finland
Jaime Wisniak, Israel
King Lun Yeung, Hong Kong
Zhibing Zhang, UK

Contents

Ion-Exchange Membranes, Yoshinobu Tanaka, Seung-Hyeon Moon, Victor V. Nikonenko, and Tongwen Xu
Volume 2012, Article ID 906952, 3 pages

Ion Transport through Diffusion Layer Controlled by Charge Mosaic Membrane, Akira Yamauchi
Volume 2012, Article ID 417179, 7 pages

Enhancing Ion Transfer in Overlimiting Electrodialysis of Dilute Solutions by Modifying the Surface of Heterogeneous Ion-Exchange Membranes, Natalia Pismenskaya, Nadezhda Melnik, Ekaterina Nevakshenova, Kseniya Nebavskaya, and Victor Nikonenko
Volume 2012, Article ID 528290, 11 pages

Reactivity of Phenol Allylation Using Phase-Transfer Catalysis in Ion-Exchange Membrane Reactor, Ho Shing Wu and Yeng Shing Fu
Volume 2012, Article ID 196083, 8 pages

Performance of a 1 kW Class Nafion-PTFE Composite Membrane Fuel Cell Stack, Pattabiraman Krishnamurthy, Ramya Krishnan, and Dhathathreyan Kaveripatnam Samban
Volume 2012, Article ID 512803, 7 pages

Study of Chromium Removal by the Electrodialysis of Tannery and Metal-Finishing Effluents, Ruan C. A. Moura, Daniel A. Bertuol, Carlos A. Ferreira, and Franco D. R. Amado
Volume 2012, Article ID 179312, 7 pages

Ion-Exchange Membranes Based on Polynorbornenes with Fluorinated Imide Side Chain Groups, Arlette A. Santiago, Joel Vargas, Mikhail A. Tlenkopatchev, Mar López-González, and Evaristo Riande
Volume 2012, Article ID 835378, 11 pages

Measurement of Membrane Characteristics Using the Phenomenological Equation and the Overall Mass Transport Equation in Ion-Exchange Membrane Electrodialysis of Saline Water, Yoshinobu Tanaka
Volume 2012, Article ID 148147, 12 pages

Ultrathin Sicopion Composite Cation-Exchange Membranes: Characteristics and Electrolytic Performance following a Conditioning Procedure, Erik Ayala-Bribiesca, Mario Boucher, and Laurent Bazinet
Volume 2012, Article ID 932723, 12 pages

Hybrid Anion Exchange Hollow Fiber Membrane for Delivery of Ionic Drugs, Na Wang, Mengbing Cui, Cuiming Wu, Yiyun Cheng, and Tongwen Xu
Volume 2012, Article ID 832190, 9 pages

Editorial

Ion-Exchange Membranes

Yoshinobu Tanaka,¹ Seung-Hyeon Moon,² Victor V. Nikonenko,³ and Tongwen Xu⁴

¹ IEM Research, 1-46-3 Kamiya, Ushiki-shi, Ibaraki 3001216, Japan

² Department of Environmental Science and Engineering, Gwangju Institute of Science and Technology (GIST),
261 Cheomdan-Gwagiro, Buk-gu, Gwangju 500-712, Republic of Korea

³ Membrane Institute, Kuban State University, Stavropolskaya Street 149, Krasnodar 350040, Russia

⁴ CAS Key Laboratory of Soft Matter Chemistry, Laboratory of Functional Membranes, School of Chemistry and Material Science,
University of Science and Technology of China, Jinzai Road 96, Hefei, Anhui 230026, China

Correspondence should be addressed to Yoshinobu Tanaka, fwis1202@mb.infoweb.ne.jp

Received 7 August 2012; Accepted 7 August 2012

Copyright © 2012 Yoshinobu Tanaka et al. This is an open access article distributed under the Creative Commons Attribution License, which permits unrestricted use, distribution, and reproduction in any medium, provided the original work is properly cited.

Principles of ion transport across ion-exchange membranes had been investigated using biological membranes in old time. Industrial application of the membranes started after the invention of artificial membranes in 1950. Ion-exchange membrane electrodialysis is now one of the basic technology in saline water desalination industry. It is also applied to many fields such as demineralization and reuse of sewage or industrial waste, refining of amino acid solutions, production of organic and inorganic chemicals, membrane reactors, among others. Further, the membranes are applied to the succeeding technology such as electrodialysis reversal, bipolar membrane electrodialysis, electrodeionization, electrolysis, diffusion dialysis, fuel cell, reverse electrodialysis, among others.

This special issue presents the newest investigation on ion-exchange membranes submitted from each field. It includes topics in the fundamental studies and application studies such as membrane preparation, membrane characterization, membrane application, environmental problem; process design and operation, among others. Fundamental studies are the basis of the application studies. At the same time, the application studies induce the development of the fundamental studies. Both studies influence each other and consequently contribute to the technology development. Based on the history of ion-exchange membranes, the following ten articles published in this special issue must induce the development of succeeding technology.

In the first article “*Reactivity of phenol allylation using phase-transfer catalysis in ion-exchange membrane reactor*,” Wu and Fu have reported the reactivity of phenol allylation

using quaternary ammonium salt phase-transfer catalysts in ion-exchange membrane reactors incorporated with the laboratory-produced membrane. They have immobilized the catalyst in the pore of an ion-exchange membrane. That allowed them to benefit the permselective as well as the catalytic functions of the new membrane. The study investigates the reactivity of phenol allylation using quaternary ammonium salt as a phase-transfer catalyst in several types of membrane reactors. Optimum reactivity and turnover of phenol allylation were obtained using a respond surface methodology. The contact angle, water content, and crosslinkage degree were measured to understand the microenvironment in the ion-exchange membrane.

The second article is “*Performance of a 1 kW class nafion-PTFE composite membrane fuel cell stack*” addressed by Kirshnamurthy et al. The membranes have been prepared by impregnation of Nafion into the expanded polytetrafluoroethylene (EPTFE) matrix. Nafion loading in the membranes was kept at lower amount of 2 mg/cm². The lower amount of electrolyte per unit area in the composite membranes offers cost advantageous compared to conventional membranes. The composite membranes (30 μ m thickness) had higher thermal stability and mechanical strength compared to the conventional membranes (50 μ m thickness). The durability of single pass cells was tested. The performance of the membrane electrode assembly (20-cell stack, 330 cm² active area) have been reported and it was comparable to that of the conventional membrane.

In the third article, “*Study of chromium removal by electrodialysis of tannery and metal-finishing effluents*” by Moura

et al., the membranes were synthesized from blends of polystyrene and polyaniline. The electrodialysis experiments were performed using a three-compartment cell with a capacity of 200 mL each. The unit was incorporated with the synthesized cation-exchange membranes (and Nafion 450) and anion-exchange membranes Selemion AMT. Supplying metal-finishing effluents collected at two industries, chromium removal percentage was evaluated. The synthesized membranes presented similar chromium transport to that observed in the Nafion 450. The study proved the feasibility of a technology in the treatment of tannery and metal finishing effluents, bringing great advantageous to water reuse.

In the fourth article “*Ion-exchange membranes based on polynorbornenes with fluorinated imide side chain groups*”, Santiago et al. have prepared cation-exchange membranes based on polynorbornenes with fluorinated and sulfonated dicarboximide side chain groups. The study was extended to block copolymer containing structural units with phenyl and 4-oxybenzenesulfonic acid, 2,3,5,6-tetrafluorophenyl moieties replacing the hydrogen atom of the dicarboximide group. They discuss electrochemical characteristics of the membranes, electromotive forces of concentration cells, proton conductivity, and also proton permselectivity. The efficient segregation of hydrophilic from hydrophobic moieties, presumably favored by the low polarity of bonds attached to the phenyl groups, gives raise to the formation of percolation paths responsible for the rather high proton conductivity of the homopolymeric membranes.

The fifth article is “*Measurement of membrane characteristics using phenomenological equation and the overall mass transport equation in ion-exchange membrane electrodialysis of saline water*” by Tanaka. In saline water electrodialysis, the author found that the overall solute permeability μ occasionally takes minus value. For understanding this phenomenon, new concept of the overall concentration reflection coefficient σ^* was introduced. σ^* was defined for describing the permselectivity between solutes and water molecules (solvent) in the electrodialysis system just after an electric current interruption. Negative μ ($\sigma^* < 1$) means that ions are transferred with water molecules from desalting cells toward concentrating cells just after an electric current interruption, indicating up-hill transport or coupled transport between water molecules and solutes.

The sixth article by Ayala-Bribiesca et al. “*Ultrathin sicopion composite cation-exchange membrane: characteristics and electrodialytic performance following a conditioning procedure*” has addressed the preparation of ultrathin ($\approx 20\ \mu\text{m}$) highly conductive composite cation-exchange membranes. The membranes were made from sulphonated poly(ether-ether-ketone) containing different levels of sulphonic functionalized silica particles (SFSPs). Sicopion membranes were conditioned according to the French normalizing association procedure, and their electrodialytic characteristics were compared to an existent commercial food-grade membrane (CMX-SB). Electrical conductivity of Sicopion membranes was higher than that of CMX-SB membranes as well as their water content. As the SFSP level was reduced, the ion-exchange capacity increased. Sicopion membranes presented

a lower demineralization rate than CMX-SB membranes due to an OH^- leakage through the pores created by dislodging the SFSP particles during the conditioning procedure.

The seventh article is “*Hybrid anion exchange hollow fiber membrane for delivery of ionic drugs*”. Wang et al. prepared anion-exchange hollow fiber membranes based on bromomethylated poly(2,6-dimethyl-1,4-phenylene oxide) as drug carriers for some anionic model drugs such as sodium salts of benzoate, salicylate, among others. The above organic-inorganic hybrid anion exchange hollow fiber membrane was used for controlled release of the model drugs. They have established that the adsorption/release behavior of the membrane depends on the drug nature. In particular, the physicochemical characteristics of drugs are crucial to the interaction patterns between the drugs and the membrane, including electrostatic interactions and nonelectrostatic interactions (hydrophobic interactions and hydrogen bonding). The hydrogen bonding capacity of the drugs significantly affects the loading capacity and the release rate.

In the eighth article “*Obtaining the zwitterionic Form of L-Lysine from L-Lysine monohydrochloride by electrodialysis*” by Aghajanyan et al., L-lysine monohydrochloride was transformed to its zwitterionic form in four- and two-chamber electrodialysis apparatus. The process of transformation at various concentration of L-lysine monohydrochloride (0.1–0.7 mol/l) was studied. It was established that at the optimum current density in the chosen range of salt concentration, total transformation into its zwitterionic form occurred. In the process of transformation, changes in Cl^- ion concentration, pH, dry matter content, electroconductivity, as well as in current voltage depending on time were determined. Studies have shown that the process of total transformation was accomplished when pH of the lysine solution achieved 10. The losses of lysine diffused into the next chamber was less than 1.0%. The specific energy consumption in two- and four-chamber electrodialyzer was 1.85 and 3.82 kWh/kg and the current efficiency was ~ 76 and $\sim 73\%$ correspondingly.

In the ninth article “*Enhancing ion transfer in overlimiting electrodialysis of dilute solutions by modifying the surface of heterogeneous ion exchange membranes*”, Pismenskaya et al. have studied the effect of surface modification of heterogeneous ion-exchange membranes on the ion transfer rate in overlimiting electrodialysis of dilute solutions. One of the membranes was obtained by casting a thin film of a Nafion-type material on the surface of a heterogeneous cation-exchange membrane. The other membrane was made by grafting quaternary ammonium bases onto the surface layer of an anion-exchange membrane to replace secondary and tertiary ammonium groups initially present. The surface modification resulted in a considerable increase, up to two times, of mass transfer rate due to enhanced electroconvection at the cation-exchange membrane and suppressed water splitting at the anion-exchange membrane.

In the tenth article, “*Ion transport through diffusion layer controlled by charge mosaic membrane*”, Yamauchi has studied charged mosaic membranes imposed on a cation-exchange membrane or on an anion-exchange membrane. The author found that these complex two-layer membranes show properties typical for monopolar (selective transfer at

the interface of monomer and mosaic layers) as well as for bipolar membranes (water splitting at the interface of monomer and mosaic layers). It was also established that the transition time in chronopotentiometric measurements was function of what monopolar membrane was used together with the mosaic one: in the case of the cation-exchange membrane, the transition time was higher, and in the case of the anion-exchange membrane, lower than that found for relative monopolar membranes. The thickness of the boundary layer was derived with conjugation with the limiting current density and the transition time.

In publishing the special issue, the editors thank deeply the authors for their excellent contributions and reviewers for their time and effort in reviewing the manuscripts.

Yoshinobu Tanaka
Seung-Hyon Moon
Victor V. Nikonenko
Tongwen Xu

Research Article

Ion Transport through Diffusion Layer Controlled by Charge Mosaic Membrane

Akira Yamauchi

Department of Chemistry, Faculty of Science, Fukuoka University, 8-19-1 Nanakuma, Jonan-ku, Fukuoka 814-0180, Japan

Correspondence should be addressed to Akira Yamauchi, yamakira42@yahoo.co.jp

Received 2 April 2012; Revised 21 June 2012; Accepted 22 July 2012

Academic Editor: Victor V. Nikonenko

Copyright © 2012 Akira Yamauchi. This is an open access article distributed under the Creative Commons Attribution License, which permits unrestricted use, distribution, and reproduction in any medium, provided the original work is properly cited.

The kinetic transport behaviors in near interface of the membranes were studied using commercial anion and cation exchange membrane and charge mosaic membrane. Current-voltage curve gave the limiting current density that indicates the ceiling of conventional flux. From chronopotentiometry above the limiting current density, the transition time was estimated. The thickness of boundary layer was derived with conjunction with the conventional limiting current density and the transition time from steady state flux. On the other hand, the charge mosaic membrane was introduced in order to examine the ion transport on the membrane surface in detail. The concentration profile was discussed by the kinetic transport number with regard to the water dissociation (splitting) on the membrane surface.

1. Introduction

It is well known that electrodialysis using ion exchange membrane makes drinking water or table salt from sea water. In Japan especially it is popular to use this electrodialysis in various fields such as food, medical pharmacy and ultrapure water [1–3]. However, the more efficient and improved electrodialysis have been required for pure water production because conventional system costs much of electric power at present. One of the main problems originates from the limiting current density that restricts the direct current for supplying through the system and depends on the thickness of diffusion layers. In this study, the way to see the thickness of the depleted solution layer was examined in order to improve the efficiency on the electrodialysis from fundamental standpoint.

As mentioned above, the aim will be focused on the ionic behavior of ion transport from bulk solution to membrane surface. In addition, so far developed charge mosaic membrane [4–6] is introduced into electrodialysis model system and the ion transport mechanism is investigated. As experimental strategies, electrical methods were mainly adopted, and 4 kinds of membrane systems were selected to study: cation exchange membrane system (CMV), anion exchange membrane system (AMV), charge mosaic membrane and

cation exchange membrane system (MM + CMV), and anion exchange membrane and charge mosaic membrane system (AMV + MM).

The potentiometry was also used on the same membrane systems to elucidate the diffusion layer. The chronopotentiometry has been carried out to obtain the transition time [7–9]. The technique was adopted for 4 membrane arrangements to examine the contribution to the boundary layer of the charge mosaic membrane. The kinetic parameter about the boundary layer was noticed and introduced for understanding of the experimental results. The boundary layer thickness was already studied using chronopotentiometric technique in the underlimiting current-range [10], but in this paper different other methods were adopted to measure the boundary layer thickness.

2. Experimental

2.1. Materials. The membranes used in the experiments were commercial Selemion CMV as cation exchange membrane, Selemion AMV as anion exchange membrane (Asahi glass Co.), and charge mosaic membrane MM, which was developed in Dainichi Seika. Co. and contained both strong acid-type cation exchange group and strong base-type anion

exchange group fixed in the direction perpendicular to the membrane surface [4–6]. The KCl solution was prepared from 10^{-5} to 10^{-1} mol dm $^{-3}$ in this study.

2.2. Membrane Arrangement. A study in laboratory scale was carried out with 4 kinds of membrane systems, which imagined ED (electrodialysis) and EDI (electrodeionization) model membrane systems.

4 membrane arrangement systems for this research were taken as following.

CMV : KCl solution/CMV/KCl solution (ED model).

AMV : KCl solution/AMV/KCl solution (ED model).

MM + CMV : KCl solution/MM + CMV/KCl solution (EDI model).

AM + MMV : KCl solution/AMV + MM/KCl solution (EDI model).

The membranes arrangements of two tops and two bottoms are similar to conventional ED and EDI device, respectively. Then, for convenience, sometimes ED or EDI symbols were used in this paper.

2.3. Apparatus

2.3.1. Current-Voltage Curve. Current-voltage curves were determined with a gradual increase of potential difference imposed through the cells, and current density across the membrane was measured. The obtained combination of potential difference and current density gave the experimental current-voltage curve.

2.3.2. Chronopotentiometry. The potentiostat (Potentiostat/Galvanostat, HA-151, Hokutodenko. Co.) allowed the current-voltage measurement and the chronopotentiometry measurement on different membrane arrangements. Chronopotentiogram was driven with a function generator (function generator, HB-111, Hokutodenko. Co.) and recorded by X-Y-t recorder (XY recorder F-35C, Riken Denshi. Co.). The experimental cell for the current-voltage measurement and the chronopotentiometry was the four-electrodes cell as depicted in Figure 1. The voltage drops across the membranes under investigation are measured by Haber-Luggin capillaries in which 3 M KCl solution was filled with agar and each connected to potentiostat or galvanostat where Ag/AgCl electrode was connected as reference electrode.

Chronopotentiometry is one of the electrochemical characterization methods that measure the electric potential response of a system to the imposed current [10–12]. It was performed with 4 membrane arrangements under investigation. It is not the same measurement as the current-voltage curve measurement at the point where the current instead of voltage drop was applied into the system by means of outer supply. The method of chronopotentiometry was firstly developed for electrochemistry of electrode and now used also for studies in membrane science field almost without any changes [13]. Then the Sand equation, which had concerned with electrode reaction was introduced toward the membrane system.

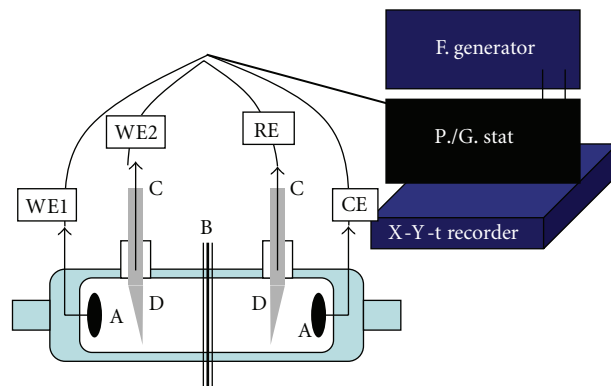


FIGURE 1: Experimental cell with electrochemical apparatus. A; Ag/AgCl electrode. B: Membrane system (Monopolar or Monopolar + Mosaic membranes). Membranes parts are fixed by two rubbers with holes, 1 cm in diameter from both sides to avoid the leak of solution. C: Ag/AgCl electrode. D: 3 M KCl in agar.

The transition time obtained by chronopotentiometry corresponds to the moment, where the initial salt concentration on the membrane surface decrease until it becomes zero [12]. On the other hand, it means the time to reach overlimiting current density by applied current. The obtained kinetic parameters were analyzed by the Sand equation.

2.3.3. pH Measurement. pH indicators, phenolphthalein, and methyl red were put into the KCl solution to check simply the occurrence of water dissociation during operation of chronopotentiometry. It indicated that the pH change, H $^{+}$ take place from slight red color qualitatively.

3. Results and Discussion

3.1. Limiting Current Density. Current-voltage curve measurement was carried out to obtain the limiting current density in the membrane systems of 4 arrangements under investigation. The limiting current density was determined from current-voltage curve and explained by the well-known schematic picture [11] in which three regions can be distinguished. Firstly, a linear part appears in the low-potential drop region, called the ohmic region. Secondly, the current density attains a plateau region due to the depleted ion layer adjacent to membrane surface. The concentration on the membrane surface became zero finally. Hence the current density on this step was defined as the limiting current density, and there the salt flux is dominated by the diffusion between the bulk solution and membrane surface. After the plateau, the current density begins to increase again. The third region is called the overlimiting region [11]. The limiting current densities about ED or EDI model system were determined from the current-voltage curves. In fact, the limiting current density on EDI was slightly larger than on ED. The salt flux across the membrane is in agreement with the salt flux, which passed from the bulk solution to the membrane surface. Therefore, it is important to consider the flux until the concentration on the membrane surface reach zero.

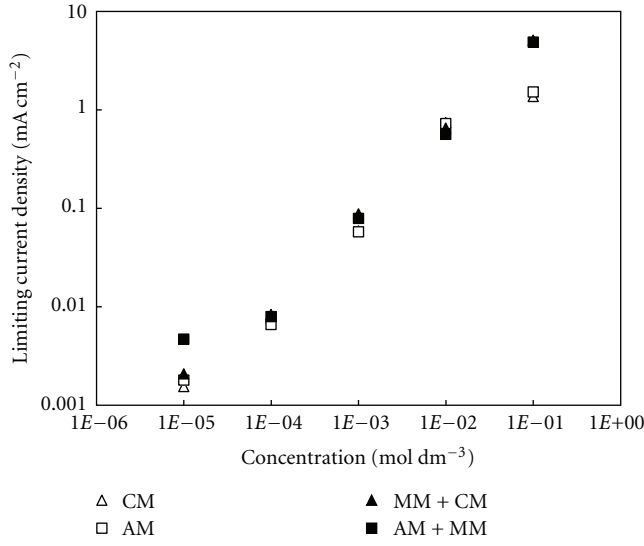


FIGURE 2: Limiting current density of 4 membrane arrangements in KCl solution. Symbols are inserted in the figure.

The limiting current density is given by a following equation derived in the literatures [10–14]:

$$i_{\text{lim}} = \frac{FD_{\text{KCl}}C_O}{\delta(\bar{t}_i - t_i)} \quad (1)$$

Here F is Faraday constant, C_O the bulk solution concentration, D the salt diffusion coefficient, δ the diffusion boundary thickness, \bar{t}_i the counter ion transport number in the membrane, and t_i the transport number in the solution.

Here if one assumes that D the salt diffusion coefficient, δ the diffusion boundary thickness and \bar{t}_i the counter ion transport number in the membrane are known, t_i the transport number in the solution can be obtained. It will be done about the detailed discussion later.

3.2. Transition Time. Chronopotentiogram, one of electrochemical methods, is given as schematic explanation in Figure 3. The result in 0.01 M KCl solution with using CMV was shown in Figure 4. All current densities imposed for the chronopotentiometry were always larger than the limiting current density obtained by the current-voltage curve measurement. In the case where such a large current was imposed on the membrane system, the concentration polarization should occur rapidly on the membrane surface and the concentration on the membrane surface becomes zero immediately. The situation is the same as the case mentioned in previous section. The transition time, τ was defined as the time when the concentration on the membrane surface became zero, that is, inflection point of shadow in Figure 3.

Now, the transition time is given by Sand as following equation [12, 13]:

$$\tau = \frac{\pi D_{\text{KCl}}}{4} \frac{1}{i^2} \left(\frac{Fz_i C_O}{\bar{t}_i - t_i} \right)^2 \quad (2)$$

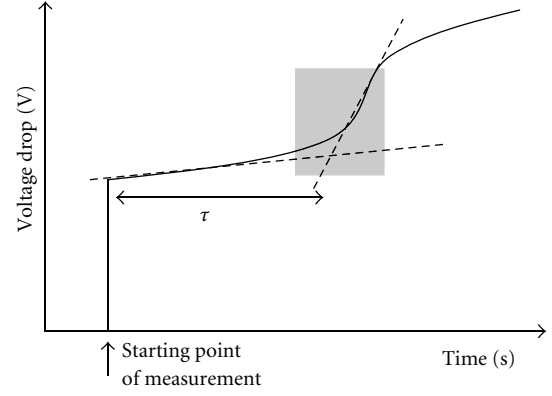


FIGURE 3: Schematic drawing of chronopotentiogram.

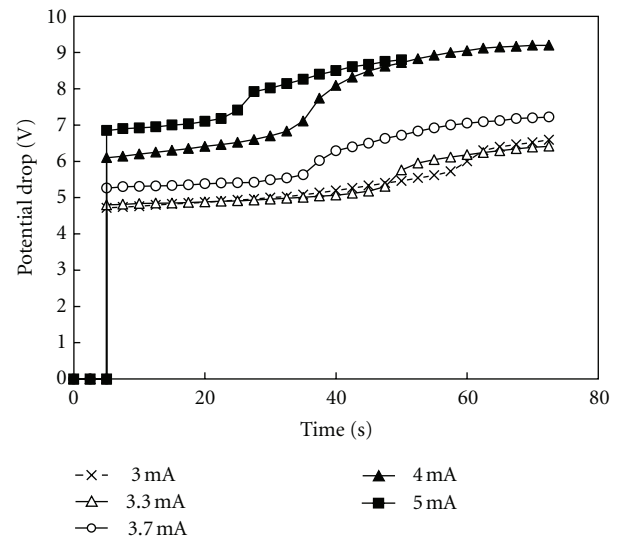


FIGURE 4: Chronopotentiogram with a cation exchange membrane in 0.01 M KCl solution. Current densities are inserted in the figure.

Here D is the diffusion coefficient of electrolyte, C_O and z_i the concentration in the bulk and the charge of the counter ion, \bar{t}_i and t_i the transport number of the counter ion in the membrane and solution, respectively, i the current density, and F the Faraday coefficient. Then the measured transition times were indicated as a function of inverse of square of current densities in Figure 5. According to Figure 5, there were hardly difference between CMV and AMV membrane arrangements. On the other hand, in the case where the charged mosaic membrane was introduced additionally on cation- and anion exchange membrane like arrangements, MM + CMV and AMV + MM, the transition time was changed remarkably. The transition time, τ , increased on the arrangement, MM + CMV, while τ on the arrangement, AMV + MM decreased. At present, it is not clear, but there seems to be influence of boundary layer, δ .

3.3. Kinetic Transport Number in Boundary Layer. When $z_i = 1$, (2) was rearranged to evaluate the transport number at

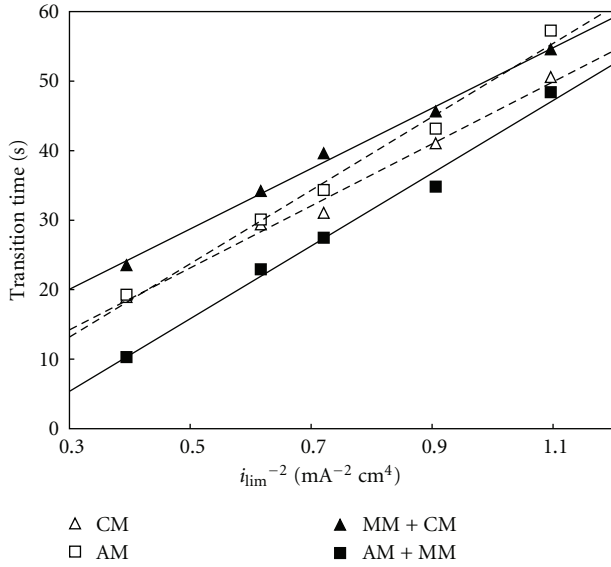


FIGURE 5: Transition time versus i_{lim}^{-2} in 0.01 M KCl solution. Symbols are inserted in the figure.

the boundary layer in the case of KCl solution as follows:

$$t_i = \bar{t}_i - C_0 F \frac{1}{i} \sqrt{\frac{\pi D_{\text{KCl}}}{4\tau}}. \quad (3)$$

Potential changes along the time and increases after the current density value reached on the transition time are shown at the grey portion in Figure 3. The fact suggests that any ion transport process also changes after the transition time. The transport number might be changed under a certain condition, although the transport number had been almost unity in membrane when the relation between the voltage and the current has been simply ohmic at the moment. The kinetic transport number on the membrane surface was defined and derived from the above (3) on the moment when ion concentrations on the membrane reached zero.

The kinetic transport number in the boundary layer was shown in Figure 6, where the diffusion coefficient was assumed to be constant values in KCl solution and also transport number in membrane, $\bar{t}_i = 1$. According to Figure 6, an addition of the charged mosaic membrane resulted in the change of transport number at the boundary layer and the transport number tended to change remarkably with the extent of current density. In particular, it was supposed that the kinetic transport number in the boundary layer decreased remarkably in the case of AM + MM. Hence we define the transport number as kinetic transport number in boundary layer.

3.4. Thickness of Boundary Layer. Equation (1) on the limiting current density was rearranged to derive the thickness of boundary layer as follows:

$$\delta = \frac{FD_{\text{KCl}}C_0}{i_{\text{lim}}(\bar{t}_i - t_i)}. \quad (4)$$

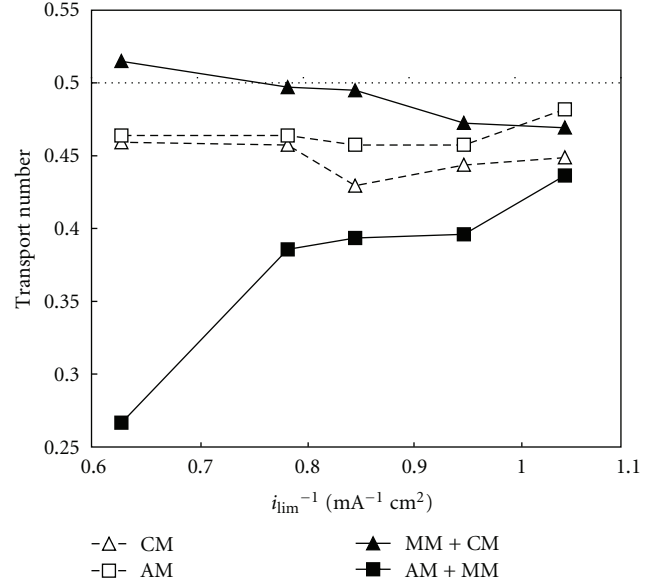


FIGURE 6: Relation between transport number and various i_{lim}^{-1} value in 0.01 M KCl solution on 4 membrane arrangements. Symbols are inserted in the figure.

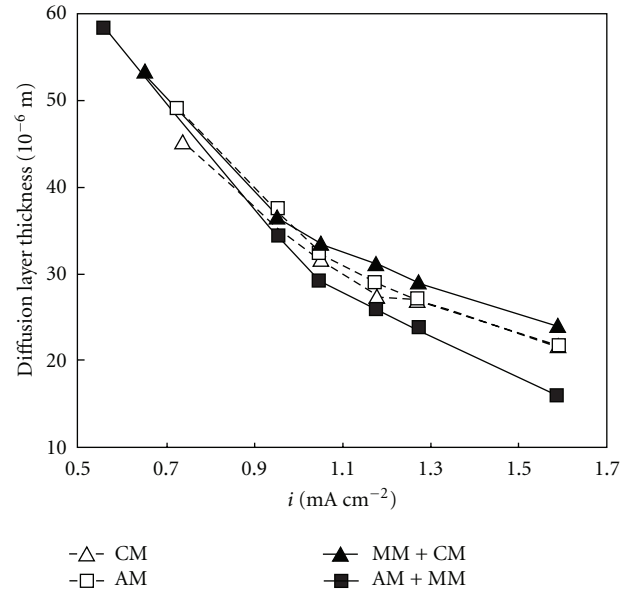


FIGURE 7: Diffusion layer thickness versus current density. Symbols are inserted in the figure.

The estimated limiting current density was already given in Figure 2. The transport number on designated ion should be unity through the membrane. This condition was equivalent with that in the chronopotentiometry at the transition time just before. It was supposed that the transport number and the current density obtained from the chronopotentiometry were able to be substituted by using (4) because the conditions on the surface of membrane are same. Then, the thickness of the boundary layer was represented in Figure 7. The added charge mosaic membrane

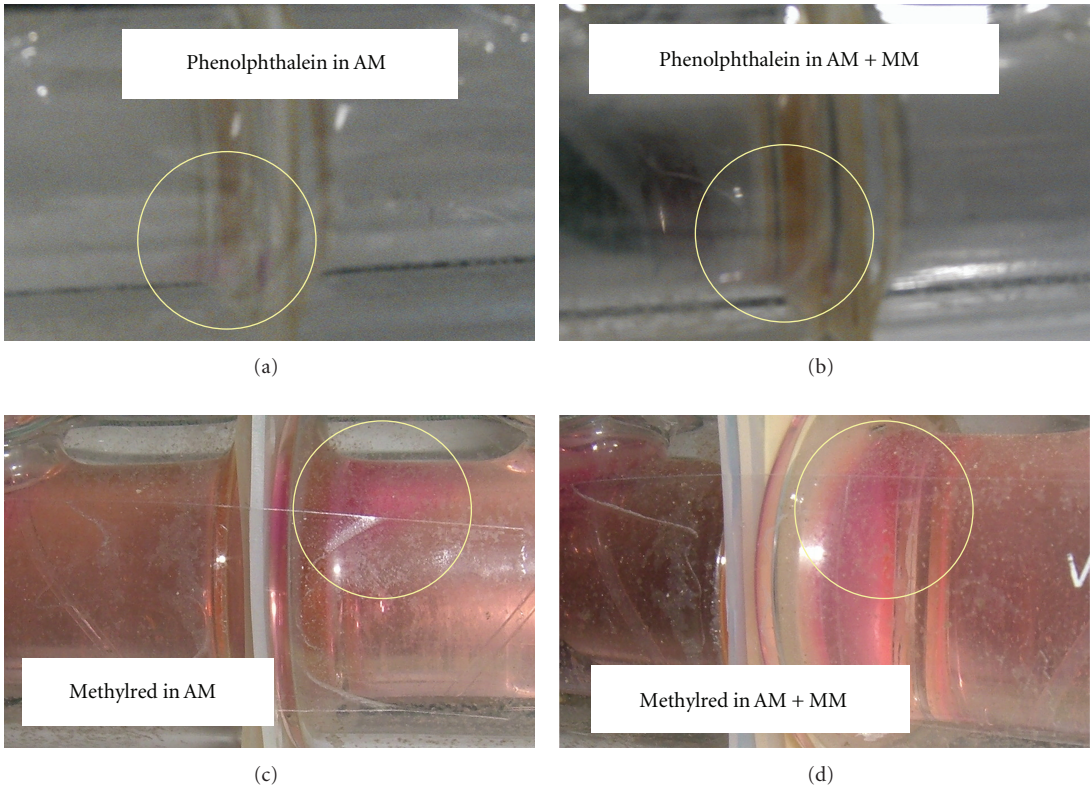


FIGURE 8: Indicator, methyl red in cell of two bottoms changed in red. This shows the existence of H^+ in a bulk solution.

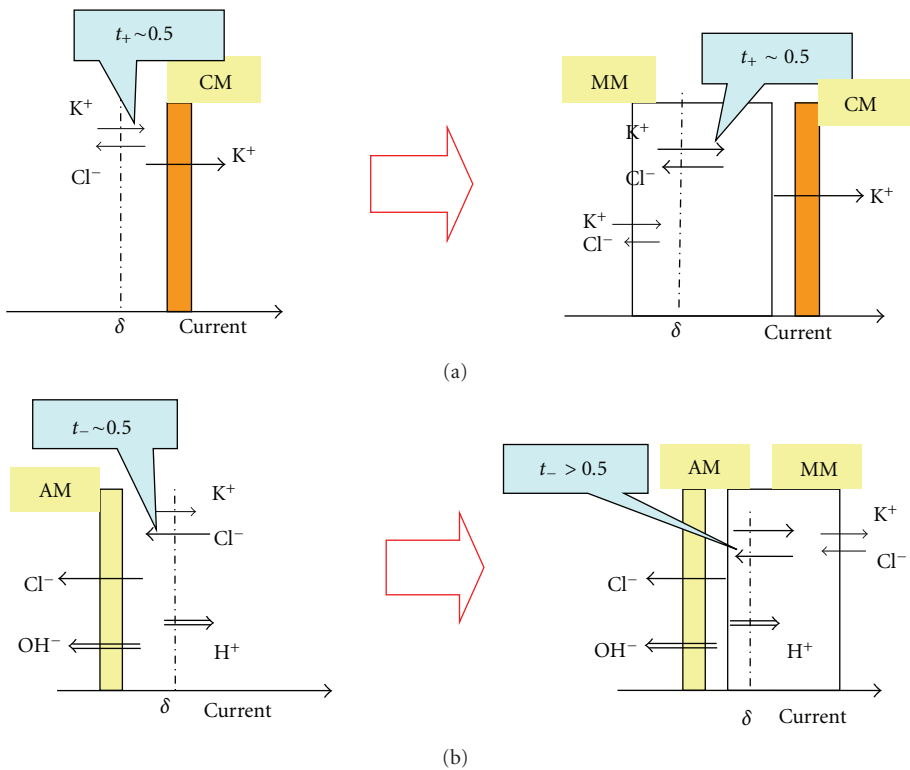


FIGURE 9: Schematic model of ion transport on the membrane surface. Dotted lines are hypothetical boundary lines.

caused the increase of the thickness of boundary layer on the cation exchange membrane and the decrease on the anion exchange membrane. The tendency of change became remarkable depending on the current density.

Finally, it was suggested that the introduction of the charge mosaic membrane into ion exchange membrane resulted in the change of boundary layer's thickness, and this result supported the speculation in Section 3.2. Transition Time.

3.5. Water Splitting. During the chronopotentiometry, the pH measurement was carried out at the same time under the presence of pH indicators, phenolphthalein, and methyl red, and the results were shown in Figure 8. The color changes were not recognized in CMV and MM + CM systems at all, but the red color changes appeared in AMV and AM + MM systems. The pH change suggested that the water splitting took place near the surfaces on anion exchange membrane systems only. The water splitting seems to give an affect to the ion transport process on membrane, in particular anion membrane systems. Then the experimental results were tentatively examined by the following model in Figure 9.

The arrow toward right indicates the current direction in Figure 9 on which the dotted line is hypothetically located as the end of diffusion layer from each membrane surface. Cation passage through the cation exchange membrane is K^+ in the Figure 9(a)(left) because the transport number on the cation exchange membrane is theoretically unity. K^+ is also transported toward the current direction in the diffusion layer and Cl^- is transported toward the reverse direction. The width of arrow depends on the amount of transported ion in Figure 9.

The arrangement, MM + CMV, is represented in Figure 9(a)(right) where the water splitting phenomenon on the membrane did not appear but the diffusion layer indicated the growth by introduction of the charge mosaic membrane on the cation exchange membrane as indicated in Figure 7. This is caused by that ion transport process may depend on difference in movement of ions in a mosaic membrane and in solution under overlimiting current. In other words, the ions in free solution, cation, and anion affected each other by the interaction between the ions of the positive and negative to some extent, while ions in charge mosaic membrane under electricity moves smoothly along the fixed charge sites faster than them in free solution. It means the increase of K^+ transport number and finally the thickness of diffusion layer will be reflected from the equivalent properties of (3) and (4) at the same limiting current.

The arrangement, AMV, was shown in Figure 9(b)(left) on which the water splitting was observed sufficiently. In the case, the produced H^+ seems to affect the Cl^- transport number. The transport numbers, however, did not change so much as seen in Figure 6 because the protons would be compensated by Cl^- of high concentration in bulk solution next to the diffusion layer.

The arrangement, AMV + MM, was indicated in Figure 9(b)(right). The transport number was remarkably changed on this model, as clear from the result in Figure 6,

and the diffusion layer turned to be decreased as shown in Figure 7. It is supposed that the water splitting occurred at the membrane surface participates in the decrease. The produced protons promptly are connected with Cl^- on mosaic membrane introduced to this systems. As one possibility, though the situation is not clear, it is guessed as follows. As the Cl^- from the bulk solution is slow rate compared to those in mosaic membrane, Cl^- could not compensate the anionic depletion due to the produced proton in the diffusion layer. As a result, the anion transport number would decrease or the thickness of diffusion layer would be getting smaller. Figure 8 indicated the color's change by methyl red indicators. The red sign due to a generated proton appeared on the solution toward the cathode. It means that H^+ was transported toward the bulk solution as a part of charge carriers from the end of diffusion layer.

According to Figure 9, it was supposed that the ionic transport was changed by an addition of the charge mosaic membrane to electrodialysis.

4. Conclusion

Kinetic transport number on ionic transport in the diffusion layer in near the membrane surface was obtained by means of the chronopotentiometry. The equation was developed to obtain the thickness of the diffusion layer from equation of limiting current density. The diffusion layers were indicated as function given current densities.

On the other hand, the water splitting phenomenon was observed from pH measurement in both cases of anion exchange membrane system and anion exchange + charge mosaic membrane system. The phenomena together with relation to the thickness of diffusion layer were considered schematically in Figure 9.

In this study, it was examined whether the limit of current density could be increased by introducing the charge mosaic membrane.

References

- [1] T. Sata, "Ion exchange membrane," in *Royal Society of Chemistry*, pp. 215–240, London, UK, 2004.
- [2] Y. Tanaka, *Ion Exchange Membrane: Fundamentals and Applications*, vol. 12 of *Membrane Science and Technology*, Elsevier, Amsterdam, The Netherlands, 2007.
- [3] T. Hamano, P. B. Chebi, L. Gerdes, and T. D. Wolfe, "The development of a new electrodialysis system for brackish water," *Desalination*, vol. 96, pp. 23–31, 1994.
- [4] A. Yamauchi, J. Tateyama, B. I. Etoh, M. Takizawa, Y. Sugito, and S. Doi, "Charged mosaic membrane prepared from microsphere gel and its characterization," *Journal of Membrane Science*, vol. 173, no. 2, pp. 275–280, 2000.
- [5] M. Takizawa, Y. Sugito, N. Oguma, M. Nakamura, S. Horiguchi, and T. Fukutomi, "Charge-mosaic membrane prepared from microspheres," *Journal of Polymer Science A*, vol. 41, no. 9, pp. 1251–1261, 2003.
- [6] D. L. Grzenia, A. Yamauchi, and S. R. Wickramasinghe, "Electrolyte dialysis using charge-mosaic membranes," *Desalination and Water Treatment*, vol. 4, pp. 306–310, 2009.

- [7] N. Pismenskaia, P. Sistat, P. Huguet, V. Nikonenko, and G. Pourcelly, "Chronopotentiometry applied to the study of ion transfer through anion exchange membranes," *Journal of Membrane Science*, vol. 228, no. 1, pp. 65–76, 2004.
- [8] J. J. Krol, M. Wessling, and H. Strathmann, "Concentration polarization with monopolar ion exchange membranes: current-voltage curves and water dissociation," *Journal of Membrane Science*, vol. 162, no. 1-2, pp. 145–154, 1999.
- [9] J. J. Krol, M. Wessling, and H. Strathmann, "Chronopotentiometry and overlimiting ion transport through monopolar ion exchange membranes," *Journal of Membrane Science*, vol. 162, no. 1-2, pp. 155–164, 1999.
- [10] P. Sistat and G. Pourcelly, "Chronopotentiometric response of an ion-exchange membrane in the underlimiting current-range. Transport phenomena within the diffusion layers," *Journal of Membrane Science*, vol. 123, no. 1, pp. 121–131, 1997.
- [11] R. Ibanez, D. F. Stamatialis, and M. Wessling, "Role of membrane surface in concentration polarization at cation exchange membranes," *Journal of Membrane Science*, vol. 239, no. 1, pp. 119–128, 2004.
- [12] A. J. Bard and L. R. Faulkner, *Electrochemical Methods, Fundamentals and Applications*, Wiley International Edition, 1980.
- [13] A. Yamauchi, A. M. E. Sayed, K. Mizuguchi, M. Kodama, and Y. Sugito, "Ion transport behavior in diffusion layer of new designed ion exchange-mosaic composite polymer membrane," *Journal of Membrane Science*, vol. 283, no. 1-2, pp. 301–309, 2006.
- [14] T. Yawataya, *Ion Exchange Membrane For Engineer*, Kyoritsu Shuppan, 1982.

Research Article

Enhancing Ion Transfer in Overlimiting Electrodialysis of Dilute Solutions by Modifying the Surface of Heterogeneous Ion-Exchange Membranes

Natalia Pismenskaya, Nadezhda Melnik, Ekaterina Nevakshenova, Kseniya Nebavskaya, and Victor Nikonenko

Membrane Institute, Kuban State University, Krasnodar 350040, Russia

Correspondence should be addressed to Victor Nikonenko, v_nikonenko@mail.ru

Received 30 March 2012; Accepted 24 May 2012

Academic Editor: Tongwen Xu

Copyright © 2012 Natalia Pismenskaya et al. This is an open access article distributed under the Creative Commons Attribution License, which permits unrestricted use, distribution, and reproduction in any medium, provided the original work is properly cited.

The desalination of dilute NaCl solutions with heterogeneous Russian commercial and modified ion-exchange membranes was studied in a laboratory cell imitating desalination channels of large-scale electrodialysers. The modification was made by casting a thin film of a Nafion-type material on the surface of cation-exchange membrane, and by processing with a strong polyelectrolyte the surface of anion-exchange membrane. It was shown that the modifications resulted in an increase of mass transfer coefficient and in a decrease in water splitting rate, both by up to 2 times. The effect of mass transfer growth is explained by higher surface hydrophobicity of the modified membrane that enhances electroconvection. The decrease in water splitting rate in the case of cation-exchange membrane is due to homogenization of its surface layer. In the case of anion-exchange membrane the effect is due to grafting of quaternary ammonium bases onto the original membrane surface layer. The suppression of water splitting favors development of electroconvection. In turn, intensive electroconvection contributes to deliver salt ions to membrane surface and thus reduces water splitting.

1. Introduction

The applications of electrodialysis (ED) for water recovery in hybrid systems with RO [1] and in near zero liquid discharge (ZLD) systems [2], for ultrapure water production [3, 4], and for salt production from sea water [5] are some examples of successful use of this process, characterized by high economic and ecological effectiveness [6]. Desalination/deionization of dilute solutions is one of the largest ED applications [6, 7]. However, the process rate in this case is limited by the delivery of electrolyte from bulk solution to the membrane interface. This delivery occurs mainly as electrolyte diffusion while the contribution of forced convection is vanishing when approaching the interface [8–10]. The usage of intensive current modes might be of practical interest, since it can significantly raise the ED process rate [6, 10].

The latest researches [10–12] show that one of the most promising ways of reducing diffusion limitations and

enhancing the ED rate is the stimulation of current-induced convection, namely electroconvection. Electroconvection occurs as volume transport under the effect of an electric field imposed through the charged solution, in particular, through the electrical double layer (EDL). In the case where the space charge region (SCR) remains quasiequilibrium, electroconvection occurs as classical electroosmotic flow, named electroosmosis of the first kind [13–15]. When the applied current density is high enough, the SCR becomes nonequilibrium, it extends far beyond the quasiequilibrium EDL. Electroconvection caused by the action of the applied electric field upon the extended nonequilibrium SCR induced by the same electric field, is known as electroosmosis of the second kind [13–15]. Electroconvection produces microvortices, which actively mix the solution and may partially destroy diffusion boundary layer (DBL) in desalination channel at membrane surface [11, 15]. Since the EDL thickness increases with decreasing electrolyte solution

TABLE 1: Some characteristics of commercial MK-40, MA-40, and surface-modified MK-40/Nf and MA-40M membranes.

Membranes	Cation exchange		Anion exchange	
	MK-40	MK-40/Nf	MA-40	MA-40M
Ion exchange groups, bulk	$-\text{SO}_3^-$	$-\text{SO}_3^-$	$=\text{NH}, \equiv\text{N}$	$=\text{NH}, \equiv\text{N}$
Idem, surface	$-\text{SO}_3^-$	$-\text{SO}_3^-$	$=\text{NH}, \equiv\text{N}$	$-\text{N}^+(\text{R})_3$
Thickness, μm	480 ± 10	500 ± 10	470 ± 20	470 ± 20
Ion exchange capacity ¹ , mM cm^{-3} wet	1.7 ± 0.1	1.7 ± 0.1	3.2 ± 0.08	3.2 ± 0.08
Surface fraction of ion exchange material ² , %	22 ± 3	100	19 ± 4	19 ± 4
Contact angle ³ , degrees	55 ± 3	64 ± 3	50 ± 2	47 ± 2
Specific electrical conductivity in 0.5 M NaCl solution ⁴ , mS cm^{-1}	7.7 ± 0.3	8.3 ± 0.3	7.5 ± 0.3	5.5 ± 0.3
Diffusion permeability ⁵ , $10^{-8} \text{ cm}^2 \text{ s}^{-1}$	6.7 ± 0.4	6.6 ± 0.4	7.0 ± 0.4	6.7 ± 0.4

¹ Ion exchange capacity was determined for wet membranes in the sodium form (cation exchange membranes) or in the chloride form (anion exchange membranes).

² Surface fraction of ion exchange material was determined for a wet membrane using SEM images by the method described in [21].

³ Contact angle on the surface of wet membrane was found 20 s after placing a test drop, according to the method described in [18].

⁴ Specific electrical conductivity of membrane in 0.5 M NaCl solution was determined by a difference method using a clip cell [28].

⁵ Diffusion permeability of membranes was determined in $\text{H}_2\text{O}/\text{IEM}/0.5 \text{ M NaCl}$ system using the cell described in [29]; the modified side of MK-40/Nf membrane was facing the NaCl solution; the left- and right-hand sides of MK-40, MA-40, and MA-40M membranes are symmetrical.

concentration, the rate of electroconvection should grow with diluting solution. This feature is especially important because it allows ED rate to be increased when treating diluted solutions [10, 15, 16]. Note that the extended SCR may be also used as a barrier for separating coions from counterions in a microchannel ED device [17].

In experiments using small-scale laboratory cells described in earlier publications [10, 18, 19], we have shown that ion-exchange membrane surface modification can significantly enhance the ED rate in the range of 10^{-4} to 10^{-2} M electrolyte solutions. Hydrophobization of cation-exchange membrane surface can stimulate the development of electroconvection due to change of the no-slip hydrodynamic boundary condition to the slip one [10, 18, 20]. In case of anion-exchange membranes, the treatment of surface by a strong polyelectrolyte containing quaternary ammonium bases leads to a decrease in the water splitting rate at the depleted membrane interface under intensive current densities. The effect is due to the substitution of secondary and tertiary amine groups, characterized by high catalytic activity in respect to water splitting reaction, by quaternary ammonium groups of low catalytic activity [10, 21, 22].

In this paper we will study the behavior of modified ion-exchange membranes in conditions close to those applied in large-scale electrodialysers. It will be shown that appropriate modification of heterogeneous membrane surface allows significant enhance of salt-ion transfer in real ED desalination processes.

2. Ion-Exchange Membranes and Their Characteristics

Heterogeneous cation-exchange MK-40 and anion-exchange MA-40 membranes (Shchekinoazot, Russia) are produced using a hot pressing method from polyethylene (as an inert binder) and ion-exchange resin powders, KU-2 and EDE-10P, respectively. KU-2 is a sulfonated styrene-divinylbenzene copolymer; EDE-10P is produced by polycondensation of polyethylenepolyamines and epichlorohydrin. SEM

images of surface and cross sections of a dry MK-40 membrane are shown in Figures 1(a), 1(b), 1(c), and 1(d). SEM images of MA-40 membranes look similarly. As it can be seen in Figures 1(b), 1(c), and 1(d), the diameter of ion-exchange resin particles is 10 to 30 μm .

Some characteristics of these ion-exchange membranes (IEMs) are represented in Table 1.

The membrane bulk contains from 35% (MK-40) to 45% (MA-40) of polyethylene [23]. However, the surfaces of wet MK-40 and MA-40 membranes are covered with polyethylene by about 80% (Table 1). The higher content of the binder in the near-surface layer is explained by the fact that at elevated temperatures used during the hot pressing, polyethylene is more fluent than the ion-exchange resin material.

Effective contact angle found experimentally for heterogeneous membranes under study is an average between its local values corresponding to the polyethylene and to the resin particles. The surface of MA-40 membrane is more hydrophilic, apparently due to higher exchange capacity of the resin in this membrane (Table 1).

The MK-40 membrane has sulfonic ion-exchange groups, which have low catalytic activity with respect to water splitting reaction [24, 25]. The MA-40 membrane contains mostly secondary and tertiary amines as ion-exchange groups, which are effective catalysts of this reaction [24, 25]. Thereby the MA-40 membrane is characterized by a high rate of H^+/OH^- ions generation at its depleted surface in intensive current modes [21]. In order to reduce water splitting, it is possible to replace secondary and tertiary amines on MA-40 surface with quaternary ones which are characterized by low catalytic activity. For this purpose, a commercial MA-40 membrane was modified by a copolymer of dimethyldiallylammonium chloride [21, 26].

The surface of MK-40/Nf membrane is completely covered with a thin (20 μm) homogeneous film (Nf) with the same functional groups as that of the MK-40 membrane (Figures 1(e) and 1(f), Table 1). The film is formed by casting

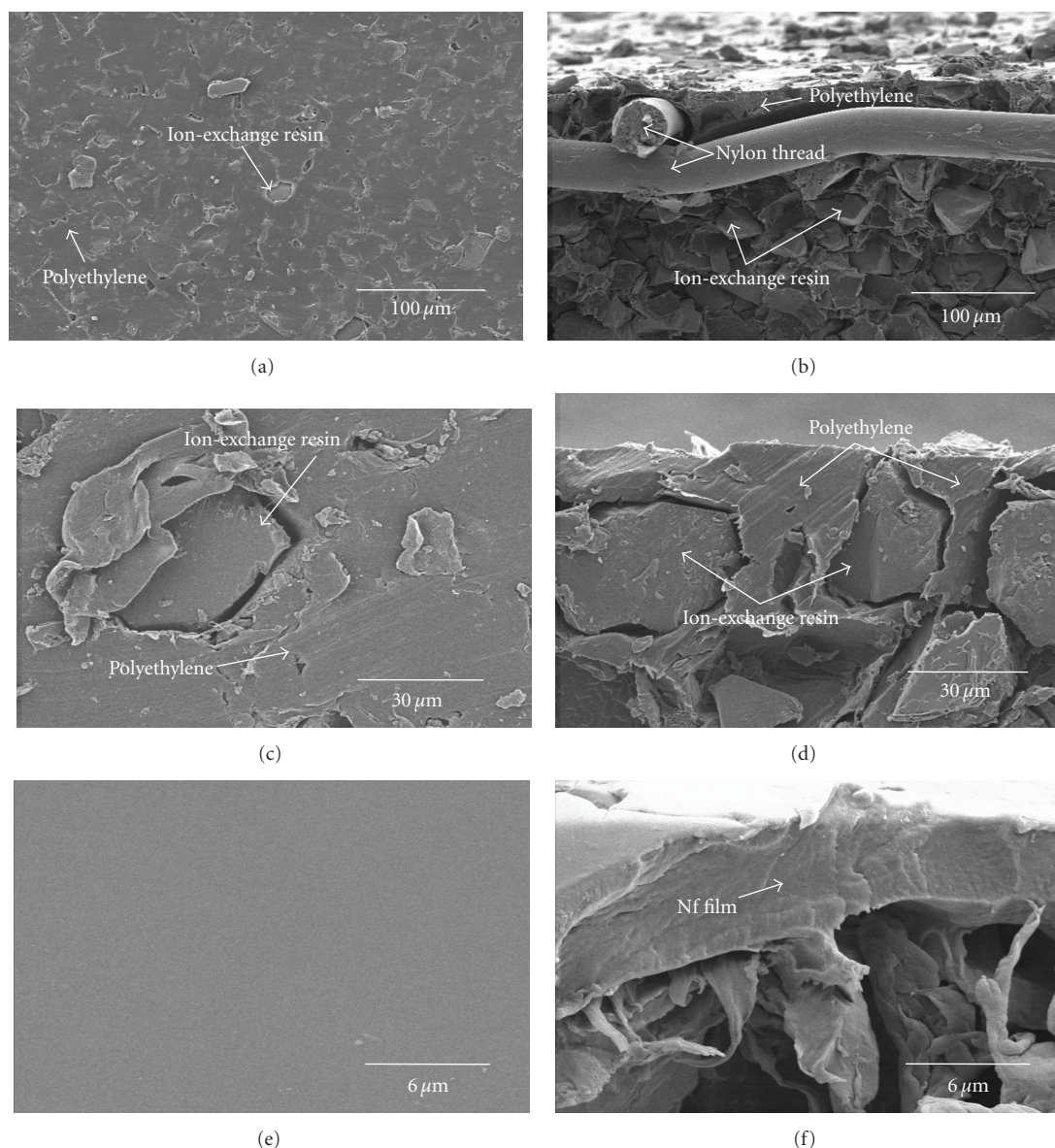


FIGURE 1: SEM images of the surface (a, c, and e), the cross sections (b, d, and f) of a MK-40 (a, b, c, and d), and a MK-40/Nf (e, f) ion-exchange membranes.

a 7% MF-4SK solution in isopropyl alcohol (Plastpolymer, Russia) on the MK-40 membrane as substrate. MF-4SK is a sulfonated tetrafluorethylene and perfluorovinyl (alcohol) ether copolymer. The structure and properties of MF-4SK material are close to those of Nafion (DuPont Co.); they are thoroughly studied by Berezina et al. [27, 28]. As a result of casting perfluorinated film, the contact angle on MK-40/Nf membrane is increased (Table 1), and the membrane surface becomes homogeneous (Figure 1(e)). However, this modification does not lead to significant changes in electrical conductivity and diffusion permeability of modified MK-40/Nf membrane compared to the commercial MK-40 (Table 1).

3. Method of Mass-Transfer Characteristics Measurements

The principal scheme of experimental setup for mass-transfer characteristics measurements is shown in Figure 2.

The membranes forming desalination (DC), concentration (CC), and electrode (EC) compartments are separated from one another by an inert net spacer (S) of extrusion type with rhombic cells, situated at 45° to ingoing stream. The step of the spacer cell is 5 mm, the thickness is 1.0 mm, and the porosity is 0.91.

The membranes under study are designated with an asterisk (MK*-40, MA*-40, the numbers "40" are not

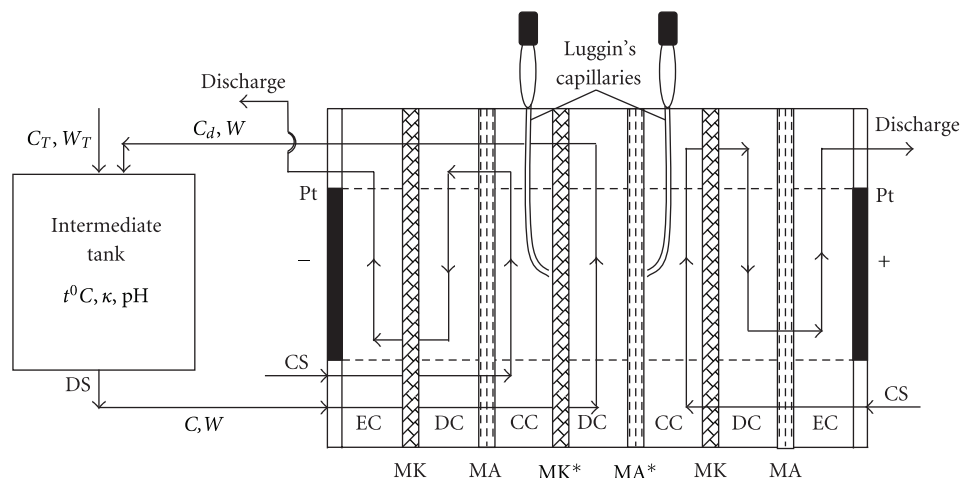


FIGURE 2: Principal scheme of the experimental setup used for measuring mass-transfer characteristics. A desalting (DS) and two concentrating (CS) streams, desalination (DC), concentration (CC) and electrode (EC) channels, and polarizing platinum electrodes (Pt) are shown. Dashed straight lines mark out the active section of membrane stack polarized by electric current.

shown). They can be commercial membranes or modified ones. Auxiliary commercial MK-40 and MA-40 membranes serve to separate the products of electrode reactions from the central compartment under study.

Two plastic Luggin's capillaries (0.5 mm in external diameter) are built in the spacer. Both capillary tips are situated at the center of polarized area in CC at about 0.5 mm from the surface of the membrane forming the central DC. Another end of each capillary is connected to a reservoir with a (0.02 M) NaCl solution where a measuring Ag/AgCl electrode is inserted.

The membrane stack imitates an industrial electro-dialyser with internal collectors. At the stack entrance, each compartment has a nonpolarized section of 5 cm length for hydrodynamic stabilization of the solution flow. The polarized membrane area is 3 cm in width (a) and 10 cm in length (L), the total membrane length is 22 cm. Our previous investigations [29, 30] showed that the mass-transfer characteristics obtained in a stack of $L = 10$ cm in length can be quantitatively scaled to predict the behavior of industrial electro-dialysers.

An intermediate tank, inserted into the desalting stream (Figure 2), contains a stirrer and sensors to control temperature, pH, and specific electrical conductivity (κ). In the concentrating streams (CS), a 0.02 M NaCl solution is supplied from a separate tank (not shown in Figure 2), it continuously passes through auxiliary CC and DC, then through EC and is discharged. The average linear flow velocity in all compartments is equal to 2.5 cm s^{-1} .

Before the experiment, the tank, the central desalination compartment, and the hoses were filled with 1200 mL of a 0.03 M NaCl solution. Then a constant voltage controlled with the Luggin's capillaries (Figure 2) was applied and electro-dialysis process was realized at $25 \pm 0.5^\circ\text{C}$ maintained in the tank. The solution circulated through the intermediate tank and the central DC with volume flow rate W . The salt concentration in the tank decreased with time because of the

electro-dialysis desalination: the outlet concentration, C_d , was lower than the inlet one, C . Besides, there were changes in pH of the solution passed through the DC due to different rates of water splitting at the cation-exchange (MK-40 or MK-40/Nf) and the anion-exchange (MA-40 or MA-40M) membranes. In order to maintain pH = 7 in the solution in the tank, alkaline (NaOH) or acid (HCl) solution was added into the tank, depending on the sign of the pH changes in the outlet solution. The desalination process was realized in quasi-steady-state conditions, the amount of the solution put in the system so that allowed us to keep a slow (less than 1% per minute) [29] decrease in the electrolyte concentration of the solution in the intermediate tank. The total duration of every run was 8–10 hours. The electric current, as well as the specific conductivity of the solution (converted then into the NaCl concentration) in the tank were measured as functions of time.

The range of NaCl concentrations used in the experiments ($0.001 \text{ M} \leq C \leq 0.03 \text{ M}$) is chosen in a way to be sure that the co-ion transfer through the membranes is negligible, as well as that of carbonic acid dissociation products, which may appear in the desalinated solution due to dissolved atmospheric carbon dioxide. Experimental data by Sheldeshov et al. [31] and Gnusin et al. [32] as well as our calculations with help of the microheterogeneous model [33] show that the co-ion transfer through MK-40, MA-40, and similar heterogeneous membranes at current densities close to the limiting one becomes negligible if the difference between the salt concentration at the enriched and depleted membrane interfaces is less than 0.1 M. According to our estimations made earlier [29], noticeable carbon dioxide absorption from air and contribution of carbonic acid dissociation products to charge transfer through anion-exchange membranes occur at feed NaCl concentrations lower than $0.5 \times 10^{-3} \text{ M}$.

The mass-transfer rate may be found from the rate of the salt concentration decrease in the tank. In fact, the salt

concentration in the tank varies due to ion transfer through IEMs in the DC and due to addition of alkaline (or acid) solution into the tank in order to maintain $\text{pH} = 7$. The description of material balance in the tank conducts to [18, 19]:

$$k_i = \frac{i_i}{FC} = -\frac{V_{\text{sol}}}{SC} \frac{dC}{dt} + \frac{c_T W_T}{SC}, \quad (1)$$

where i_i is the partial current density of salt counterion (in our case it is ion Na^+ for cation-exchange membrane and ion Cl^- for anion-exchange membrane) through the membrane under study; C is the current salt (NaCl) concentration in the tank; k_i (defined as i_i/FC) is the mass-transfer coefficient characterizing the salt counterion transfer rate through the membrane under study; V_{sol} is the volume of solution in the desalting stream (including its volume in the tank, in the DC, and in the hoses); W_T and c_T are the volume flow rate and the concentration of the solution (NaOH or HCl) added into the tank to maintain $\text{pH} = 7$, respectively; S is the membrane active surface. The first term in right-hand side of (1) shows the rate of concentration variation in the tank ($V_{\text{sol}}(dC/dt)$) divided by SC . The rate of concentration variation in the tank depends on the rate of ED desalination ($k_i SC$) and the rate of alkaline or acid addition ($c_T W_T$).

Equation (1) assumes that there is no salt co-ion flux through both membranes forming the desalination compartment. As it is noted above, the range of feed concentrations was chosen in a way to satisfy the negligible co-ion flux assumption.

Equation (1) is applied if the mass-transfer coefficient is calculated for the salt counterion passing through the membrane, which generates less H^+ and OH^- ions than the other one forming the desalination compartment. For example, it is the case of Na^+ transfer through the MK-40 membrane making a pair with a MA-40 membrane. In this case, NaOH is added into the tank to compensate the excess of H^+ ions produced at the MA-40 membrane. To calculate the mass-transfer coefficient of Cl^- ion for the MA-40 only the first term in the right-hand side of (1) should be taken into account, as no Cl^- is added into the tank, and (1) becomes

$$k_i = \frac{i_i}{FC} = -\frac{V_{\text{sol}}}{SC} \frac{dC}{dt}. \quad (2)$$

We have a similar situation in the case of MK-40/Nf membrane making the DC with MA-40M membrane ($\Delta\varphi > 4\text{ V}$). The rate of water splitting is essentially less than that in MK-40/MA-40 system; however, a small quantity of NaOH is needed to compensate the excess of H^+ ions produced at the MA-40M membrane.

The evaluated maximal measurement error in determination of k_i was 6%.

The effective transport number of an ion transported through the membrane is defined as the ratio of the partial current density of this ion to the total current density i :

$$T_i = \frac{i_i}{i}. \quad (3)$$

If the co-ion transport is not taken into account, the sum of salt cation (Na^+) and proton (H^+) transport numbers in a cation-exchange membrane, as well as the sum of salt anion (Cl^-) and hydroxyl (OH^-) transport numbers in an anion-exchange membrane is equal to unity:

$$T_{\text{Na}^+} + T_{\text{H}^+} = T_{\text{Cl}^-} + T_{\text{OH}^-} = 1. \quad (4)$$

T_{H^+} and T_{OH^-} characterize the rate of water splitting in a membrane system. Their values are readily found after determination of k_i , according to (1)–(4).

4. Concentration Dependence of Mass-Transfer Coefficient and Effective Transport Numbers

The results of study of mass-transfer characteristics of desalination channels in a cell shown in Figure 2 and formed by MK-40//MA-40 and MK-40/Nf//MA-40M membrane pairs are shown in Figures 3 and 4 and Table 2. The data were obtained at a potential difference $\Delta\varphi$ (registered with Luggin's capillaries as shown in Figure 2) equal to 2.5, 4.0, or 6.0 V per cell pair. A potential difference was fixed while the feed concentration decreased with time since a fixed volume of solution circulated through a central desalination compartment and a tank, as it is described in Section 3. Total (i_{tot}) and partial (Na^+ and H^+ ions through cation-exchange membranes and Cl^- and OH^- ions through anion-exchange ones, resp.) current densities are shown in Figure 5 as functions of the feed NaCl concentration, in the case where the potential drop across a cell pair was 4 V.

The data presented in Figure 3 show that when the value of potential drop per cell pair $\Delta\varphi$ is fixed, the mass-transfer coefficients of salt counterions grow with decreasing feed NaCl concentration for all investigated membranes. For both cation- and anion-exchange membranes, this growth is more important in the case of surface-modified membranes (Figure 3, Table 2).

The dependence of mass-transfer coefficient on $\Delta\varphi$ in case of fixed NaCl concentration is more complicated. When $\Delta\varphi$ is growing, there is a tendency to equalization of the mass-transfer rates found in systems with both modified and commercial membranes. After passing 4 V, a deceleration of mass-transfer rate growth or even its descend with rising $\Delta\varphi$ occurs, Figures 3(b) and 3(c).

As expected [34], the effective transport numbers of water splitting products $T_{\text{H}^+(\text{OH}^-)}$ (Figure 4) grow with diluting solution at fixed $\Delta\varphi$ and with increasing $\Delta\varphi$ at fixed feed solution concentration, for all membranes. At $\Delta\varphi = 2.5\text{ V}$ and $\Delta\varphi = 4.0\text{ V}$, the values of $T_{\text{H}^+(\text{OH}^-)}$ are relatively low, especially for modified membranes ($T_{\text{H}^+(\text{OH}^-)} < 0.15$) (Figures 4(a) and 4(b)), while a high increase of Na^+ and Cl^- mass-transfer coefficients is registered (Figures 3(a) and 3(b)). Further growth of potential drop ($\Delta\varphi > 4\text{ V}$) leads to a more significant raise of $T_{\text{H}^+(\text{OH}^-)}$ (Figure 4(c)). At $\Delta\varphi = 6.0\text{ V}$ and $C_{\text{NaCl}} = 0.005\text{ M}$, T_{H^+} and T_{OH^-} in commercial MK-40 and MA-40 membranes reach 0.22 and 0.35, respectively. Hence, in these conditions H^+ and especially OH^- ions make a noticeable competition with

TABLE 2: Ratio of Na^+ to Cl^- mass-transfer coefficients for ED cells with modified and commercial membranes at different feed solution concentrations and potential drops per cell.

$C_{\text{NaCl}}, \text{mol dm}^{-3}$	$k_{\text{Na}^+}^{\text{MK-40/Nf}}/k_{\text{Na}^+}^{\text{MK-40}}$			$k_{\text{Cl}^-}^{\text{MA-40M}}/k_{\text{Cl}^-}^{\text{MA-40}}$		
	2.5 V	4.0 V	6.0 V	2.5 V	4.0 V	6.0 V
0.02	1.0 ± 0.1	1.2 ± 0.1	1.0 ± 0.1	1.0 ± 0.1	1.2 ± 0.1	1.0 ± 0.1
0.01	1.2 ± 0.1	1.4 ± 0.1	1.0 ± 0.1	1.3 ± 0.1	1.3 ± 0.1	1.0 ± 0.1
0.005	2.0 ± 0.1	1.7 ± 0.1	1.2 ± 0.1	1.8 ± 0.1	1.7 ± 0.1	1.2 ± 0.1

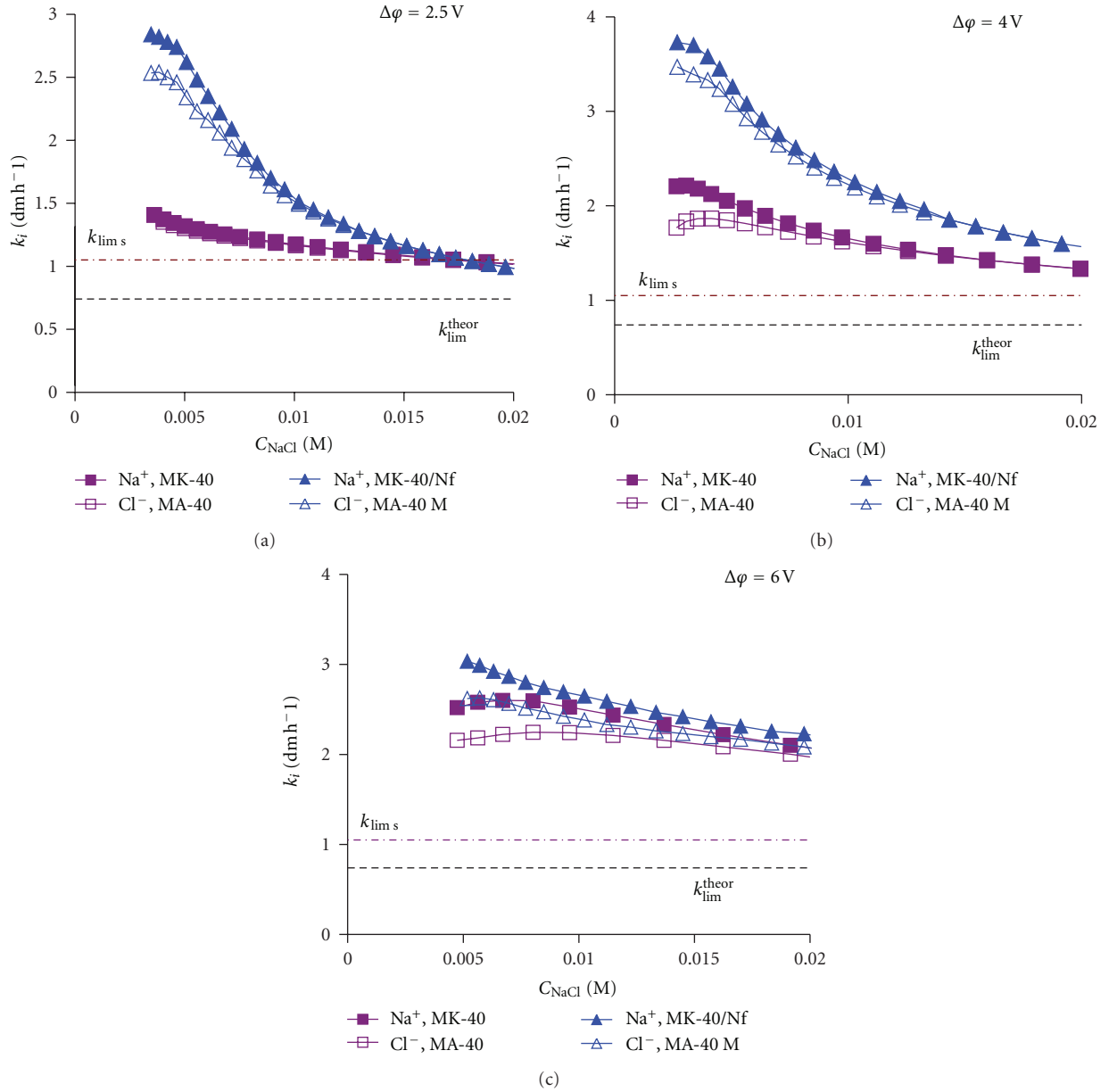


FIGURE 3: Concentration dependence of Na^+ mass-transfer coefficients across MK-40 and MK-40/Nf cation-exchange membranes and Cl^- across MA-40 and MA-40M anion-exchange membranes forming desalination channels in a cell shown in Figure 2 under different potential drops ($\Delta\phi$) per cell pair: 2.5 V (a), 4.0 V (b), and 6 V (c). The limiting mass-transfer coefficient for the DC without spacer, $k_{\text{lim}}^{\text{theor}}$, is calculated according to (7); the limiting mass-transfer coefficient for DC with spacer, $k_{\text{lim s}}$, is evaluated as described in the text.

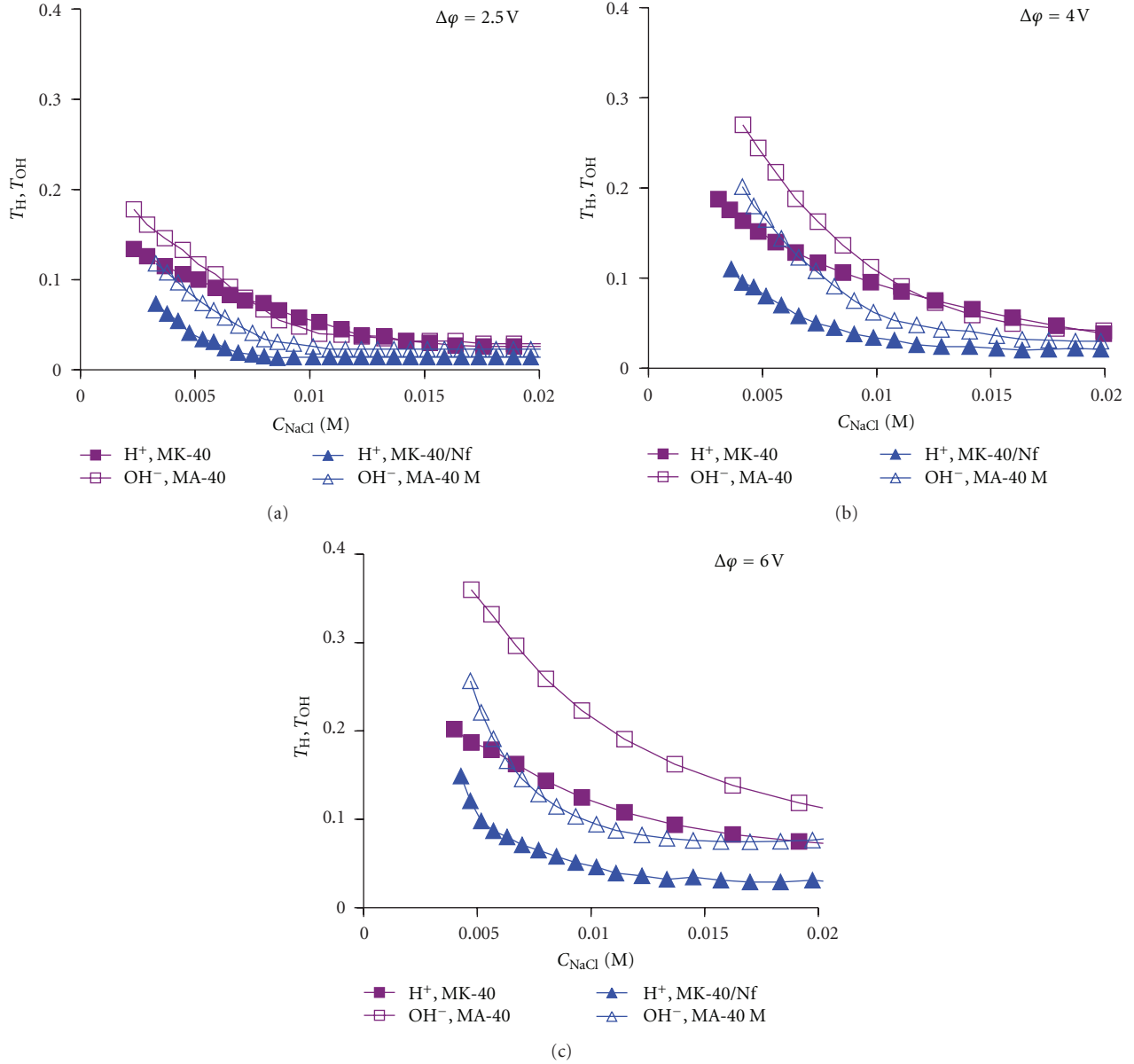


FIGURE 4: Concentration dependence of effective transport number of protons in cation-exchange membrane and that of hydroxyl ions in anion-exchange membranes forming MK-40//MA-40 and MK-40/Nf//MA-40M desalination channels at potential drops ($\Delta\phi$) 2.5 V (a), 4.0 V (b), and 6.0 V (c) per cell pair.

Na^+ and Cl^- ions in the electric charge transfer through the membranes.

As to the membranes with modified surface, MK-40/Nf and MA-40M, both chemical treatment of a MA-40 membrane and casting a homogeneous ion conducting film onto a MK-40 membrane lead to a substantial decrease in water splitting product transport numbers. For example, at $C_{\text{NaCl}} = 0.005 \text{ M}$ and $\Delta\phi = 4.0$ (Figure 4(b)), T_{OH^-} is equal to 0.23 and 0.15, for MA-40 and MA-40M membranes, respectively, while T_{H^+} is equal to 0.14 and 0.06 for MK-40 and MK-40/Nf membranes, respectively.

The obtained results are in good agreement with the actual theoretical concepts of overlimiting mass-transfer

mechanisms [10, 11, 15, 35, 36] and with the experimental data found earlier with laboratory-scale ED cells [10, 18, 19]. First, these data confirm that electroconvection is the main mechanism of salt-ion transfer enhancement in intensive current modes. Following “classical” theoretical basics [37–39], the mass-transfer coefficient has its limiting value, which corresponds to the limiting current density and does not depend on the concentration of feed solution. It follows from the combination of well-known Peers equation [38]:

$$i_{\text{lim } i}^{\text{theor}} = \frac{FDC}{\delta(T_i - t_i)} \quad (5)$$

and the mass-transfer coefficient definition $k_i = i_i/FC$ (1), when assuming that no water splitting occurs and the

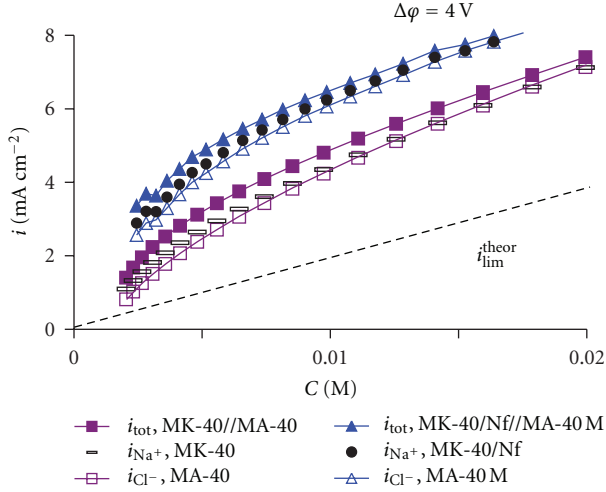


FIGURE 5: Total (i_{tot}) and partial current densities in the electro-dialysis cell shown in Figure 2 as functions of the feed NaCl concentration. i_{Na^+} and i_{H^+} are the partial current densities of Na^+ and H^+ ions through cation-exchange membrane, respectively; i_{Cl^-} and i_{OH^-} are those of Cl^- and OH^- ions through anion-exchange membrane, respectively. The potential drop across the cell pair is 4 V.

thickness of the Nernst diffusion boundary layer (DBL), δ , is constant. Combining (1) and (5) leads to a simple equation:

$$k_{\text{lim}i}^{\text{theor}} = \frac{D}{\delta(T_i - t_i)}. \quad (6)$$

Here D is the electrolyte diffusion coefficient; t_i is the transport number of the salt counterion in solution.

The limiting state in a desalination channel is determined by the membrane whose hosted counterions have lower mobility in solution [7]. It can be seen from (5): the difference $(T_i - t_i)$ is higher for lower t_i , as T_i is very close to 1; hence, $i_{\text{lim}i}^{\text{theor}}$ is lower. For this reason, when current density increases, the limiting state in the cell under study is first achieved at the cation-exchange membrane. According to “classical” theories, the salt concentration at this membrane becomes zero when the current density reaches $i_{\text{lim Na}^+}^{\text{theor}}$. In desalination channels without spacer, $i_{\text{lim Na}^+}^{\text{theor}}$ may be evaluated according to (7) [22], which is derived from the known L  v  que equation [40, 41]:

$$i_{\text{lim Na}^+}^{\text{theor}} = \frac{1.43CFD_{\text{NaCl}}^{2/3}V^{1/3}}{L^{1/3}h^{1/3}(T_{\text{Na}^+} - t_{\text{Na}^+})}, \quad (7)$$

where V is the average flow rate, L is the desalination length, and h is the intermembrane distance. Equation (7) is valid for relatively short channels, $L < 0.02Vh^2/D$.

Combining (5)–(7), it is relatively easy to find the limiting value of the mass-transfer coefficient for a desalination channel with the dimensions used in this study, but without spacer: $k_{\text{lim}}^{\text{theor}} = 0.74 \text{ dm hr}^{-1}$ ($D_{\text{NaCl}} = 1.61 \cdot 10^{-9} \text{ m}^2 \text{ s}^{-1}$; $t_{\text{Na}^+} = 0.40$ [42]; $T_{\text{Na}^+} = 1$). This value is plotted in Figure 3 with dashed line. Usually introduction of a spacer into desalination channel results in a decrease of diffusion layer

thickness due to enhancing convective transfer. Hence, $i_{\text{lim}}^{\text{theor}}$ and $k_{\text{lim}}^{\text{theor}}$ should increase according to (5) and (6). We can evaluate the increase in $k_{\text{lim}}^{\text{theor}}$ resulted from the introduction of spacer in DC as follows. In our former experiments [22, 34, 43] it was shown that in the DC formed by MK-40 and MA-40 membranes, water splitting arises when the current density is close to the limiting current density at the cation-exchange membrane ($i_{\text{lim Na}^+}$): the solution outgoing from the DC becomes slightly alkaline. With increasing current density up to $(1.05\text{--}1.1) i_{\text{lim Na}^+}$, the rate of H^+ and OH^- ion generation at the anion-exchange membrane becomes higher than that at the cation-exchange membrane: the outgoing solution becomes acid. In actual experiments, a slight increase in pH of desalinated solution is registered for the DC, formed by MK-40 and MA-40 membranes, when the NaCl concentration is in the range 0.015–0.020 M and $\Delta\phi = 2.5 \text{ V}$. In these conditions T_{H^+} and T_{OH^-} are close to zero. This fact allows us to assume that in these conditions the MK-40/S/MA-40 system is close to its limiting state; hence, $i \approx i_{\text{lim Na}^+}$. The mass-transfer coefficient corresponding to this state is $k_{\text{lim s}} = (i_{\text{lim Na}^+}/FC)$. The value of $k_{\text{lim s}}$ is plotted in Figure 3 with dash-dotted line. This value is about 35% higher than that of $k_{\text{lim}}^{\text{theor}}$ (valid for the same channel, but without spacer).

The increase in mass-transfer coefficients over $k_{\text{lim s}}$ may be caused by the following effects coupled with the concentration polarization: exaltation effect connected with water splitting, gravitational convection, or electroconvection [10]. Our estimations show that at $\Delta\phi \leq 4.0 \text{ V}$ and at the values of the partial current densities of H^+ (OH^-) reached in our experiments (Figure 4), exaltation effect [10] cannot provide an increase in ion transfer more than 3–5%. However, k_{Na^+} and k_{Cl^-} can exceed $k_{\text{lim s}}$ in several times. For example, at $C_{\text{NaCl}} = 0.005 \text{ M}$ and $\Delta\phi \leq 4.0 \text{ V}$ (Figure 4(b)) $k_{\text{Na}^+}/k_{\text{Cl}^-}$ is equal to 2.5 and 3.3 for MK-40 and MK-40/Nf membranes, respectively, and $k_{\text{Cl}^-}/k_{\text{lim s}}$ is equal to 1.8 and 3.1 for MA-40 and MA-40M, respectively. Gravitational convection weakens with diluting solution and is practically negligible in conditions of this experiment [10]. In contrast, electroconvection is enhanced with diluting solution [10, 11, 22]. Apparently, it is the only mechanism able to enhance salt-ion transfer in conditions of our experiment.

The reasons for more prominent electroconvection in the DC with modified membranes are as follows. The application of sulfonated polytetrafluoroethylene (Nf) film on MK-40 surface results in a significant increase of water contact angle (Table 1). Water slips easier at more hydrophobic surface [20], facilitating the onset of electroconvection [10, 18, 19]. Another reason may be in lower water splitting in the cell with modified membranes. As it was shown by Choi et al. [44], mass-transfer rate through ion-exchange membranes rises with increasing Stokesian radius of counterion. This is apparently caused by the fact that a more hydrated counterion can involve a bigger volume in motion during electroconvection. H^+ and OH^- ions carry the charge by “tunneling” from one water molecule to another without bringing liquid volume into motion (the Grotthuss transport mechanism) hence, Stokesian radius of these ions is very small. As a result, an increase in the contribution of water

splitting products to the charge transfer through the membrane weakens electroconvection. Moreover, the H^+ and OH^- ions generated at the membrane/solution interface are carried away into the extended SCR and reduce the space charge density at a fixed current density [34], as a result, the electric body force generating electroconvection is also reduced.

The negative impact of H^+ and OH^- ions generation on mass-transfer rate is especially noticeable in the case of commercial MA-40 membrane: the mass-transfer coefficient of both Na^+ and Cl^- ions decreases at low feed concentrations when the voltage increases from 4.0 V to 6.0 V (Figures 3(b) and 3(c)). This result is typical for majority of anion-exchange membranes, which generate more intensively H^+ and OH^- ions in comparison with the neighboring cation-exchange membranes in a desalination channel [45].

It follows from experiments carried out with small laboratory-scale cells that a noticeable decrease in mass-transfer rate (apparently due to suppression of electroconvection) takes place when $T_{H^+(OH^-)}$ reaches a value in the range from 0.2 to 0.3 [34]. The decrease of k_{Na^+} and k_{Cl^-} in the DC imitating large-scale electrodialysers starts at somewhat smaller $T_{H^+(OH^-)}$ values (0.1–0.15) (Figures 3(b), 3(c), 4(b), and 4(c)). Perhaps, this is caused by the fact that we register integral (averaged over the DC length) transport numbers. $T_{H^+(OH^-)}$ can easily reach values of 0.2–0.3 near the exit of DC, where the solution concentration decreases by 20–30% compared to the inlet.

As noted above, the difference in the behavior of commercial and modified membranes decreases with increasing potential difference: the rates of mass transfer and water splitting are getting close (Figures 3 and 4). It is possible that the reason for that is in the convergence of water splitting rates for different membranes under high $\Delta\phi$. Apparently the impact of the field effect [46] into water splitting rate increases with increasing $\Delta\phi$, and in the range of high $\Delta\phi$ the difference in catalytic activity of different fixed group is no longer the dominating factor. Thus, the benefit of the replacement of the secondary and tertiary amino groups with the quaternary ammonium bases (MA-40M) is not so noticeable at high $\Delta\phi$ (Figure 3(c)).

In long desalination channels, $H^+(OH^-)$ ions, produced at one of the membranes forming the channel, can reach the other membrane and then participate in competitive transfer through this membrane. Even if a part of the ions generated at the first membrane will be neutralized by the products of water splitting at the second one, the remained ions will reduce the current efficiency and contribute to suppression of electroconvection. Generally, as mentioned above, it is anion-exchange membrane which splits water more intensively. In addition of negative effects noted above, an excess of H^+ ions in the desalination compartment decreases the degree of dissociation of weak acids presented in natural waters, such as silicic acid, and hence, reduces their removal. An increase of pH in the concentrate compartment leads to formation of salt deposits. For these reasons, a decrease in water splitting rate at anion-exchange membrane is a key point in improvement of overlimiting electrodialysis.

Synergetic effect is achieved when both membranes are improved: the cation-exchange one in order to enhance electroconvection and the anion-exchange one in order to suppress water splitting.

5. Conclusions

Overlimiting electrodialysis can be essentially improved by applying specially modified ion-exchange membranes. The cation-exchange membrane was modified by a thin homogeneous ion-conducting but relatively hydrophobic (Nafion-type) layer in order to stimulate electroconvection and to reduce water splitting. The modification of the anion-exchange membrane was aimed only at lowering water splitting rate at its surface. The behavior of modified and original commercial membranes (MA-40 and MK-40) was compared in a desalination channel imitating that in large-scale electrodialysers. It is shown that, as well as in small-scale laboratory cells studied earlier, the H^+ and OH^- effective transport numbers in the membranes are reduced by about 2 times and hence, current efficiency increased correspondingly, when the commercial membranes were replaced with the modified ones. The salt-ion transfer intensified by electroconvection increases up to 3.5 times. The effect is maximum in rather diluted (0.005 M NaCl) solution at 4 V per cell pair. With increasing voltage, the mass-transfer coefficient continues to grow in the range 0.01 to 0.025 M concentrations. However, it decreases at feed concentrations <0.005 M NaCl and a fixed voltage. Apparently, the reason is in high water splitting rate, which occurs in very dilute solutions in spite of the modification of both membranes. Another reason is in participation in current transfer of hydrogen carbonate anions issued from dissolving of atmospheric CO_2 in water, but this effect takes place at feed concentrations <0.0005 M NaCl.

Note that the ways and materials of modification are commercially available. In practical terms, this means that there are new opportunities to produce inexpensive ion-exchange membranes effective in electrodialysis of dilute solutions.

Acknowledgments

Part of the work was realized within a French-Russian laboratory “Ion-exchange membranes and related processes”. The authors are grateful to CNRS, France and to RFBR (Grants no. 11-08-93107-NCNIL, 11-08-96511, and 11-08-93107), Russia, as well as FP7 “CoTraPhen” project PIRSES-GA-2010-269135 for financial support of this work.

References

- [1] Y. Zhang, K. Ghyselbrecht, B. Meesschaert, L. Pinoy, and B. Van der Bruggen, “Electrodialysis on RO concentrate to improve water recovery in wastewater reclamation,” *Journal of Membrane Science*, vol. 378, no. 1–2, pp. 101–110, 2011.
- [2] Y. Oren, E. Korngold, N. Daltrophe et al., “Pilot studies on high recovery BWRO-EDR for near zero liquid discharge approach,” *Desalination*, vol. 261, no. 3, pp. 321–330, 2010.

- [3] J. Wood, J. Gifford, J. Arba, and M. Shaw, "Production of ultra-pure water by continuous electrodeionization," *Desalination*, vol. 250, no. 3, pp. 973–976, 2010.
- [4] V. I. Zabolotsky, V. V. Nikonenko, N. D. Pismenskaya, and A. G. Istoshin, "Electrodialysis technology for deep demineralization of surface and ground water," *Desalination*, vol. 108, no. 1–3, pp. 179–181, 1997.
- [5] Y. Tanaka, R. Ehara, S. Itoi, and T. Goto, "Ion-exchange membrane electrodialytic salt production using brine discharged from a reverse osmosis seawater desalination plant," *Journal of Membrane Science*, vol. 222, no. 1–2, pp. 71–86, 2003.
- [6] H. Strathmann, "Electrodialysis, a mature technology with a multitude of new applications," *Desalination*, vol. 264, no. 3, pp. 268–288, 2010.
- [7] Y. Tanaka, *Ion Exchange Membranes: Fundamentals and Applications*, vol. 12 of *Membrane Science and Technology*, Elsevier, Amsterdam, The Netherlands, 2007.
- [8] K. S. Spiegler, "Polarization at ion exchange membrane-solution interfaces," *Desalination*, vol. 9, no. 4, pp. 367–385, 1971.
- [9] P. Długołęcki, B. Anet, S. J. Metz, K. Nijmeijer, and M. Wessling, "Transport limitations in ion exchange membranes at low salt concentrations," *Journal of Membrane Science*, vol. 346, no. 1, pp. 163–171, 2010.
- [10] V. V. Nikonenko, N. D. Pismenskaya, E. I. Belova et al., "Intensive current transfer in membrane systems: modelling, mechanisms and application in electrodialysis," *Advances in Colloid and Interface Science*, vol. 160, no. 1–2, pp. 101–123, 2010.
- [11] I. Rubinstein and B. Zaltzman, "Electro-osmotically induced convection at a permselective membrane," *Physical Review E*, vol. 62, no. 2, pp. 2238–2251, 2000.
- [12] J. Balster, M. H. Yildirim, D. F. Stamatialis et al., "Morphology and microtopology of cation-exchange polymers and the origin of the overlimiting current," *Journal of Physical Chemistry B*, vol. 111, no. 9, pp. 2152–2165, 2007.
- [13] S. S. Dukhin, "Electrokinetic phenomena of the second kind and their applications," *Advances in Colloid and Interface Science*, vol. 35, no. C, pp. 173–196, 1991.
- [14] N. A. Mishchuk and P. V. Takhistov, "Electroosmosis of the second kind," *Colloids and Surfaces A*, vol. 95, no. 2–3, pp. 119–131, 1995.
- [15] N. A. Mishchuk, "Concentration polarization of interface and non-linear electrokinetic phenomena," *Advances in Colloid and Interface Science*, vol. 160, no. 1–2, pp. 16–39, 2010.
- [16] S. S. Dukhin and N. A. Mishchuk, "Intensification of electrodialysis based on electroosmosis of the second kind," *Journal of Membrane Science*, vol. 79, no. 2–3, pp. 199–210, 1993.
- [17] S. J. Kim, S. H. Ko, K. H. Kang, and J. Han, "Direct seawater desalination by ion concentration polarization," *Nature Nanotechnology*, vol. 5, no. 4, pp. 297–301, 2010.
- [18] E. D. Belashova, N. A. Melnik, N. D. Pismenskaya et al., "Overlimiting mass transfer through cation-exchange membranes modified by NAFION film and carbon nanotubes," *Electrochimica Acta*, vol. 59, pp. 412–423, 2012.
- [19] N. D. Pismenskaya, V. V. Nikonenko, N. A. Melnik et al., "Evolution with time of hydrophobicity and microrelief of a cation-exchange membrane surface and its impact on overlimiting mass transfer," *The Journal of Physical Chemistry B*, vol. 116, no. 7, pp. 2145–2161, 2012.
- [20] M. Z. Bazant and O. I. Vinogradova, "Tensorial hydrodynamic slip," *Journal of Fluid Mechanics*, vol. 613, pp. 125–134, 2008.
- [21] N. D. Pismenskaya, E. I. Belova, V. V. Nikonenko et al., "Lower rate of $H^+(OH^-)$ ions generation at an anion-exchange membrane in electrodialysis," *Desalination and Water Treatment*, vol. 21, no. 1–3, pp. 109–114, 2010.
- [22] E. I. Belova, G. Y. Lopatkova, N. D. Pismenskaya, V. V. Nikonenko, C. Larchet, and G. Pourcelly, "Effect of anion-exchange membrane surface properties on mechanisms of overlimiting mass transfer," *Journal of Physical Chemistry B*, vol. 110, no. 27, pp. 13458–13469, 2006.
- [23] G. Z. Nefedova, Z. V. Klimov, G. S. Sapozhnikov, and Katalog, "Ionitovye membrany" (Russian), M: NIITEKhim, 1977.
- [24] R. Simons, "Electric field effects on proton transfer between ionizable groups and water in ion exchange membranes," *Electrochimica Acta*, vol. 29, no. 2, pp. 151–158, 1984.
- [25] V. I. Zabolotsky, N. V. Sheldeshov, and N. P. Gnusin, "Dissociation of water molecules in systems with ion-exchange membranes," *Russian Chemical Reviews*, vol. 57, pp. 801–808, 1988.
- [26] N. D. Pismenskaya, Y. A. Fedotov, V. V. Nikonenko et al., Patent 2008141949 Russian Federation, B 01D71/60 (2006.01), B01D7/06 (2006.01). Method of ion exchange membrane preparation, Filing date 22.10.2008, Issue date 27.04.2010.
- [27] N. P. Berezina, S. V. Timofeev, and N. A. Kononenko, "Effect of conditioning techniques of perfluorinated sulphocationic membranes on their hydrophylic and electrotransport properties," *Journal of Membrane Science*, vol. 209, no. 2, pp. 509–518, 2002.
- [28] N. P. Berezina, N. A. Kononenko, O. A. Dyomina, and N. P. Gnusin, "Characterization of ion-exchange membrane materials: properties vs structure," *Advances in Colloid and Interface Science*, vol. 139, no. 1–2, pp. 3–28, 2008.
- [29] E. V. Laktionov, N. D. Pismenskaya, V. V. Nikonenko, and V. I. Zabolotsky, "Method of electrodialysis stack testing with the feed solution concentration regulation," *Desalination*, vol. 151, no. 2, pp. 101–116, 2003.
- [30] V. V. Nikonenko, N. D. Pismenskaya, A. G. Istoshin, V. I. Zabolotsky, and A. A. Shudrenko, "Description of mass transfer characteristics of ED and EDI apparatuses by using the similarity theory and compartmentation method," *Chemical Engineering and Processing: Process Intensification*, vol. 47, no. 7, pp. 1118–1127, 2008.
- [31] N. V. Sheldeshov, V. V. Ganych, and V. I. Zabolotskii, "Transport number of salt ions and water dissociation products in cation and anion-exchange membranes," *Soviet Electrochemistry*, vol. 23, pp. 11–15, 1991.
- [32] N. P. Gnusin, N. P. Berezina, N. A. Kononenko, and O. A. Dyomina, "Transport structural parameters to characterize ion exchange membranes," *Journal of Membrane Science*, vol. 243, no. 1–2, pp. 301–310, 2004.
- [33] V. I. Zabolotsky and V. V. Nikonenko, "Effect of structural membrane inhomogeneity on transport properties," *Journal of Membrane Science*, vol. 79, no. 2–3, pp. 181–198, 1993.
- [34] V. V. Nikonenko, N. D. Pismenskaya, and E. I. Volodina, "Rate of generation of ions H^+ and OH^- at the ion-exchange membrane/dilute solution interface as a function of the current density," *Russian Journal of Electrochemistry*, vol. 41, no. 11, pp. 1205–1210, 2005.
- [35] I. Rubinstein and B. Zaltzman, "Extended space charge in concentration polarization," *Advances in Colloid and Interface Science*, vol. 159, no. 2, pp. 117–129, 2010.
- [36] M. A.-K. Urtenov, E. V. Kirillova, N. M. Seidova, and V. V. Nikonenko, "Decoupling of the Nernst-Planck and Poisson equations. Application to a membrane system at overlimiting currents," *Journal of Physical Chemistry B*, vol. 111, no. 51, pp. 14208–14222, 2007.

- [37] K. S. Spiegler, "Transport processes in ionic membranes," *Transactions of the Faraday Society*, vol. 54, pp. 1408–1428, 1958.
- [38] A. M. Peers, "Membrane phenomena," *Discussions of the Faraday Society*, vol. 21, pp. 124–125, 1956.
- [39] F. G. Helfferich, *Ion Exchange*, McGraw-Hill, New York, NY, USA, 1962.
- [40] J. S. Newman, *Electrochemical Systems*, Prentice Englewood Cliffs, New York, NY, USA, 1973.
- [41] M. A. L  v  que, *Les Lois de la Transmission de Chaleur par Convection*, vol. 12-13 of *Annales des Mines, Memoires*, 1928.
- [42] R. A. Robinson and R. H. Stokes, *Electrolyte Solutions*, Butterworths, London, UK, 1968.
- [43] V. I. Zabolotsky, V. V. Nikonenko, N. D. Pismenskaya et al., "Coupled transport phenomena in overlimiting current electrodialysis," *Separation and Purification Technology*, vol. 14, no. 1–3, pp. 255–267, 1998.
- [44] J. H. Choi, H. J. Lee, and S. H. Moon, "Effects of electrolytes on the transport phenomena in a cation-exchange membrane," *Journal of Colloid and Interface Science*, vol. 238, no. 1, pp. 188–195, 2001.
- [45] Y. Tanaka, "Water dissociation reaction generated in an ion exchange membrane," *Journal of Membrane Science*, vol. 350, no. 1-2, pp. 347–360, 2010.
- [46] S. Maf  , P. Ram  rez, and A. Alcaraz, "Electric field-assisted proton transfer and water dissociation at the junction of a fixed-charge bipolar membrane," *Chemical Physics Letters*, vol. 294, no. 4-5, pp. 406–412, 1998.

Research Article

Reactivity of Phenol Allylation Using Phase-Transfer Catalysis in Ion-Exchange Membrane Reactor

Ho Shing Wu and Yeng Shing Fu

Department of Chemical Engineering and Materials Science, Yuan Ze University, Zhongli, Taiwan

Correspondence should be addressed to Ho Shing Wu, cehswu@saturn.yzu.edu.tw

Received 16 February 2012; Revised 16 May 2012; Accepted 17 May 2012

Academic Editor: Victor V. Nikonenko

Copyright © 2012 H. S. Wu and Y. S. Fu. This is an open access article distributed under the Creative Commons Attribution License, which permits unrestricted use, distribution, and reproduction in any medium, provided the original work is properly cited.

This study investigates the reactivity of phenol allylation using quaternary ammonium salt as a phase-transfer catalyst in three types of membrane reactors. Optimum reactivity and turnover of phenol allylation were obtained using a response surface methodology. The contact angle, water content, and degree of crosslinkage were measured to understand the microenvironment in the ion exchange membrane.

1. Introduction

Phase-transfer catalytic techniques have been used in manufacturing industry synthesis processes, such as insecticidal and chemical production [1–3]. However, a traditional liquid-liquid phase-transfer catalytic reaction has many disadvantages, because separating the catalyst and purifying the reaction system are difficult. Hence, the liquid-solid-liquid phase-transfer catalyst technique was developed. Although this type of catalyst is easy to use and recover from a solution, the reactant pore diffusion in the catalyst affects the reaction and decreases the reaction rate. A catalyst immobilized in an ion exchange membrane could solve these problems.

When a catalyst is immobilized in an inert membrane pore, the catalytic reactivity and separation functions are engineered in a complex system. The membrane technique offers advantages of (i) separating the catalyst from the reaction solution, (ii) maintaining phase separation to minimize the potential of emulsions forming, and (iii) a high surface area per unit volume of the reactor. Furthermore, Zaspalis et al. [4] reported that a reaction using a membrane catalyst could be 10 times more active than a pellet catalyst reaction. Yadav and Mehta [5] presented a theoretical and experimental analysis of capsule membrane phase-transfer catalysis for the alkaline hydrolysis of benzyl chloride to benzyl alcohol. Okahata and Ariga [6] examined the reaction

of sodium azide with benzyl bromide in the presence of a capsule membrane with pendant quaternary ammonium groups and polyethylene glycol groups on the outside. A capsule membrane is unsuited to mass industrial production because of the inconvenience of working with capsules.

Various methods of preparing ion-exchange membranes for different purposes have been proposed and practiced by industry. One of these methods is copolymerizing divinylbenzene and other vinyl monomers (e.g., styrene, chloromethylstyrene, and vinylpyridine) into a membranous copolymer using the paste method and then introducing ion-exchange groups into the copolymer [7–9]. The polymer solution (which contains polymers with ion-exchange groups and other polymers) is then cast on a flat plate to remove the solvent [10, 11]. Most commercial anion-exchange membranes contain benzyl trimethylammonium or *N*-alkyl pyridinium groups as anion-exchange groups and are cross-linked with divinylbenzene. The membrane backbone polymer is hydrophobic because of aromatic or heterocyclic groups and the active ion-exchange group is hydrophilic. A study [12, 13] that used commercially and laboratory-produced membranes as phase-transfer catalysts in the allylation of phenol showed that the reactivity of quaternary ammonium catalysts in the ion-exchange membrane was lower than that of general phase-transfer catalysts because the ion-exchange group was hydrophilic. The types

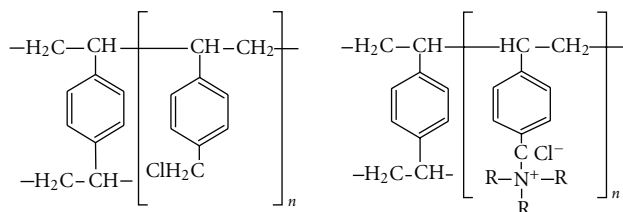


FIGURE 1: The structure of the base membrane and anion exchange membrane.

of ion-exchange groups were hydrophobic and hydrophilic to test the reactivity of phenol allylation. This study presents a discussion on the reactor design problem in a membrane reactor in a two-phase system and examines the relationship between the reactivity of phenol allylation and the membrane reactor. This study also uses membrane properties and the transfer of phenolate ions in the membrane to research the reactivity of quaternary ammonium catalysts in the membrane.

2. Experimental Section

2.1. Materials. Allyl bromide (Fluka, 99.5%), phenol (RDH, 99%), chloromethylstyrene (Aldrich, 97%), and allyl phenyl ether (PhOR, Aldrich, 99%) were provided by the indicated suppliers. Anion-exchange membrane A-172 (a polymer of 1-methyl-4-vinyl-pyridinium crosslinked with 1,4-divinylbenzene) was purchased from ASAHI CHEM Ind. Co. Ltd. (Japan). The characteristics of the A-172 membrane were thickness 0.12–0.15 mm; ion-exchange capacity 1.8–1.9 meq/g of dry membrane; water content 24%–25%; electrical resistance 1.7–20 Ω/cm^2 ; character: monoanion permselectivity membrane; reinforcement PP fabric.

3. Preparation of Anion Exchange Membrane

The preparation procedure was identical to that described by H. S. Wu and Y. K. Wu (2005) [13]. Four types of anion exchange membranes with different amine functional groups (trimethylamine (TMA), triethylamine (TEA), tri-*n*-propylamine (TPA), and tri-*n*-butylamine (TBA) were prepared by a reaction of a membranous copolymer composed of chloromethylstyrene (CMS type) and divinylbenzene with various tertiary amines (TMA, TEA, TPA, and TBA). Figure 1 shows the structure of the base membrane and anion exchange membrane. H. S. Wu and Y. K. Wu [13] described the synthesis of the base membrane and the process of immobilizing amine in the base membrane.

4. Water Content in the Membrane

The membrane was washed with deionized water and then immersed in deionized water for 60 min. This process was completed twice. The wet membrane was weighed after removing its surface moisture. This process was conducted at least three times to obtain accuracy within 5%. The dry membrane was weighed after drying at 60°C. Water content

was calculated using $W_C(\%) = (W_W - W)/W_W \times 100$, where W_C , W_W , and W are water content in the membrane, weight of the wet membrane after wiping, and weight of the dry membrane, respectively.

5. Kinetics of Phenol Allylation in a Membrane Reactor

Figure 2 shows the experiment apparatus of a membrane reactor. An external circulatory bath was the membrane reactor thermostat to maintain isothermal conditions. An aqueous solution (55 cm^3) of sodium hydroxide (0.00334 mol) and phenol (0.002 mol) was prepared and introduced into the membrane reactor, which was set at the desired temperature. Quantities of allyl bromide (0.03 mol), dichloroethane (55 cm^3), and diphenyl ether (internal standard) were prepared and set to the desired temperature and then introduced into the reactor. The interfacial area between the two phases was $6.0 \times 10^{-4} \text{ m}^2$. The reaction temperature was 45–65°C. The reaction rate did not decrease below 5% after repeating four reaction runs.

For a kinetic run, a sample was withdrawn from the reaction solution at selected time intervals. The sample (0.1 cm^3) was immediately added to dichloroethane (0.3 cm^3) to quench the reaction. The organic phase content was then quantitatively analyzed with a high-performance liquid chromatograph using the internal standard method. The accuracy of these analytical techniques was within 2%–3% and the data were correctly reproduced within 5% of the values reported by this study. Liquid chromatography was conducted with a Shimadzu LC-SPD-10A instrument using a column packed with Phenomenex C12 (150 \times 4.6 mm, SYNERGI 4u MAX-RP 80A, USA). The eluant was $\text{CH}_3\text{OH}/\text{H}_2\text{O} = 3/1$ with a flow rate of 1.0 $\text{cm}^3 \text{ min}^{-1}$ monitored at 254 nm (UV detector).

6. Measurement of Contact Angle

Numerous types of membranes (the A172 membrane and laboratory-produced membranes) can be used to measure contact angles. A syringe needle was used to draw solvents and then the syringe was squeezed five times until it was clean. Solvents were drawn into the syringe needle without bubbles. Membranes were placed on a table with a flat surface and the syringe needle was placed on the apparatus. One drop was dropped onto the membrane until the shape of the drop did not change. The contact angle was recorded. Measurements were taken three times.

7. Results and Discussion

Phase-transfer catalysis is a useful tool in organic synthesis and has many applications in commercial processes. However, it cannot separate a product from its catalyst. Hence, liquid-solid-liquid phase-transfer catalysis was developed to immobilize the quaternary ammonium group onto the resin and membrane [12–15]. Wu and Wang [14] proposed two

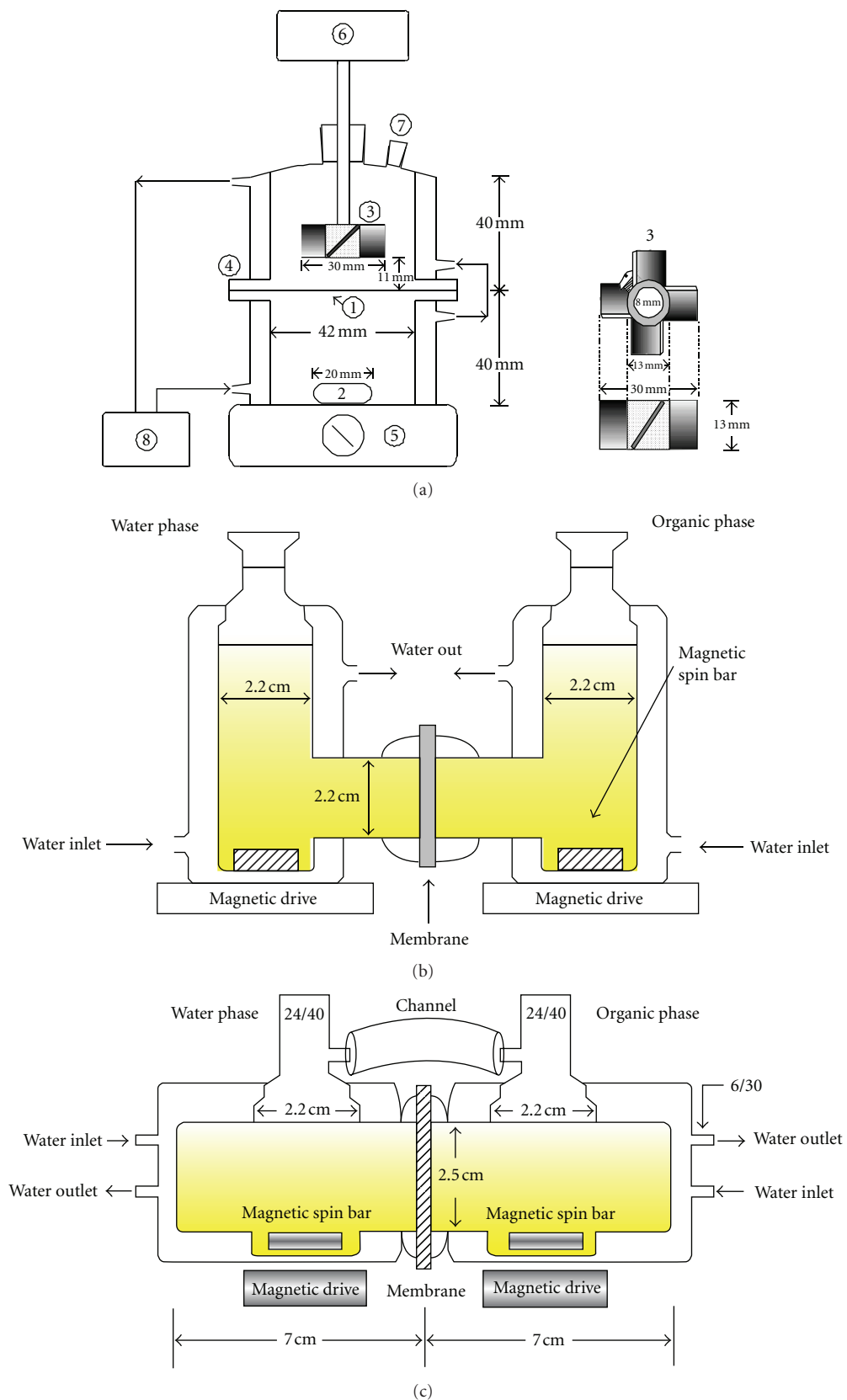


FIGURE 2: Schematic of (a) membrane reactor V1: membrane, 2; Teflon stir bar, 3; stainless stirrer, 4; membrane reactor, 5; magnetic stirrer, 6; mechanical stirrer, 7; sampling point, 8; cooling circulator bath [12]. (b) Membrane reactor H1. (c) Membrane reactor H2.

TABLE 1: Advantages and disadvantages of three reactors.

	V1 reactor	H1 reactor	H2 reactor
Diameter of membrane (cm)	6.2	2.2	2.5
Area of membrane (m ²)	$3.02 \cdot 10^{-3}$	$3.8 \cdot 10^{-4}$	$4.91 \cdot 10^{-4}$
Working volume (cm ³)	55	35	35
Activation energy (kcal/mole)	12.11	13.12	11.69
Turnover number (s ⁻¹)	$1.53 \cdot 10^{-3}$	$2.58 \cdot 10^{-3}$	$2.74 \cdot 10^{-3}$
Recovery rate of phenol in 90 min (ppm/(min m ²))	13794	45263	38452
Pressure drop	△	△	○
Gravity	×	△	○
Area of membrane	×	○	○
Apparatus	△	○	○
Cost	△	○	○
Operating difficulty	△	○	○
Reactivity	×	○	○

○ good, △ fair, × poor.

reactors: the slurry reactor and fixed-bed reactor using quaternary ammonium poly(styrene-co-chloromethylstyrene) resin, to evaluate a liquid-solid-liquid triphase reaction. However, the catalyst was always suspended in the solution and could flow out of the reactor during a reaction. Hence, developing a method to secure the catalyst on the reactor bed is crucial to improve product and catalyst separation. A membrane reactor could solve these problems, but some design issues must be addressed to improve reaction rates.

8. Membrane Reactor Design Problems

Previous research [13] reported that the organic solution leaked into the aqueous solution during a reaction because gravity reduced the reactivity of the active site on the membrane in the vertical membrane reactor. Hence, the vertical membrane reactor was replaced with a horizontal membrane reactor to avoid the gravity problem, to test the reactivity of phenol allylation. The leaking phenomenon decreased in the horizontal membrane reactor. Wu and Lo [12] and H. S. Wu and Y. K. Wu [13] used the design shown in Figure 2(a). The reactor (V1) was used to recover phenol from simulated wastewater. The reaction system was prepared by pouring the aqueous solution into the bottom cell, covering the anion exchange membrane and locking the reactor. The organic solution was introduced into the top cell, starting the reaction.

Some engineering problems must be overcome in this system and the membrane structure is an important factor. Before the experiment, some bubbles may appear in the aqueous solution during the preparation step. This could influence the mass transfer of aqueous reactant from the bulk solution to the membrane. If the boiling points of both solvents (1-2 dichloroethane and water) are different, there is a large pressure drop between two cells, which forces the solution to pass through the membrane into the other phase because the membrane reactor is a closed system. If the density of the solution in the top cell is larger than in the other cells, gravity is also a problem. Gravity could

force the top solution to pass through the membrane into the bottom phase. Hence, gravity, pressure, membrane, and bubbles influence reactivity in the reactor type, as shown in Figure 2(a). The sample was also only drawn from the top cell and not from the bottom cell.

H. S. Wu and Y. K. Wu [13] proposed that the membrane reactor (H1) design shown in Figure 2(b) could solve these problems and produce better reactivity than membrane reactor V1. Moreover, the sample was simultaneously drawn from two phases in reactor H1, but from only one point in the top cell in membrane reactor V1, as shown in Figure 2(a). Reactor H1 has some disadvantages; for example, the solution is higher than the height of the membrane and the density of 1-2 dichloroethane is more than that of water. Although the gravity effect was less than in reactor V1, the organic phase still passes through the membrane during the long reaction time. Reactor H1 used a closed system for each cell; therefore, the pressure drop between two cells was large, which could be problematic.

Reactor H2 in Figure 2(c) was designed to compensate for these problems. The height of the solution was equal to that of the membrane and there was a channel tube between both phases, solving the effects of gravity and pressure. Table 1 shows the advantages and disadvantages of the three membrane reactors.

9. Optimal Reactivity in Reactors H1 and H2 Using Response Surface Methodology

Increasing the concentration of the organic reactant (allyl-bromide) increases the reaction rate. In this case, increasing the concentration of organic reactants could also increase the mass transfer rate of the organic reactant because the mass transfer of the organic reactant from the organic phase to the membrane phase was slow. However, increasing aqueous reactant concentrations (phenol) could decrease the reaction rate. An increase in the concentration of aqueous reactants allows aqueous reactants to block the

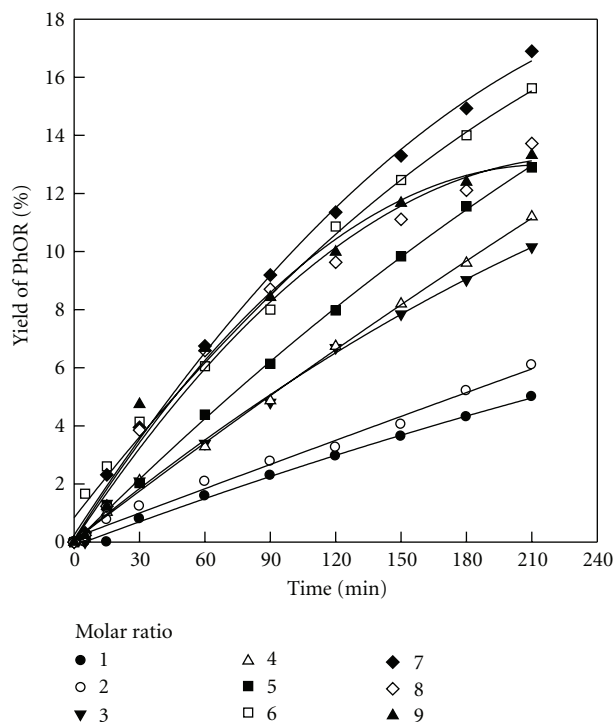


FIGURE 3: Effect of molar ratio of allylbromide to PhONa. $T = 50^{\circ}\text{C}$, agitation = 400 rpm. Aqueous phase (35 cm^3): deionized water, phenol = 0.011 mol, NaOH = 0.018 mole. Organic phase (35 cm^3): 1,2- $\text{C}_2\text{H}_4\text{Cl}_2$, membrane reactor H1, membrane = A172.

membrane, decreasing the mass transfer rate [12]. Hence, the reaction mechanism in a liquid-liquid membrane phase-transfer catalyzed reaction is different from that in a liquid-liquid phase-transfer catalyzed reaction. This study used the Respond Surface Methodology (RSM) [16–18] to investigate the reactivity of phenol allylation in H1 and H2 reactors.

The molar ratio of organic reactant (allylbromide) to aqueous reactant (phenol) was generally an important factor. The reaction rate increased in conjunction with the molar ratio of allylbromide to phenol. Molar ratios between 1 and 9 were tested in this system. After testing, the best molar ratio (7) was used in the next step. The result is shown in Figure 3. Organic and aqueous reactant concentrations affected the reaction rate. Previously, researchers wanting to obtain optimum conditions in traditional reaction kinetics used experimental runs, which increased the number of runs. This method was time consuming and expensive. This study used RSM to test different concentrations to examine the relationship between organic and aqueous reactant concentrations. The best molar ratio of organic to aqueous reactant concentrations was found and this ratio was used in the steepest ascent path method. After the experiment design, reaction rates were calculated to obtain (9).

$$R = 2.47 \times 10^{-4} + 3.8 \times 10^{-5} [\text{Phenol}] + 1.18 \times 10^{-4} [\text{Allylbromide}]$$

$$\begin{aligned} & -8 \times 10^{-5} [\text{Phenol}]^2 \\ & -3.51 \times 10^{-3} [\text{Allylbromide}]^2, \end{aligned} \quad (1)$$

where R is the reaction rate ($\text{mol}/(\text{m}^2 \cdot \text{s})$). The respond surface of the reaction in reactor H1 is shown in Figure 4(a).

The turnover number is the number of substrate molecules converted to produce by one molecule of catalyst per unit of time when the reaction rate is maximal and the substrate is saturated. That is, the turnover number (s^{-1}) is the maximal mole of substrate consumed per catalyst per time. The turnover number is calculated using

$$\text{Turnover Number} = \frac{R}{M_c}, \quad (2)$$

where M_c is the amount of the catalyst per area (mol/m^2). Based on previous research, the yield of allyl phenyl ether increased when the excess organic concentration increased. Figure 4(a) shows that after calculation, the optimal reaction rate was $8.54 \times 10^{-4} \text{ mol}/\text{s} \cdot \text{m}^2$ when phenol and allylbromide were $7.41 \times 10^{-3} \text{ mol}$ and 0.106 mol , respectively. The average membrane weight was 0.086 g and the ion-exchange capacity was $1.6 \text{ mmol}/\text{g}$; therefore, the mole of the catalyst was $1.22 \times 10^{-4} \text{ mol}$. The turnover number was $2.58 \times 10^{-3} \text{ s}^{-1}$ at 328 K . Previous researchers [12] found a turnover number of $1.53 \times 10^{-3} \text{ s}^{-1}$ in reactor V1, as shown in Figure 2(a). This value was smaller than that of reactor H1.

Table 1 shows the similar optimal reactivity of reactor H2. The optimal reaction rate and turnover number for reactor H2 are larger than those for reactor H1. Figure 4 shows that the operating concentration of allylbromide or phenol in reactor H2 is also larger than those for reactor H1. Therefore, reactor H2 performs better than reactor H1.

10. Effect of Membrane Structure

Wu and Lo [12] showed that the reaction rate increased with an increasing molar ratio of allylbromide to phenol. Figure 5 shows that the allyl phenyl ether yield varies with different types of membranes. To determine what occurred in the reaction, different membrane types were tested to measure contact angles. This is shown in Figures 6 and 7.

The dry A172 membrane and laboratory-produced base membranes were polymeric membranes. Generally, the polymer membranes were hydrophobic. The contact angles of the dry A172 membrane and laboratory-produced base membranes decreased with an increasing concentration of phenol in the aqueous solution. The contact angles for the dry A172 membrane in aqueous or organic solvents were larger than those for the laboratory-produced base membranes. This could indicate that the interaction between solvents and the membrane of the laboratory-produced membranes was larger than the interaction of the A172 membrane. The reaction rate for laboratory-produced membranes could be higher than for the A172 membrane. For wet membranes, the contact angles were zero because the solvent drops were drawn into the membrane.

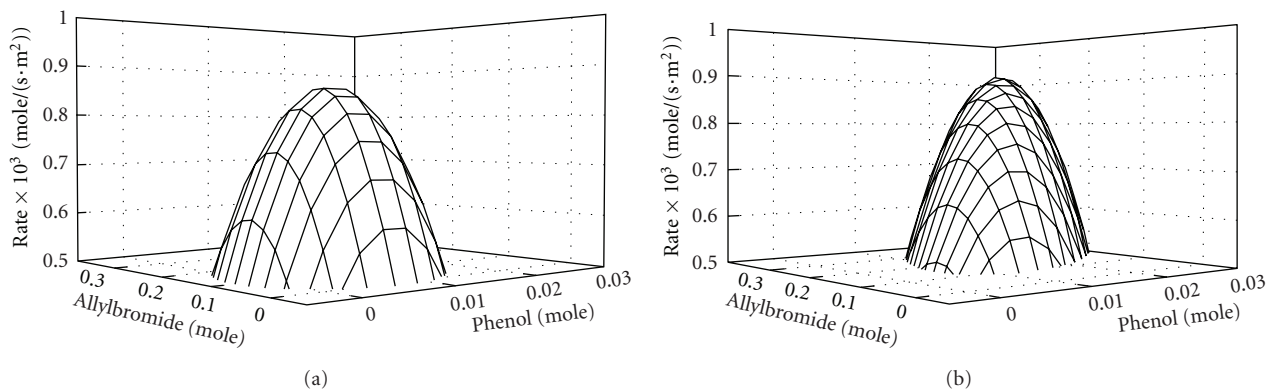


FIGURE 4: Respond surface of reaction in membrane reactors (a) H1 and (b) H2.

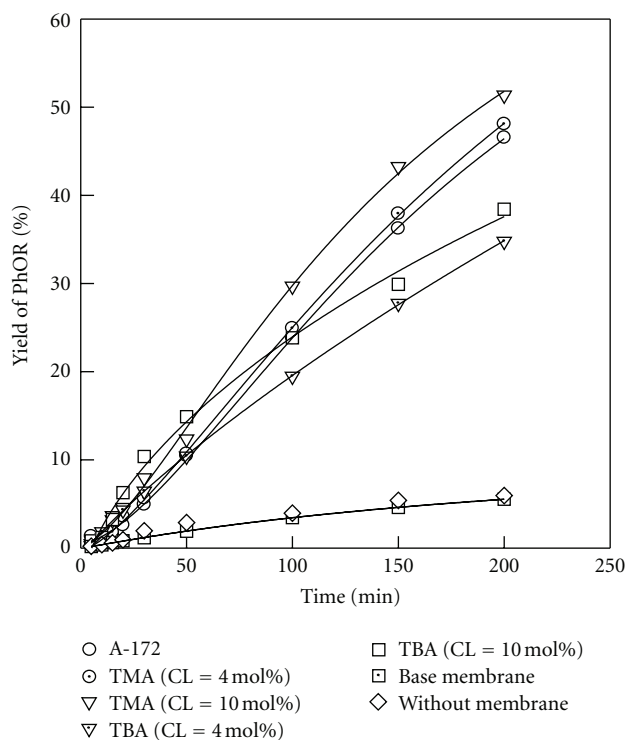
FIGURE 5: PhOR yield from various membranes with an excess of organic reactant. 45°C, 400 rpm. Aqueous phase (55 cm³): 0.004 mol of phenol, NaOH = 0.0064 mol. Organic phase (55 cm³): 1,2-C₂H₄Cl₂, 0.06 mol of C₃H₅Br. Data quoted from Wu and Lo [12].

Figure 8 shows that the water content decreased with increasing crosslinkage when the ion-exchange capacity did not change. Because the physical strength of the membrane increased with crosslinkage, it was difficult for water to exist in the membrane, and the swelling decreased.

The aqueous ion-exchange reaction of phenolate ion (PhO⁻) and bromide ion (Br⁻) is shown by

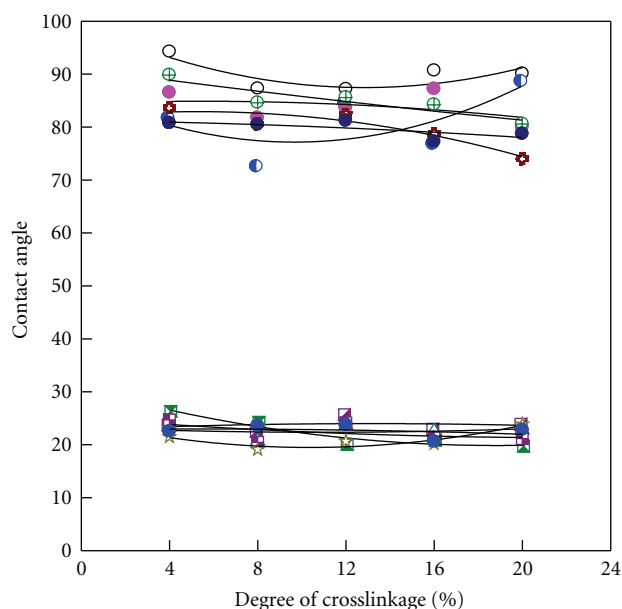
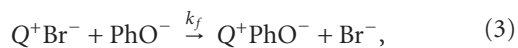


FIGURE 6: Contact angles of laboratory-produced base membranes with different degrees of crosslinkage with different concentrations of phenol and molar ratios of allylbromide to phenol.

where Q⁺ is a phase-transfer catalyst. The reaction expression is:

$$r = -\frac{d[PhO^-]}{dt} = k_f[PhO^-][Q^+Br^-]. \quad (4)$$

The k_f value was calculated from the slope in Figure 9 (upper panel) using the initial reaction rate method. The reaction rate has an optimal value. k_f decreased with increasing initial amounts of PhONa. This verifies that increasing concentrations of aqueous reactant does not increase the reaction rate, as shown in Figure 9 (lower panel). Therefore, the contact angle, water content, and ion exchange of

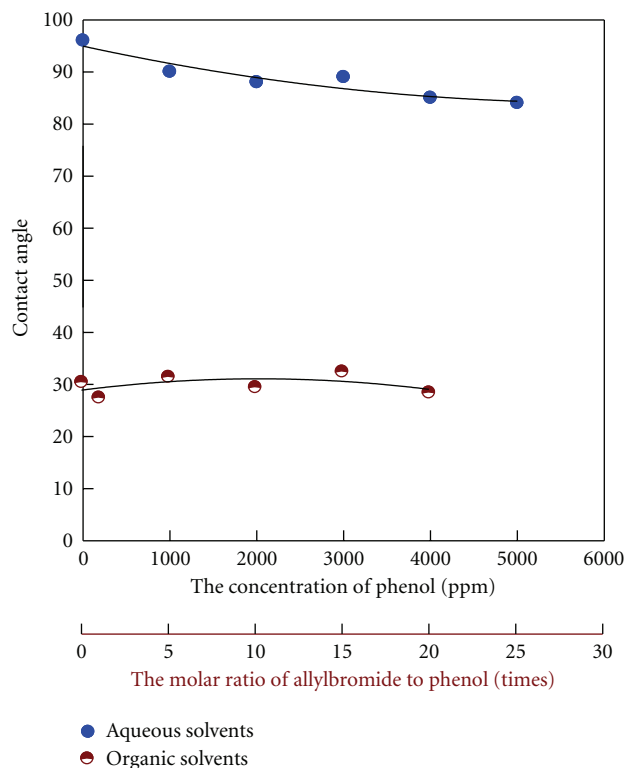


FIGURE 7: Contact angles of dry A172 membrane with different concentrations of phenol and molar ratios of allylbromide to phenol.

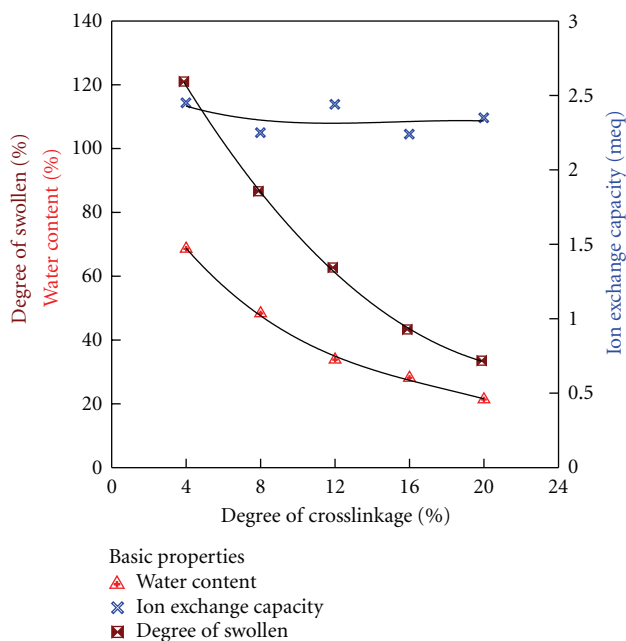


FIGURE 8: Effects of degree of crosslinkage on swelling, water content, and ion exchange capacity of a tetra-methylamine membrane.

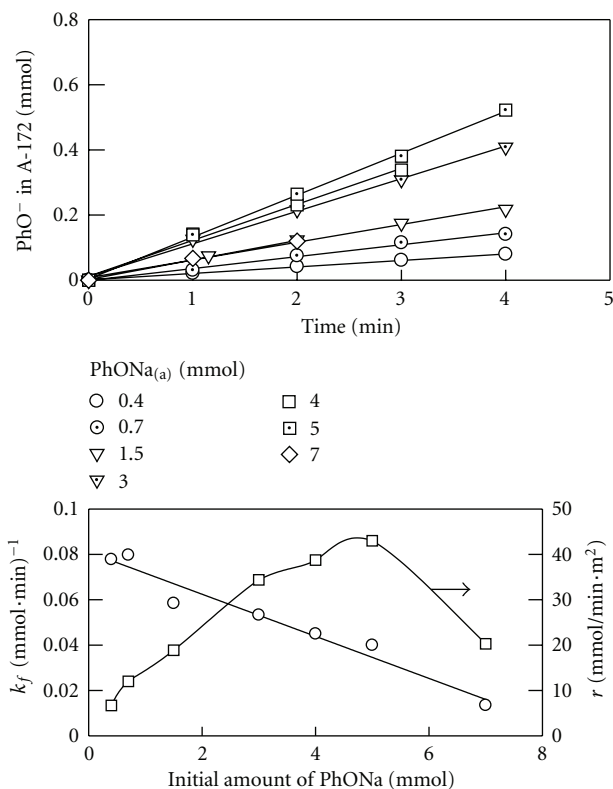


FIGURE 9: PhO^- in A172 versus time and the effect of PhONa on the forward ion-exchange rate. 65°C , 400 rpm, 30.2 cm^2 of A-172 membrane, aqueous phase 55 cm^3 .

phenolate ions with bromide in the membrane are essential for applying this membrane technique to phase-transfer catalysis.

11. Conclusion

Gravity and pressure are important factors in reactor design. The catalytic reactivity in the H2 reactor design was better than in the V1 reactor. The RSM could be used to obtain the optimal turnover number and reaction rate to verify the reactivity of a catalyst in a membrane. For phase-transfer catalytic membrane systems to perform well, the membrane structure for reactants and solvents must be studied to obtain optimal conditions.

Acknowledgment

We would like to thank the National Science Council of Taiwan for financially supporting this research under Grant nos. NSC 94-2214-E155-004 and 95-2214-E155-006.

References

- [1] V. V. Dehmlo and S. S. Dehmlo, *Phase Transfer Catalysis*, Chemie, Weinheim, Germany, 1993.
- [2] C. M. Starks, C. L. Liotta, and M. Halpern, *Phase-Transfer Catalysis, Fundamentals, Applications, and Industrial Perspectives*, Chapman & Hall, New York, NY, USA, 1994.

- [3] H. M. Yang and H. S. Wu, "Interfacial mechanism and kinetics of phase-transfer catalysis," in *Interfacial Catalysis*, A. G. Volkov, Ed., vol. 285, chapter 11, Marcel Dekker, 2003.
- [4] V. T. Zaspalis, W. Van Praag, K. Keizer, J. G. Van Ommen, J. R. H. Ross, and A. J. Burggraaf, "Reactions of methanol over catalytically active alumina membranes," *Applied Catalysis*, vol. 74, no. 2, pp. 205–222, 1991.
- [5] G. D. Yadav and P. H. Mehta, "Theoretical and experimental analysis of capsule membrane phase transfer catalysis: selective alkaline hydrolysis of benzyl chloride to benzyl alcohol," *Catalysis Letters*, vol. 21, no. 3–4, pp. 391–403, 1993.
- [6] Y. Okahata and K. J. Ariga, "Functional capsule membranes. 27. A new type of phase-transfer catalysts (PTC). Reaction of substrates in the inner organic phase with the outer aqueous anions catalyzed by PTC grafted on the capsule," *Journal of Organic Chemistry*, vol. 51, p. 5064, 1986.
- [7] Y. Mizutani, R. Yamane, H. Ihara, and H. Motomura, "Studies of Ion Exchange Membranes. XVI. The preparation of ion exchange membranes by the "Paste Method"," *Bulletin of The Chemical Society of Japan*, pp. 361–366, 1963.
- [8] Y. Mizutani, R. Yamane, and H. Motomura, "Studies of Ion Exchange Membranes. XXII. Semicontinuous preparation of ion exchange membrane by the paste method," *Bulletin of The Chemical Society of Japan*, pp. 689–694, 1964.
- [9] Y. Mizutani, "Studies of Ion Exchange Membranes. The tetrahydrofuran extraction of the ion-exchange membrane and its base membrane prepared by the "Paste Method"," *Bulletin of The Chemical Society of Japan*, vol. 42, no. 1969, pp. 2459–2463, 1969.
- [10] H. P. Gregor, H. Jacobson, R. C. Shair, and D. M. Wetstone, "Interpolymer ion-selective membranes. I. Preparation and characterization of polystyrenesulfonic acid-dynel membranes," *Journal of Physical Chemistry*, vol. 61, p. 141, 1957.
- [11] P. Zschocke and D. Quellmatz, "Novel ion exchange membranes based on an aromatic polyethersulfone," *Journal of Membrane Science*, vol. 22, pp. 325–332, 1985.
- [12] S. Wu and M. H. Lo, "Modeling and kinetics of allylation of phenol in a triphase-catalytic membrane reactor," *American Institute of Chemical Engineers*, vol. 51, pp. 960–970, 2005.
- [13] H. S. Wu and Y. K. Wu, "Preliminary study on the characterization and preparation of quaternary ammonium membrane," *Industrial & Engineering Chemistry Research*, vol. 44, p. 1757, 2005.
- [14] H. S. Wu and C. S. Wang, "Liquid—solid—liquid phase-transfer catalysis in sequential phosphazene reaction: kinetic investigation and reactor design," *Chemical Engineering Science*, vol. 58, no. 15, pp. 3523–3534, 2003.
- [15] H. S. Wu, "Catalytic activity and kinetics of liquid—solid—liquid phase-transfer catalysts," in *New Developments in Catalysis Research*, L. P. Bevy, Ed., chapter 1, pp. 1–38, Nova Science Publishers, 2005.
- [16] G. E. P. Box and J. S. Hunter, "Multi-factor experimental designs for exploring response surfaces," *Annals of Mathematical Statistics*, vol. 28, p. 195, 1957.
- [17] G. E. P. Box and K. B. J. R. Wilson, "On the experimental attainment of optimum conditions," *Journal of the Royal Statistical Society B*, vol. 13, p. 1, 1951.
- [18] J. J. Cilliers, R. C. Austin, and J. P. Tucker, "An evaluation of formal experimental design procedures for hydrocyclone modelling," in *Proceeding of the 4th International Conference of Hydrocyclones*, L. Svarovsky and M. T. Thew, Ed., pp. 31–49, Kluwer Academic Publishers, Southampton, UK, 1992.

Research Article

Performance of a 1 kW Class Nafion-PTFE Composite Membrane Fuel Cell Stack

Pattabiraman Krishnamurthy, Ramya Krishnan, and Dhathathreyan Kaveripatnam Samban

Centre For Fuel Cell Technology, ARC-International, IIT M Research Park, Phase I, 2nd Floor, No. 6, Kanagam Road, Taramani, Chennai 600113, India

Correspondence should be addressed to Ramya Krishnan, ramya.k.krishnan@gmail.com

Received 29 February 2012; Revised 16 May 2012; Accepted 19 May 2012

Academic Editor: Yoshinobu Tanaka

Copyright © 2012 Pattabiraman Krishnamurthy et al. This is an open access article distributed under the Creative Commons Attribution License, which permits unrestricted use, distribution, and reproduction in any medium, provided the original work is properly cited.

Composite membranes have been prepared by impregnation of Nafion into the expanded polytetrafluoroethylene (EPTFE) matrix. Nafion loading in the composite membranes was kept constant at 2 mg/cm². The lower amount of electrolyte per unit area in the composite membranes offers cost advantages compared to conventional membrane of 50 μ m thickness with an electrolyte loading of \sim 9 mg/cm². Composite membranes (30 μ m thickness) were found to have higher thermal stability and mechanical strength compared to the conventional membranes (50 μ m thickness). The performance of the membrane electrode assembly made with these composite membranes was comparable to that of the conventional membranes. Single cells fabricated from these MEAs were tested for their performance and durability before scaling them up for large area. The performance of a 20-cell stack of active area 330 cm² fabricated using these membranes is reported.

1. Introduction

Polymer electrolyte membrane fuel cell (PEMFC) presents an attractive alternative to traditional power sources, due to high efficiency and low pollution. The efficiency of the fuel cell vehicle using direct hydrogen fuel cells has been reported to be twice that of the gasoline vehicles [1, 2]. Fuel cell efficiency is high even at partial loads compared to the internal combustion engines, which operate at high efficiency only at full loads. The only emissions in vehicles operating on hydrogen as fuel is water and is hence non-polluting. Fuel cell stacks of sub-kW and 1 kW level find applications as power sources in electronic equipments and as power source in portable applications. A 3 kW fuel cell stack has been projected for applications in the telecommunication sectors as highly reliable and durable on-site power generation technology is required for these applications. Stacks of 5 kW and above are used as power sources in various stationary and vehicular applications. Combined heat and power generation using fuel cells is especially attractive for stationary power generation. Further, these short stacks hybridized with electrical storage devices

(batteries and/or ultra-capacitors) can have several benefits, including capturing regenerative braking energy, enhancing fuel economy, providing a more flexible operating strategy, overcoming fuel cell cold-start and transient shortfalls, and lowering the cost per unit power. In a PEMFC, the proton-conducting membrane is located between the cathode and anode and transports protons from anode to cathode. The membranes for high performance PEM fuel cells have to meet the requirements of low cost, high proton conductivity, good water uptake, low gas permeability (<1 mA/cm² at 60°C) [3], and so forth. Nafion, the widely used polymer electrolyte membrane, is a fast proton-conducting separator and shows excellent performance at low temperatures and high humidities. However, the cost of the membrane is high thus limiting its applications in commercial systems. Other disadvantages include the loss of conductivity at high temperature, decrease in strength in thin sections of the membrane and significant dimensional change on hydration [4, 5]. Composite membranes based on substrate and ionomer offer advantages in terms of cost and strength while retaining similar conductivities. Gore Tex materials are made of porous inert polytetrafluoroethylene filled with ion

exchange polymer (usually Nafion) [6]. The same approach was adopted by another company (Johnson Matthey) using a nonwoven silica substrate [7]. Very thin membranes could be made due to better mechanical properties compensating for the higher intrinsic resistance. The concept of using porous substrate-based composite membranes has been used to prepare a low proton resistance PBI/PTFE composite membrane [8]. Nafion composite membranes with porous Teflon, polypropylene, nylon, and Celgard substrates have been studied and their properties are reported in the literature [9, 10]. The composite membranes based on expanded PTFE has been the subject of study of many researchers and studies on methods to reduce the resistance of the membranes through surface modification of EPTFE [11–13], changes in the solvent solubility parameter [14], addition of additives during membrane fabrication [15] have been investigated.

Present PEMFC fuel cell stacks use conventional commercially available materials. As bipolar plates, membranes and catalysts form the major cost component in a fuel cell, most of the research is carried out on alternative substitutes for these materials. PEMFC stacks are being developed with alternate materials to meet the cost targets set for various transport and stationary applications. PEMFC stacks have been designed, assembled, and tested at the 1 kWe, 5 kWe, and 10 kWe size from a range of materials including uncoated stainless steel (type 904) coated stainless steel (type 316) and coated titanium [16, 17]. Performance of a 1 kW-class PEMFC stack using TiN-coated 316 stainless steel bipolar plates have been reported by Cho et al. [16]. The authors have concluded that TiN-coated stainless steel performed better than bare stainless steel. LF11 Al alloy bipolar plates with gold plating (coated by surface plasma technique) were used to develop 1 kW fuel cell stack [17] to study its properties as these bipolar plates had preferable properties compared to graphite- and gold-coated stainless steel plates. Nafion/SiO₂ composite membrane stack have been developed using sol-gel technique to control the SiO₂ particle size in Nafion NRE 212 membrane [18]. A ten cell stack developed using the composite membrane could be operated at 110°C using 90% glycol solution as the coolant and pure hydrogen and oxygen as the reactant. Bandlamudi et al. [19] have studied the properties of 150 W PBI/H₃PO₄ Gel-Based Polymer Electrolyte Membrane Fuel Cells under the Influence of Reformates. Stacks based on Celtec-P commercial high temperature membranes are also being tested [20]. Bonville et al. [21] have studied the effect of scaling up (from 25 cm² to 300 cm²) on the cell performance and properties using Ionomem corporations composite membrane based on PTFE, Nafion and phosphotungstic acid at 120°C and 35% RH. Based on the performance, the process of scaling up was verified.

Although a number of papers based on composite membranes are available in the literature, papers on fuel cell stack are mainly based on commercial membranes. Composite-membrane-based stack are being developed only by the manufacturers of these membranes. The present paper illustrates a simple method to prepare composite membranes with comparable performance to those reported in the

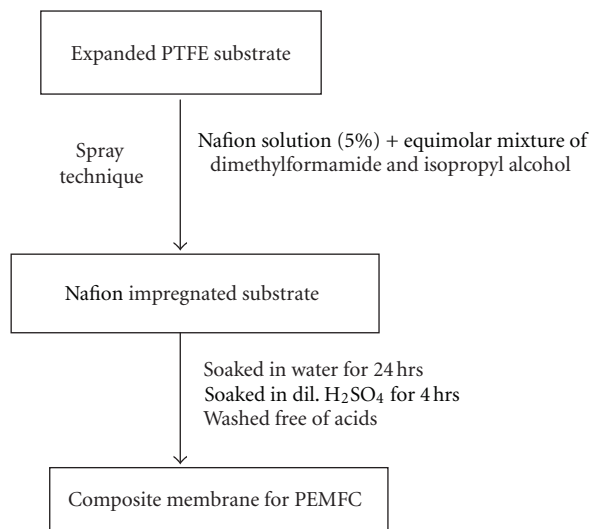


FIGURE 1: Fabrication procedure for composite membranes.

literature that can be easily scaled up to fabricate membranes of large size for development of fuel cell stacks for various applications. The results of the properties of the composite membrane developed using a PTFE matrix and Nafion ionomer and that of the 1 kW stack fabricated using them are presented in the current paper.

2. Experimental

2.1. Preparation of Nafion/EPTFE Composites. Figure 1 gives the general procedure for preparation of the composite membrane. Porous EPTFE was first washed with alcohol and dried in oven and mounted on a frame. The film was soaked in acetone for 30 min before impregnating with ionomer. Nafion solution (5%) obtained from Dupont Co, with an equivalent weight of 1000, was used for impregnating the porous EPTFE film. Nafion solution was mixed with dimethylformamide to make the solution into 2.5% of polymer in the solvent. The Nafion loading in the porous EPTFE film was maintained constant at 2 mg/cm² for all the membranes. Impregnation was carried out in steps to ensure that all the pores of the membrane were fully blocked to avoid gas crossover by spray method. Membranes were pressed at 30 kg/cm² (using a Carver, USA hot press) at 120°C for 3 minutes followed by annealing. The membranes were soaked in water for 24 hrs and then in dilute H₂SO₄ for 4 hrs and washed free of acid before use.

2.2. Characterization of the Composite Membranes. The composite membranes were characterized by IR spectroscopy (Perkin Elmer FTIR), thermogravimetric analysis (Netzsch thermal analyzer model no. STA 449 F1, Germany), dynamic mechanical analysis (Dynamic mechanical analyzer model Q800 by TA instruments, USA.), and conductivity measurement (by Impedance analysis using Solatron Analytical frequency analyzer model 1400 Test system) before fuel cell testing. Gas permeability across the membranes were tested

TABLE 1: Properties of the composite membrane.

S. No	Property	
1	Substrate	Expanded PTFE
2	Substrate pore size	5 μm
3	Substrate porosity	85%
4	Substrate thickness	25 $\mu\text{m} \pm 5$
5	Composite membrane thickness	28 ± 5 μm
6	Composite membrane conductivity	16 mS/cm

by assembling the membrane in a fuel cell set up and passing the gas on one side of the cell. The other inlet is capped and the outlet is dipped into a water reservoir after applying a differential pressure of 1 Kg/cm² on one side. Membranes that did not show any permeability were only used for making MEA. The maximum pressure up to which these membranes were tested was 3 Kg/cm².

The membrane electrode assemblies were made by a proprietary technique developed in our lab using 40% Pt/C (Arora Mathey, India), 5% Nafion Solution (DuPont, USA), and Carbon substrate from Ballard, USA. The catalyst layers were coated on a Gas diffusion layer by brush and the catalyst loading (total) was 1 mg/sq cm. Pure hydrogen and air were used as fuel and the oxidant. The cells were operated at ambient pressure conditions. Preliminary performance comparison, durability studies (by cycling between two different potentials) were carried out in 30 cm² active area MEA before scaling up the membrane production to prepare MEAs with an active area of 330 cm². The MEAs were tested using an Arbin Fuel cell test station, USA. A 1 kW stack was built using 20 MEAs of 330 cm² active area. The stack was operated at the cell temperature of 50°C using water as the coolant.

3. Results and Discussion

Composite membranes based on expanded PTFE substrate were prepared by spray method as described in Figure 1. The properties of the substrate used and the membrane are given in Table 1. The SEM images of the substrate and the composite membrane have been discussed in detail earlier [14]. Conductivity measurements were made by sandwiching the membrane between conducting plates and measuring the impedance. The composite membranes have good conductivity due to their reduced thickness even though a substrate of high resistance is used.

3.1. Composite Membrane Characterization. Figure 2 shows the IR spectrum of the substrate and Nafion impregnated EPTFE membrane. The plain EPTFE shows characteristic peaks in the region 503 cm⁻¹ due to -CF₂ rocking mode, 620–640 cm⁻¹ due to -CF₂ wagging, 1150 cm⁻¹ due to -CF₂ stretching, and 1240 cm⁻¹ due to -CF₃ stretching. As the plain EPTFE does not absorb any moisture, no characteristic peak is seen in the region 3000–4000 cm⁻¹. In the composite Nafion membrane, the finger print region due to the PTFE background is still retained and no significant shift is observed due to any interactions in this region. Additional peaks due to -C-O-C-stretching band (970 cm⁻¹), weak

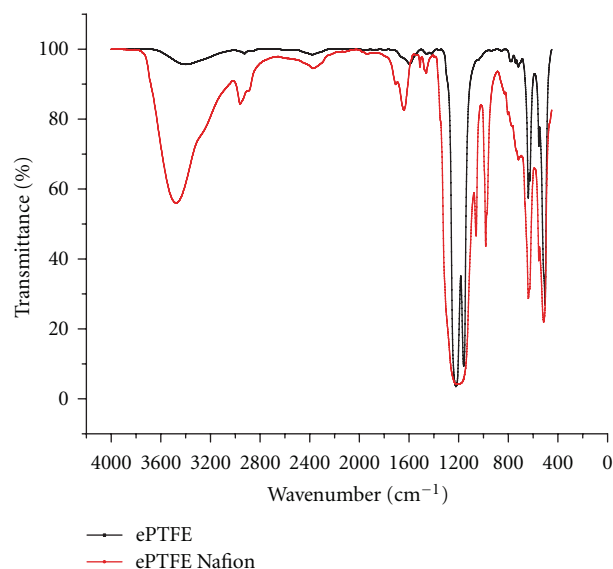


FIGURE 2: IR curves for the substrate and the composite membrane.

band at 805 cm⁻¹ due to -C-S-stretching, a band in the 1100–1200 cm⁻¹ region due to highly polar sulphonic acid groups, -OH bending vibration in the 1600–1800 cm⁻¹ region, and band in the 3200–3800 cm⁻¹ region due to water fundamental vibrations, are seen. These results confirm the impregnation of Nafion in PTFE and correspond with the Nafion and the PTFE bands observed in the literature [23].

Figure 3 shows the TGA curves obtained for the substrate PTFE and that of Nafion impregnated PTFE. It was found that pure PTFE is very stable and shows no transitions below 500°C. The composite Nafion membrane due to the presence of the ionomer shows transition around 300°C and 450°C due to degradation of the sulphonic acid groups and the main chain scission of Nafion ionomer. Nafion 112 membranes have been shown to have 3–5°C lower initial thermal decomposition temperature than the composite membranes by Huang et al. [22]. Figure 4 shows the stress-strain curves of Nafion and Composite membrane at 30°C. The composite membrane shows low-dimensional changes to applied stress compared to pure Nafion membrane. This property would be advantageous while operating a fuel cell. The membrane electrode assembly in a fuel cell undergoes stress due to tensile/compressive forces, hydration of the membrane due to water present in the vapor and liquid phase, cycling temperatures, and dynamic load cycles. Such stresses can lead to changes in the performance of the MEA. As these stresses are related more to the membrane than the other components of the MEA, the composite membrane that shows low variations in the stress is more advantageous. Further, it can also be seen that the composite membranes have higher modulus even though they are thinner than the pure Nafion membrane. Table 2 shows the comparison in properties between the developed composite membranes and Nafion 112 membranes.

3.2. Fuel Cell Characterization. Figure 5 compares the performance of the MEAs fabricated using the composite membrane and Nafion 212 membrane tested using a 30 cm²

TABLE 2: Comparison of the properties of the composite membrane with Nafion 112 membranes.

S. No	Property	Composite membrane	Nafion 112
1	Thickness	$28 \pm 5 \mu\text{m}$	$50 \mu\text{m}$
2	Water uptake	16	30
3	Thermal stability	$>300^\circ\text{C}$	$<300^\circ\text{C}^*$
4	Youngs modulus (Mpa)	241	117.7
5	Ionomer content (mg/cm^2)	2	9

* [22]

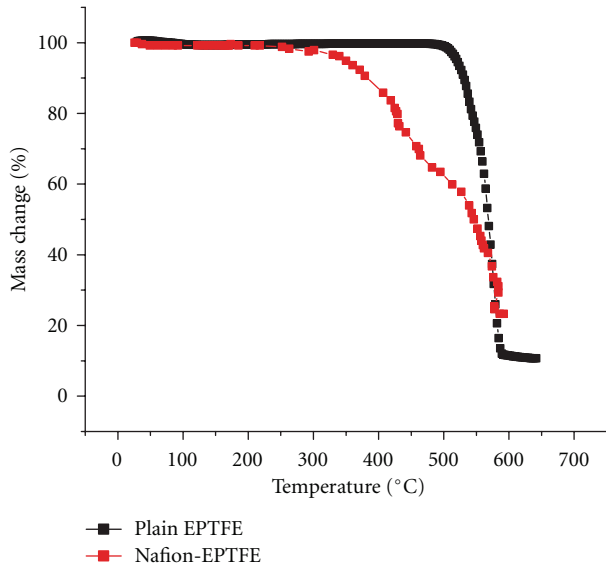


FIGURE 3: TGA curves for the substrate and the composite membrane.

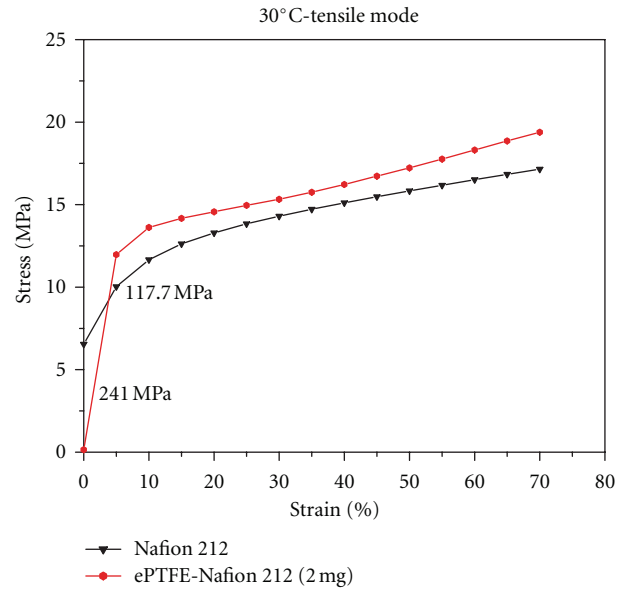
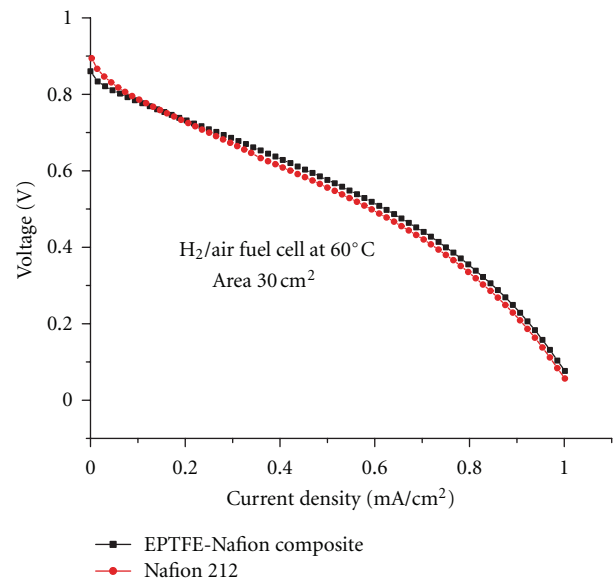


FIGURE 4: Stress-strain curves for the composite membrane and Nafion 212 membrane.

active area MEA with hydrogen and air as fuel and oxidant, respectively, at 60°C . The open circuit voltage for the composite PTFE-Nafion membrane is lower than that of pure Nafion membrane. This could be attributed to higher permeability of the composite membranes to reactant gases. Higher gas permeability for the composite membranes has been reported in the literature [24] in comparison to recast Nafion membranes and commercial Nafion 212 membranes. Polarization curves obtained for composite Nafion membrane and pure Nafion membranes show comparable performance at 60°C under humidified reactant conditions. The reactant gases were humidified at 10°C and 5°C higher than the cell temperature for hydrogen gas and air, respectively. As the polarization curves are a complex function of kinetic and mass transport-related parameters in addition to the ohmic resistance, similar performances indicate the applicability of these membranes for fuel cell applications.

3.3. Durability Testing of the MEAs. Cost and lifetime of the cells are two interrelated parameters, which have to be considered while development of new materials. As a lower

FIGURE 5: Comparison in performance between composite membrane and Nafion 112 at 60°C and ambient pressure conditions.

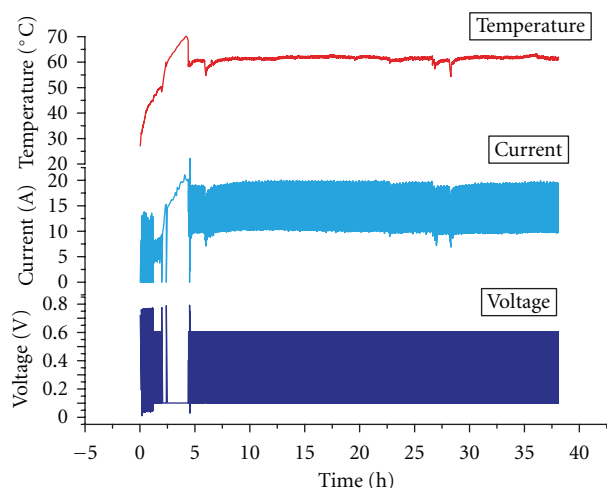


FIGURE 6: Durability of the composite membrane performance to repeated cycling.

cost, thinner alternative material is currently being considered, lifetime studies have to be carried out to study its applicability. Lifetime of the cell is dependent on many parameters like platinum particle dissolution and sintering, carbon corrosion, membrane thinning, operating parameters like voltage and current, cell temperature, pressure of the reactants, transient or continuous operation, number of startups and shut down, and so forth. As it is important to test durability under various conditions, one of the parameters, that is, cycling between operating voltage and very low voltage was carried out to study the membrane durability. Such extreme voltage parameters ensure that the cell is operated between high current density and nominal current density leading to differences in the water contents in the cell and induce enough stress to test the membrane properties and their durability. Figure 6 shows the results of the cycling studies carried out on the composite MEA. The MEA was held at a potential of 0.6 V for a period 30 s and 0.1 V for a period of 30 s. The entire cycle was thus completed in 1 min. It can be seen that the characteristics of the cell are constant for more than 2000 cycles studied. Further, during the long-term operation, ac impedance was also measured as shown in Figure 7. Ohmic and charge transfer resistance of the single cells employed using these composite membranes changed only marginally during cycling (after 2000 cycles). It has been reported that Nafion 112 membrane [25, 26] shows higher degradation at low humidity and high temperature of operation due to water-dependent glass transition temperature of Nafion and the humidity and temperature-dependent peroxide formation rates. Studies by Janssen et al. [27] on PEMFC durability by load on/off cycling with near saturated H_2 and air at ambient pressure concluded that membrane degradation did not contribute significantly to losses and that losses were mainly due to decrease in kinetic parameters and transport losses due to change in hydrophilicity of the electrodes. As the present study has been carried using fully saturated gases and optimal temperatures, it can be concluded that membrane degradation is not taking place.

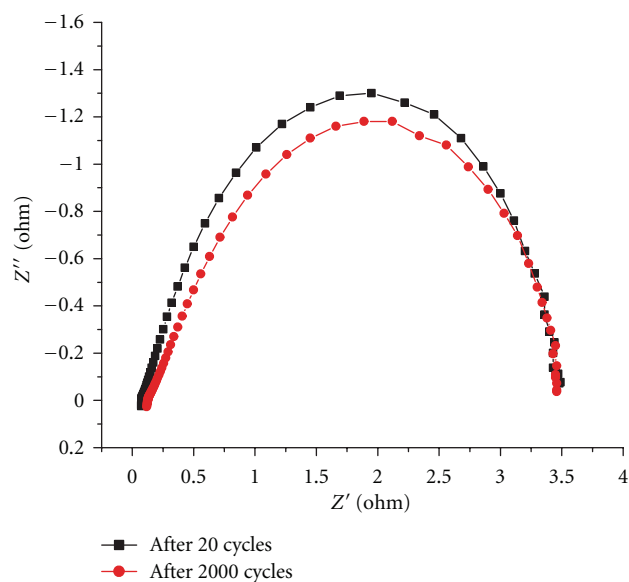


FIGURE 7: Comparison of impedance curves during cycling.

3.4. Fuel Cell Stack Characterization. Based on the results obtained from single cell studies, membrane fabrication was scaled up to form MEAs with an active area of 330 cm^2 . The major challenges to be faced during the scaling up process include nonuniformity in coating and incomplete coverage of the pores of ePTFE substrate. The spray method used for coating of the membrane included repetitive spraying in the longitudinal and transverse directions on the entire surface of the membrane to ensure complete coverage. Also the solution viscosity was maintained at constant level and evaporation losses were minimized by addition of high boiling solvents so as to have a uniform coating. The process developed produced membranes with less than 10% wastage. A fuel cell stack with 20 cells was fabricated from these membranes after testing individual membranes for permeability characteristics as mentioned in Section 2.1. Figure 8 shows the composite membrane of 30 cm^2 active area and a 330 cm^2 active area membrane along with the 20 cell stack assembled with these membranes. The stack design selected had the following configuration: number of cells—20, Active area 330 cm^2 , commercial supported catalyst (40%) for both anode and cathode, Serpentine flow field channels, water cooling channels after 2 cells, and internal fuel and oxidant manifold. After assembly of the stack, it was tested for electrical short circuits, internal or external leakage of gases, coolants, and so forth. The stack was operated using hydrogen and air as reactants at ambient pressure conditions and 50°C . The performance data for the stack is shown in Figure 9. The open circuit voltage for the stack was 16.04 V with the average individual cell open circuit voltage of $\sim 810\text{ mV}$. The voltage lowered to 15.28 V, 14.48 V, and 14.01 V as the current increased from 10 A to 20 A and 30 A, respectively. A peak power of 1.01 kW was obtained at the voltage of 11.22 V and 90 A current. In a fuel cell stack, uniform performance of each unit cell is preferable. The performances of the individual cells at

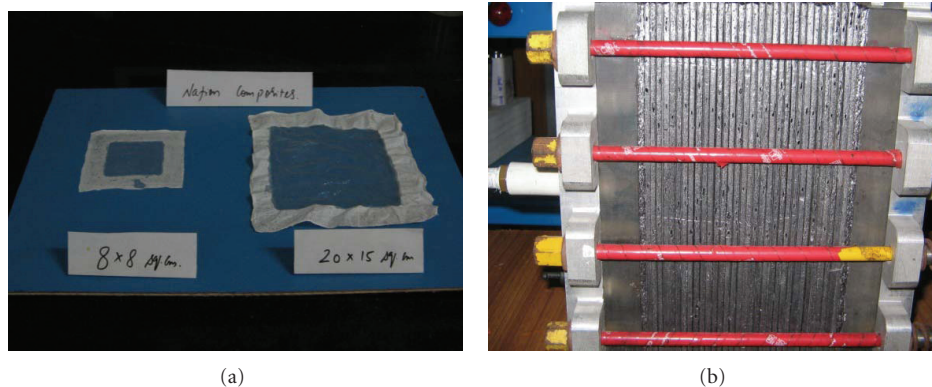


FIGURE 8: Composite membranes fabricated and the 20 cell PEMFC stack.

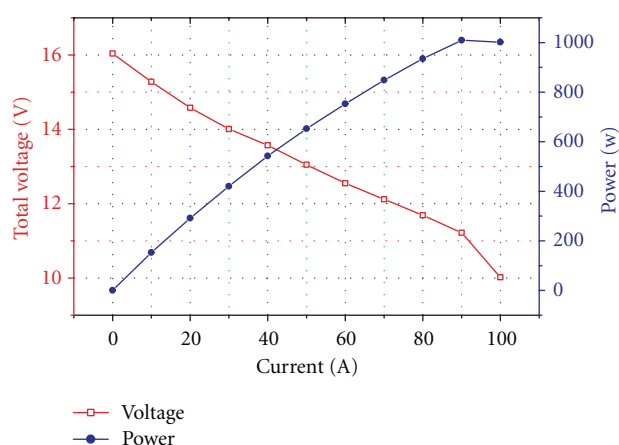


FIGURE 9: Performance of 20 cell fuel cell stack using the composite membrane.

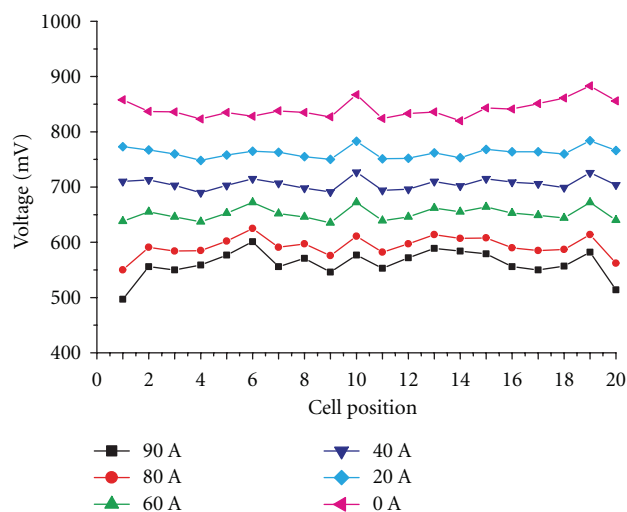


FIGURE 10: Performance of the individual cells at various current.

various currents are shown in Figure 10. The results show that the voltage distribution is fairly uniform. The deviation from the mean voltage at current densities up to 200 mA/cm^2 was less than 6% and increasing to 12% at a current density of 250 mA/cm^2 . These results suggest that the membranes

of comparable uniformity and quality have been prepared using the spray method, and the slight differences in the voltages of the various cells could be the result of slight differences in the internal resistance of the cells, nonuniform distribution of the reactant gases from the gas inlet to the outlet, and differences in the activation polarization of the electrodes, and so forth. With respect to endurance testing, the stack was not continuously tested at any particular power for long duration. The stack has been tested for more than 300 hrs at various conditions. The research and development program thus resulted in the development of 1 kW stack demonstrated using a composite membrane prepared in the lab. The process can be scaled up further to produce large stacks.

4. Conclusions

Composite Nafion membranes were fabricated by impregnating expanded PTFE substrate with the ionomer solution. Composite membranes with ionomer loading of 2 mg/cm^2 and thickness of $30 \mu\text{m}$ were found to have higher thermal stability and mechanical strength than conventional membranes with ionomer loading of $\sim 9 \text{ mg/cm}^2$ and $50 \mu\text{m}$ thickness. The composite membranes also offered cost advantages due to lower active material loading compared to the conventional membranes besides having comparable performance. Durability of the MEAs was tested by carrying out cycling studies between two voltages of 0.6 V and 0.1 V. The MEAs were cycled to ~ 2000 cycles, and it was found to give stable performance. Impedance analysis of the MEAs before and after cycling showed that the differences in the solution and the charge transfer resistances were almost the same indicating negligible membrane degradation. Based on the results, the membrane fabrication was scaled up and a 20 cell stack with an active area of 330 cm^2 were fabricated. A peak power of 1.01 kW was obtained with fairly uniform performance of the individual cells.

Acknowledgments

The authors would like to thank Dr. G. Sundararajan, Director, ARCI, Hyderabad, for supporting this work and Department of Science and Technology (DST), Government

of India for financial support. The authors recognized that there is no conflict of interests concerning the quality of results obtained.

References

- [1] L. Carrette, K. A. Friedrich, and U. Stimming, "Fuel cells: principles, types, fuels, and applications," *Fuel Cells*, vol. 1, no. 4, pp. 163–193, 2000.
- [2] K. S. Jeong and B. S. Oh, "Fuel economy and life-cycle cost analysis of a fuel cell hybrid vehicle," *Journal of Power Sources*, vol. 105, no. 1, pp. 58–65, 2002.
- [3] K. V. Kordesch and G. R. Simader, *Fuel Cells and Their Applications*, VCH, Weinheim, Germany, Chapter 4, 1996.
- [4] O. Savadogo, "Emerging membranes for electrochemical systems: (I) solid polymer electrolyte membranes for fuel cell systems," *Journal of New Materials for Electrochemical Systems*, vol. 1, no. 1, pp. 47–66, 1998.
- [5] P. Costamagna and S. Srinivasan, "Quantum jumps in the PEMFC science and technology from the 1960s to the year 2000: part I. Fundamental scientific aspects," *Journal of Power Sources*, vol. 102, no. 1–2, pp. 242–252, 2001.
- [6] B. Bahar, A. R. Hobson, J. A. Kolde, and D. Zuckerbrod, "Ultra-thin integral composite membrane," 1996, US Patent 5547551.
- [7] J. M. Gascoyne, G. A. Hards, J. Denton, and T. R. Ralph, "Composite membranes," 1999, european patent 875524.
- [8] H.-L. Lin, T. L. Yu, W. K. Chang, C. P. Cheng, C. R. Hu, and G. B. Jung, "Preparation of a low proton resistance PBI/PTFE composite membrane," *Journal of Power Sources*, vol. 164, no. 2, pp. 481–487, 2007.
- [9] K. M. Nouel and P. S. Fedkiw, "Nafion-based composite polymer electrolyte membranes," *Electrochimica Acta*, vol. 43, no. 16–17, pp. 2381–2387, 1998.
- [10] B. K. Dutta, D. Randolph, and S. K. Sikdar, "Thin and composite high-flux membranes of perfluorosulfonated ion-exchange polymer," *Journal of Membrane Science*, vol. 54, no. 1–2, pp. 51–61, 1990.
- [11] H. Tang, M. Pan, S. P. Jiang, X. Wang, and Y. Ruan, "Fabrication and characterization of PFSI/ePTFE composite proton exchange membranes of polymer electrolyte fuel cells," *Electrochimica Acta*, vol. 52, no. 16, pp. 5304–5311, 2007.
- [12] Z. Jie, T. Haolin, and P. Mu, "Fabrication and characterization of self-assembled Nafion-SiO₂-ePTFE composite membrane of PEM fuel cell," *Journal of Membrane Science*, vol. 312, no. 1–2, pp. 41–47, 2008.
- [13] K. Pattabiraman and K. Ramya, "Phosphotungstic acid modified expanded PTFE based nafion composites," *Journal of New Materials for Electrochemical Systems*, vol. 14, no. 4, pp. 217–222, 2011.
- [14] K. Ramya, G. Velayutham, C. K. Subramaniam, N. Rajalakshmi, and K. S. Dhathathreyan, "Effect of solvents on the characteristics of Nafion/PTFE composite membranes for fuel cell applications," *Journal of Power Sources*, vol. 160, no. 1, pp. 10–17, 2006.
- [15] H. L. Lin, T. L. Yu, K. S. Shen, and L. N. Huang, "Effect of Triton-X on the preparation of Nafion/PTFE composite membranes," *Journal of Membrane Science*, vol. 237, no. 1–2, pp. 1–7, 2004.
- [16] E. A. Cho, U.-S. Jeon, S. A. Hong, I.-H. Oh, and S.-G. Kang, "Performance of a 1 kW-class PEMFC stack using TiN-coated 316 stainless steel bipolar plates," *Journal of Power Sources*, vol. 142, no. 1–2, pp. 177–183, 2005.
- [17] M. Wang, K.-D. Woo, D. K. Kim, X. Zhu, and S. Sui, "Development of a kilowatt class PEMFC stack using Au-coated LF11 Al alloy bipolar plates," *Metals and Materials International*, vol. 12, no. 4, pp. 345–350, 2006.
- [18] X. Li, C. C. Ke, S. G. Qu, J. Li, Z. G. Shao, and B. L. Yi, http://www.intechopen.com/download/pdf/pdfs_id/20373.
- [19] G. C. Bandlamudi, M. Saborni, P. Beckhaus, F. Mähendorf, and A. Heinzel, "PBI/H₃PO₄ gel based polymer electrolyte membrane fuel cells under the influence of reformates," *Journal of Fuel Cell Science and Technology*, vol. 7, no. 1, pp. 0145011–0145012, 2010.
- [20] P. Mocotéguy, B. Ludwig, J. Scholta, Y. Nedellec, D. J. Jones, and J. Rozière, "Long-term testing in dynamic mode of HT-PEMFC H₃PO₄/PBI celtec-P based membrane electrode assemblies for micro-CHP applications," *Fuel Cells*, vol. 10, no. 2, pp. 299–311, 2010.
- [21] L. J. Bonville, H. R. Kunz, Y. Song et al., "Development and demonstration of a higher temperature PEM fuel cell stack," *Journal of Power Sources*, vol. 144, no. 1, pp. 107–112, 2005.
- [22] L. N. Huang, L. C. Chen, T. L. Yu, and H. L. Lin, "Nafion/PTFE/silicate composite membranes for direct methanol fuel cells," *Journal of Power Sources*, vol. 161, no. 2, pp. 1096–1105, 2006.
- [23] A. Gruger, A. Régis, T. Schmatko, and P. Colomban, "Nanostructure of Nafion membranes at different states of hydration: an IR and Raman study," *Vibrational Spectroscopy*, vol. 26, no. 2, pp. 215–225, 2001.
- [24] E. Endoh, S. Terazono, H. Widjaja, and Y. Takimoto, "Degradation study of MEA for PEMFCs under low humidity conditions," *Electrochemical and Solid-State Letters*, vol. 7, no. 7, pp. A209–A211, 2004.
- [25] V. Ramani, H. R. Kunz, and J. M. Fenton, "Effect of particle size reduction on the conductivity of Nafion/phosphotungstic acid composite membranes," *Journal of Membrane Science*, vol. 266, no. 1–2, pp. 110–114, 2005.
- [26] J. Healy, C. Hayden, T. Xie et al., "Aspects of the chemical degradation of PFSA ionomers used in PEM fuel cells," *Fuel Cells*, vol. 5, no. 2, pp. 302–308, 2005.
- [27] G. J. M. Janssen, E. F. Sitters, and A. Pfrang, "Proton-exchange-membrane fuel cells durability evaluated by load-on/off cycling," *Journal of Power Sources*, vol. 191, no. 2, pp. 501–509, 2009.

Research Article

Study of Chromium Removal by the Electrodialysis of Tannery and Metal-Finishing Effluents

Ruan C. A. Moura,¹ Daniel A. Bertuol,² Carlos A. Ferreira,³ and Franco D. R. Amado¹

¹ PROCIMM, State University of Santa Cruz, Road Ilhéus-Itabuna km 16, 45662-000 Ilhéus, BA, Brazil

² DEQ, Federal University of Santa Maria, 97105-900 Santa Maria, RS, Brazil

³ PPGEM, Federal University of Rio Grande do Sul, 91501-970 Porto Alegre, RS, Brazil

Correspondence should be addressed to Ruan C. A. Moura, ruan_moura@yahoo.com.br

Received 16 December 2011; Revised 17 April 2012; Accepted 3 May 2012

Academic Editor: Yoshinobu Tanaka

Copyright © 2012 Ruan C. A. Moura et al. This is an open access article distributed under the Creative Commons Attribution License, which permits unrestricted use, distribution, and reproduction in any medium, provided the original work is properly cited.

The metal-finishing and tannery industries have been under strong pressure to replace their current wastewater treatment based on a physicochemical process. The electrodialysis process is becoming an interesting alternative for wastewater treatment. Electrodialysis is a membrane separation technique, in which ions are transported from one solution to another through ion-exchange membranes, using an electric field as the driving force. Blends of polystyrene and polyaniline were obtained in order to produce membranes for electrodialysis. The produced membranes were applied in the recovery of baths from the metal-finishing and tannery industries. The parameter for electrodialysis evaluation was the percentage of chromium extraction. The results obtained using these membranes were compared to those obtained with the commercial membrane Nafion 450.

1. Introduction

Over the past few decades, there has been increased concern for the preservation of water resources. Industrial activities have led to widespread heavy metal contamination of soils and natural waters. Among the various sources of water contamination, the electroplating industry stands out as one of the most important, because it generates a considerable volume of effluents containing high concentrations of metal ions and, often, high concentrations of organic matter [1]. Another aggravating factor is that the traditional process for the treatment of these effluents, not very efficient and in some cases totally inefficient, produces dangerous solid waste (electroplating sludge), which should, therefore, be disposed of in appropriate landfills.

The most commonly used technology for the treatment of effluents is the physicochemical one, followed by units of biological treatment, usually consisting of activated sludge or aerated lagoon systems [2]. These conventional treatments are generally not able to reduce all the polluting parameters. Chemical Oxygen Demand (COD), chlorides, sulfates, and chromium often do not reach the required limits [3].

In this context, the leather and metal-finishing industries urge researchers to investigate new technologies for the recovery or recycling of chemical wastewater [4]. Because of their toxicity, these effluents cannot be rejected without pretreatment in the environment [5, 6].

Membrane technology has become increasingly attractive for wastewater treatment and recycling [7]. The main advantage of a membrane process is that concentration and separation are achieved without changing the physical state or using chemical products. Because of their modularity, membrane techniques in general and electromembrane techniques in particular are very well adapted to pollution treatment at its source; within this process, the electrodialysis process is becoming a good alternative when compared to the traditional methods of wastewater treatment [8, 9].

Electrodialysis (ED) is a membrane separation process based on the selective migration of aqueous ions through an ion-exchange membrane as a result of an electrical driving force. The transport direction and rate for each ion depend on a number of conditions, such as, its charge, mobility, relative concentrations, and applied voltage. Ion separation

is closely associated with the characteristics of the ion-exchange membrane, especially its permselectivity. ED was first used for the desalination of saline solutions, but other applications, such as, the treatment of industrial effluents, have gained importance [10, 11].

The purpose of this study is the investigation of the transport of some ions through synthesized membranes and a commercial one by electrodialysis. For the tannery effluents, photoelectrochemical oxidation (PEO) processes were previously used to degrade organic matter [12–14].

2. Experimental

For this study, two different real effluents were collected at two industries in the Southern Brazil. One effluent was collected at the discharge point of the conventional effluent treatment plant (CET) of a tannery plant. This plant carries out all the industrial processes from raw hides to finished leather. This effluent was then photoelectrooxidized for 24 hours and then treated by ED. A scheme of the PEO system used in this work is shown in Figure 1. It is made up of two serial, one liter PVC electrolytic reactors.

A 400 W high-pressure mercury-vapor lamp was used as a light source. Before each experiment, the UV light was turned on for 15 min to allow the UV energy to become stable. Two pairs of electrodes were used. The cathode and anode were DSA (70TiO₂/30RuO₂). The electrode area inside the cell was 118 cm². During the experiments, the reactor was operated in a batch recirculation mode. The effluent was recirculated at a flow rate of 4 L·h⁻¹, and 50 L effluent was treated by PEO for each experiment. The photoelectrochemical oxidation experiments were carried out using a DC power supply with an applied current density of 20 mA cm⁻².

In the metal-finishing plant, the effluent was also collected at the discharge point of the conventional effluent treatment plant (CET). The chromium concentrations were 0.5 ppm for the tannery effluent and 60 ppm for the metal-finishing effluent.

2.1. Membranes. The membranes were prepared by mixing conventional polymer (HIPS) with conducting polymers polyaniline (PAni). Two different mixing methods were tested to evaluate the effect of the production method. Dopants for polyaniline (PAni), camphorsulfonic acid (CSA), and p-toluenesulfonic acid (p-TSA) were also used.

HIPS and PAni were dissolved in 20 mL of tetrachloroethylene. After dissolution, PAni was dispersed in an HIPS polymeric matrix for 30 minutes. This dispersion was performed at 1,000 rpm in a mixer (Fisaton). The membranes were molded on glass plates using a laminator to keep thickness constant, and the solvent evaporated slowly for 24 hours under room temperature. The membranes were referred to as MCS and MTS.

2.2. Membrane Characterization

2.2.1. Infrared Spectroscopy. The samples were prepared with potassium bromide (KBr) powder. All of the samples were

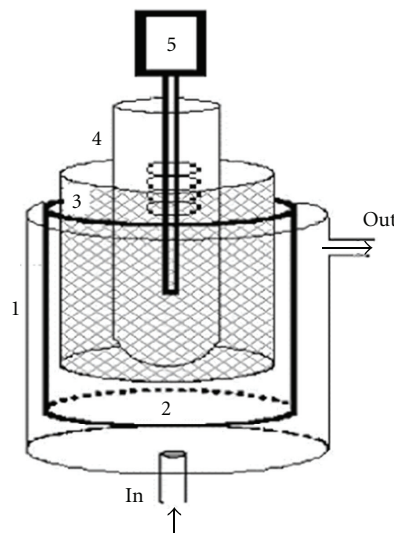


FIGURE 1: Schematic representation of PEO system: (1) PVC reservoir; (2) titanium oxide cathode; (3) titanium oxide recovered with TiO₂/RuO₂ anode; (4) quartz tube; (5) mercury steam lamp.

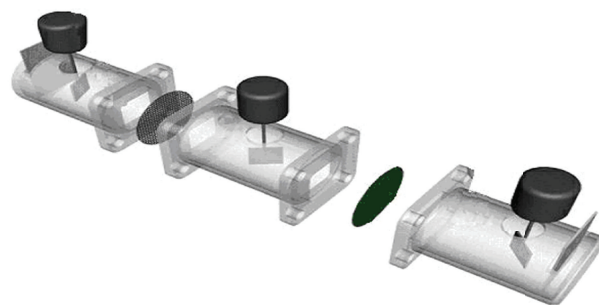


FIGURE 2: Three-compartment cell used for electrodialysis.

analyzed using an FTIR Perkin Elmer spectrometer model Spectrum 1000. The spectra were recorded in the spectral range of 400–4,000 cm⁻¹.

2.2.2. Swelling. Excess water was removed with a paper filter, and the membranes were weighed and kept in the oven at 80°C for 10 hours and then weighed again. The uptake of water was determined by the mass difference between the wet and the dried membranes (after heating at 80°C). Water absorption is expressed in percentage.

2.2.3. Morphology. Scanning electron micrographs of the membranes' surface were obtained using a microscope (Philips XL20) after the samples were sputter-coated with gold.

2.2.4. Electrodialysis. The membranes were synthesized (MTS and MCS) [15–17] and the commercial membrane (Nafion 450) was used as a cation selective membrane. Selemion AMV was used as an anion selective membrane. All of the membranes were maintained in contact with the solutions for 48 h in order to achieve equilibrium.

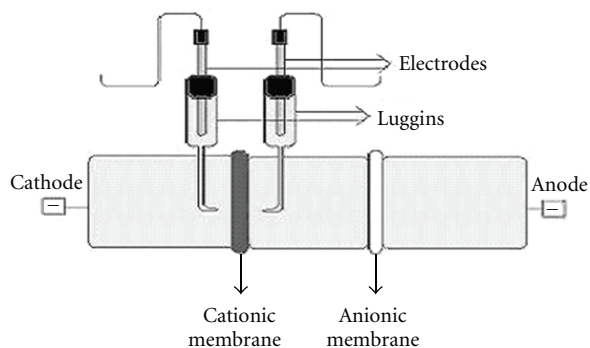


FIGURE 3: Three-compartment cell used to determine polarizations curves.

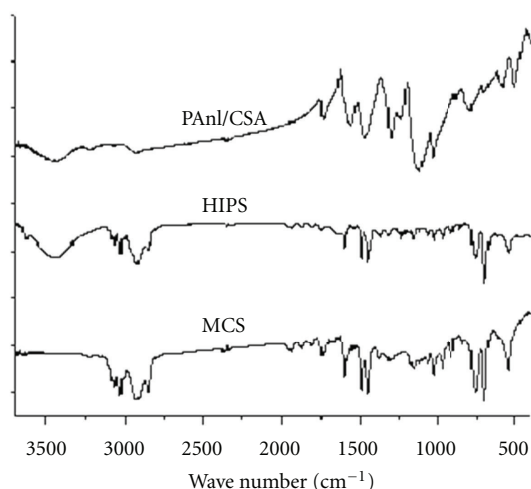


FIGURE 4: FTIR spectrum of PAni/CSA, HIPS sample, and MCS membrane.

The membranes were also equilibrated in deionized water at room temperature for 24 hours, with the aim of testing the hydrophilic behavior of $-\text{SO}_3^-$ from the doping acid that was used in polyaniline.

The electro dialysis experiments were performed using a three-compartment cell with a capacity of 200 mL each, as shown in Figure 2. A platinized titanium electrode was used as the anode and cathode. A Selemion AMT anionic membrane was utilized and the cationic membranes were the synthesized membranes (MCS and MTS) and Nafion 450. The area of the membranes was 16 cm^2 and all the experiments were galvanostatic, with a current density of $10 \text{ mA} \cdot \text{cm}^{-2}$. All of the electro dialysis experiments were carried out during 180 minutes.

The evaluation of the electro dialysis process was expressed in percent extraction, that is, how much of the ion in question was transferred from the diluted to the concentrated compartment:

$$\text{Pe \%} = \frac{M_i - M_f}{M_i} \times 100, \quad (1)$$

where Pe is the percent extraction (%), M_i is the ion concentration considered in the diluted compartment in

TABLE 1: Solutions used in electro dialysis tests for recovery of metals tannery and metal-finishing effluents.

Experiment	Cathodic compartment	Intermediary compartment	Anodic compartment
1	0.1 M Na_2SO_4	Tannery effluent photoelectro-oxidized with 20 A and 5 h	0.1 M Na_2SO_4
2	0.1 M Na_2SO_4	Metal-finishing effluent	0.1 M Na_2SO_4

TABLE 2: Thickness and swelling of the membranes.

Membrane	Thickness (mm)	Swelling (%)
MCS	0.20–0.25	13.6
MTS	0.20–0.25	12.9
Nafion 450	0.40	28.6

time zero, and M_f is the ion concentration considered in the diluted compartment at the final time.

Table 1 shows the solution's distributions that were used in the experiments.

2.2.5. Polarization Curves. Current-voltage curves (CVCS) were obtained in galvanostatic mode using a classical three compartment cell [18, 19]. This cell was composed of three symmetrical 200 cm^3 half cells. These compartments were separated by gaskets, which clamp the membrane. In the geometrical center of the gaskets there was a cylindrical hole. The working area of the AMV membrane was 16 cm^2 . Two Ag/AgCl electrodes, immersed in Luggin's capillaries, allowed the measurement of the potential difference between the two sides of the membrane. Mechanical stirrers were placed in each compartment. The same solutions were used on both sides of the membrane. The electrical current was supplied with two platinum electrodes (Figure 3). Electric current was applied using a DC power source for 120 seconds. The curves were obtained by potential measurements through the membrane corresponding to the applied current.

3. Results and Discussion

3.1. Thickness and Swelling. Table 2 shows the thickness and swelling of the membranes produced for this study and of the Nafion 450 membrane.

The swelling capacity of the membrane affects not only its dimensional stability but also its selectivity, electric resistance, and hydraulic permeability. Dimensional stability increases as the polymer affinity for water decreases. Conversely, as the polymer affinity for water increases, ionic transport resistance decreases [20].

Membranes that use CSA as a doping acid show slightly greater swelling than other membranes. However, the Nafion 450 membrane showed much greater swelling than the synthesized membranes. This difference may be associated with the fact that Nafion is a supported membrane and is thicker than the membranes under study.

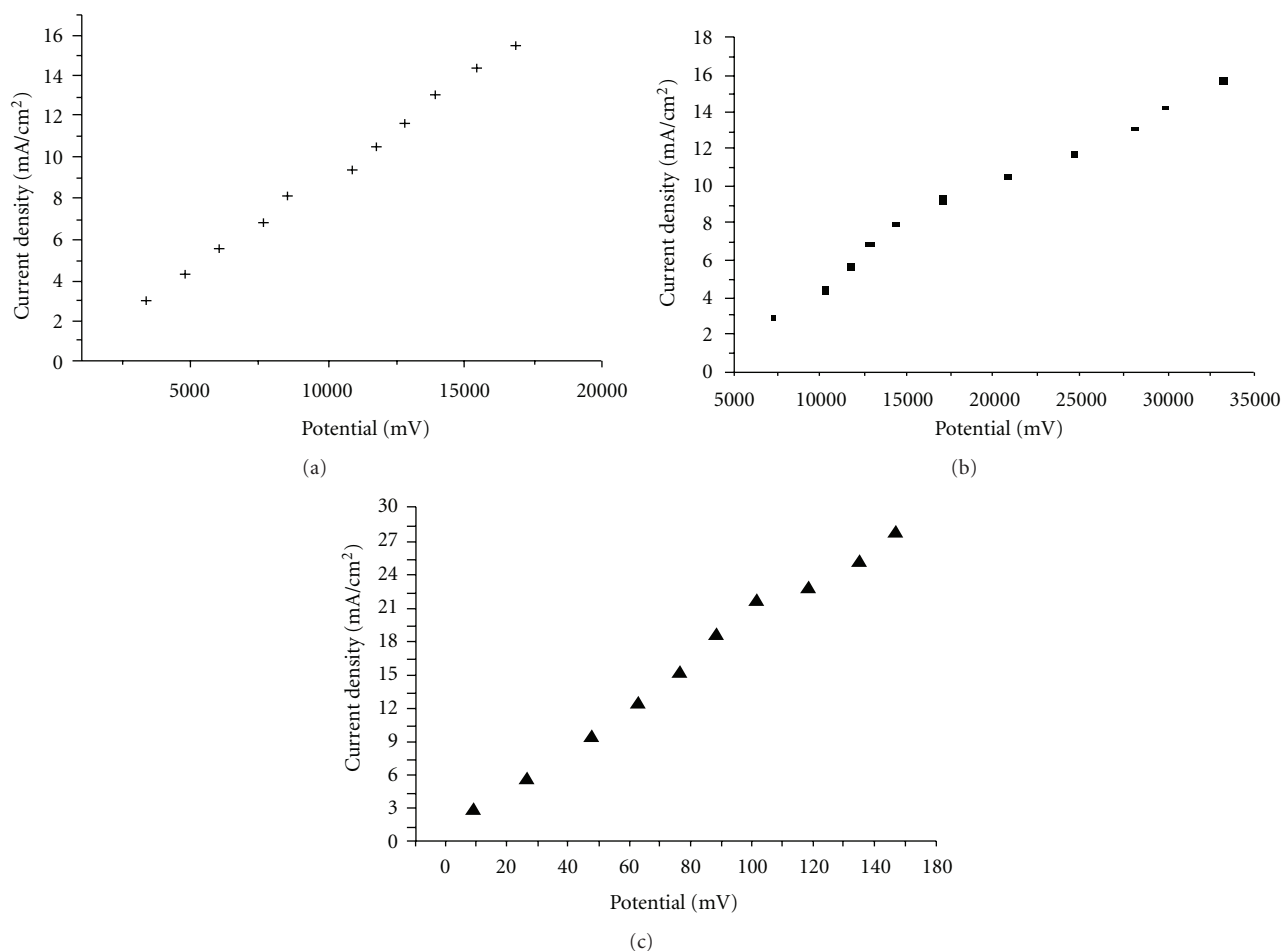


FIGURE 5: Polarization curves of the synthesized membranes and commercial membrane using the metal-finishing effluents. (a) MCS, (b) MTS, and (c) Nafion 450.

MPC for HIPS membrane with polyaniline doped with camphorsulfonic acid (CSA), MPT for HIPS membrane with polyaniline doped with p-toluenesulfonic acid (TSA). This difference between the transport numbers may be related to the structure of polyaniline dopant acid because its dopant (CSA) is more hydrophilic than the other one (p-TSA).

3.2. Infrared Spectroscopy. To ensure incorporation into the polymeric matrix, samples of PANi/CSA, HIPS, and MCS membrane were analyzed. Figure 4 shows the FTIR spectra of these samples.

In Figure 4, HIPS spectrum and different peaks were observed. The peak at $2,948\text{ cm}^{-1}$ corresponds to an angular deformation of CH_3 . At $1,731\text{ cm}^{-1}$, there is a peak attributed to the stretching of C=O groups. The peaks at $1,645\text{ cm}^{-1}$ and $1,554\text{ cm}^{-1}$ correspond to N_2H stretching. The peaks at $1,075\text{ cm}^{-1}$ and $1,140\text{ cm}^{-1}$ are associated to the stretching of C-O-C groups [17].

The MCS membrane spectrum displays peaks of PANi and HIPS spectra, thus showing the incorporation of PANi into the plastic matrix. Some of the peaks are overlapped, as seen in the stretching of N-H groups, in approximately $3,430\text{ cm}^{-1}$.

3.3. Polarization Curves. Figure 5 presents the polarization curves of the synthesized membranes and commercial membrane Nafion 450 using the metal-finishing effluents.

According to the classical theory [21, 22] of concentration polarization for ion-exchange membranes, the current-voltage response shows three regions. The shape of current-voltage curves can be distinguished. In the first region, a linear relationship is obtained between the current and voltage drop that is referred to as the ohmic region. In the second region, the current varies very slightly with voltage, denoting an almost unrelated current applied voltage, corresponding to the so-called limiting current. In the region III is an over-limiting current region, and then current intensity increases again with the applied voltage.

The MCS and MTS membranes presented a higher electric resistance than the Nafion 450 membrane and the limit current density was around $11\text{ mA}\cdot\text{cm}^{-2}$. For the Nafion 450 membrane, the limit current density was around $20\text{ mA}\cdot\text{cm}^{-2}$, thus showing that electric resistance is lower.

Figure 6 presents the polarization curves of the synthesized membranes and commercial membrane Nafion 450, using the tannery effluents.

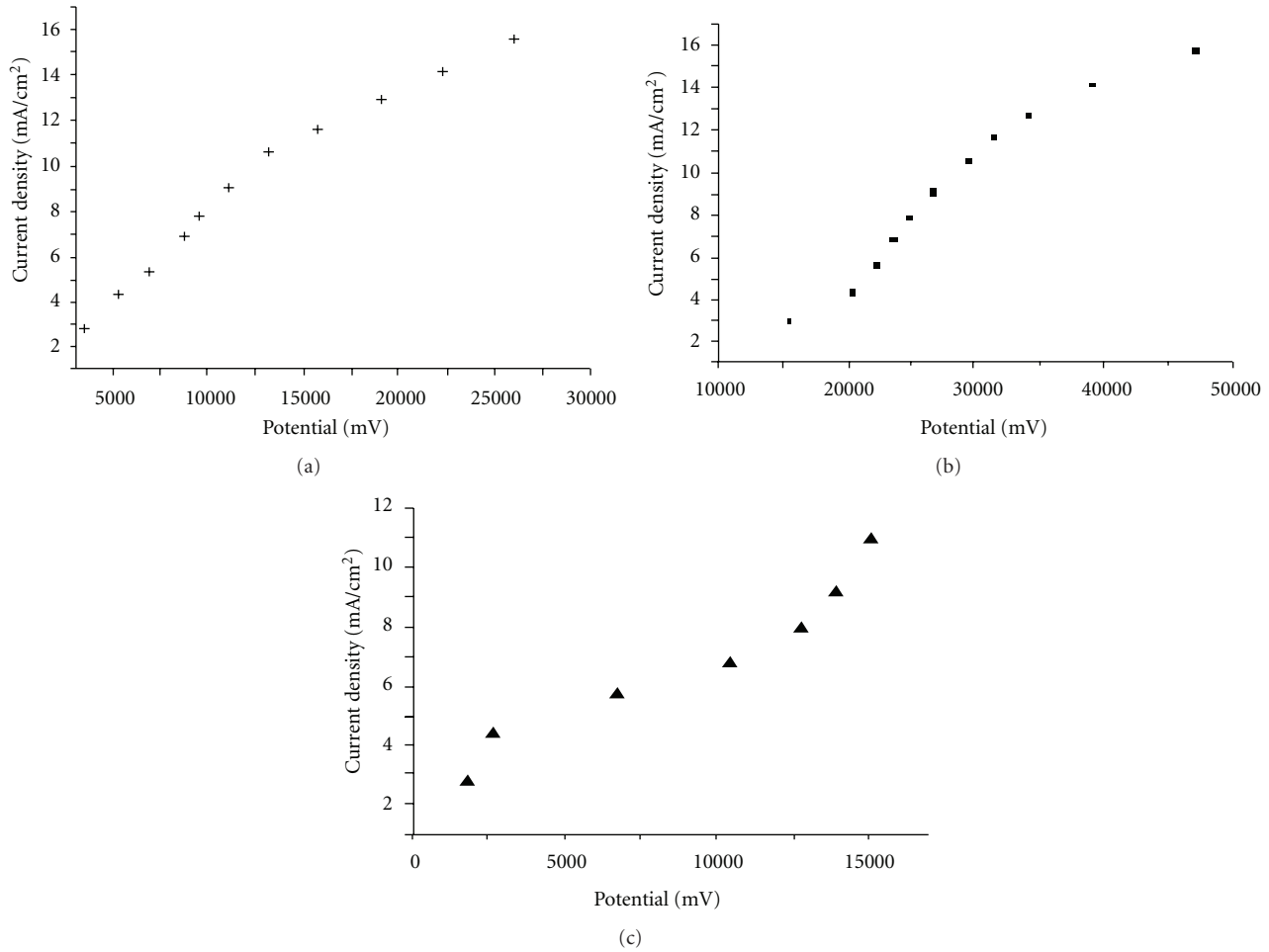


FIGURE 6: Polarization curves of the synthesized membranes and commercial membrane using the tannery effluents (a) MCS, (b) MTS, and (c) Nafion 450.

In Figure 6, it is possible to observe the current-potential curves of the membranes used for the treatment of the tannery effluents after photoelectrochemical oxidation. It is verified that the curves present the same behavior as the curves obtained with the metal-finishing effluent.

The membranes had higher resistance due to the residual organic matter present in the effluent, which might have caused the membranes fouling, hindering the transport, and consequently increasing electric resistance. This phenomenon was also observed for the commercial membrane Nafion 450.

3.4. Electrodialysis. Table 3 shows the chromium transport from metal-finishing effluents through the synthesized membranes and the commercial membrane. It is possible to verify that the Nafion 450 membrane presented better results when compared to the synthesized membranes (MTS and MCS).

The analysis of chromium in the tannery effluent is shown in Table 4. The MCS membrane had better chromium transport than the MTS membrane. The commercial Nafion membrane showed a better result, once again. Transport results confirmed the effect of the acid structure used

TABLE 3: Chromium percent extraction through membranes using the metal-finishing effluents.

Membrane	Pe Cr ³⁺ (%)
MCS	18.7
MTS	19.3
Nafion 450	37.9

as polyaniline dopant. TSA (toluenesulfonic acid) is an aromatic acid and CSA (camphorsulfonic acid) is a cyclic acid; this difference may affect the interactions between the (HSO₃⁻) groups from the dopant acid and nitrogen from polyaniline, which may, in turn, affect ionic transport through the membrane.

3.5. Morphology. Regarding the morphology of membranes (Figure 7), it is possible to observe the MTS (A) and MCS (B) surfaces. The addition of polyaniline clearly promoted changes in the morphology of the HIPS polymeric matrix. The main differences between the MCS and MTS membranes were observed in the polyaniline structure. The morphology

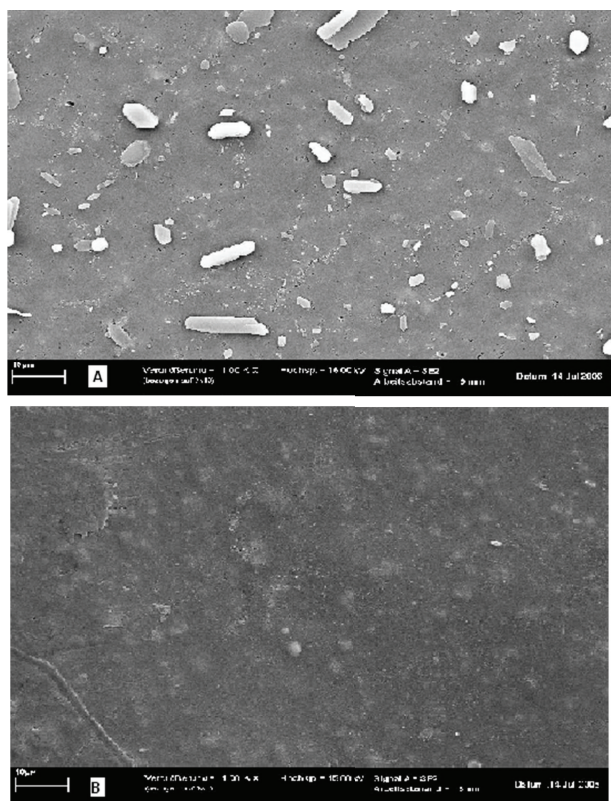


FIGURE 7: Microscopy (A) MTS and (B) MCS membrane surface.

TABLE 4: Chromium percent extraction through membranes using tannery effluents.

Membrane	Pe Cr ³⁺
MTS	95
MCS	96
Nafion 450	100

of the MTS membrane resembles needles; such a difference is due to the fact that during the synthesis of polyaniline doped with p-toluenesulfonic acid (p-TSA), the complete oxidation reaction of the aniline took place.

4. Conclusions

Infrared spectroscopy showed characteristic bands of PANi in the spectra of the membranes, especially the peak at $1,034\text{ cm}^{-1}$ regarding the S=O group. The synthesized membranes presented similar chromium transport to that observed in the Nafion 450 membrane using the tannery effluent. Electric resistance was higher in the synthesized membrane than in the commercial membrane.

Using the metal-finishing effluent, it was possible to verify that the MCS and MTS membranes presented similar results in chromium transport. The Nafion 450 membrane, however, presented better results, because its electric resistance is lower.

The study proved the feasibility of using an alternative technology in the treatment of tannery and metal-finishing effluents, bringing great advantages to water reuse.

References

- [1] M. Haroun, A. Idris, and S. R. Syed Omar, "A study of heavy metals and their fate in the composting of tannery sludge," *Waste Management*, vol. 27, no. 11, pp. 1541–1550, 2007.
- [2] A. A. Dantas Neto, T. N. de Castro Dantas, and M. C. P. Alencar Moura, "Evaluation and optimization of chromium removal from tannery effluent by microemulsion in the Morris extractor," *Journal of Hazardous Materials*, vol. 114, no. 1–3, pp. 115–122, 2004.
- [3] A. Cassano, R. Molinari, M. Romano, and E. Drioli, "Treatment of aqueous effluents of the leather industry by membrane processes: a review," *Journal of Membrane Science*, vol. 181, no. 1, pp. 111–126, 2001.
- [4] V. Sivakumar, V. J. Sundar, T. Rangasamy, C. Muralidharan, and G. Swaminathan, "Management of total dissolved solids in tanning process through improved techniques," *Journal of Cleaner Production*, vol. 13, no. 7, pp. 699–703, 2005.
- [5] G. Tiravanti, D. Petruzzelli, and R. Passino, "Low and non waste technologies for metals recovery by reactive polymers," *Waste Management*, vol. 16, no. 7, pp. 597–605, 1996.
- [6] Z. Bajza and I. V. Vrcek, "Water quality analysis of mixtures obtained from tannery waste effluents," *Ecotoxicology and Environmental Safety*, vol. 50, no. 1, pp. 15–18, 2001.
- [7] J.-H. Tay and S. Jeyaseelan, "Membrane filtration for reuse of wastewater from beverage industry," *Resources, Conservation and Recycling*, vol. 15, no. 1, pp. 33–40, 1995.
- [8] A. Cassano, J. Adzet, R. Molinari, M. G. Buonomenna, J. Roig, and E. Drioli, "Membrane treatment by nanofiltration of exhausted vegetable tannin liquors from the leather industry," *Water Research*, vol. 37, no. 10, pp. 2426–2434, 2003.
- [9] S. M. Kulikov, O. M. Kulikova, O. V. Scharikova, R. I. Maximovskaya, and I. V. Kozhevnikov, "Use of electromembrane technology for waste water treatment and modern acidic catalyst synthesis," *Desalination*, vol. 104, no. 1–2, pp. 107–111, 1996.
- [10] X. Tongwen, "Electrodialysis processes with bipolar membranes (EDBM) in environmental protection—a review," *Resources, Conservation and Recycling*, vol. 37, no. 1, pp. 1–22, 2002.
- [11] H. Strathmann, "Electrodialysis and related processes," in *Membrane Separations Technology—Principles and Applications*, R. D. Noble and S. Stern, Eds., p. 213, Elsevier, New York, NY, USA, 1995.
- [12] L. Pinhedo, R. Pelegrini, R. Bertazzoli, and A. J. Motheo, "Photoelectrochemical degradation of humic acid on a (TiO₂) 0.7(RuO₂)0.3 dimensionally stable anode," *Applied Catalysis B*, vol. 57, no. 2, pp. 75–81, 2005.
- [13] L. Szpyrkowicz, G. H. Kelsall, S. N. Kaul, and M. De Faveri, "Performance of electrochemical reactor for treatment of tannery wastewaters," *Chemical Engineering Science*, vol. 56, no. 4, pp. 1579–1586, 2001.
- [14] M. A. S. Rodrigues, F. D. R. Amado, J. L. N. Xavier, K. F. Streit, A. M. Bernardes, and J. Z. Ferreira, "Application of photoelectrochemical-electrodialysis treatment for the recovery and reuse of water from tannery effluents," *Journal of Cleaner Production*, vol. 16, no. 5, pp. 605–611, 2008.
- [15] F. D. R. Amado, E. Gondran, J. Z. Ferreira, M. A. S. Rodrigues, and C. A. Ferreira, "Synthesis and characterisation

- of high impact polystyrene/polyaniline composite membranes for electrodialysis,” *Journal of Membrane Science*, vol. 234, no. 1-2, pp. 139–145, 2004.
- [16] F. D. R. Amado, L. F. Rodrigues Jr., M. A. S. Rodrigues, A. M. Bernardes, J. Z. Ferreira, and C. A. Ferreira, “Development of polyurethane/polyaniline membranes for zinc recovery through electrodialysis,” *Desalination*, vol. 186, no. 1–3, pp. 199–206, 2005.
- [17] F. D. R. Amado, M. A. S. Rodrigues, F. D. P. Morisso, A. M. Bernardes, J. Z. Ferreira, and C. A. Ferreira, “High-impact polystyrene/polyaniline membranes for acid solution treatment by electrodialysis: preparation, evaluation, and chemical calculation,” *Journal of Colloid and Interface Science*, vol. 320, no. 1, pp. 52–61, 2008.
- [18] P. Sistat and G. Pourcelly, “Chronopotentiometric response of an ion-exchange membrane in the underlimiting current-range. Transport phenomena within the diffusion layers,” *Journal of Membrane Science*, vol. 123, no. 1, pp. 121–131, 1997.
- [19] M. Taky, G. Pourcelly, F. Lebon, and C. Gavach, “Polarization phenomena at the interfaces between an electrolyte solution and an ion exchange membrane. Part I. Ion transfer with a cation exchange membrane,” *Journal of Electroanalytical Chemistry*, vol. 336, no. 1-2, pp. 171–194, 1992.
- [20] R. F. D. Costa, M. A. S. Rodrigues, and J. Z. Ferreira, “Transport of trivalent and hexavalent chromium through different ion-selective membranes in acidic aqueous media,” *Separation Science and Technology*, vol. 33, no. 8, pp. 1135–1143, 1998.
- [21] R. Valerdi-Pérez and J. A. Ibáñez-Mengual, “Current-voltage curves for an electrodialysis reversal pilot plant: determination of limiting currents,” *Desalination*, vol. 141, no. 1, pp. 23–37, 2001.
- [22] N. Pismenskaya, V. Nikonenko, B. Auclair, and G. Pourcelly, “Transport of weak-electrolyte anions through anion exchange membranes: current-voltage characteristics,” *Journal of Membrane Science*, vol. 189, no. 1, pp. 129–140, 2001.

Research Article

Ion-Exchange Membranes Based on Polynorbornenes with Fluorinated Imide Side Chain Groups

Arlette A. Santiago,¹ Joel Vargas,² Mikhail A. Tlenkopatchev,³
Mar López-González,⁴ and Evaristo Riande⁴

¹Facultad de Química, Universidad Nacional Autónoma de México, CU, Coyoacán, 04510 México, DF, Mexico

²Facultad de Ingeniería, Universidad Autónoma del Carmen, Avenida Central S/N Esq. con Fracc. Mundo Maya, 24115 Ciudad del Carmen, CAM, Mexico

³Instituto de Investigaciones en Materiales, Universidad Nacional Autónoma de México, CU, Apartado Postal 70-360, Coyoacán, 04510 México, DF, Mexico

⁴Instituto de Ciencia y Tecnología de Polímeros (ICTP-CSIC), C/Juan de la Cierva 3, 28006 Madrid, Spain

Correspondence should be addressed to Mikhail A. Tlenkopatchev, tma@unam.mx

Received 3 February 2012; Revised 11 April 2012; Accepted 15 April 2012

Academic Editor: Seung Hyeon Moon

Copyright © 2012 Arlette A. Santiago et al. This is an open access article distributed under the Creative Commons Attribution License, which permits unrestricted use, distribution, and reproduction in any medium, provided the original work is properly cited.

The electrochemical characteristics of cation-exchange membranes based on polynorbornenes with fluorinated and sulfonated dicarboximide side chain groups were reported. This study was extended to a block copolymer containing structural units with phenyl and 4-oxybenzenesulfonic acid, 2,3,5,6-tetrafluorophenyl moieties replacing the hydrogen atom of the dicarboximide group. A thorough study on the electrochemical characteristics of the membranes involving electromotive forces of concentration cells and proton conductivity is reported. The proton permselectivity of the membranes is also discussed.

1. Introduction

Ion-exchange membranes have received considerable attention for many applications. Thus, the desalination of sea-water and brackish-water, treatment of industrial effluents, concentration or separation of food and pharmaceutical products containing ionic species are some of the examples of these kinds of applications [1, 2].

Ion-exchange membranes should exhibit high conductance, high permselectivity, low free diffusion of ionic species, low osmotic flow, good mechanical properties, and high chemical stability. Many polyelectrolytes based on perfluorinated polyimides, polyetherketones, polysulfones, polyphosphazenes; have been synthesized, and their electrochemical characteristics have been studied [3]. It is well known that norbornene monomers can be easily functionalized and membranes from functionalized polynorbornenes with adamantyl, phenyl, cyclohexyl, and pentafluorophenyl dicarboximide side groups have been prepared [4–6]. Taking

into account these antecedents and searching for new ion-exchange membranes, a study was undertaken focused on the preparation of cation-exchange membranes based on modified polynorbornenes.

In an earlier work, the preparation of hydrogenated and sulfonated poly(*N*-phenyl-*exo-endo*-norbornene-5,6-dicarboximide) has been reported [7]. A drawback of these membranes is that the sulfonation procedure does not guarantee a uniform sulfonation of the phenyl groups, and even it can produce degradative processes in the polymer chains. In order to circumvent these difficulties, we have synthesized poly(*N*-pentafluorophenyl-*exo-endo*-norbornene-5,6-dicarboximide) and successfully replaced the fluorine atom in position 4 of the phenyl group by sulfonation in mild conditions [8].

The fluorine atoms in the polyelectrolyte side chains can decrease attractive intermolecular interactions between phenyl groups thus avoiding the molecular piling of the phenyl rings. This behavior is a direct consequence of the

high electronegativity of the fluorine atom which severely reduces the polarizability of the $C^{ar}-F$ bond and as a result the formation of nonpermanent or flitting dipoles which are the basis of the London dispersion forces [9]. It should be noted that earlier studies on gas transport in polynorbornene-based membranes showed that fluorinated moieties in the polymer chains cause a significant increase in gas permeability as a consequence of the decrease in intramolecular interactions [10]. The cation-exchange membranes were also prepared from copolymers resulting from partially replacing the phenyl groups of poly(*N*-phenyl-*exo-endo*-norbornene-5,6-dicarboximide) by 4-oxybenzenesulfonic acid, 2,3,5,6-tetrafluorophenyl groups [11]. The aim of this study was to find out how the decrease of the density of sulfonic acid in the membranes affects their transport characteristics. The acronyms used for the homopolymeric and the copolymeric acidic membranes were, respectively, P5FNDIHS and C5FNDIHS, and the structural units of the respective chains are shown in Figure 1.

2. Experimental Part

2.1. Synthesis of the Monomer. By reaction of norbornene-5,6-dicarboxylic anhydride (NDA) with 2,3,4,5,6-pentafluoroaniline an amic acid (AA) that is obtained which further treated with anhydrous sodium acetate/acetic anhydride produces the monomer *N*-pentafluorophenyl-*exo-endo*-norbornene-5,6-dicarboximide (5FNDI) (see Scheme 1). More details of the synthesis are given elsewhere [8].

2.2. Polymerization. Polymerization of 5FNDI was carried out by ring opening metathesis polymerization (ROMP) (Scheme 1). The reaction was performed at 45°C for 2 h in glass vials, under nitrogen atmosphere. The polymerization was terminated by adding ethyl vinyl ether to the reaction medium which was further poured into methanol, solubilized with chloroform containing a few drops of 1 N HCl, and precipitated again into methanol. The product was dried in a vacuum oven at 40°C to constant weight. Then, the polymer was hydrogenated quantitatively at room temperature and 115 bar using a Wilkinson's catalyst (Scheme 2).

2.3. Sulfonation Procedure. Hydrogenated poly(*N*-pentafluorophenyl-norbornene-5,6-dicarboximide) (P5FNDI) (0.5 g, 1.51 mmol), sodium 4-hydroxybenzenesulfonate dihydrate (0.70 g, 3.02 mmol), and potassium carbonate (0.52 g, 3.77 mmol) were mixed in a round flask equipped with a Dean-Stark trap and stirred in 15 mL of solvent (*N,N*-dimethylacetamide-toluene 2:1) at 120°C for 9 h (Scheme 2). Progressive precipitation overtime was observed. The product was then filtered off, washed several times with distilled water and dried in a vacuum oven at 40°C overnight. The resulting polymer P5FNDIHS, a pale-brown powder, was soluble in DMF and DMSO. Yield: 94%, $T_g = 228^\circ\text{C}$, $T_{d1} = 260^\circ\text{C}$ (sulfonic group loss), $T_{d2} = 430^\circ\text{C}$ (main chain decomposition).

^1H NMR (300 MHz, DMF- d_7): δ (ppm) = 7.80 (2H, s), 7.18 (2H, s), 3.56 (2H, s), 2.73, 2.31, 1.83, 1.58, 1.91.

^{13}C NMR (75 MHz, DMF- d_7): δ (ppm) = 175.0 (C=O), 145.5, 145.0, 140.4, 139.7, 128.2 (C-O), 115.1, 107.2, 49.0, 43.0.

^{19}F NMR (300 MHz, DMSO- d_6 , ref. TFA [-77 ppm]): δ (ppm) = -141.9 , -143.0 , -153.1 .

FT-IR (thin film, cm^{-1}): 2926 (C-H asym str), 2860 (C-H sym str), 1787 (C=O), 1726, 1636, 1509, 1406, 1356, 1295 (C-F), 1140 ($-\text{SO}_3\text{H}$, asym str), 1132, 1039 ($-\text{SO}_3\text{H}$, sym str), 981, 833, 698, 561. The acronym for this polymer will be P5FNDIHS (Figure 1).

2.4. Copolymerization. The copolymer was prepared via ROMP in a block fashion [11]. Firstly, monomer PhNDI, synthesized according to literature [8] and catalyst I were stirred in 1,2-dichloroethane at 65°C for 0.33 h. Then, monomer 5FNDI dissolved in 1,2-dichloroethane was added to the polymer solution and stirred at 65°C for 0.66 h (Scheme 1). The obtained copolymer C5FNDI was soluble in chloroform and dichloroethane. The incorporation of 5FNDI in copolymer was 32 mol% as determined by ^1H NMR. The block copolymer obtained was hydrogenated as mentioned above and the pentafluorophenyl moieties of hydrogenated poly(*N*-phenyl-*exo-endo*-norbornene-5,6-dicarboximide-*co-N*-pentafluorophenyl-*exo-endo*-norbornene-5,6-dicarboximide) (C5FNDI) were sulfonated with 4-hydroxybenzenesulfonate dihydrate using the procedure used for the sulfonation of hydrogenated poly(*N*-pentafluorophenyl-*exo-endo*-norbornene-5,6-dicarboximide) (Scheme 2). The acronym for this copolymer will be C5FNDIHS and its composition is shown in Figure 1.

2.5. Membranes Preparation and Atomic Force Microscopy (AFM). P5FNDIHS and C5FNDIHS membranes (in sodium salt form) were cast, respectively, from hot *N,N*-dimethylformamide solutions (~ 2 wt %) of P5FNDIHS and C5FNDIHS chains in a Teflon mold and dried at 70°C for 12 h. The films were immersed firstly in stirring methanol at room temperature for 3 h and secondly in deionized water for 1 h in order to remove the residual solvent. Afterwards, the membranes underwent a proton exchange treatment with 1.0 N hydrochloric acid during 12 h. Then, the films were washed repeatedly with deionized water until the rinse water became neutral. Finally, the membranes were dried under a vacuum at 120°C for 10 h.

The surface morphology of the thin films was observed using tapping mode AFM (Multimode Nanoscope IVa, Digital Instrument/Veeco) under ambient conditions. In tapping mode, the stylus oscillates and touches the sample only at the end of its downward movement. The nominal resonance frequency for the tapping mode was between 265–309 kHz with a phosphorous (*n*) doped Si cantilever which had a spring constant that ranged from 20 to 80 N m^{-1} . The set point in the AFM control program was adjusted to change the contact force between the tip and surface in order to detect the existence of morphologies.

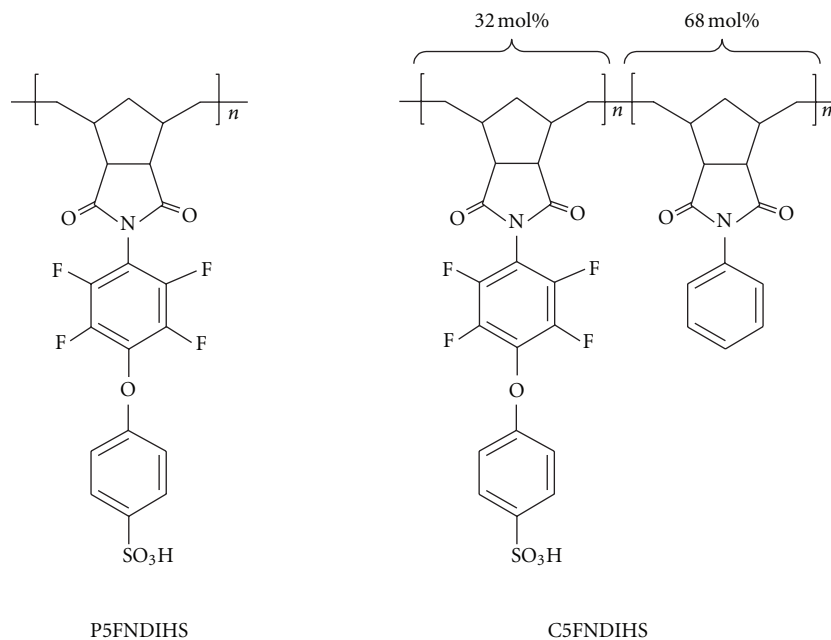
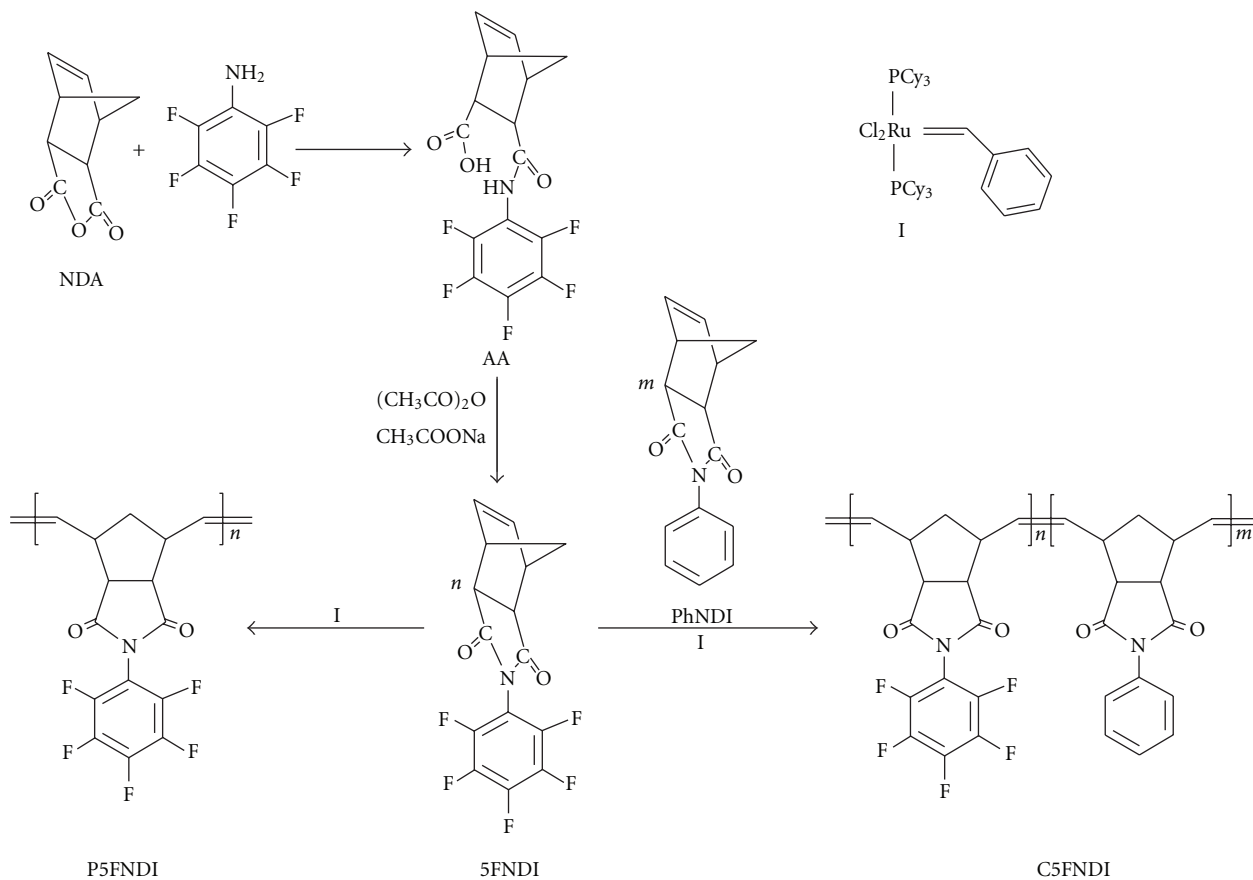
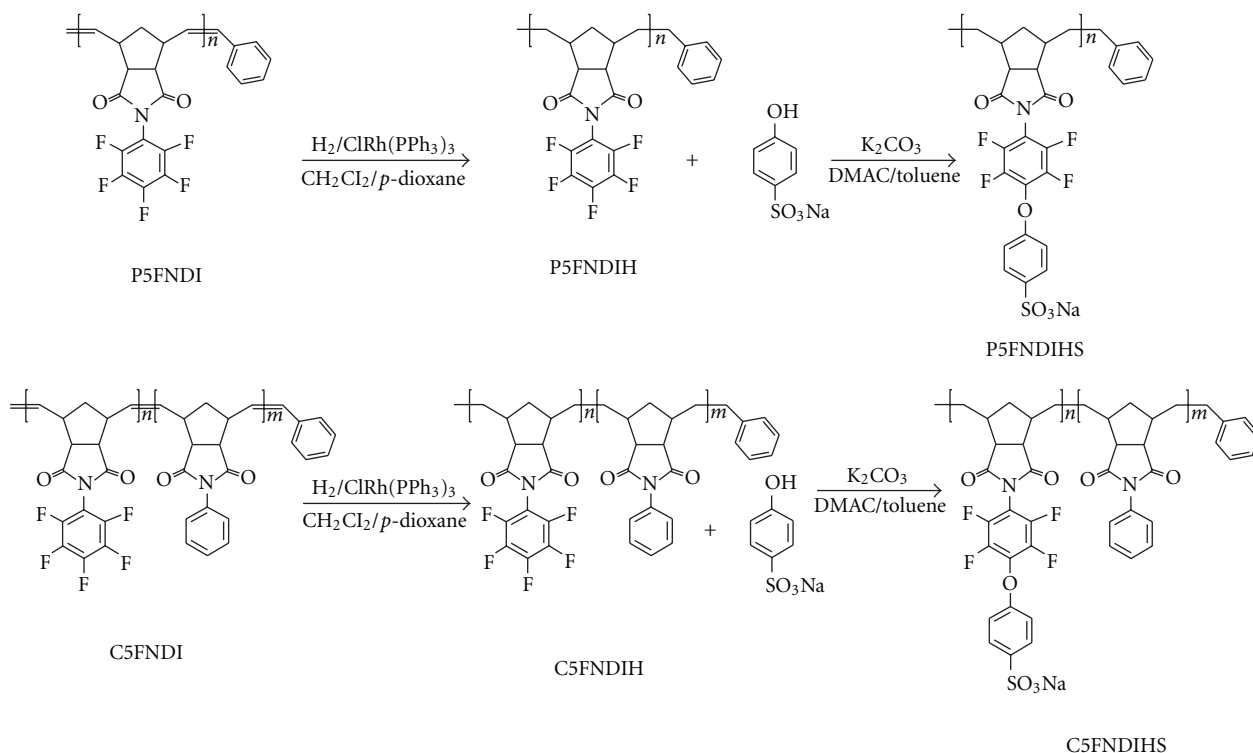


FIGURE 1: Acid form structural units of hydrogenated-sulfonated poly(*N*-pentafluorophenyl-*exo-endo*-norbornene-5,6-dicarboximide) (P5FNDIHS) and hydrogenated-sulfonated poly(*N*-phenyl-*exo-endo*-norbornene-5,6-dicarboximide-co-*N*-pentafluorophenyl-*exo-endo*-norbornene-5,6-dicarboximide) (C5FNDIHS).



SCHEME 1: Monomer synthesis and further polymerization.



SCHEME 2: Synthesis of sulfonated polymer and copolymer.

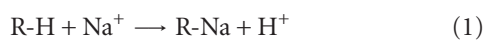
TABLE 1: Density in Kg m^{-3} , ρ , water uptake in $\text{Kg H}_2\text{O/Kg dry membrane}$, w_u , IEC in equivalents of fixed anionic groups per Kg dry membrane obtained by titration, X^- , and NMR, X_{NMR}^- , molecules of water per fixed ionic group, λ , and conductivity, σ , in S/m , at 30°C .

Membrane	ρ	w_u	X^-	X_{NMR}^-	λ_{x^-}	λX_{NMR}^-	σ
P5FNDIHS	1500	0.617	1.750	2.060	19.6	16.6	2.24
C5FNDIHS	1380	0.373	0.286	0.204	72.5	101.6	0.0134

2.6. Density, Water Uptake, and Ion-Exchange Capacity of the Membranes. The density of the dry membranes was measured by the flotation method using isooctane as solvent. The values of this parameter are shown in the first column of Table 1.

Weighed dry membranes were immersed in distilled water for several hours, removed from the solution, gently blotted with filter paper to remove superficial water, and weighed. From the weights of the dry membranes, m_d , and the membranes equilibrated with water, m_w , the water uptake, w_u , in $\text{g H}_2\text{O/g dry membrane}$ is obtained as $w_u = (m_w/m_d) - 1$.

The ion-exchange capacity (IEC) of a given membrane was measured by immersing the weighed dry membrane in a 1 N HCl solution for 1 h. Then the membrane was removed from the solution, washed several times with distilled water to eliminate the chloride acid absorbed, and finally immersed in a 1 N sodium chloride solution. The protons exchanged in the reaction



were estimated by titration with a very diluted NaOH solution. The values of IEC in equiv/Kg dry membrane were obtained as $\text{IEC} = VN/m_d$ where V is the volume in L of the solution of NaOH of normality N (equiv/L) used in the titration, and m_d is the mass of the membrane in Kg.

2.7. Electromotive Forces of Concentration Cells. Electromotive forces of concentration cells made up of two semicells separated by the ion-exchange membrane were measured (Figure 2). The configuration of the cells was $\text{Ag}|\text{AgCl}|\text{HCl solution}(c_1)|\text{cation-exchange membrane}|\text{HCl solution}(c_2)|\text{AgCl}|\text{Ag}$, where c_1 and c_2 are the concentrations of the electrolyte in the left-hand and right-hand compartments of the concentration cells. Notice that the anion of the electrolyte must be reversible with that of the electrodes. The solution in each compartment was kept under strong stirring to minimize the formation of membrane-solution interface layers. The evolution of electromotive force, emf , of the cell with time was measured at 25°C with a 3645-20 Hioki voltage logger and recorded every second with a 3911-20 communication base apparatus via a PC. The emf

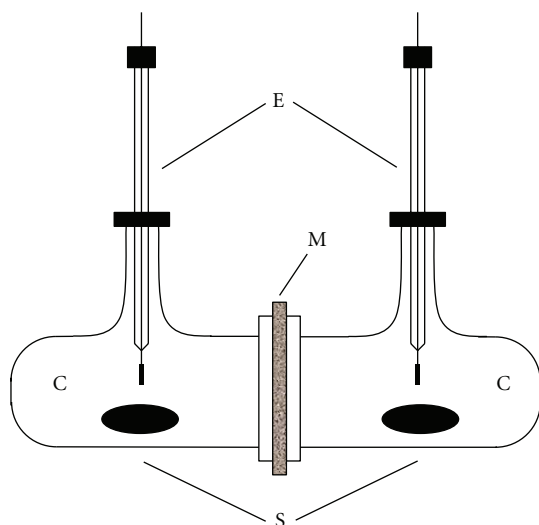


FIGURE 2: Concentration cell used to measure the electromotive force: (C) half cell, (E) electrodes, (M) ion-exchange membrane, and (S) magnetic stirrers.

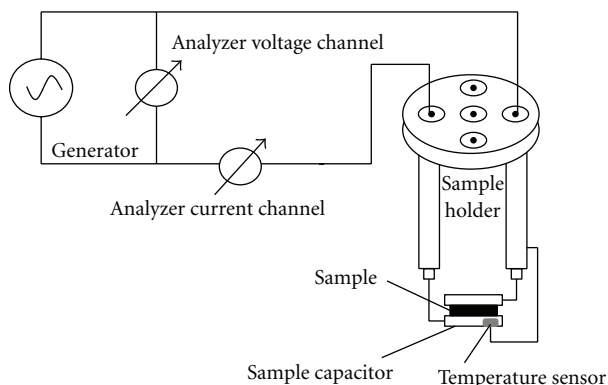


FIGURE 3: Cell used to measure the ionic conductivity of the membranes.

of the concentration cell was taken as that one at which this quantity reaches a maximum.

2.8. Ohmic Resistance Measurements. The ohmic resistance of the membranes in the acid form was measured with a Novocontrol BDS system comprising a frequency response analyzer (Solartron Schlumberger FRA 1260) and a broadband dielectric converter with an active sample head. Gold disk electrodes were used in the impedance measurements carried out at several temperatures in the frequency window $4.9 \times 10^{-2} - 1 \times 10^7$ Hz. The temperature was controlled by a nitrogen jet (QUATRO from Novocontrol) with a temperature error of 0.1 K during every single sweep in frequency (Figure 3). Measurements were carried out on molded disk-shaped samples of 60–100 μm thickness with diameters of 20 and 10 mm.

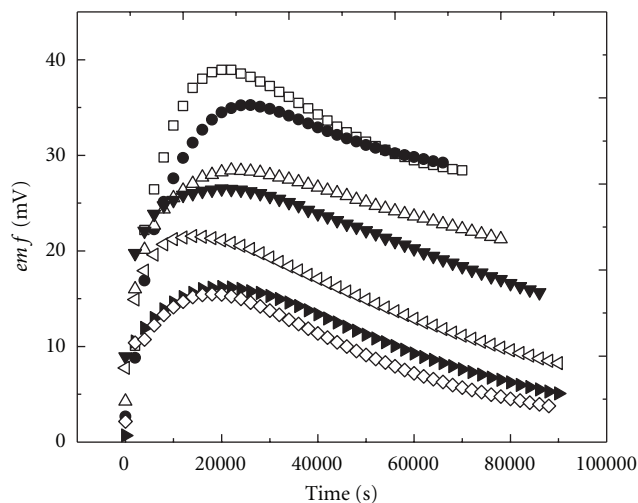


FIGURE 4: Evolution of the *emf* of the P5FNDIHS membrane for different c_2/c_1 ratios: (\square) 0.01/0.005, (\bullet) 0.02/0.01, (\triangle) 0.1/0.05, (\blacktriangledown) 0.2/0.1, (\triangleleft) 0.4/0.2, (\blacktriangleright) 0.8/0.4, and (\diamond) 1.0/0.5.

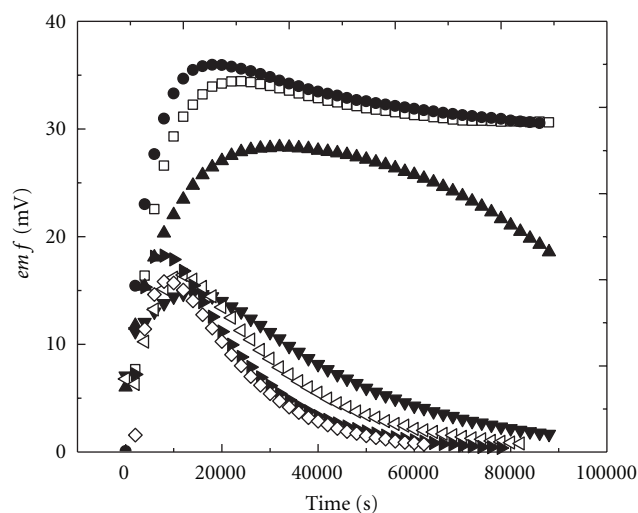


FIGURE 5: Evolution of the *emf* of the C5FNDIHS membrane for different c_2/c_1 ratios: (\square) 0.01/0.005, (\bullet) 0.02/0.01, (\blacktriangle) 0.1/0.05, (\blacktriangledown) 0.2/0.1, (\triangleleft) 0.4/0.2, (\blacktriangleright) 0.8/0.4, and (\diamond) 1.0/0.5.

3. Results and Discussion

Values of the water uptake and the ion-exchange capacity (IEC) of the membranes measured by titration are given in Table 1. The values of the IEC estimated from the NMR spectra, also given in Table 1, somewhat differ from those determined by titration. Moreover, the number of moles of water per $-\text{SO}_3^-$ group anchored to the polymer chains of the membranes are also shown in Table 1. It is worth noting that in spite of its relatively low IEC, the C5FNDIHS membrane exhibits a rather large number of molecules of water per anionic fixed group.

The variation of the electromotive force, *emf*, of the concentration cell with time for several HCl solutions flanking the membrane of interest is shown in Figures 4 and 5.

The ratio between the concentrations of the solutions in the concentrated, c_2 , and diluted, c_1 , compartments lies in the vicinity of 2. In all cases, prior to each experiment, the membrane was washed several times with distilled water until exhausting the free electrolyte inside the membrane and then was equilibrated with the solution used in the dilute compartment of the concentration cell. An inspection of the evolution of the curves in the figures shows that the *emf* of the concentration cell increases with time needing nearly 3 h in most cases to reach the maximum value and then decreases as time increases. The *emf* at the maximum of the curves was taken as the apparent electromotive force of the concentration cell flanked by electrolyte solutions with concentration c_2/c_1 .

The *emf* of a concentration for an electrolyte $A_{\nu^+}^{z_+} B_{\nu^-}^{z_-} \rightarrow \nu^+ A^{z_+} + \nu^- B^{z_-}$ is given by [12]

$$emf = \frac{\nu RT}{z_+ F} \int_{a_1}^{a_2} t_+(c) d \ln a_{\pm} = \frac{\nu RT}{F} \int_{a_1}^{a_2} \tau_+(c) d \ln a_{\pm}, \quad (2)$$

where a_1 and a_2 are, respectively, the activities of the electrolyte solutions in the compartments 1 and 2 of the concentration cell, t_+ and τ_+ ($= t_+/z_+$) are, respectively, the number of equivalents and moles of cations transported across the membrane by a Faraday of current, F , and $\nu = \nu_+ + \nu_-$ is the total number of moles of ions proceeding from the dissociation of the electrolyte. For monovalent electrolytes, such as HCl, (2) becomes

$$emf = -\frac{2RT}{F} \int_{a_1}^{a_2} t_+(c) d \ln a_{\pm}. \quad (3)$$

Notice that for monovalent electrolytes, $t_+ = \tau_+$. Since transport numbers depend on the concentration of electrolyte, solution of (3) requires measuring the $t_+(c)$ profile across the membrane using the Hirthoff method, that is, determining the variation of concentration of electrolyte in a concentration cell flanked by the electrolyte at the same concentration c after passing a known amount of dc current across the membrane. However, if the concentration ratio c_2/c_1 is 2 or lower, the average transport number of the cation can approximately be estimated as

$$t_+ = \frac{emf}{emf_{\max}}, \quad (4)$$

where *emf* is the experimental value of the concentration cell and emf_{\max} can be obtained doing $t_+ = 1$ in (3), that is,

$$emf_{\max} = -\frac{2RT}{F} \ln \frac{a_2}{a_1}. \quad (5)$$

Values of the apparent proton transport numbers for different concentrations flanking the membrane are shown in Figure 6.

The response of cation-exchange membranes in acid form to an alternating electric field of angular frequency ω is modeled by an electric circuit consisting of an ohmic resistance R_M accounting for proton transport in the membrane

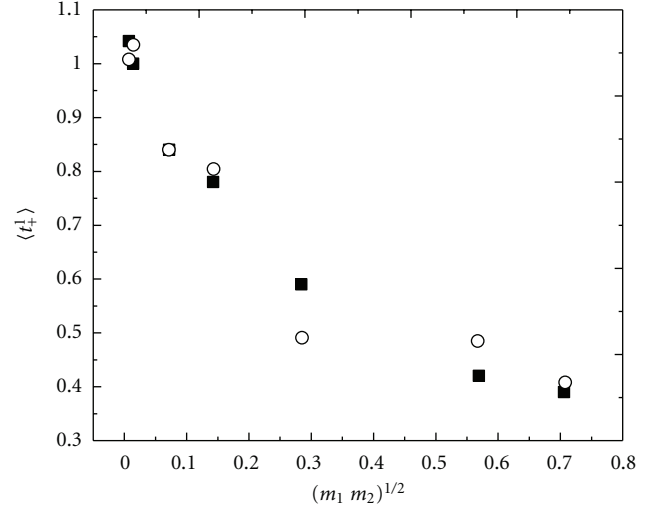


FIGURE 6: Variation of the apparent proton transport number with the geometric average of the molality of the solutions flanking the membrane in P5FNDIHS (squares) and C5FNDIHS (circles).

in series with a parallel RC circuit. The RC circuit represents a Debye relaxation process with a single relaxation time $\tau = RC$. Strictly speaking, relaxation processes are described by a distribution of relaxation times and as a result it is more realistic to replace the capacitor by a constant phase element of admittance $Y^*(\omega) = Y_0(j\omega\tau)^n$, $0 < n \leq 1$ [13]. The impedance of the circuit is given by

$$Z^*(\omega) = R_M + \frac{R}{1 + Y_1(j\omega\tau)^n}, \quad (6)$$

where $Y_1 = RY_0$ is a dimensionless parameter. The complex plane plot $Z''(\omega)$ versus $Z'(\omega)$, called Nyquist diagram [14], is an arc intersecting the abscissa axis at $\omega \rightarrow \infty$ and $\omega \rightarrow 0$. Taking into account that $\lim_{\omega \rightarrow \infty} Z'(\omega) = R_M$ and $\lim_{\omega \rightarrow \infty} Z''(\omega) = 0$, the intersection of the arc with the abscissa axis at high frequencies gives the ohmic resistance of the membrane to proton transport. However, Nyquist plots for the acidic P5FNDIHS and C5FNDIHS membranes presented in Figures 7 and 8, respectively, show in addition to the polarization arc another arc, at higher frequencies, that presumably intersects with the abscissa axis at the origin. The real impedance where the two arcs intersect with the abscissa axis at the same point is the resistance R_M of the membrane. On the other hand, the polarization arc in the low-frequency region does not intersect with the abscissa axis as (6) predicts but both $|Z''|$ and Z' increase as frequency decreases. This behavior is presumably associated with a charge-transfer resistance R_{CT} and a double-layer capacitance C_{dl} . The Warburg impedance [13, 15, 16] nearly always exhibits these two characteristics in such a way that it is conditioned by the diffusion of charges in the membrane-electrode interface. The value of this impedance for an interface of infinite thickness is given by

$$Z_W^*(\omega) = \frac{\sigma}{\omega^{1/2}} - j \frac{\sigma}{\omega^{1/2}}, \quad (7)$$

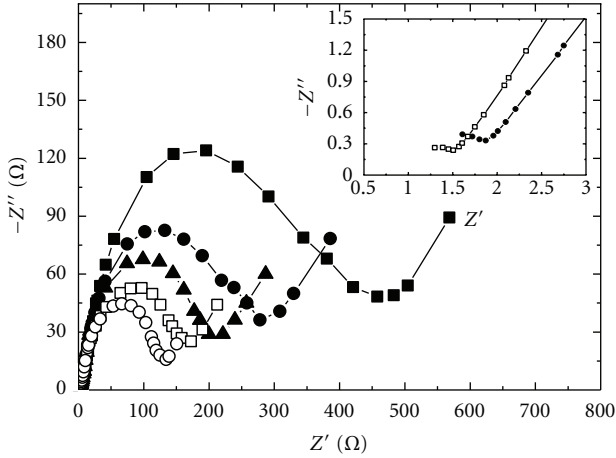


FIGURE 7: Nyquist plots at 10 (■), 20 (●), 30 (▲), 40 (□) y 50°C (○) for the P5FNDIHS membrane in the acid form equilibrated with distilled water. Inset: zoom of the Nysquit plots at 20°C and 40°C in the high-frequency region.

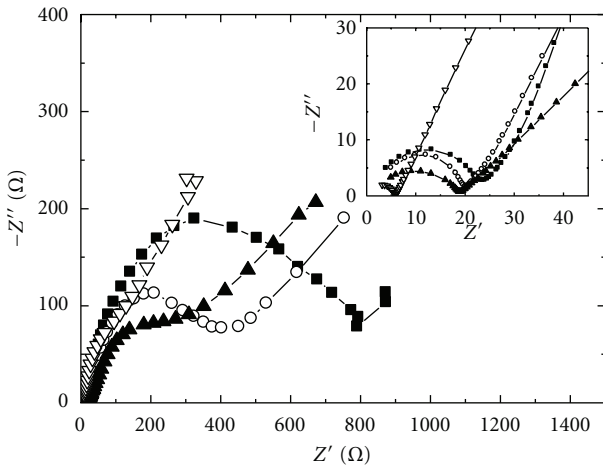


FIGURE 8: Nyquist plots at 20 (■), 30 (○), 50 (▲) y 70°C (▽) for the C5FNDIHS membrane in the acid form equilibrated with distilled water. Inset: zoom of the Nyquist plots at high frequencies.

where σ is a constant that depends on $\Sigma_i (1/C_i^b D_i^{1/2})$ where C_i^b and D_i are, respectively, the bulk concentration and diffusion coefficients of the reactant species i . As a result the modulus of the impedance scales as $|Z_W^*(\omega)| \sim \omega^{-1/2}$, that is, the double logarithmic plot of the modulus of the complex impedance is a straight line of slope $-1/2$ in the case of a double layer of infinite thickness. Although the results seem to support the existence of a Warburg impedance, there are not enough data in the low-frequency region that allow to reach a definite conclusion concerning the membrane-electrode double layer thickness.

To account for the arc intersecting with the origin at high frequencies, the equivalent circuit of the membrane (ohmic resistance of the membrane in series with a circuit made up of constant phase element in parallel with the polarization resistance) should be in parallel with a capacitor, in the case of a semicircle, or a constant phase element for an arc.

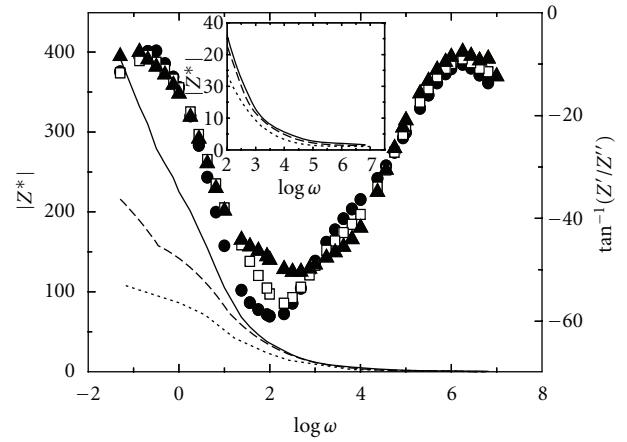


FIGURE 9: Bode diagram showing the variation of the modulus of the impedance $|Z^*|$ (lines) and the out-of-phase angle ($\phi = \tan^{-1}(Z''/Z')$) (symbols) with the frequency at 20°C (solid line and filled circles), 40°C (dash line and open squares) and 60°C (dot line and filled triangles) for the P5FNDIHS membrane in the acid form equilibrated with distilled water.

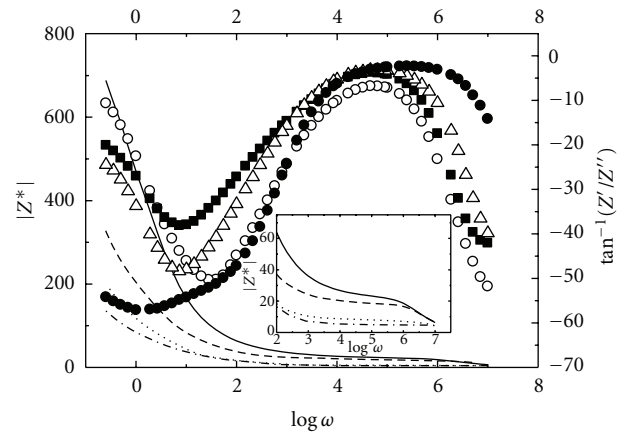


FIGURE 10: Bode diagram showing the variation of the modulus of the impedance $|Z^*|$ (lines) and the out-of-phase angle ($\phi = \tan^{-1}(Z''/Z')$) (symbols) with the frequency at 20°C (solid line and filled circles), 40°C (dash line and filled squares), 60°C (dot line and open triangles), and 80°C (dash dot line and filled circles) for the C5FNDIHS membrane in the acid form equilibrated with distilled water.

An alternative method to determine the resistance of the membranes is the Bode diagram [17] consisting in the plot of both the modulus of the impedance and $\tan^{-1}(Z''/Z')$ against frequency. According to (6),

$$\lim_{\omega \rightarrow 0} |Z^*(\omega)| = R_p + R_M; \quad \lim_{\omega \rightarrow 0} \tan^{-1} \left[\frac{Z''(\omega)}{Z'(\omega)} \right] = 0, \quad (8)$$

Illustrative Bode plots for the P5FNDIHS and C5FNDIHS membranes are plotted in Figures 9 and 10, respectively. The curves show that the modulus of the impedance undergoes a sharp decrease reaching a plateau whereas ϕ reaches

TABLE 2: Comparative and illustrative results for the ohmic resistance, R_M , and conductivity, σ , of the membranes at 30°C obtained from Nyquist and Bode diagrams.

Membrane	R_M (Nyquist), Ω	R_M (Bode), Ω	σ (Nyquist), S/m	σ (Bode), S/m
P5FNDIHS	1.79	1.70	2.13	2.24
C5FNDIHS	20.24	20.41	0.0135	0.0134

a maximum at the plateau. The resistance of the membrane is taken as the value of $|Z^*(\omega)|$ at the maximum of ϕ . It can be seen at very high frequencies that the modulus drops as a result of the fact that the capacitor in parallel with R_M governs the impedance of the circuit. The results obtained for R_M by the two methods are in rather good agreement. For examples the value of R_M for the P5FNDIHS membrane at 30°C estimated from Nyquist and Bode plots are, respectively, 1.79 and 1.70 Ω . These results are 20.24 and 20.41 Ω for the C5FNDIHS membrane (see Table 2). For consistency, the results of the Bode plots obtained for R_M will be used in the analysis below.

The resistance R_M of the membranes was measured at different temperatures and the corresponding conductivities were obtained by means of the familiar expression

$$\sigma = \frac{l}{R_0 S}, \quad (9)$$

where l and S are, respectively, thickness and area of the membrane in contact with the electrodes. For comparative purposes the values of the conductivity at 30°C are shown in Table 1. Illustrative Arrhenius plots showing the temperature dependence of the conductivity of the membranes obtained from the resistances of the membranes estimated from Bode plots are shown in Figure 11.

Figure 12 shows representative morphologies of the P5FNDIHS and C5FNDIHS membranes. The molecular chains of the latter membranes contain, respectively, 68% and 32% molar fractions of phenyl and 4-oxybenzenesulfonic acid, 2,3,5,6-tetrafluorophenyl moieties bonded to the dicarboximide side groups. It is expected that these moieties are mutually incompatible and therefore segregations occur giving rise to nanosize domains observed in the AMF of C5FNDIHS. It is worth noting that the AFM of P5FNDIHS suggests a much more homogeneous membrane surface than that of C5FNDIHS. Moreover, it is expected that the surface of the dry P5FNDIHS and C5FNDIHS membranes has significant surface fluorine content compared to the theoretical bulky fluorine content owing to the low-surface energy of the tetrafluorophenyl moieties which provide a thermodynamic-driving force for the self-assembly at the surface air-polymer interface [18, 19].

In spite of the high water uptake of the P5FNDIHS membrane, the moles of water per anionic fixed group in the membrane, λ , are of the same order as that reported for Nafion [20] and copolyimide acid membranes [21, 22]. However, it is surprising that the value of λ for the low IEC C5FNDIHS membrane is nearly four times that of the P5FNDIHS. This fact suggests that microphases separation in the latter membrane serves to compartmentalize an excess of water into the hydrophilic polar side chain domains,

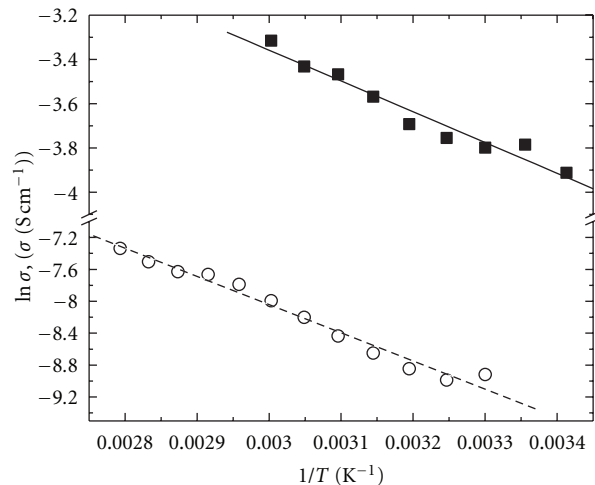


FIGURE 11: Arrhenius plot showing the temperature dependence of the P5FNDIHS (squares) and C5FNDIHS (circles) membranes.

specifically in the vicinity of the dicarboximide side groups. It is worth noting in this regard that apparently dried naphthalenic polyimides may contain up to 10% of water. Moreover, ^1H NMR experiments carried out on acidic naphthalenic polyimide membranes heated at 130°C under vacuum show peaks at 0.7–1 ppm corresponding to water associated with imide groups [23]. This water may be absorbed by the membranes during the NMR experiments handling.

An inspection of the dependence of the electromotive force on time for the C5FNDIHS and P5FNDIHS membranes shows that a certain time is required to reach a maximum value and then decreases as time increases. The *emf* of the concentration cell containing the former membrane falls to zero. The change is not so dramatic for the concentration cell with the P5FNDIHS membrane. The drop of t_+ to zero for the C5FNDIHS membrane at long times, even for dilute concentration solutions, suggests that the concentration of electrolyte equalizes in the two compartments of the concentration cell presumably as a consequence of strong electrolyte diffusion. The drop of t_+ with increasing concentration is not so dramatic for the P5FNDIHS membrane at low concentrations, but the decrease of the transport parameter is still significant. To explain this behavior the membranes can be viewed formed by hydrophilic pores to the walls of which anionic SO_3^- groups are anchored. These groups prevent the diffusion of coions across the pores and therefore hinder electrolyte diffusion thus increasing the transport number of counterions. The strong dependence of the counterion transport on electrolyte concentration suggests that the number of anionic fixed groups in the walls is not large enough to

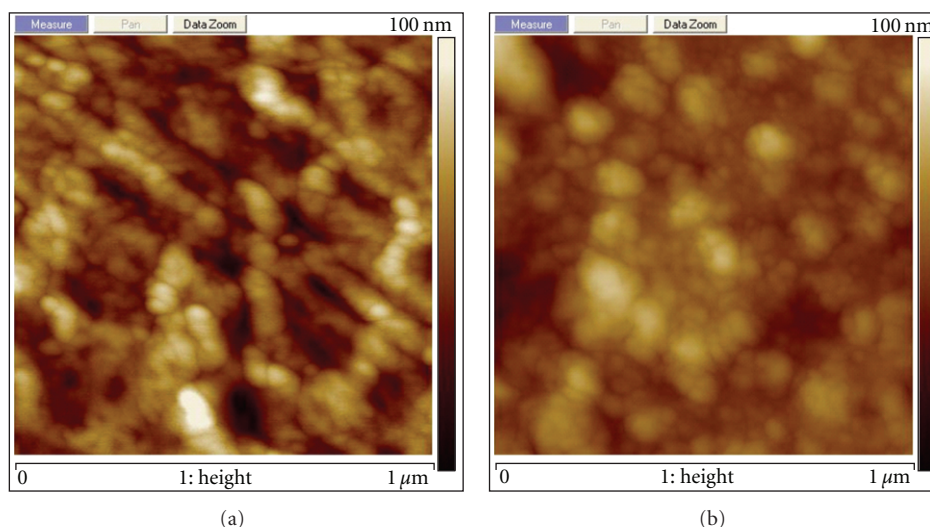


FIGURE 12: AFM topographic image for C5FNDIHS (a) and P5FNDIHS (b) membranes.

prevent ions diffusion across the membranes. As a result, electrolyte diffusion from the high- to the low-concentration compartment occurs, c_2/c_1 decreases, and the electromotive force of the concentration goes down. Owing to the rather high time necessary to reach a maximum and the rather high free ionic diffusion taking place in that period of time, the ratio a_2/a_1 presumably undergoes a significant decrease for the more concentrated solutions. Therefore, the *emf* at the maximum is the lower bound of this quantity and the transport number corresponding to the nominal values of c_2/c_1 should be higher than those obtained by means of (4).

The curves showing the variation of the transport number of protons with the geometrical average of the molality of the solutions flanking the membranes show that both membranes are ideally permselective for very dilute solutions, but the permselectivity undergoes a rather fast drop with increasing concentration. When the electrolyte solutions are flanking the membranes, protons in the concentrated HCl solution migrate to the side of the membrane facing the diluted HCl solution. Because fixed ions in the membrane hinder chloride anions transport across the membrane, the side of the membrane in contact with the concentrated HCl solution is negatively charged whereas that in contact with diluted HCl solution is positively charged. As a result an electric potential is created inside the membrane that drags the pore liquid positively charged toward the concentrated electrolyte solution compartment, enhancing the osmotic flow.

As the concentrations of the electrolyte solutions increase, chloride anions are not totally rejected by the fixed anions of the membrane, and diffusion of hydrochloric acid from the concentrated HCl solution compartment to the diluted HCl solution compartment occurs. Both the ionic diffusion across the membranes and the osmotic flow may be responsible for the low permselectivity of the membranes at high electrolyte solution concentration.

In an earlier work we carried out the synthesis of the nonfluorinated poly(*N*-phenyl-*exo-endo*-norbornene-5,6-dicarboximide) which underwent nonuniform sulfonation

of the phenyl groups by using acetyl sulfate as sulfonating agent [7]. The IEC of the membrane prepared from this ionic polynorbornene dicarboximide was 0.82 eq/Kg dry membrane and in spite of having a higher IEC, in comparison with that of the fluorine-containing C5FNDIHS membrane, the former membrane exhibited a water uptake of 0.124 Kg H₂O/Kg dry membrane, about one-third of the value in this latter obtained by titration; additionally, the conductivity of the sulfonated membrane equilibrated with water was 0.0414 S/m, of the same order of that found for the fluorine-containing C5FNDIHS membrane. These results suggest that the sulfonic acid groups have not relaxed the attractive interactions between phenyl groups and that molecular piling of the aromatic rings has taken place inhibiting the emergence of microphases separation in the non fluorinated membrane and therefore decreasing the storage of an excess of water into the polar side chain domains, specifically in the vicinity of the dicarboximide side groups. As it is seen, the chemical structure plays an important role in this kind of macromolecules since the more fluorine content in the polymer the more water uptake of the membrane. Indeed, an increase in the density of sulfonic acid affects directly the proportional transport properties in the membrane as it is shown in the fluorine-containing P5FNDIHS that exhibits the highest IEC, water uptake, and ionic conductivity of all the ionic polynorbornene dicarboximides we have discussed so far.

The conductivity of membranes with high water uptake is strongly dependent on the fixed ions concentration. Thus the P5FNDIHS membrane (average IEC = 1.90 eq/Kg dry membrane) exhibits a conductivity of 2.24 S/m, at 30°C, of the same order of that reported for high-conductivity acidic membranes and about two orders of magnitude higher than that of the C5FNDIHS membrane (average IEC = 0.245 eq/Kg dry membrane). Despite the low permselectivity of the membranes at high electrolyte solution concentration, the rather high level of ionic conductivity as well as water content seems promising for low-temperature fuel cell applications. Arrhenius plots representing the temperature

dependence of the membranes, presented in Figure 11, show that the activation of energy associated with proton transport across the P5FNDIHS membrane (11.7 ± 0.8 kJ/mol) is less than one half of that corresponding to the C5FNDIHS membrane (29.3 ± 1.6 kJ/mol).

The study of the mechanism governing proton transport in acidic ion-exchange membranes has drawn the attention of many researchers [24, 25]. *Ab initio* simulations suggest that the proton state in bulk water and in water clusters fluctuates between more localized hydronium ion-like states or Eigen ions and more delocalized H_5O_2^+ -like states or Zundel ions in such a way that forming and breaking hydrogen bonds in the neighborhood of the proton location (Grotthus like hopping) may be responsible for proton transport [26–30]. Proton diffusion involving this mechanism presumably takes place in high-conductivity membranes, such as, the P5FNDIHS membrane, is named structural diffusion. In low-conductivity membranes, such as, the C5FNDIHS membrane, water acts as a carrier of protons, and the transport is called vehicular diffusion.

4. Conclusions

The efficient segregation of hydrophilic from hydrophobic moieties, presumably favored by the low polarity of $\text{C}^{\text{ar}}-\text{F}$ bonds attached to the phenyl groups, gives rise to the formation of percolation paths responsible for the rather high proton conductivity of the homopolymeric membranes. The copolymeric membranes absorb an unusual quantity of water despite their low IEC. It seems that microphases separation in the membranes serves to compartmentalize an excess of water into the polar side chain domains, specifically in the vicinity of the dicarboximide side groups.

The electromotive force of the concentration cells undergoes a strong decrease at long times in the case of the homopolymeric membrane dropping to zero for the copolymeric membranes. The performance of the membranes in separation processes in diluted solutions is rather poor, unless the concentrations of the solutions at both sides of the membranes are continuously renewed.

Abbreviations

5FNDI:	<i>N</i> -pentafluorophenyl- <i>exo-endo</i> -norbornene-5,6-dicarboximide
<i>a</i> :	Activity coefficient of the electrolyte solution
AA:	Amic acid
C_1 :	Concentration of the solution in the diluted compartment
C_2 :	Concentration of the solution in the concentrated compartment
C5FNDI:	Poly(<i>N</i> -pentafluorophenyl-norbornene-5,6-dicarboximide- <i>co-N</i> -pentafluorophenyl-1- <i>exo-endo</i> -norbornene-5,6-dicarboximide)
C5FNDIH:	Hydrogenated copolymer
C5FNDIHS:	Copolymeric acid membrane
<i>emf</i> :	Electromotive force
<i>F</i> :	Faraday constant

IEC:	Ion exchange capacity
<i>l</i> :	Thickness of the membrane in contact with the electrodes
<i>m</i> :	Molality of the solution
m_d :	Weight of the dry membrane
m_w :	Weight of the membrane equilibrated with water
NDA:	Norbornene-5,6-dicarboxylic anhydride
P5FNDI:	Poly(<i>N</i> -pentafluorophenyl-norbornene-5,6-dicarboximide)
P5FNDIH:	Hydrogenated homopolymer
P5FNDIHS:	Homopolymeric acid membrane
PhNDI:	<i>N</i> -phenyl- <i>exo-endo</i> -norbornene-5,6-dicarboximide
ROMP:	Ring opening metathesis polymerization
R_M :	Ohmic resistance of the membrane to proton transport
<i>S</i> :	Area of the membrane in contact with the electrodes
T_{d1} :	Temperature of sulfonic group loss
T_{d2} :	Temperature of main chain decomposition
T_g :	Glass transition temperature
t_+ :	Number of equivalents of cations transported across the membrane by a Faraday of current
W_u :	Water uptake
Z^* :	Impedance of the circuit
Z_w^* :	The Warburg impedance
ϕ :	out-of-phase angle
λ :	Moles of water per anionic fixed group in the membrane
ν :	Total number of moles of ions
ρ :	Density of the membrane
σ :	Conductivity of the membrane in acid form
τ_+ :	Number of moles of cations transported across the membrane by a Faraday of current
ω :	Angular frequency of an alternating electric field.

Acknowledgments

The authors thank CONACYT-SEMARNAT, CONACYT-FORDECYT, and ICyTDF for generous support with contracts 23432, 116157, and 4312. The authors are grateful to Alejandrina Acosta, Carlos Flores Morales, and Miguel Ángel Canseco for their assistance in NMR, AFM, and thermal properties, respectively. This work was also supported by the CICYT through the Project MAT2011-29174-C02-02.

References

- [1] T. Sata, *Ion-Exchange Membranes*, RSC, Cambridge, UK, 2004.
- [2] T. Xu, "Ion exchange membranes: state of their development and perspective," *Journal of Membrane Science*, vol. 263, no. 1–2, pp. 1–29, 2005.
- [3] M. A. Hickner, H. Ghassemi, Y. S. Kim, B. R. Einsla, and J. E. McGrath, "Alternative polymer systems for proton exchange membranes (PEMs)," *Chemical Reviews*, vol. 104, no. 10, pp. 4587–4612, 2004.

- [4] A. P. Contreras, M. A. Tlenkopatchev, M. M. López-González, and E. Riande, "Synthesis and gas transport properties of new high glass transition temperature ring-opened polynorbornenes," *Macromolecules*, vol. 35, no. 12, pp. 4677–4684, 2002.
- [5] M. Tlenkopatchev, J. Vargas, M. A. Almaraz-Girón, M. López-González, and E. Riande, "Gas sorption in new fluorine containing polynorbornenes with imide side chain groups," *Macromolecules*, vol. 38, no. 7, pp. 2696–2703, 2005.
- [6] J. Vargas, A. A. Santiago, M. A. Tlenkopatchev, M. López-González, and E. Riande, "Gas transport in membranes based on polynorbornenes with fluorinated dicarboximide side moieties," *Journal of Membrane Science*, vol. 361, no. 1–2, pp. 78–88, 2010.
- [7] J. Vargas, A. A. Santiago, M. A. Tlenkopatchev et al., "Gas transport and ionic transport in membranes based on polynorbornenes with functionalized imide side groups," *Macromolecules*, vol. 40, no. 3, pp. 563–570, 2007.
- [8] A. A. Santiago, J. Vargas, S. Fomine, R. Gaviño, and M. A. Tlenkopatchev, "Polynorbornene with pentafluorophenyl imide side chain groups: synthesis and sulfonation," *Journal of Polymer Science A*, vol. 48, no. 13, pp. 2925–2933, 2010.
- [9] D. O'Hagan, "Understanding organofluorine chemistry. An introduction to the C-F bond," *Chemical Society Reviews*, vol. 37, no. 2, pp. 308–319, 2008.
- [10] Y. P. Yampol'skii, N. B. Bepalova, E. S. Finkel'shtein, V. I. Bondar, and A. V. Popov, "Synthesis, gas permeability, and gas sorption properties of fluorine-containing norbornene polymers," *Macromolecules*, vol. 27, no. 10, pp. 2872–2878, 1994.
- [11] A. A. Santiago, J. Vargas, J. Cruz-Gómez et al., "Synthesis and ionic transport of sulfonated ring-opened polynorbornene based copolymers," *Polymer*, vol. 52, no. 19, pp. 4208–4220, 2011.
- [12] V. Compañ, F. J. Fernández-Carretero, E. Riande, A. Linares, and J. L. Acosta, "Electrochemical properties of ion-exchange membranes based on sulfonated EPDM-polypropylene blends," *Journal of the Electrochemical Society*, vol. 154, no. 2, pp. B159–B164, 2007.
- [13] E. Barsoukov and J. R. Macdonalds, *Impedance Spectroscopy: Theory, Experiment and Applications*, chapter 2, Wiley, Hoboken, NJ, USA, 2nd edition, 2005.
- [14] H. Nyquist, "Thermal agitation of electric charge in conductors," *Physical Review*, vol. 32, no. 1, pp. 110–113, 1928.
- [15] E. Warburg, "About the behaviour of so-called impolarizable electrodes in the presence of alternating current," *Annals of Physics and Chemistry*, vol. 67, p. 493, 1899.
- [16] A. J. Bard and L. R. Faulkner, *Electrochemical Methods. Fundamentals and Applications*, section 10.3, Wiley, 2nd edition, 2001.
- [17] W. W. Bode, *Network Analysis in Feedback Amplifier Design*, Van Nostrand, Princeton, NJ, USA, 1956.
- [18] S. Wu, *Polymer Interface and Adhesion*, chapter 5, Marcel Dekker, New York, NY, USA, 1982.
- [19] H. Ghassemi, J. E. McGrath, and T. A. Zawodzinski Jr., "Multiblock sulfonated-fluorinated poly(arylene ether)s for a proton exchange membrane fuel cell," *Polymer*, vol. 47, no. 11, pp. 4132–4139, 2006.
- [20] R. O'Hayre, S.-W. Cha, W. Colella, and F. B. Prinz, *Fuel Cell Fundamentals*, chapter 4, Wiley & Sons, New York, NY, USA, 2006.
- [21] X. Guo, F. Zhai, J. Fang, M. F. Heras-Laguna, M. López-González, and E. Riande, "Permeability and conductivity of membranes based on sulfonated naphthalenic copolyimides," *Journal of Physical Chemistry B*, vol. 111, p. 13694, 2007.
- [22] S. Yuan, C. del Rio, M. López-González, X. Guo, J. Fang, and E. Riande, "Impedance spectroscopy and performance of cross-linked new naphthalenic polyimide acid membranes," *Journal of Physical Chemistry C*, vol. 114, no. 51, pp. 22773–22782, 2010.
- [23] L. Garrido, J. Pozuelo, M. López-González, J. Fang, and E. Riande, "Simulation and experimental studies on proton diffusion in polyelectrolytes based on sulfonated naphthalenic copolyimides," *Macromolecules*, vol. 42, no. 17, pp. 6572–6580, 2009.
- [24] S. J. Paddison, "Proton conduction mechanisms at low degrees of hydration in sulfonic acid-based polymer electrolyte membranes," *Annual Review of Materials Research*, vol. 33, pp. 289–319, 2003.
- [25] K. D. Kreuer, S. J. Paddison, E. Spohr, and M. Schuster, "Transport in proton conductors for fuel-cell applications: simulations, elementary reactions, and phenomenology," *Chemical Reviews*, vol. 104, no. 10, pp. 4637–4678, 2004.
- [26] M. Tuckerman, K. Laasonen, M. Sprik, and M. Parrinello, "Ab initio molecular dynamics simulation of the solvation and transport of hydronium and hydroxyl ions in water," *The Journal of Chemical Physics*, vol. 103, no. 1, pp. 150–161, 1995.
- [27] M. Tuckerman, K. Laasonen, M. Sprik, and M. Parrinello, "Ab initio molecular dynamics simulation of the solvation and transport of H_3O^+ and OH^- ions in water," *Journal of Physical Chemistry*, vol. 99, p. 5749, 1995.
- [28] M. E. Tuckerman, D. Marx, M. L. Klein, and M. Parrinello, "On the quantum nature of the shared proton in hydrogen bonds," *Science*, vol. 275, no. 5301, pp. 817–820, 1997.
- [29] D. Marx, M. E. Tuckerman, J. Hutter, and M. Parrinello, "The nature of the hydrated excess proton in water," *Nature*, vol. 397, no. 6720, pp. 601–604, 1999.
- [30] D. Marx, M. Tuckerman, and M. Parrinello, "Solvated excess protons in water: quantum effects on the hydration structure," *Journal of Physics*, vol. 12, no. 8, pp. A153–A159, 2000.

Research Article

Measurement of Membrane Characteristics Using the Phenomenological Equation and the Overall Mass Transport Equation in Ion-Exchange Membrane Electrodialysis of Saline Water

Yoshinobu Tanaka

IEM Research, 1-46-3 Kamiya, Ushiku-shi, Ibaraki 300-1216, Japan

Correspondence should be addressed to Yoshinobu Tanaka, fwis1202@mb.infoweb.ne.jp

Received 6 November 2011; Accepted 18 January 2012

Academic Editor: Seung Hyeon Moon

Copyright © 2012 Yoshinobu Tanaka. This is an open access article distributed under the Creative Commons Attribution License, which permits unrestricted use, distribution, and reproduction in any medium, provided the original work is properly cited.

The overall membrane pair characteristics included in the overall mass transport equation are understandable using the phenomenological equations expressed in the irreversible thermodynamics. In this investigation, the overall membrane pair characteristics (overall transport number λ , overall solute permeability μ , overall electro-osmotic permeability ϕ and overall hydraulic permeability ρ) were measured by seawater electrodialysis changing current density, temperature and salt concentration, and it was found that μ occasionally takes minus value. For understanding the above phenomenon, new concept of the overall concentration reflection coefficient σ^* is introduced from the phenomenological equation. This is the aim of this investigation. σ^* is defined for describing the permselectivity between solutes and water molecules in the electrodialysis system just after an electric current interruption. σ^* is expressed by the function of μ and ρ . σ^* is generally larger than 1 and μ is positive, but occasionally σ^* becomes less than 1 and μ becomes negative. Negative μ means that ions are transferred with water molecules (solvent) from desalting cells toward concentrating cells just after an electric current interruption, indicating up-hill transport or coupled transport between water molecules and solutes.

1. Introduction

Mass transport across the membrane must be discussed fundamentally on the basis of the thermodynamics because the thermodynamics describes the rule of energy changes inevitably generating in the mass transport. However, the classical thermodynamics discusses only reversible phenomena and it does not treat transport rate. The irreversible thermodynamics came to succeed in discussing the transport rate by introducing the concept of “time” in its system [1–4]. Basic theory of the irreversible thermodynamics is established on the assumption of “microscopic irreversibility” [5–7]. This assumption holds more strictly in the circumstance being more close to equilibrium states. The actual electrodialysis process is not formed in the equilibrium states, so that the irreversible thermodynamics is assumed to exhibit only approximated meaning in the

electrodialysis system. However, the irreversible thermodynamics is considered to be applicable in the circumstances being apart to some extent from equilibrium states [8, 9]. The irreversible thermodynamics is the fundamental rule of mass transport and it is expressed by the functions including phenomenological coefficients. On the other hand, the performance of an electrodialyzer is expressed by the functions including parameters such as electrodialysis conditions and process specifications. These parameters cannot be discussed directly based on the irreversible thermodynamics. In the previous investigation, the overall mass transport equation was related to the irreversible thermodynamics and developed for analyzing the performance of an electrodialyzer [10]. It was successfully employed in the computer simulation of an electrodialysis process [11–13]. The overall mass transport equation includes the parameters such as the overall transport number λ , the overall solute permeability

μ , the overall electro-osmotic permeability ϕ , and the overall hydraulic permeability ρ . Among these parameters, μ is very small values and further in some cases, μ was found to take negative values. In such cases, μ has been conventionally neglected by setting $\mu = 0$. The aim of this investigation is to establish reasonable explanation of the negative μ . For understanding this phenomenon, the concept of the overall concentration reflection coefficient σ^* [10] must be supplied.

2. Theoretical

2.1. Phenomenological Equation and Overall Mass Transport Equation. When two kinds of ions are transported with solvent in a solution, their fluxes influence each other, because the fluxes and driving forces are not independent and coupled together. The interactions are presented in the irreversible thermodynamics. Kedem and Katchalsky introduced the following phenomenological equation expressing the electric current I , volume flow of a solution J and mass flux of component i ; J_i in a membrane system [14],

$$\begin{aligned} I &= L_E \Delta\psi + L_{EP} \Delta P + \sum_i L_{Ei} \Delta\mu_i, \\ J &= L_{PE} \Delta\psi + L_P \Delta P + \sum_i L_{Pi} \Delta\mu_i, \\ J_i &= L_{iE} \Delta\psi + L_{iP} \Delta P + \sum_k L_{ik} \Delta\mu_k \end{aligned} \quad (1)$$

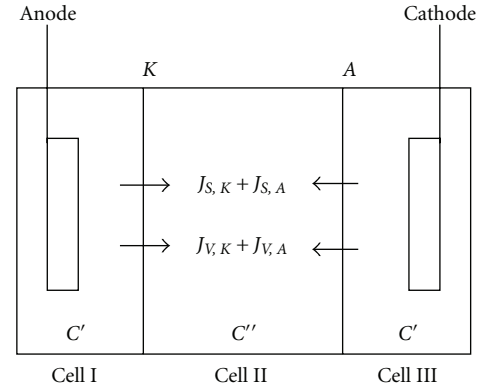
$\Delta\psi$ is a potential difference, ΔP is a pressure difference, and $\Delta\mu_i$ is a chemical potential difference across the membrane. House [15] discussed an electrokinetic phenomenon based on the approaches of Kedem and Katchalsky [14]. Referring to this suggestion, Schultz discussed the principle of salt and solvent (water) transport in a two-cell electrodialysis system (cell I and cell II) incorporated with a cation-exchange membrane and introduced the following equations expressing the flux of solutes $J_{S,K}$ and a solution $J_{V,K}$ across the membrane [16],

$$\begin{aligned} J_{S,K} &= t_K \frac{i}{F} + \{\omega_K - L_{P,K} \sigma_K (1 - \sigma_K) C_S^*\} RT \Delta C_S, \\ J_{V,K} &= \beta_K i - \sigma_K L_{P,K} RT \Delta C_S \end{aligned} \quad (2)$$

in which t is the transport number, ω is the solute permeability, β is the electro-osmotic permeability, L_P is the hydraulic permeability, σ_K is the reflection coefficient of the cation-exchange membrane, and these phenomenological coefficients are membrane characteristics. R is the gas constant, F is the Faraday constant, and T is the absolute temperature. $\Delta C_S = (C_S^{\text{II}} - C_S^{\text{I}})$ is salt concentration difference between cell II and cell I. C_S^* is the logarithmic mean concentration across the membrane defined by

$$C_S^* = \frac{\Delta C_S}{\ln(C_S^{\text{II}}/C_S^{\text{I}})}. \quad (3)$$

The principle of separating salt from water is introduced based on the theory mentioned above using a three-cell



K: Cation-exchange membrane
A: Anion-exchange membrane

FIGURE 1: Three-cell electrodialysis system.

electrodialysis system (Figure 1). The system consists of a central cell (cell II) and electrode cells (cell I and cell III) placed on both outsides of cell II. A cation-exchange membrane (K) is placed between cell I and cell II, and an anion-exchange membrane (A) is placed between cell II and cell III. Supplying a salt solution into cell I and cell III, constant current density i is applied and a salt solution being collected in cell II is taken out from the system until the salt concentration in cell II reaches steady constant. Salt accumulation $J_{S,K} + J_{S,A}$ and solution accumulation $J_{V,K} + J_{V,A}$ in cell II in the steady state are given by the following equation introduced from (2) [10]:

$$\begin{aligned} J_{S,K} + J_{S,A} &= (t_K + t_A - 1) \frac{i}{F} - RT \\ &\times [(\omega_K + \omega_A) - \{L_{P,K} \sigma_K (1 - \sigma_K) \\ &\quad + L_{P,A} \sigma_A (1 - \sigma_A)\} C_S^*] \Delta C, \\ J_{V,K} + J_{V,A} &= (\beta_K + \beta_A) i + RT (\sigma_K L_{P,K} + \sigma_A L_{P,A}) \Delta C. \end{aligned} \quad (4)$$

Here, we put $\Delta C = C'' - C' = \Delta C_S$. t_K and t_A are transport number of counter ions of a cation- and an anion-exchange membrane respectively. Subscripts K and A denote a cation- and an anion-exchange membrane. Superscripts ' and ' ' denote desalting sides (cells I and III) and a concentrating side (cell II), respectively. C_S^* is logarithmic mean concentration defined by (3).

The overall mass transport equation was developed from electrodialysis experiments as described in Section 3 experiment. Namely, a strong electrolyte solution is supplied to an electrodialyzer illustrated in Figure 2 keeping the linear solution velocities in desalting cells to be constant. Passing a constant electric current i (A/cm²) through electrodes, concentrate is extracted from concentrating cells. After the electrolyte concentration reaches constant (C''), salt concentration in desalting cells (C' (equiv./cm³), ion flux J_S (equiv./cm²s) and volume flux J_V (cm³/cm²s) transported across a membrane pair are measured. Plotting J_S/i and J_V/i against $(C'' - C')/i = \Delta C/i$ creates linear lines as exemplified

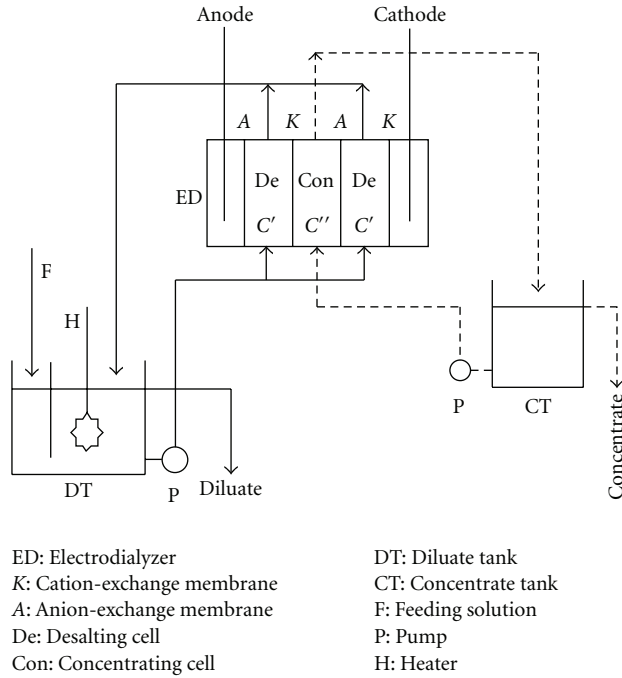


FIGURE 2: Electrodesialysis process.

in Figures 3 and 4. These lines are expressed by the following overall mass transport equation [10]:

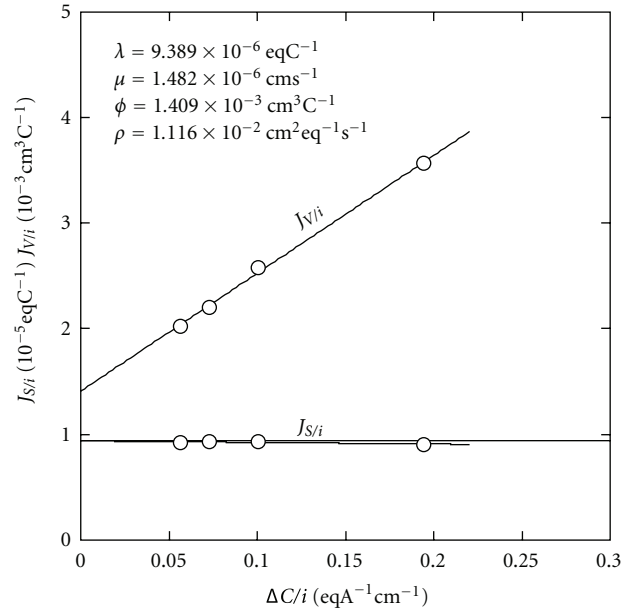
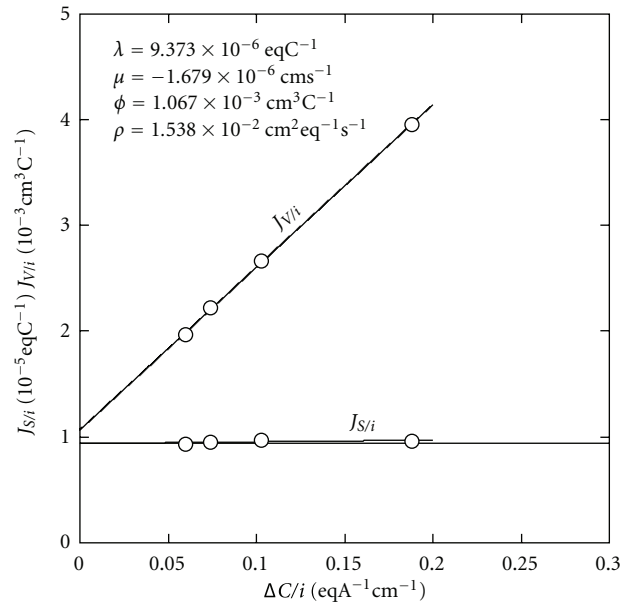
$$J_S = C'' J_V = \lambda i - \mu(C'' - C') = \lambda i - \mu \Delta C, \quad (5)$$

$$J_V = \phi i + \rho(C'' - C') = \phi i + \rho \Delta C, \quad (6)$$

in which λ (eqC^{-1}) is the overall transport number, μ (cm s^{-1}) is the overall solute permeability, ϕ ($\text{cm}^3 \text{C}^{-1}$) is the overall electro-osmotic permeability, and ρ ($\text{cm}^4 \text{eq}^{-1} \text{s}^{-1}$) is the overall hydraulic permeability. These parameters are termed the overall membrane pair characteristics and they are measured easily from the intercepts and gradients of the linear lines. The term "overall" means that the coefficients express the contributions of a cation- and an anion-exchange membrane. It means also that the coefficients express the contributions of many types of ions dissolving in a strong electrolyte solution. Terms λi and $\mu \Delta C$ in (5) stand for migration and diffusion of ions. Terms ϕi and $\rho \Delta C$ in (6) correspond to electro-osmosis and hydraulic osmosis of a solution. Osmosis refers to the movement of solvent in the original definition. However, the osmosis referred in (6) consists of the osmotic flow of solvent and of the volume flow associated with solutes.

The overall mass transport equation does not hold in the equilibrium state because it was developed from saline water electrodesialysis experiments. It describes the mass transport in the nonequilibrium state. It is conceptually simple and available for discussing electrodesialysis phenomena without contradictions.

In the electrodesialysis experiments, the solutions supplied to desalting cells are mixed vigorously by spacers integrated. Thus, the boundary layer effects on the membrane surfaces

FIGURE 3: J_S/i versus $\Delta C/i$ plot and J_V/i versus $\Delta C/i$ plot. Selemion CMR/ASR 25°C.FIGURE 4: J_S/i versus $\Delta C/i$ plot and J_V/i versus $\Delta C/i$ plot. Neosepta CIM/ACS3 35°C.

are assumed to be negligible. The influence of concentration polarization on the overall membrane pair characteristics were discussed in the previous investigation [10] and concluded that the membrane pair characteristics are not influenced by the concentration polarization.

2.2. Overall Membrane Pair Characteristics and Phenomenological Coefficients. The overall mass transport equation ((5)

and (6)) is substantially identical to the phenomenological equation expressed in irreversible thermodynamics (4):

$$\begin{aligned} J_S &= J_{S,K} + J_{S,A}, \\ J_V &= J_{V,K} + J_{V,A}. \end{aligned} \quad (7)$$

From (7), the overall membrane pair characteristics λ , μ , ϕ and ρ are presented by the functions of the membrane characteristics defined in the phenomenological equation as follows:

$$\lambda = \frac{t_K + t_A - 1}{F} = \left(\frac{J_S}{i} \right)_{\Delta C=0} \quad (8)$$

$$\begin{aligned} \mu &= RT[(\omega_K + \omega_A) \\ &\quad - \{L_{P,K}\sigma_K(1 - \sigma_K) + L_{P,A}\sigma_A(1 - \sigma_A)\}C_S^*] \\ &= RT[(\omega_K + \omega_A) - \sigma(1 - \sigma)(L_{P,K} + L_{P,A})C_S^*] \\ &= \left(\frac{J_S}{\Delta C} \right)_{i=0}, \end{aligned} \quad (9)$$

$$\phi = \beta_K + \beta_A = \left(\frac{J_V}{i} \right)_{\Delta C=0}, \quad (10)$$

$$\begin{aligned} \rho &= RT(\sigma_K L_{P,K} + \sigma_A L_{P,A}), \\ &= RT\sigma(L_{P,K} + L_{P,A}) = \left(\frac{J_V}{\Delta C} \right)_{i=0}. \end{aligned} \quad (11)$$

Here, σ_K and σ_A are reflection coefficients of a cation- and an anion-exchange membrane respectively ((18) and (19)). σ expresses the contributions of a cation- and an anion-exchange membrane, so it is termed the overall reflection coefficient (Equation (20)) and it is introduced as follows. From (9):

$$\sigma(1 - \sigma) = \frac{L_{P,K}\sigma_K(1 - \sigma_K) + L_{P,A}\sigma_A(1 - \sigma_A)}{L_{P,K} + L_{P,A}}. \quad (12)$$

From (11),

$$\sigma = \frac{\sigma_K L_{P,K} + \sigma_A L_{P,A}}{L_{P,K} + L_{P,A}}. \quad (13)$$

From (12) and (13),

$$\sigma = \frac{L_{P,K}\sigma_K^2 + L_{P,A}\sigma_A^2}{L_{P,K}\sigma_K + L_{P,A}\sigma_A}, \quad (14)$$

when $\sigma_K = 0, \sigma = \sigma_A$
 when $\sigma_A = 0, \sigma = \sigma_K$
 when $\sigma_K = \sigma_A = 1, \sigma = 1$.

2.3. Reflection Coefficient. Equations (8)–(11) show that σ_K and σ_A appear in μ and ρ , and disappear in λ and ϕ . These events and (5) and (6) suggest that σ_K and σ_A do not exert an influence on electric current-driven mass transport, that is, migration and electro-osmosis. Reflection coefficient is a parameter indicating the permselectivity between solutes and solvent passing through the membrane. It is essentially the concept developed in pressure-driven dialysis. This phenomenon is conceivable in electrodialysis,

but the concept developed in pressure dialysis is not directly applicable to the phenomenon in electrodialysis. In order to understand the behavior of the reflection coefficient in an electrodialysis process, it is necessary to establish a concept of zero current density. In other words, it is reasonable to image the electric current interruption (switch off) for a moment in the electrodialysis process operating under a constant electric current, and assume the disappearance of the migration and electro-osmosis in this moment. Here, we assume further that solute diffusion and hydraulic osmosis remain as they are just after the electric current interruption [10].

In order to discuss the behavior of the reflection coefficient in an electrodialysis process, we express the volume flow J_V and exchange flow J_D in an ion-exchange membrane pair by the following equations introduced by Schloegel [17]:

$$\begin{aligned} J_V &= (L_{P,K} + L_{P,A})\Delta P \\ &\quad + (L_{PD,K} + L_{PD,A})RT\Delta C = \left(\frac{J_S}{C_S^*} \right) + \left(\frac{J_W}{C_W^*} \right), \end{aligned} \quad (15)$$

$$\begin{aligned} J_D &= (L_{DP,K} + L_{DP,A})\Delta P \\ &\quad + (L_{D,K} + L_{D,A})RT\Delta C = \left(\frac{J_S}{C_S^*} \right) - \left(\frac{J_W}{C_W^*} \right), \end{aligned} \quad (16)$$

ΔP and ΔC are pressure difference and concentration difference across the membrane, respectively. L_P is the hydraulic conductivity and L_D is the exchange flow parameter. L_{PD} is the osmotic volume flow coefficient and L_{DP} is the ultrafiltration coefficient. J_W is the flux of water molecules. C_S^* and C_W^* are respectively, logarithmic mean concentration (3) of solutes and water (solvent) between a desalting cell and a concentrating cell. It should be noticed that (15) and (16) are originally defined in the pressure-driven transport (pressure dialysis) of neutral species with no electric current. Equation (15) presents the sum of the solute flux J_S and solvent flux J_W , while (16) shows the difference between J_S and J_W . It should be added that (6) expresses the solution flux J_V and not expresses the solvent flux J_W .

In a pressure-driven process, putting $\Delta C = 0$ in (15) and (16) introduces the following equation applicable to pressure dialysis:

$$\begin{aligned} (J_V)_{\Delta C=0} &= (L_{P,K} + L_{P,A})\Delta P, \\ (J_D)_{\Delta C=0} &= (L_{DP,K} + L_{DP,A})\Delta P, \end{aligned} \quad (17)$$

σ_K and σ_A included in (4) are defined by Staverman [18] and Kedem-Katchalsky [19] as follows:

$$\sigma_K = - \left(\frac{J_{D,K}}{J_{V,K}} \right)_{\Delta C=0} = - \left(\frac{L_{DP,K}}{L_{P,K}} \right), \quad (18)$$

$$\sigma_A = - \left(\frac{J_{D,A}}{J_{V,A}} \right)_{\Delta C=0} = - \left(\frac{L_{DP,A}}{L_{P,A}} \right). \quad (19)$$

We define the overall reflection coefficient σ (14) using (18) and (19):

$$\sigma = - \left(\frac{J_D}{J_V} \right)_{\Delta C=0} = - \frac{L_{DP,K} + L_{DP,A}}{L_{P,K} + L_{P,A}}. \quad (20)$$

σ given in (20) is the reflection coefficient defined in the pressure-driven dialysis. Here, we term σ “overall pressure reflection coefficient,” because it is the membrane pair characteristic and reflects pressure difference ΔP -driven phenomenon.

σ given in (18)–(20) defines the permselectivity between water (solvent) and solutes and it is originally established in pressure-dialysis. For understanding the permselectivity between water and solutes (ions) in electrodialysis, σ is fundamentally inapplicable. The permselectivity between water and ions in electrodialysis must be explained on the basis of σ^* (overall concentration reflection coefficient) described below.

In the electrodialysis process, ΔP is relatively low and negligible, and just after an electric current interruption (switch off), ΔC remains as it is. Putting $\Delta P = 0$ in (15) and (16) introduces the following equations applicable to electrodialysis:

$$\begin{aligned} (J_V)_{\Delta P=0} &= (L_{PD,K} + L_{PD,A})RT\Delta C, \\ (J_D)_{\Delta P=0} &= (L_{D,K} + L_{D,A})RT\Delta C. \end{aligned} \quad (21)$$

We define here another reflection coefficient σ^* introduced from (21) and generated just after an electric current interruption as follows:

$$\sigma^* = -\left(\frac{J_D}{J_V}\right)_{\Delta P=0} = -\frac{L_{D,K} + L_{D,A}}{L_{PD,K} + L_{PD,A}}. \quad (22)$$

σ^* (22) is the reflection coefficient defined in electrodialysis, and it is termed “the overall concentration reflection coefficient” because it reflects a concentration difference ΔC -driven phenomenon.

Koter [20] suggests that the Onsager reciprocity [5, 6] is not satisfied and the relationship between L_{PD} and L_{DP} depends on the concentration difference across the membrane. One example for Nafion 417 in NaCl/H₂O at $C''/C' = 2$ is $L_{DP}/L_{PD} = 0.40$. Thus, the reciprocal equation is presented as follows:

$$L_{DP,K} + L_{DP,A} = k(L_{PD,K} + L_{PD,A}) \quad k \neq 1, \quad (23)$$

in which, k is defined as the Onsager reciprocity coefficient. From (20), (22), and (23):

$$\sigma\sigma^* = k \frac{L_{D,K} + L_{D,A}}{L_{P,K} + L_{P,A}}. \quad (24)$$

Cancelling, J_W/C_W^* in (15) and (16):

$$J_D = 2 \frac{J_S}{C_S^*} - J_V. \quad (25)$$

From (22) and (25),

$$\sigma^* = 1 - 2 \left(\frac{1}{C_S^*} \right) \left(\frac{J_S}{J_V} \right)_{\Delta P=0}. \quad (26)$$

σ^* presented in (26) gives the permselectivity between ions and water molecules just after an electric current interruption. J_S and J_V are expressed as the following equations

just after an electric current interruption by putting $i = 0$ in (5) and (6):

$$\begin{aligned} J_S &= -\mu(C'' - C'), \\ J_V &= \rho(C'' - C'). \end{aligned} \quad (27)$$

Substituting (27) into (26):

$$\sigma^* = 1 + 2 \left(\frac{\mu}{\rho} \right) \left(\frac{1}{C_S^*} \right). \quad (28)$$

2.4. Membrane Characteristics. Yamauchi and Yasuko Tanaka [21] measured σ_K , $L_{P,K}$, and ω_K of a cation-exchange membrane (Neosepta CL-25T, Tokuyama Soda Co. Ltd.) by means of pressure-driven dialysis of a KCl solution and found σ_K to be unity. This phenomenon means that K⁺ ions do not pass through the cation-exchange membrane due to the Donnan exclusion of co-ions (Cl[−] ions). σ_K and σ_A included in (9), (11) and (14) are equivalent to σ_K measured in the above experiment. So, (8)–(11) are simplified as follows by substituting $\sigma_K = \sigma_A = 1$ in (9), (11), and (14):

$$t_K + t_A = \lambda F + 1, \quad (29)$$

$$\omega_K + \omega_A = \frac{\mu}{RT}, \quad (30)$$

$$\beta_K + \beta_A = \phi, \quad (31)$$

$$L_{P,K} + L_{P,A} = \frac{\rho}{RT}. \quad (32)$$

Putting $\sigma = 1$ in (20),

$$L_{DP,K} + L_{DP,A} = L_{P,K} + L_{P,A}. \quad (33)$$

From (24) and (32),

$$k(K_{D,K} + L_{D,A}) = \frac{\rho\sigma^*}{RT} = (L_{P,K} + L_{P,A})\sigma^*. \quad (34)$$

3. Experimental

3.1. Electrodialysis 1. The following commercially available ion-exchange membranes were integrated into an electro-dialyzer ED and formed an electrodialysis system [22] as illustrated in Figure 2.

Aciplex K172/A172, Asahi Chemical Co.

Selemion CMV/ASR, Asahi Glass Co.

Neosepta CIMS/ACS3, Tokuyama Inco.

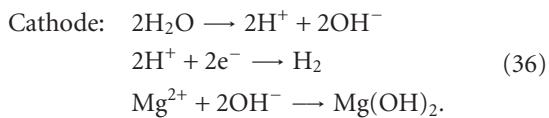
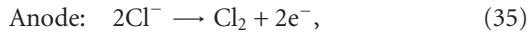
The specifications of the membranes are listed in Table 1. The effective membrane area was maintained to 1.72 dm² (18 cm length, 10 cm width). The flow-pass thickness in a desalting and a concentrating cell was 0.075 cm. Number of cell pairs was 9. Seawater was supplied into the diluate tank DT, then it was supplied to desalting cells De at a linear velocity of 5 cm/s keeping temperature to 25, 35, 50, or 60°C. Passing a constant electric current through the Ti/Pt-anode

TABLE 1: Specifications of ion-exchange membranes.

		Thickness mm	Electric resistance $\Omega \text{ cm}^2$	Transport number	Exchange capacity meq/dry memb.	Water content %	Intensity kg/cm^2
Aciplex	K172	0.11–0.13	1.9–2.2	> 0.99	1.5–1.6	20–30	2.6–3.3
	A172	0.11–0.15	1.7–2.1	>0.99	1.8–1.9	24–25	2.2–3.0
	CK2	0.23	3.3	0.91			
	CA3	0.09–0.12	1.5–2.0				1.3–2.0
Selemin	CMR	0.11	2.36	0.94	3.7	34	2.0
	ASR	0.11	1.80	0.96	3.5	33	2.0
	CMV2	0.11–0.15	2.0–3.5	>0.91	1.5–1.8	18–20	3–5
	AST	0.11–0.13	1.5–2.5	>0.95			1.5–2.5
Neosepta	CIMS	0.14–0.17	1.5–1.6	>0.98	2.2–2.5	30–35	3.1–4.1
	ACS3	0.09–0.12	1.5–2.0	>0.98	2.0–2.4	20–30	1.3–2.0
	CL25T	0.15–0.17	2.2–3.0	>0.98	1.5–1.8	25–35	3–5
	AVS4T	0.15–0.17	3.7–4.7	>0.98	1.5–2.0	25–30	4–6

and stainless (SUS 304) cathode, concentrate was extracted from concentrating cells. Confirming the salt concentration of the concentrate to be stable, diluate and concentrate were sampled. Electrodialysis was repeated changing current density incrementally.

In Figure 2, partition cells were incorporated between the desalting cells and electrode cells and seawater was supplied to the partition cells for preventing the influence of electrode reactions to the performance of electrodialysis. Seawater was also supplied to the electrode cells. The electrode reactions are as follows:



An HCl solution was supplied to the cathode cell to dissolve $\text{Mg}(\text{OH})_2$.

3.2. Electrodialysis 2. The following commercially available membranes were integrated into an electrodialyzer [10] similar to the unit in Figure 2: Aciplex CK2/CA3, Selemin CMV2/AST, Neosepta CL25T/AVS4T.

The specifications of the membranes are listed in Table 1. The effective membrane area was 5 dm^2 (25 cm length, 20 cm width). The flow-pass thickness in a desalting cell and concentrating cell was 0.12 cm. Number of cell pairs was 10. Diluted seawater (0.294 eq/dm^3), seawater (0.577 eq/dm^3), and concentrated seawater (1.131 and 1.920 eq/dm^3) were supplied into the diluate tank DT, then it was supplied to desalting cells De at a linear velocity of 5 cm/s keeping temperature to 29°C . Passing a constant electric current through graphite-stainless electrodes, concentrate was extracted from concentrating cells. Diluate and concentrate were sampled and electrodialysis was repeated changing current density step by step as described in the electrodialysis 1.

3.3. Chemical Analysis. Concentration (eq/dm^3) of K^+ , Mg^{2+} , Ca^{2+} , Cl^- , and SO_4^{2-} ions in diluate and concentrate were analyzed. In seawater electrodialysis, total salt concentration C is given as $C = C_{\text{Na}} + C_{\text{K}} + C_{\text{Mg}} + C_{\text{Ca}} = C_{\text{Cl}} + C_{\text{SO}_4}$. So, sodium ion concentration is given by $C_{\text{Na}} = C_{\text{Cl}} + C_{\text{SO}_4} - C_{\text{K}} - C_{\text{Ca}} - C_{\text{Mg}}$.

4. Results and Discussion

4.1. Overall Mass Transport Equation and Overall Membrane Pair Characteristics; λ , μ , ϕ and ρ . J_s/i and J_v/i are plotted against $\Delta C/i$ and exemplified in Figures 3 and 4. From these plots, overall transport number λ , overall solute permeability μ , overall electro-osmotic permeability ϕ , and overall hydraulic permeability ρ are calculated as shown in the figures. The gradient of J_s/i versus $\Delta C/i$ is usually negative, so μ is positive (Figure 3). However, the gradient occasionally gives positive, so μ becomes negative (Figure 4). μ values of the commercially available membranes are generally very small due to the Donnan exclusion of the membranes against co-ions and their dense structure. Using the overall mass transport equation, μ can be detected from the above gradients. Overall membrane pair characteristics observed in this investigation are listed in Table 2. μ values of the Neosepta CIMS/ACS3 membranes (Electrodialysis 1) and the Selemin CMV2/AST membranes (Electrodialysis 2) are found to be negative.

4.2. Membrane Characteristics t , ω , β , and L_P . Substituting λ , μ , ϕ , and ρ into (29)–(32), membrane characteristics (phenomenological coefficients) such as transport number $t_K + t_A$, solute permeability $\omega_K + \omega_A$, electro-osmotic permeability $\beta_K + \beta_A$, and hydraulic conductivity $L_{P,K} + L_{P,A}$ are calculated. $L_{DP,K} + L_{DP,A}$ is equivalent to $L_{P,K} + L_{P,A}$ as defined in (33).

Figures 5–8 show the relationship between temperature T and the membrane characteristics obtained in Section 2.1 Electrodialysis 1. It is seen that $L_{P,K} + L_{P,A}$ increases

TABLE 2: Overall membrane pair characteristics.

(a) Electrodialysis 1.

Ion-exchange membrane	Temp. °C	$\lambda \times 10^6$ eq/C	$\mu \times 10^6$ cm/s	$\phi \times 10^3$ cm/C	$\rho \times 10^2$ cm ⁴ /eq s
Aciplex K172/A172	25	9.724	1.434	1.403	1.218
	35	9.736	1.289	1.370	1.626
	50	9.972	4.515	1.542	1.996
	60	9.692	2.123	1.405	2.765
Selemion CMR/ASR	25	9.389	1.482	1.409	1.116
	35	9.422	2.421	1.501	1.377
	50	9.475	3.614	1.563	1.937
	60	9.583	5.103	1.621	2.380
Neosepta CIMS/ACS3	25	9.349	-1.055	1.004	1.254
	35	9.373	-1.679	1.067	1.538
	50	9.459	-1.239	1.067	1.835
	60	9.547	-0.561	1.405	2.059

(b) Electrodialysis 2.

Ion-exchange membrane	Conc. eq/dm ³	$\lambda \times 10^6$ eq/C	$\mu \times 10^6$ cm/s	$\phi \times 10^3$ cm ³ /C	$\rho \times 10^2$ cm ⁴ /eq s
Aciplex CK2/CA3	0.294	9.482	6.028	1.699	1.226
	0.576	9.407	8.570	1.619	1.234
	1.131	8.970	6.977	1.514	1.280
	1.920	8.953	9.690	1.367	1.387
Selemion CMV2/AST	0.294	9.055	-1.443	1.294	5.945
	0.577	9.371	-0.731	1.316	5.787
	1.131	9.389	-0.424	1.296	5.893
	1.921	9.139	0.850	1.193	6.371
Neosepta CL25T/AVS4T	0.294	9.584	1.458	1.513	6.354
	0.577	9.633	3.208	1.394	6.788
	1.132	9.228	0.908	1.304	7.566
	1.920	9.269	3.575	1.254	7.691

apparently with T . $\omega_K + \omega_A$ and $\beta_K + \beta_A$ increase slightly with T . $t_K + t_A$ is not influenced by T . $\omega_K + \omega_A$ for Neosepta CIMS/ACS3 membranes is negative (Figure 6) because $\mu < 0$ (Table 2).

Figures 9–12 show the relationships between salt concentrations in desalting cells C' and membrane characteristics obtained in Section 2.2 Electrodialysis 2. $\beta_K + \beta_A$ decreases and $L_{P,K} + L_{P,A}$ increases to some extent with the increase of C' . $t_K + t_A$ is not influenced by C' . $\omega_K + \omega_A$ increases slightly with C' and it takes negative for Selemion CMV2/AST membranes (Figure 10) due to $\mu < 0$ (Table 2).

4.3. Overall Concentration Reflection Coefficient σ^* . σ^* is defined by the functions of current density because σ^* is given by the function of logarithmic mean concentration C_S^* (Equation (28)). However, the experimental results show that σ^* is not influenced by current density. Thus, the observed σ^* is averaged for each current density. Figures (13) and (14) show the σ^* versus T and C' . σ^* is generally larger than 1, however, less than 1 for Neosepta CIMS/ACS3 membranes

and for Selemion CMV2/AST membranes. The phenomena exhibited in Figures (13) and (14) are understandable as follows.

σ^* defined in (26) gives the permselectivity between ions and water molecules just after an electric current interruption. Physical rationale of σ^* is given by the following relationships realized in an electrodialysis system (Figure 15) incorporated with a cation- and an anion-exchange membrane and cells I, II and III in which electrolyte solutions are filled:

$$J_{\text{solute}} > 0, \quad \sigma^* < 1 \quad \mu < 0, \quad (37)$$

$$J_{\text{solute}} = 0, \quad \sigma^* = 1 \quad \mu = 0, \quad (38)$$

$$J_{\text{solute}} < 0, \quad \sigma^* > 1 \quad \mu > 0. \quad (39)$$

In Figure 15, an electric current is passed through reversible electrodes and electrolyte concentration in cells I

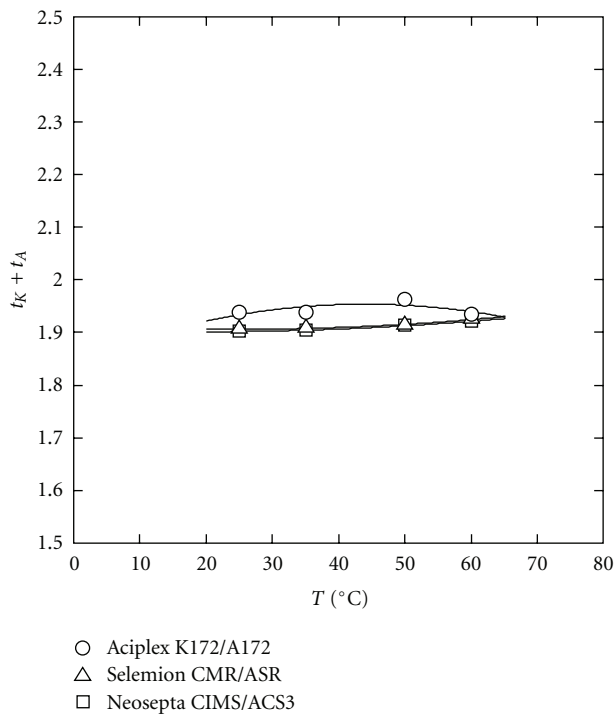


FIGURE 5: Relationship between temperature and transport number.

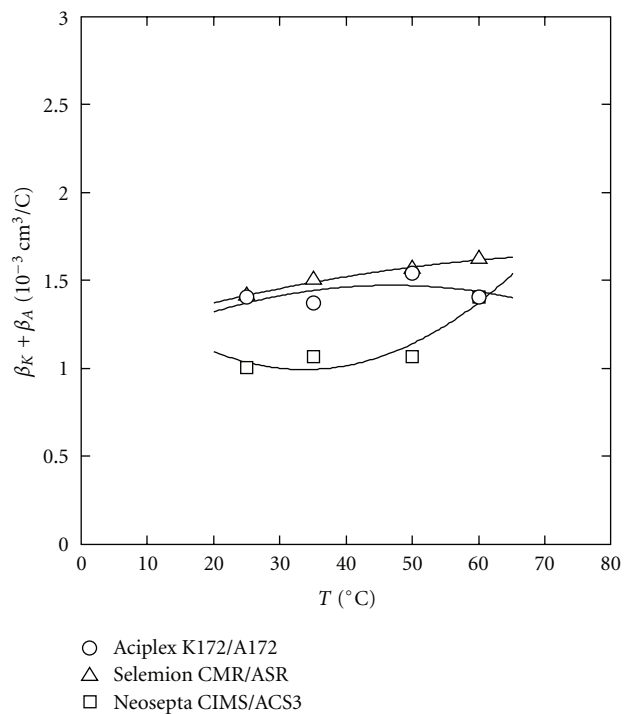


FIGURE 7: Relationship between temperature and electro-osmotic permeability.

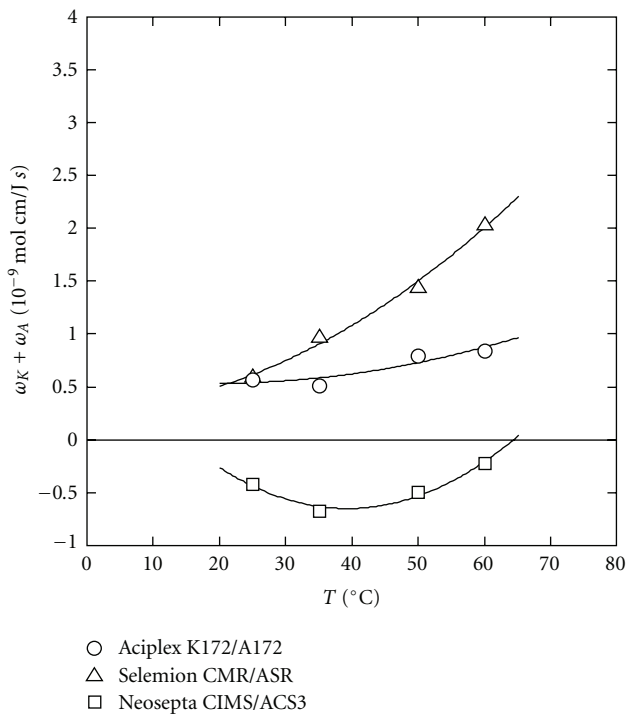


FIGURE 6: Relationship between temperature and solute permeability.

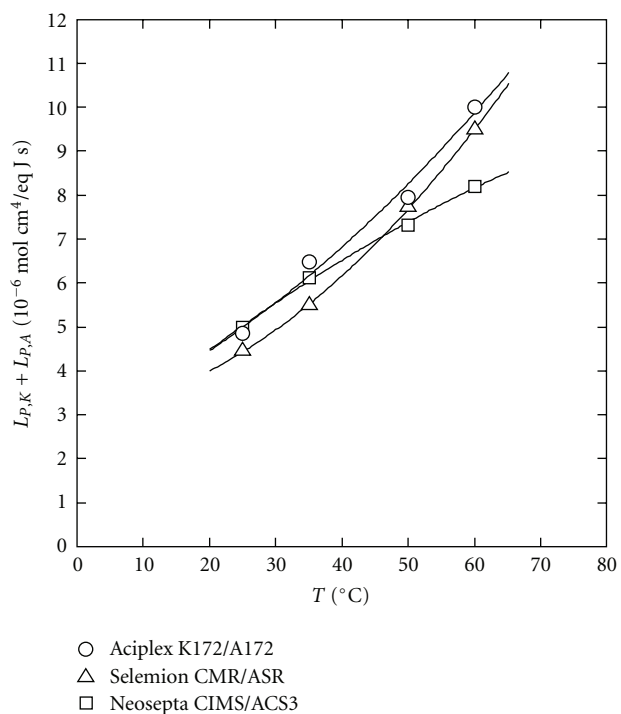


FIGURE 8: Relationship between temperature and hydraulic permeability.

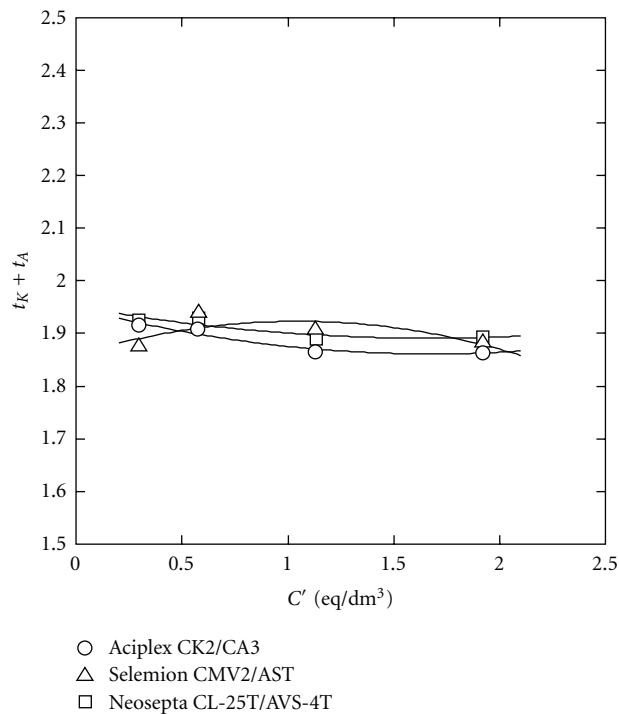


FIGURE 9: Relationship between salt concentration in a feeding solution and transport number.

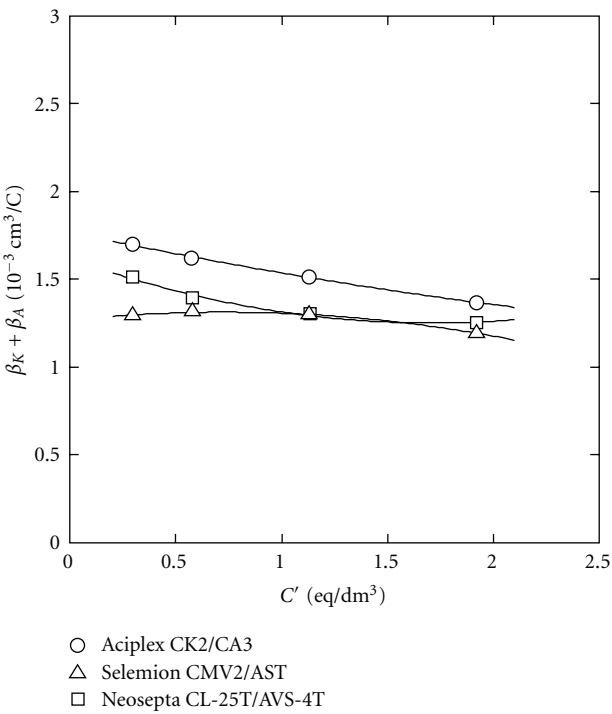


FIGURE 11: Relationship between salt concentration in a feeding solution and electro-osmotic permeability.

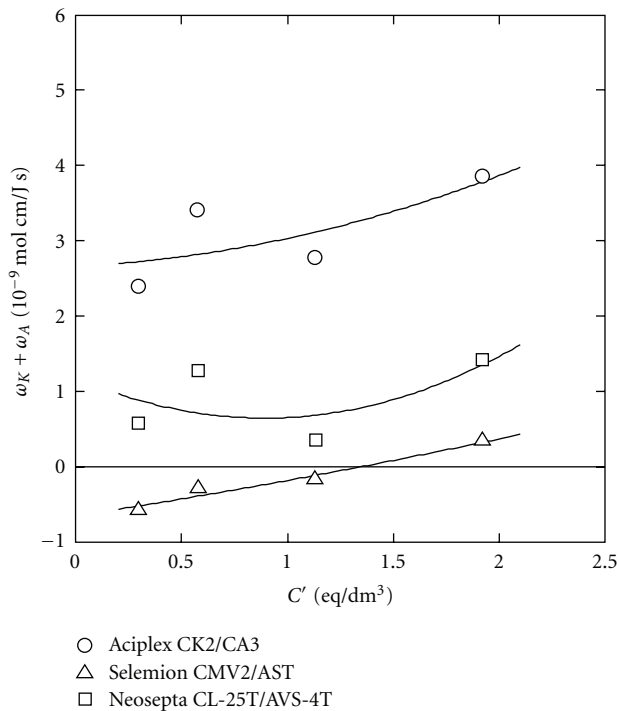


FIGURE 10: Relationship between salt concentration in a feeding solution and solute permeability.

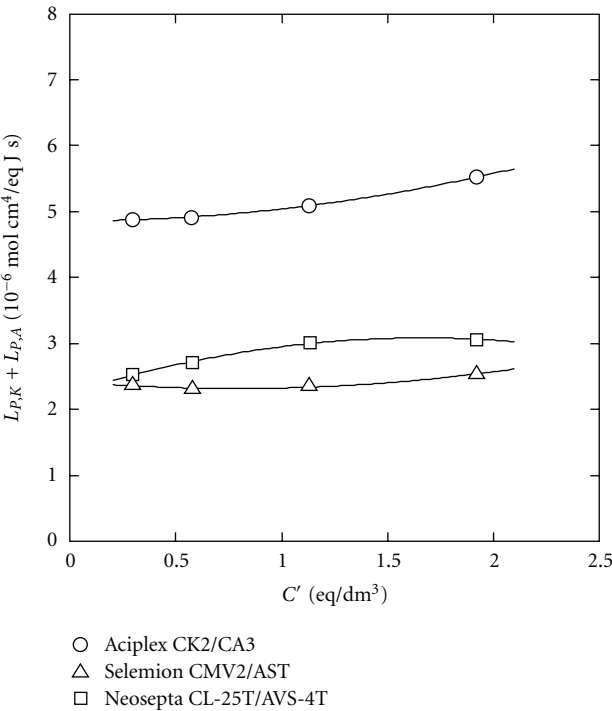


FIGURE 12: Relationship between salt concentration in a feeding solution and hydraulic conductivity.

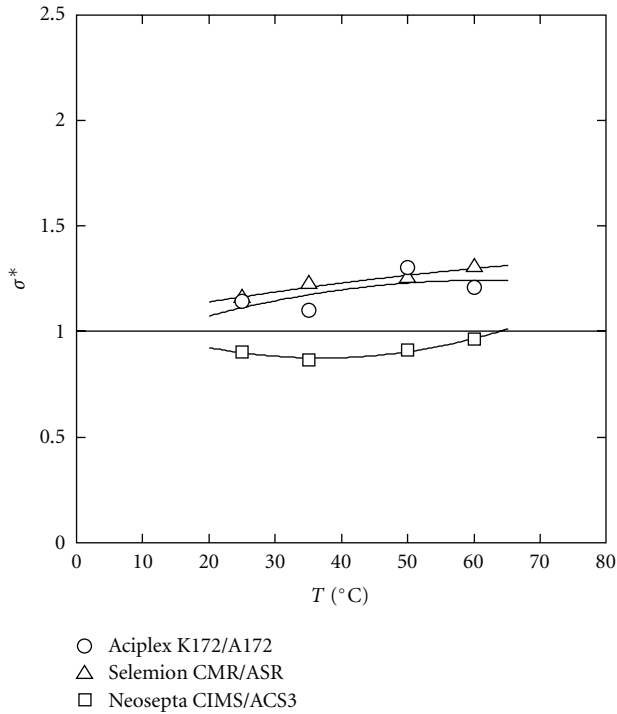


FIGURE 13: Relationship between temperature and overfull concentration reflection coefficient.

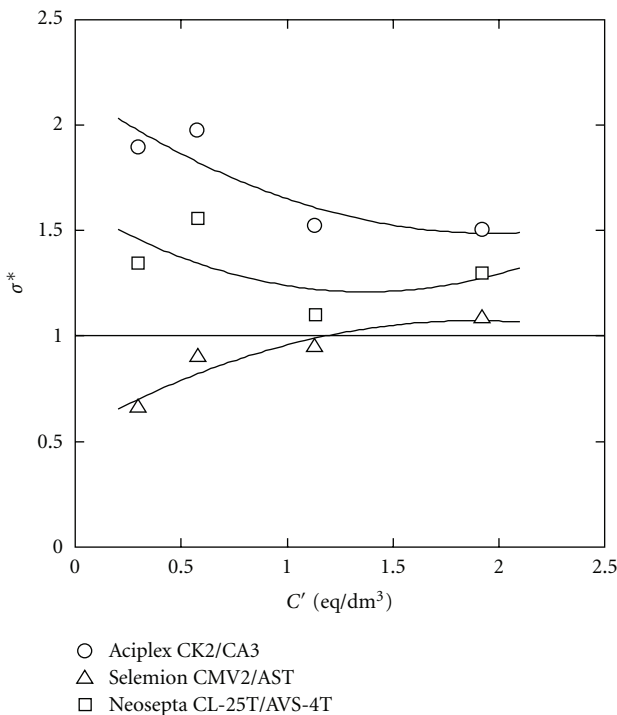


FIGURE 14: Relationship between salt concentration in a feeding solution and overfull concentration reflection coefficient.

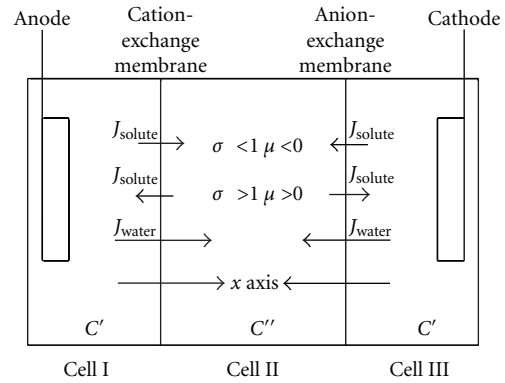


FIGURE 15: Electrodialysis system.

and III is assumed to be decreased to C' and that in cell II is increased to C'' ($C' < C''$). The x axis is drawn across each ion-exchange membrane as shown in the figure. Direction of water flux J_{water} is positive ($J_{\text{water}} > 0$); J_V is positive ($J_V > 0$) in every situation.

Solute flux across the membrane is generally negative ($J_{\text{solute}} < 0$) and it moves from the concentrating cell (cell II) toward desalting cells (cells I and III) due to solute diffusion just after an electric current interruption. In this situation, the concentration reflection coefficient is larger than 1 (Equation (39), $\sigma^* > 1$, Figures 13 and 14). This phenomenon is ordinary in electrodialysis, but extraordinary in pressure dialysis because the direction of the solute due to solute diffusion is against water flux due to hydraulic osmosis. In this case, the overall solute permeability becomes positive, that is, $\mu > 0$ (Table 2) and $\omega_K + \omega_A > 0$ (Figures 6 and 10).

In Neosepta CIMS/ACS3 membranes and Selemion CMV2/AST membranes, solutes move from the desalting cells (cells I and III) toward concentrating cell (cell II) ($J_{\text{solute}} > 0$) just after an electric current interruption. In this situation, the concentration reflection coefficient is less than 1 (Equation (37), $\sigma^* < 1$, Figures 13 and 14). This phenomenon is ordinary in pressure dialysis because the direction of the solute is the same to the water flux due to hydraulic osmosis. The overall solute permeability in this situation becomes negative ($\mu < 0$) (Table 2). The negative μ is indicative of coupled transport between water and solute, which is demonstrated also by negative $\omega_K + \omega_A$ (Figures 6 and 10). However, this phenomenon is extraordinary in electrodialysis because it means uphill transport of solutes against the concentration difference ($C'' - C'$).

In repeating words, ions (solutes) transfer (diffuse) generally from concentrating cells toward desalting cells ($\mu > 0$, $\sigma^* > 1$, $\omega_K + \omega_A > 0$). This direction of solute flux ($J_{\text{solute}} < 0$) is ordinary in electrodialysis but extraordinary in pressure dialysis because the direction of solute flux is against water flux ($J_{\text{water}} > 0$). In some cases, ions transfer from desalting cells toward concentrating cells ($\mu < 0$, $\sigma^* < 1$, $\omega_K + \omega_A < 0$). This direction of solute flux ($J_{\text{solute}} > 0$) is extra-ordinary in electrodialysis, but ordinary in pressure dialysis because the direction of solute flux is the same to water flux ($J_{\text{water}} > 0$).

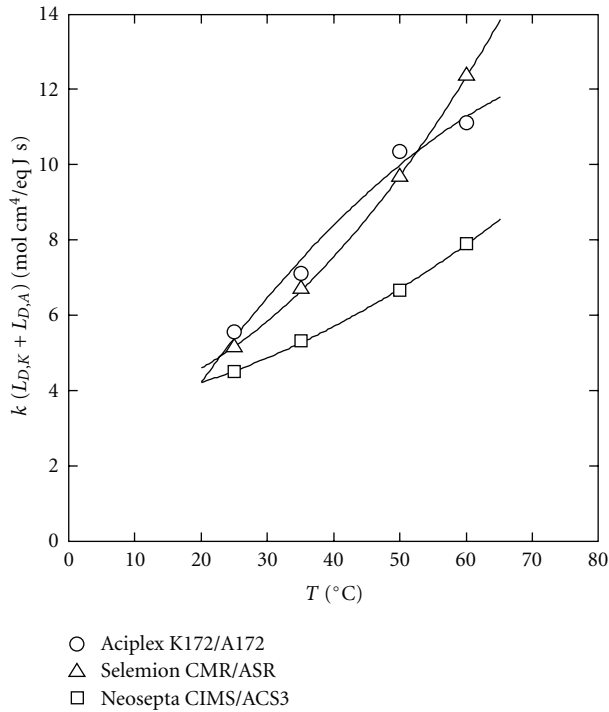


FIGURE 16: Relationship between temperature and exchange flow parameter.

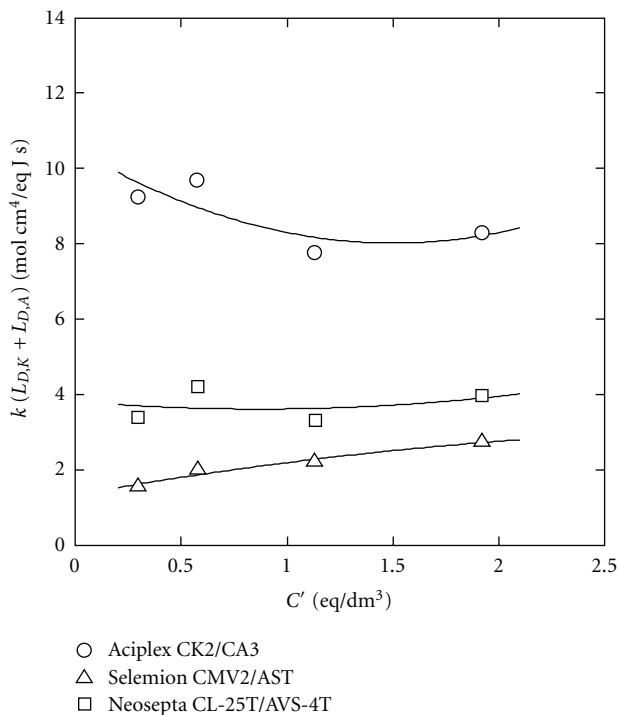


FIGURE 17: Relationship between salt concentration in a feeding solution and exchange flow parameter.

0), which indicates up-hill transport or coupled transport between water and solutes.

4.4. *Exchange Flow Parameter L_D* . $k(L_{D,K} + L_{D,A})$ is calculated from ρ and σ^* (Equation (34)). ρ is the leading parameter and the other membrane characteristics are governed by ρ . [10]. $k(L_{D,K} + L_{D,A})$ is increased with T (Figure 16) and hardly influenced by C' (Figure 17). These phenomena are caused by that ρ is increased with T and hardly influenced by C' .

5. Conclusion

Phenomenological coefficients such as transport number, solute permeability, electro-osmotic permeability, hydraulic permeability, and exchange flow parameter included in the phenomenological equations are evaluated by electrodialysis based on the overall mass transport equation. The overall reflection coefficient σ is essentially the concept applied in pressure-driven dialysis. In order to understand the behavior of the overall reflection coefficient in an electrodialysis process, the concept of the overall concentration reflection coefficient σ^* is applied. σ^* presents the permselectivity between ions and water molecules across a membrane pair just after an electric current interruption in an electrodialysis process. σ^* is generally larger than 1 and at the same time the overall solute permeability μ is positive in usual commercially available ion-exchange membranes. However, occasionally σ^* becomes less than 1 and μ becomes negative, which indicates up-hill transport or coupled transport between water and solutes.

Nomenclature

- C : Concentration (equiv. cm^{-3})
- C^* : Mean concentration (equiv. cm^{-3})
- F : Faraday constant (C equiv. $^{-1}$)
- i : Current density (A cm^{-2})
- I : Electric current (A)
- J : Volume flow ($\text{cm}^3 \text{s}^{-1}$)
- J_D : Exchange flow ($\text{cm}^3 \text{s}^{-1}$)
- J_S : Salt flux (equiv. $\text{cm}^{-2} \text{s}^{-1}$)
- J_V : Volume flux ($\text{cm}^3 \text{cm}^{-2} \text{s}^{-1}$)
- J_W : Flux of water molecules ($\text{mol cm}^{-2} \text{s}^{-1}$)
- k : Onsager reciprocity coefficient
- L_D : Exchange flow parameter ($\text{mol cm}^4 \text{equiv.}^{-1} \text{J}^{-1} \text{s}^{-1}$)
- L_{DP} : Ultrafiltration coefficient ($\text{mol cm}^4 \text{equiv.}^{-1} \text{J}^{-1} \text{s}^{-1}$)
- L_P : Hydraulic conductivity ($\text{mol cm}^4 \text{equiv.}^{-1} \text{J}^{-1} \text{s}^{-1}$)
- L_{PD} : Osmotic volume flow coefficient ($\text{mol cm}^4 \text{equiv.}^{-1} \text{J}^{-1} \text{s}^{-1}$)
- R : Gas constant ($\text{JK}^{-1} \text{mol}^{-1}$)
- t : Transport number
- T : Temperature ($^{\circ}\text{C}$, K).

Greek symbols

- β : Electro-osmotic permeability (cm^3C^{-1})
 ΔC : Concentration difference (equiv. cm^{-3})
 ΔP : Hydraulic pressure difference (dyn cm^{-2})
 $\Delta\psi$: Potential difference (V)
 $\Delta\mu$: Chemical potential difference (J mol^{-1})
 λ : Overall transport number (equiv. C^{-1})
 μ : Overall solute permeability (cm s^{-1})
 ρ : Overall hydraulic permeability ($\text{cm}^4\text{equiv.}^{-1}\text{s}^{-1}$)
 σ : Reflection coefficient, overall pressure reflection coefficient
 σ^* : Overall concentration reflection coefficient
 ϕ : Overall electro-osmotic permeability (cm^3C^{-1})
 ω : Solute permeability ($\text{mol cm J}^{-1}\text{s}^{-1}$).

Subscript

- A: Anion-exchange membrane
 i: Component
 K: Cation-exchange membrane
 S: Solute
 W: Water molecule (solvent).

Superscript

- ' : Desalting cell
 '' : Concentrating cell.

Acknowledgment

The authors are grateful to Mr. S. Nagatsuka and Mr. M. Akiyama, Odawara Salt Experimental Station, Japan Tobacco and Salt Public Corp. for their cooperation in the experimental work.

References

- [1] I. Prigogine, *Introduction to Thermodynamics of Irreversible Processes*, John Wiley, New York, NY, USA, 2nd edition, 1961.
- [2] P. Glansdorff and I. Prigogine, *Thermodynamic Theory Structure, Stability and Fluctuations*, Wiley-Interscience, London, UK, 1971.
- [3] S. R. de Groot and P. Mazur, *Nonequilibrium Thermodynamics*, North-Holland, New York, NY, USA, 1962.
- [4] D. D. Fitts, *Nonequilibrium Thermodynamics*, Mc-Graw Hill, New York, NY, USA, 1962.
- [5] L. Onsager, "Reciprocal relations in irreversible processes. I," *Physical Review*, vol. 37, no. 4, pp. 405–426, 1931.
- [6] L. Onsager, "Reciprocal relations in irreversible processes. II," *Physical Review*, vol. 38, no. 12, pp. 2265–2279, 1931.
- [7] H. B. G. Casimir, "On Onsager's principle of microscopic reversibility," *Reviews of Modern Physics*, vol. 17, no. 2-3, pp. 343–350, 1945.
- [8] P. J. Dunlop, "A study of interacting flows in diffusion of the system raffinose-KCl-H₂ at 25°C," *Journal of Physical Chemistry*, vol. 61, no. 7, pp. 994–1000, 1957.
- [9] P. J. Dunlop and L. J. Gosting, "Use of diffusion and thermodynamic data to test the Onsager reciprocal relation for isothermal diffusion in the system NaCl-KCl-H₂O at 25°C," *Journal of Physical Chemistry*, vol. 63, no. 1, pp. 86–93, 1959.
- [10] Y. Tanaka, "Irreversible thermodynamics and overall mass transport in ion-exchange membrane electrodialysis," *Journal of Membrane Science*, vol. 281, no. 1-2, pp. 517–531, 2006.
- [11] Y. Tanaka, "A computer simulation of continuous ion exchange membrane electrodialysis for desalination of saline water," *Desalination*, vol. 249, no. 2, pp. 809–821, 2009.
- [12] Y. Tanaka, "A computer simulation of batch ion exchange membrane electrodialysis for desalination of saline water," *Desalination*, vol. 249, no. 3, pp. 1039–1047, 2009.
- [13] Y. Tanaka, "A computer simulation of feed and bleed ion exchange membrane electrodialysis for desalination of saline water," *Desalination*, vol. 254, no. 1–3, pp. 99–107, 2010.
- [14] O. Kedem and A. Katchalsky, "Permeability of composite membranes Part 1. Electric current, volume flow and flow of solute through membranes," *Transactions of the Faraday Society*, vol. 59, pp. 1918–1930, 1963.
- [15] C. R. House, *Water Transport in Cells and Tissues*, Edward Arnold, London, UK, 1974.
- [16] S. G. Schultz, *Basic Principles of Membrane Transport*, Cambridge University Press, Cambridge, UK, 1980.
- [17] R. Z. Schloegel, *Fortschritte der physikalischen Chemie. Band 9*, 1964.
- [18] A. J. Staverman, "The theory of measurement of osmotic pressure," *Recueil des Travaux Chimiques des Pays-Bas*, vol. 70, no. 4, pp. 344–352, 1951.
- [19] O. Kedem and A. Katchalsky, "Thermodynamic analysis of the permeability of biological membranes to non-electrolytes," *Biochimica et Biophysica Acta*, vol. 27, no. 2, pp. 229–246, 1958.
- [20] S. Koter, "Transport of electrolytes across cation-exchange membranes. Test of Onsager reciprocity in zero-current processes," *Journal of Membrane Science*, vol. 78, no. 1-2, pp. 155–162, 1993.
- [21] A. Yamauchi and Y. Tanaka, "Salt transport phenomena across charged membrane driven by pressure difference," in *Effective Membrane Process—New Prospective*, R. Paterson, Ed., pp. 179–185, BHR Group; Information Press, Oxford, UK, 1993.
- [22] Y. Tanaka, "Ion exchange membrane electrodialysis of saline water desalination and its application to seawater concentration," *Industrial & Engineering Chemistry Research*, vol. 50, no. 12, pp. 7494–7503, 2011.

Research Article

Ultrathin Sicopion Composite Cation-Exchange Membranes: Characteristics and Electrodialytic Performance following a Conditioning Procedure

Erik Ayala-Bribiesca,¹ Mario Boucher,² and Laurent Bazinet¹

¹ Dairy Science and Technology Group (STELA), Institute of Nutraceuticals and Functional Foods (INAF) and Department of Food Sciences and Nutrition, Pavillon Paul Comtois, Laval University, Sainte-Foy, QC, Canada G1V 0A6

² SiM Composites, 4925 Rue Lionel Groulx, Bureau 11, Saint-Augustin-de-Desmaures, QC, Canada G3A 1V1

Correspondence should be addressed to Laurent Bazinet, laurent.bazinet@fsaa.ulaval.ca

Received 20 October 2011; Accepted 18 January 2012

Academic Editor: Tongwen Xu

Copyright © 2012 Erik Ayala-Bribiesca et al. This is an open access article distributed under the Creative Commons Attribution License, which permits unrestricted use, distribution, and reproduction in any medium, provided the original work is properly cited.

The aim of this work was to investigate the properties of Sicopion membranes: an ultrathin ($\approx 20 \mu\text{m}$) composite cation-exchange membrane (CEM) made from sulphonated poly(ether-ether-ketone) (SPEEK) containing different levels of sulphonic-functionalized silica particles (SFSPs). Sicopion membranes were conditioned according to the French Normalization Association procedure, consisting in a series of acid and alkaline washes, and their electrodialytic characteristics were compared to an existent commercial food-grade membrane (CMX-SB). Electrical conductivity of Sicopion membranes was higher than that of CMX-SB membranes (9.92 versus 6.98 mS/cm), as well as their water content (34.0 versus 27.6%). As the SFSP level was reduced, the ion-exchange capacity (IEC) of Sicopion membranes increased. Concerning their electrodialytic performances, Sicopion membranes presented a lower demineralization rate than CMX-SB membranes (35.9 versus 45.5%), due to an OH^- leakage through the pores created by dislodging the SFSP particles during the conditioning procedure.

1. Introduction

Sicopion is a novel type of membranes made of a composite material combining sulphonic-functionalized silica particles (SFSP) and sulphonated poly(ether-ether-ketone) (SPEEK). In this composite material, the functionalization of silica particles is accomplished by covalently grafting sulphonic acid groups [1]. In the case of SPEEK, concentrated H_2SO_4 is used to sulphonate, also by covalent bonding, an aromatic chain of poly(ether-ether-ketone) (PEEK) [1, 2]. Once the organic and the inorganic phases prepared, they are mixed in specific proportions according to the application requirements. The resulting composite material is then prepared in a membrane form. Among the factors affecting the membrane properties there is the sulphonation degree of the components and the type and amount of SFSP used. A PEEK should be partially sulphonated to decrease its hydrophobicity and produce an ion-exchanging material, but high degrees of sulphonation are to be avoided, since the polymer would then become

water soluble, which is the case of 100% SPEEK [1, 2]. The amount of SFSPs, as well as their size, determines the formation of a continuous hydrophilic phase and the mechanical properties of the material. A high content of inorganic particles (i.e., SFSP) produces higher membrane hydration and water retention capacity but, in contrast, yields a brittle membrane with lower tear resistance [1].

These materials impart to the membrane a highly functional ion-exchanging structure without inert fillers. At the same time, SFSPs enhance water retention, avoiding membrane dehydration, which has been reported to be a critical factor in cation-exchange membrane (CEM) performance in fuel cell applications [3], for which the membranes were originally designed. In food applications, dehydration of electrodialysis (ED) membranes has been linked to fouling formation on CEM membranes [4]. Hence, interest in Sicopion membranes for food applications lies on the fact they could minimize fouling caused by membrane dehydration. Another potential advantage of Sicopion membranes is their

thickness, which can be customized to very low values (i.e., under $30\ \mu\text{m}$, against $165\ \mu\text{m}$ for existing food grade CMX-SB membranes) with minimal compromise on mechanical resistance during the ED process. Since less material is used for membrane manufacture, there is an important reduction in material consumption, implying an attractive cost benchmarking with respect to other commercially available membranes.

This study was part of a broader research project aimed at the evaluation of the feasibility of existent electromembrane processes with an ultrathin membrane, as well as the development of new applications of Sicopion membranes for conventional and bipolar membrane electrodialysis of food and nutraceutical products. The aim of this work was to study the characteristics and electrodialytic performance of Sicopion membranes with different SFSP levels that have been conditioned according to the standard NF X 45-200 French Normalization Association procedure [5] for ion-exchange membranes. The conditioning procedure is a standard acid/alkaline wash applied to IEM to remove any manufacture residue prior to their study and is of interest for food applications requiring cleaning-in-place (CIP) cycles, where membranes would be required to withstand similar pH conditions [6].

2. Experimental

2.1. Material. Three different Sicopion membranes (SiM Composites, Quebec, QC, Canada) with different levels of sulphonic-functionalized silica particles (SFSPs) with an average diameter of $5\ \mu\text{m}$ (16.7, 25.0, and 35.0% of SFSP, production lots 0052, 0053, and 0054, resp.) embedded within the SPEEK backbone and one Neosepta CMX-SB cation-exchange membrane (Tokuyama Soda Ltd., Tokyo, Japan) were tested to demineralize a model salt and protein diluate solution. Anion-exchange membranes were, in all cases, Neosepta AMX-SB membranes (Tokuyama Soda Ltd.).

$\text{CaCl}_2 \cdot 2\text{H}_2\text{O}$ and KCl were obtained from MAT Laboratory (Quebec, QC, Canada). NaOH 1.0 N and HCl 1.0 N were obtained from Fisher Scientific (Nepean, ON, Canada). NaCl and Na_2CO_3 were obtained from EMD (EMD Chemicals, Gibbstown, NJ, USA). BiPRO whey protein isolate (WPI) was obtained from Davisco Foods International (Eden Prairie, MN, USA). The average concentration of protein (92.7 g), moisture (5.0 g), sodium (600.0 mg), potassium (120.0 mg), calcium (120.0 mg), phosphorous (25.0 mg), and magnesium (15.0 mg), expressed per 100 g of BiPRO WPI, as is, was obtained from the manufacturer (Davisco Foods International).

2.2. Electrodialysis Cell. The electrodialysis cell was a micro-flow-type cell (ElectroCell AB, Täby, Sweden). The stack was mounted with one Neosepta CMX-SB cation-exchange membrane separating the anode rinsing compartment from the concentrate, followed by one Neosepta AMX-SB anion-exchange membrane and the tested CEM (Sicopion or CMX-SB) defining the diluate compartment. A last Neosepta AMX-SB separated the electrode rinsing solution at the cathode end. This way, the stack defined three closed loops,

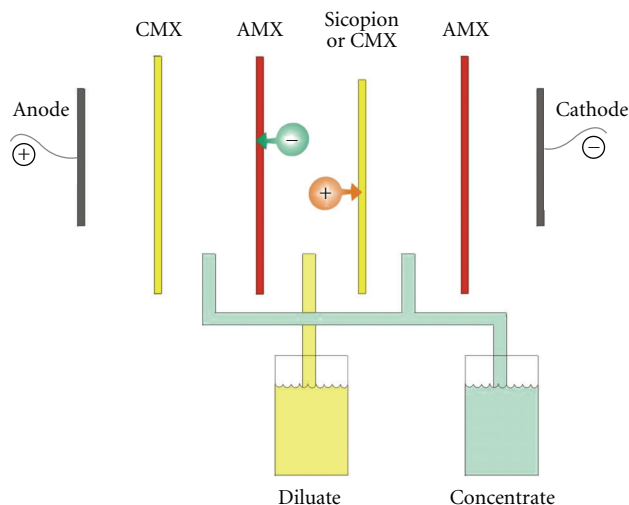


FIGURE 1: Configuration of the electrodialysis (ED) cell used for demineralization of solutions. CMX: CMX-SB cation-exchange membrane, AMX: AMX-SB anion-exchange membrane, (+) demineralizing cations, (-) demineralizing anions. The electrode-rinsing solution circuit is not shown. Adapted from [7].

as described in previous works [7]. Each closed loop was connected to a separate external plastic reservoir, allowing continuous recirculation (Figure 1). The membranes tested, with an effective surface of $10\ \text{cm}^2$, were both in contact with the model salt and protein solution (i.e., diluate) on one side and with the KCl solution (i.e., concentrate) on the other side.

2.3. Conditioning Procedure. All cation-exchange membranes were conditioned according to the NF X 45-200 procedure of the French Normalization Association (AFNOR) for IEM, Section 5.2.4.1 [5]. Anion-exchange membranes were not conditioned.

Membranes were conditioned as follows.

- Immersed in 0.1 M HCl (100 mL/ $10\ \text{cm}^2$ membrane) for 1 hour.
- Rapidly rinsed by immersion in distilled water (250 mL/ $10\ \text{cm}^2$ membrane) and pat-dried with filter paper.
- Immersed in 0.1 M NaOH (100 mL/ $10\ \text{cm}^2$ membrane) for 1 hour.
- Rapidly rinsed by immersion in 0.1 M NaCl (250 mL/ $10\ \text{cm}^2$ membrane).
- The cycle was repeated and the membranes kept in 0.1 M NaCl (100 mL/ $10\ \text{cm}^2$ membrane) until used for membrane analysis and ED procedure.

2.4. Protocol. Once the conditioning procedure completed, membrane characteristics were measured on unused membranes for further comparison with those used for the demineralization procedure. The limiting current density (LCD) value for each ED stack was determined according to the method described by Cowan and Brown [8], obtaining

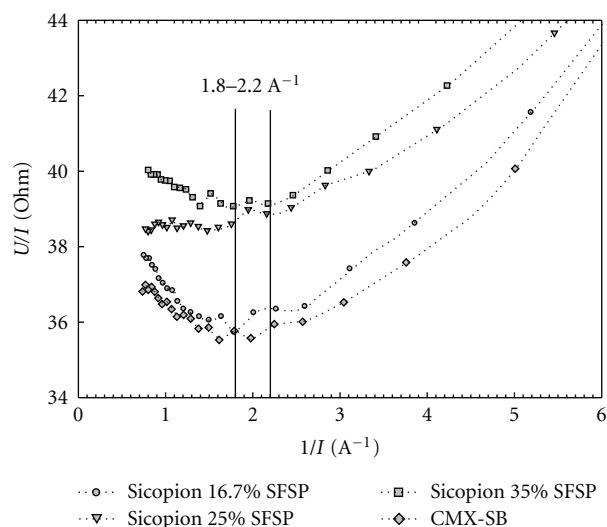


FIGURE 2: Limiting current density (LCD) value determination. Slope changes were found at 0.5 ± 0.05 A (i.e., within the 1.8 and 2.2 A^{-1} range), equivalent to a LCD value of 50 mA/cm^2 of membrane.

an overall LCD value of $50 \pm 5 \text{ mA/cm}^2$ for all membranes (Figure 2). According to this, and to assure a demineralization process under the LCD value, a current density of 13 mA/cm^2 was fixed on the power supply (model HPD 60-5SX, Xantrex, Burnaby, BC, Canada) and remained constant during the demineralization procedure.

Solutions used for the demineralization process were as follows.

- Model salt and protein solution (i.e., diluate): $1000 \text{ mg/L Na}_2\text{CO}_3$, 800 mg/L KCl , 800 mg/L CaCl_2 , 32.0 g BiPRO adjusted to pH 6.5 with $\text{HCl } 1.0 \text{ N}$ and refrigerated overnight to ensure proper hydration of proteins.
- KCl solution (i.e., concentrate): 2 g/L KCl , adjusted to pH 12 with $\text{NaOH } 1.0 \text{ N}$.
- Electrode rinsing solution: 20 g/L NaCl .

Electrodialysis was carried out during 100 minutes. Flow rates were adjusted at 900 mL/min for the electrode rinsing solution and at 600 mL/min for the diluate and concentrate solutions. 2 mL samples of diluate and concentrate solutions were taken at the beginning and at 20-minute intervals and kept frozen until analyzed by inductively coupled plasma (ICP). Three different membranes of each type were used for each demineralization (triplicate), and a fourth one was kept as a control reference. After the demineralization procedure, the ED stack was dismounted and the CEM were stored in a 0.5 M NaCl solution until further analysis. Once membrane characteristics determined, the membranes were photographed with a binocular microscope equipped with a digital camera. Finally, membrane samples were ashed, and ICP analyses were done to determine their mineral composition.

2.5. Analysis Methods

2.5.1. Membrane Parameters and Analyses

Membrane Thickness. Membrane thickness was measured using a Mitutoyo Corp. IDC-type digimatic indicator with absolute encoder (Model ID-C112 EB, Kanagawa-Ken, Japan). The indicator was equipped with a 7 mm diameter flat contact point. The membrane thickness value was averaged from ten measurements at different locations on the effective surface region of the membrane. Measurements were taken on unused conditioned membranes and on used membranes 24 hours after the ED process.

Membrane Electrical Conductivity. The membrane electrical conductivity was calculated from membrane thickness and its electrical resistance, obtained from membrane conductance. The conductance was measured after a 24-hour immersion of the membranes in a 0.5 M NaCl solution, which served as the respective reference solution. The method was carried out using a specially designed conductivity clip (Laboratoire des Matériaux Echangeurs d'Ions, Créteil, France) and a YSI conductivity meter (Model 35, Yellow Springs Instrument Co., Yellow Springs, OH, USA). Conductivity was calculated as described in previous studies [4].

Membrane Ion-Exchange Capacity (IEC). IEC of unused conditioned CEM was determined using Na^+ as counterion, according to the AFNOR procedure for IEM [5]. In the case of Sicopion membranes, given their low mass/surface ratio, the protocol was modified by increasing the defined membrane surface from 10 to 30 cm^2 , in order to have a meaningful sample.

Water Content. Water content of unused conditioned membranes was determined according to the AFNOR procedure for IEM [5].

Dimensional Stability. The dimensional stability of unused conditioned membranes in acidic and alkaline media was determined according to the official procedure of the AFNOR for IEM [5]. Complementary to this analysis, and prior to conditioning, membrane was marked and measured (i.e., according to the AFNOR procedure [5]) in dry conditions, as obtained from the manufacturer. Afterwards, this value was compared to that of the conditioned membrane to obtain a dry-to-wet dimensional stability coefficient.

Optical Microscopy. Photographs of unused and used membranes were taken at $\times 40$ and $\times 100$ magnitude on a binocular microscope (Laborlux S, Ernst Leitz Wetzlar GmbH, Wetzlar, Germany) equipped with a colour video camera (model hyper HAD, CCD-IRIS/RGB, Sony, Toronto, ON, Canada). The images were processed with Matrox Inspector software (version 3.1, Matrox Electronics Systems Ltd, Dorval, QC, Canada).

Scanning Electron Microscopy and X-Ray EDS. In order to better understand Sicopion membrane characteristics and electro-dialytic performance, SEM images of the membranes

were acquired to verify whether a fouling deposit was present or not. Scanning electron micrographs (SEMs) of uncoated Sicopion membranes used for the ED procedure were acquired at various magnifications levels at 20 kV with a scanning electron microscope (S-3000 N, Hitachi, Japan). Surface elemental analysis of one Sicopion membrane prepared with 16.7% of SFSP and used for an ED demineralization was performed on an X-ray energy-dispersive spectrometer (EDS) (INCA, Oxford Link Isis, Oxford Instruments, Concord, MA, USA). The EDS conditions were 20 kV accelerating voltage and 14.7 mm working distance. Elements of interest were silicon, potassium, sodium, phosphorous, sulfur, calcium, chlorine, oxygen, and carbon.

Membrane Ash Determination and Analysis. Samples for ash determination were prepared from 5 cm² of membrane ashed at 650°C for 16 hours in a muffle furnace. Analysis of membrane ashes for silicon quantification was performed by inductive coupled plasma optical emission spectroscopy (ICP-OES) (Optima 4300, Dual View, Perkin-Elmer, Shelton, CT, USA), in axial view at wavelengths 251.611, 212.412, and 288.158 nm.

2.5.2. Electrodialytic Parameters and Ion Migration

pH Variation of the Diluate and Concentrate Solutions. The pH of the diluate and concentrate solutions was measured along the ED process with a pH meter model SP20 (epoxy gel combination pH electrode, VWR Symphony), manufactured by Thermo Orion (West Chester, PA, USA).

Conductivity Variation of the Diluate and Concentrate Solutions. Conductivity of the diluate and concentrate solutions was measured along the ED process with an YSI conductivity instrument (model 3100-115V, YSI Inc., Yellow Springs, OH, USA) equipped with an automatic temperature compensation (ATC) immersion probe (model 3252, $k = 1/\text{cm}$, YSI Inc.).

Cation Migration. The 2 mL samples taken during the demineralization procedure were used for cation migration determination. Samples were diluted with HPLC-grade water. Potassium, sodium, and calcium concentrations were determined by ICP (ICP-OES, Optima 4300, Dual View, Perkin-Elmer, Shelton, CT, USA). Analysis was carried-out in radial view. The wavelengths used to determine each element were 766.490, 589.592, and 317.933 nm, respectively.

System Resistance. The system resistance was calculated, using Ohm's Law, from the voltage read directly from the indicators on the power supply and the current intensity read from a digital multimeter (52-0060-2, Mastercraft, Toronto, ON, Canada).

Energy Consumption. In order to compare membrane performance during ED treatment, the total energy consumption was calculated by integrating the voltage as a

function of the time multiplied by the current, according to [9]

$$E = \int_0^{100} \frac{U \cdot I}{60} dt, \quad (1)$$

where E is the energy consumption in Watt-hour (Wh), U is the potential (volt), I is the current intensity (ampere), and time is expressed in minutes.

3. Results and Discussion

3.1. Membrane Parameters and Analysis

3.1.1. Membrane Thickness. Unused conditioned Sicopion membranes were of similar thickness, with a slight decrease as SFSP level increased (22.7 ± 0.5 , 21.3 ± 0.5 , and $20.7 \pm 0.5 \mu\text{m}$, resp. for 16.7, 25.0, and 35.0% SFSP) (Figure 3). The thickness values obtained for Sicopion membranes were within the specification range established by the manufacturer. These values were, as expected, lower than those obtained for CMX-SB membranes ($165.5 \pm 0.2 \mu\text{m}$), but differences at this level were not subject to comparison, since the different nature of the membranes excludes the necessity for further explanation. Once the ED procedure was finished and the stack was dismounted, membranes (i.e., Sicopion and CMX-SB) were slightly deformed. This deformation was caused by a pressure difference forcing the membrane against spacer in the concentrate compartment. On the other hand, such deformation was not permanent, since membranes recovered their smooth and level surface after being kept 24 hours in a 0.5 N NaCl bath. To verify whether a fouling deposit was present or not, thickness was then measured and compared by Students t -tests against the corresponding unused membrane. No significant differences were found, and all results supported the absence of any detectable fouling deposit on the membrane surface.

3.1.2. Membrane Electrical Conductivity. Membrane electrical conductivity of unused conditioned Sicopion membranes was similar for all SFSP levels ($9.92 \pm 0.19 \text{ mS/cm}$) and higher than unused CMX-SB membranes ($6.98 \pm 0.24 \text{ mS/cm}$). This difference would be given by the functionalized materials composing Sicopion membranes, having less inert materials in the membrane. 24 hours after the ED treatment, membranes maintained their original conductivity, as compared by Students t -tests against the corresponding unused membrane, except for Sicopion membrane with 25.0% of SFSP ($P = 0.026$), with a $3.28 \pm 1.94 \text{ mS/cm}$ drop (Figure 4). These results indicate that the membrane integrity was not lost during the demineralization. In the case of Sicopion with 25% SFSP, the difference could be due to the slight thickness reduction, coupled to a minimal but also significant increase in its electrical resistance versus the original value ($P = 0.019$, using a Students t -test) (Figure 5), since no fouling was visible on such membrane. Nonetheless, such reduced value was still as good as that obtained for CMX-SB membranes after the ED procedures.

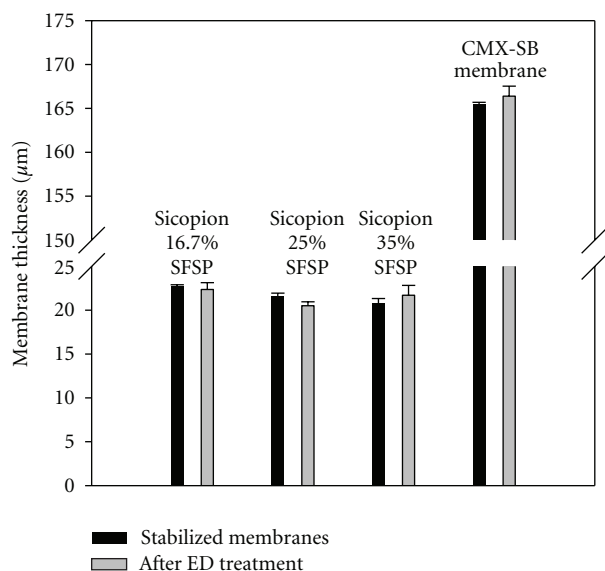


FIGURE 3: Thickness of conditioned and used (24 h after the ED procedure) Sicopion and CMX-SB membranes.

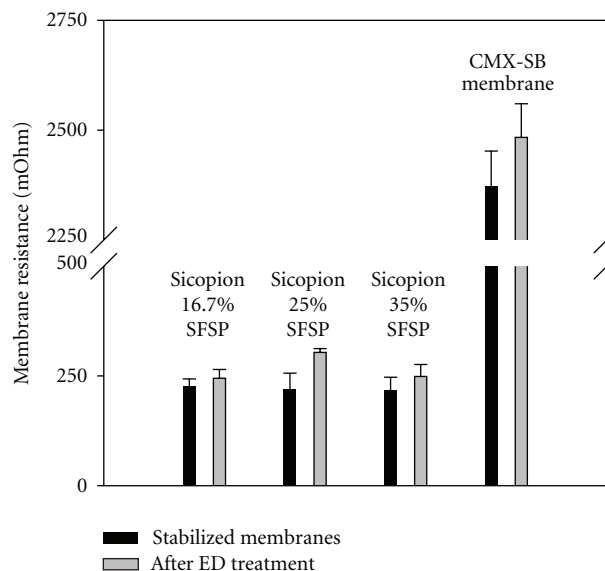


FIGURE 5: Electrical resistance of conditioned and used (24 h after the ED procedure) Sicopion and CMX-SB membranes.

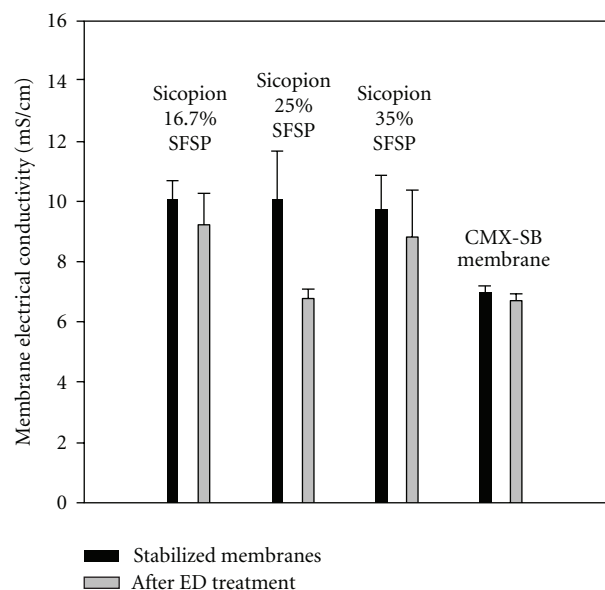


FIGURE 4: Electrical conductivity of conditioned and used (24 h after the ED procedure) Sicopion and CMX-SB membranes.

3.1.3. Membrane Ion-Exchange Capacity. From the results obtained, it appeared that the IEC decreased as a higher amount of SFSP was used to prepare the Sicopion membranes (Table 1). CMX-SB membranes had an IEC within the range of Sicopion membranes with a 16.7 and 25.0% SFSP, so membranes were similar from this point of view. Sicopion membrane with 35% SFSP presented a lower IEC than the CMX-SB membrane. The IEC of a membrane represents the amount of active ion-exchange sites present in the membrane material [5, 10] and constitutes an ionic-quality characteristic of the latter. For conditioned Sicopion

membranes, their IEC was directly proportional to their SPEEK content, suggesting a functionality loss at the SFSP ion-exchange sites. IEC analysis was not performed after the ED procedure due to the limited amount of treated membrane available.

3.1.4. Water Content. Water content of Sicopion membranes varied according to their SFSP level and was, for all levels, higher than CMX-SB water content (Table 1). Sicopion membranes prepared with higher amounts of SFSP showed higher water content of the conditioned membrane (Table 1). Although silica particles have water absorption properties [1], it is possible that their functionality loss would simply translate into higher water content within the membrane structure. If IEC values obtained are pondered according to the respective water content of each membrane to obtain a wet membrane IEC value (i.e., which better reflects the real IEC of the membrane in a working ED stack) (Table 1), it is to remark that membranes still follow the trends as described earlier in the IEC section, showing that conditioned Sicopion membranes maintain their ion-exchange capacity after membrane hydration. This particular property is especially important in fuel-cell applications to avoid membrane dehydration at high temperatures [1, 3, 11]. In food applications, dehydration has been reported to be a factor in membrane integrity alterations, such as irreversible deformation and ionic passivation [2–4], so effective water retention of membrane would reduce the risk of a membrane-fouling formation.

3.1.5. Dimensional Stability. Results for dry-to-wet stability for Sicopion membranes (Table 2) demonstrated that a minimal change in their dimensions occurs when hydration occurs. This dry-to-wet dimensional stability of Sicopion

TABLE 1: Membrane ion-exchange capacity (IEC) ($\text{mEq/g}_{\text{dry membrane}}$), water content (% of water on wet membrane basis), and IEC on wet membrane basis ($\text{mEq/g}_{\text{wet membrane}}$).

Membrane	IEC (dry basis, $\text{mEq/g}_{\text{dry}}$)	Water content (%)	IEC (wet basis, $\text{mEq/g}_{\text{wet}}$)
Sicopion 16.7% SFSP	1.394 ± 0.000	31.0 ± 0.6	0.960
Sicopion 25.0% SFSP	1.170 ± 0.000	33.5 ± 0.3	0.778
Sicopion 35.0% SFSP	1.074 ± 0.000	37.6 ± 2.4	0.667
CMX-SB	1.231 ± 0.023	27.6 ± 1.0	0.891

TABLE 2: Dimensional variation coefficients (in the X and Y dimensions) from a dry-to-wet membrane (C_{s_x} , C_{s_y}), after an acid bath (C_{a_x} , C_{a_y}) and after an alkaline bath (C_{b_x} , C_{b_y}).

CEM membrane (of diluate compartment)	Dry to wet		Acid bath		Alkaline bath	
	C_{s_x}	C_{s_y}	C_{a_x}	C_{a_y}	C_{b_x}	C_{b_y}
Sicopion 16.7 % SFSP	0.0018 ± 0.0016	0.0000 ± 0.0000	0.0031 ± 0.0008	0.0018 ± 0.0022	0.0031 ± 0.0008	0.0018 ± 0.0022
Sicopion 25.0 % SFSP	0.0000 ± 0.0000	0.0000 ± 0.0000	0.0031 ± 0.0008	0.0007 ± 0.0014	0.0038 ± 0.0013	0.0007 ± 0.0014
Sicopion 35.0 % SFSP	0.0009 ± 0.0016	0.0000 ± 0.0000	0.0014 ± 0.0016	0.0007 ± 0.0014	0.0014 ± 0.0016	0.0007 ± 0.0014
CMX-SB	n/a	n/a	0.0029 ± 0.0005	0.0023 ± 0.0027	0.0029 ± 0.0005	0.0013 ± 0.0027

membranes would allow a dry ED-stack assembly conditions. In contrast to commercially available membranes, such as CMX-SB, Sicopion membranes do not require wet environment for storage or installation procedures and are available in dry sheets or rolls from the manufacturer. As to their stability in acidic/alkaline media (Table 2), it was shown that all membranes had similar variation coefficients, although Sicopion membrane with 35% SFSP seemed to be slightly more dimensionally stable than the other Sicopion membranes. It is possible to suggest, from these results, that Sicopion membrane would be dimensionally stable in acidic and alkaline media, which would constitute an advantage for cleaning-in-place (CIP) procedures.

3.1.6. Optical Microscopy. Sicopion membranes presented a granular aspect (Figure 6), showing the sites where silica particles were embedded in the SPEEK backbone. Higher SFSP levels produced less smooth surfaces, causing the membrane to seem darker (Figure 6). Also, when compared to their respective control membranes, those used for the demineralization process appeared to be slightly darker, enhancing their texture. This darkening, given by mineral traces that remain in the membrane, is normal after an ED treatment and does not necessarily imply a fouling formation, as observed in previous work on ED membrane fouling [4]. CMX-SB membranes presented the same visual texture darkening (Figure 6) and did not present any visible fouling deposits. At the same time, the different structure of both types of membranes, given their different nature and manufacture characteristics, could be observed.

3.1.7. Scanning Electron Microscopy and X-Ray EDS. SEM showed a smooth membrane surface with no signs of fouling deposits (Figure 7). On the other hand, hollow spaces were found all over the Sicopion membranes. Such cavities would correspond to the expected location of the SFSP embedded in the SPEEK matrix. This is supported by the corresponding cavity size ($\approx 5 \mu\text{m}$) (Figure 8), corresponding to the reported average size of the SFSP used for membrane manufacture.

TABLE 3: Ash content (in dry basis %) of unused (after the stabilization procedure) and used (after the demineralization procedure) CEM.

Membrane	Unused (% ash)	After ED (% ash)
Sicopion 16.7% SFSP	13.9 ± 1.2	13.2 ± 0.4
Sicopion 25.0% SFSP	11.5 ± 0.8	13.2 ± 2.2
Sicopion 35.0% SFSP	13.4 ± 1.3	13.7 ± 0.8
CMX-SB	6.9 ± 0.5	7.8 ± 0.5

This phenomenon was the case for all Sicopion membranes (Figure 7), whose SFSP would have leached out during the alkaline wash of the conditioning procedure. The absence of the SFSP was supported by elemental analysis of the surface, where only traces of silicon were detected (Figure 9). This would explain the results found for the IEC, where no ion-exchange contribution of the SFSP was observed and for the higher water content of the membranes, by replacing the space once occupied by the SFSP.

3.1.8. Membrane Ash Determination and Analysis. Total membrane ash determination confirmed the different nature of Sicopion membranes with respect to the CMX-SB membrane. Unused Sicopion membranes presented a twofold amount of ash with respect to CMX-SB membranes (Table 3), meaning that Sicopion SPEEK contains a higher amount of inorganic material than the material used in CMX-SB membranes. No differences were found among the ash contents of Sicopion membranes, supporting the fact that SFSP were removed during the conditioning procedure and that the SPEEK backbone remaining had the same composition for all membranes. When ash content of unused membranes was compared via Student's *t*-tests to the respective ash content of the membrane after ED (Table 3), no differences were found for any membrane, confirming that no fouling took place during the ED procedure. Finally, the Sicopion membrane ash analysis confirmed the loss of the SFSP as shown by SEM and X-ray EDS mapping. As

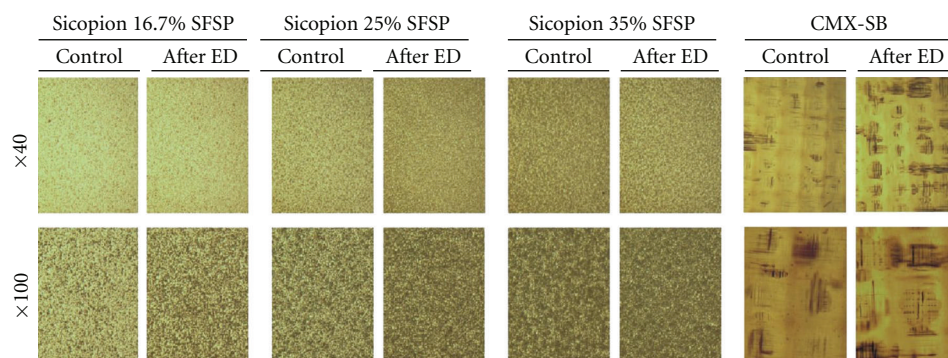


FIGURE 6: Optical microscope images of unused (control) and used (after ED) CEM at $\times 40$ and $\times 100$ magnifications.

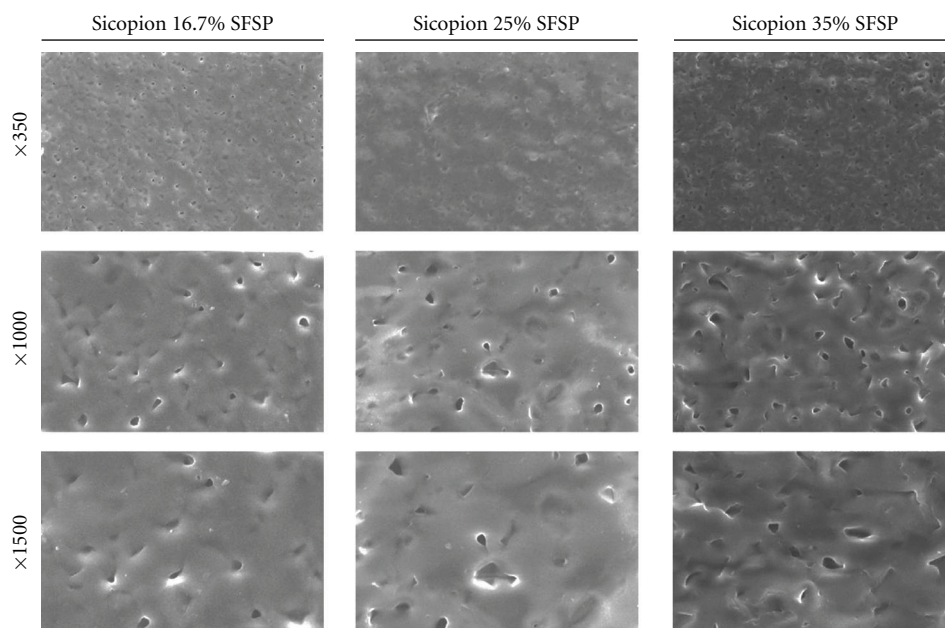


FIGURE 7: Scanning electron micrographs (SEMs) of Sicopion membranes.

expected, only traces of silicon (<0.5 mg/g dry membrane) were detected by ICP analysis.

3.2. Electrodialytic Parameters and Ion Migration

3.2.1. pH Variation of the Diluate and Concentrate Solutions.

The $\text{pH}_{(\text{diluate})}$ varied according to the CEM membrane defining the diluate compartment (Figure 10). According to the analysis of variance and a Tukey's test, all Sicopion membranes had a significantly higher effect ($P < 0.001$) on the total pH variation in the diluate after a 100-minute demineralization procedure, in contrast to CMX-SB membranes. The same case applied for the total pH variation of the concentrate solution ($P < 0.001$). In general, pH changes in the diluate were due to a more or less important leakage of OH^- through the CMX or Sicopion membrane from the concentrate, leading to the OH^- enrichment of the diluate. These mechanisms had a considerably more pronounced effect when Sicopion membranes were used (Figure 10), but OH^- leakage has also reported to occur, in lower quantities,

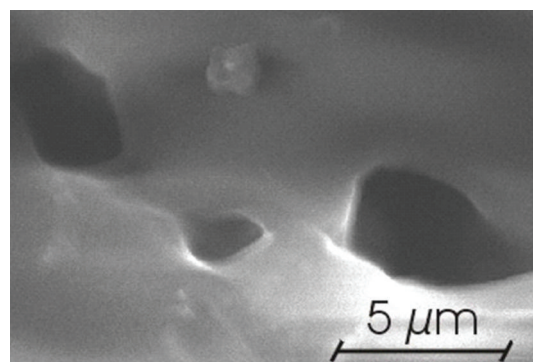


FIGURE 8: SEM of a cavity found on a Sicopion 35% SFSP membrane.

in CMX membranes [12, 13]. However, given the high concentration of OH^- ions present in the concentrate solution, for a same amount of OH^- migrating, the pH variation of the concentrate was much lower than that of the diluate.

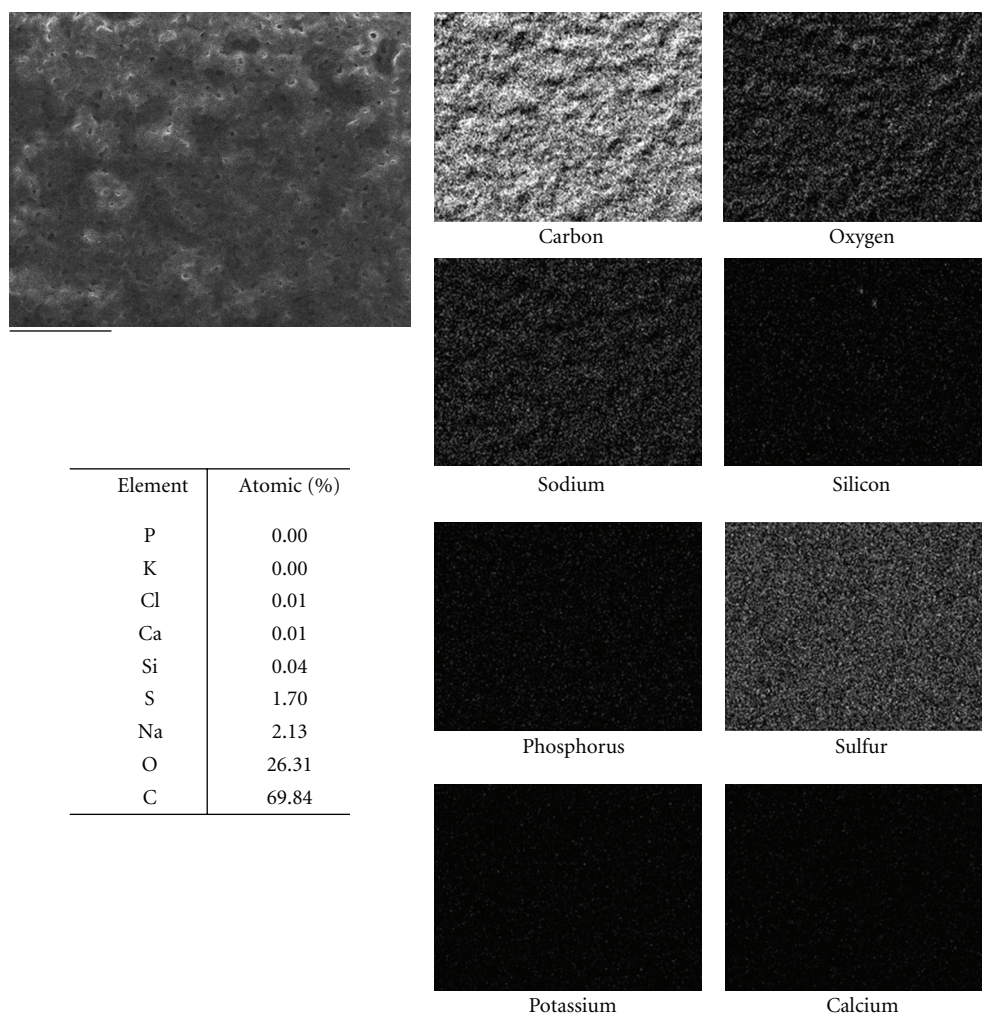


FIGURE 9: X-ray EDS mapping and relative atomic composition for a Sicopion 35% SFSP membrane. Bar under SEM is 100 μm .

Furthermore, a tendency of the pH values reaching a stabilization plateau could be observed (Figure 10). This would be due to the fact that, as OH^- ions enriched the diluate, a fraction of them could continue their path towards the anode and traverse the AEM membrane on the other side (i.e., opposite to the defining CEM) of the diluate compartment. This way, OH^- would have migrated over and over, until the pH difference between the concentrate and the diluate solutions had begun to equilibrate in OH^- concentrations.

During the demineralization process, an OH^- leakage (i.e., OH^- through the cation-exchange membrane) stands as the most probable cause for such pH variations. This hypothesis is supported by the high water content of the Sicopion membranes, given the loss of SFSP. The hydration level of a membrane can influence its microstructure and mechanical properties [11]. Hence, water present in the membranes would act as a medium through which migrating cations could create a backflow pathway for OH^- attracted towards the anode. This phenomenon would constitute the counterpart of H^+ leakage through the AEM similar to the Grøtthus mechanism (also termed proton hopping or structural diffusion mechanism) [14]. This proton hopping

(Figure 11; AEM) is due to the presence of proton acceptors (e.g., water molecules and acidic species contained in the feed solution within the AEM) [15]. Such proton acceptors may allow a certain coion (H^+ in the case of AEM) backflow, according to the electrostatic attraction towards the cathode. As more water is present in the membrane, it is easier for a relatively large ion (OH^- in contrast to H^+) to follow the same backflow pattern in CEM (Figure 11; CEM), using counterions traversing the membrane as a mobile ion-exchange site, to increase its own leakage through the CEM, as suggested by Piela and Wrona [16] for Nafion membranes. This was probably the case of Sicopion membranes. Furthermore, membrane thickness could have also had an effect on this backflow, by promoting a diffusion of OH^- by simple concentration gradient, enhanced by the microporous structure left by the SFSP leaching. It must be mentioned that the ultrathin properties of such membranes are indeed thought according to fuel cell application, where miniaturization constitutes an important advantage, which is not necessarily the case in ED applications like bulk solution demineralization. Hence, membrane thickness, at least for ED applications, could be increased to reduce OH^-

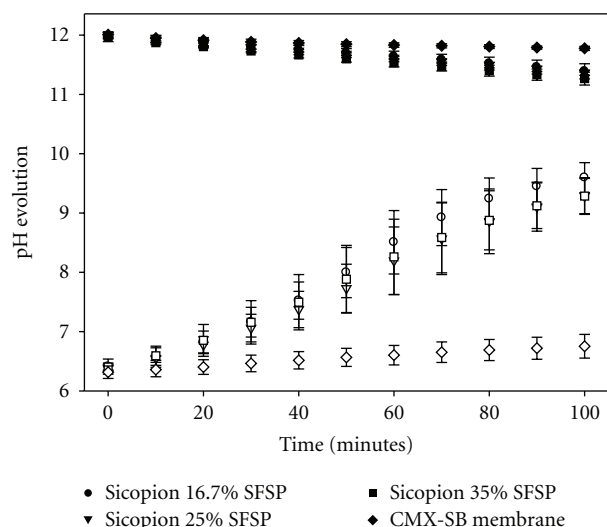


FIGURE 10: Evolution of pH in the concentrate and diluate solutions (solid and empty symbols, resp.) during the 100-minute demineralization procedure. Membranes specified in the legend indicate the CEM defining the diluate compartment.

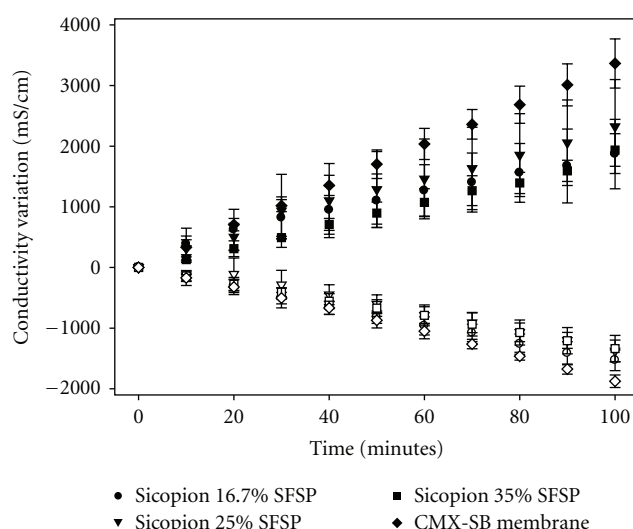


FIGURE 12: Conductivity evolution of the concentrate and diluate solutions (solid and empty symbols, resp.) during the 100-minute demineralization procedure. Membranes specified in the legend indicate the CEM defining the diluate compartment.

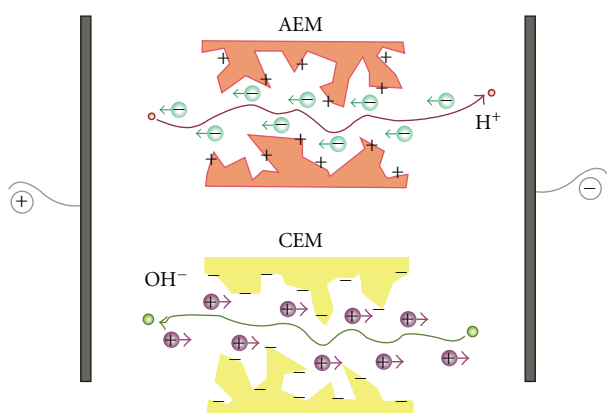


FIGURE 11: Schematic representation (offscale) of H^+ traversing an anion-exchange membrane (AEM) and the proposed counterpart for OH^- hopping through mobile counterions in the cation-exchange membrane (CEM) in a working AFNOR-conditioned Sicopion ED stack.

migration, apparently without any drawbacks on membrane performance.

It is to remark that, at least for the ED conditions used in this work, a diluate basification implied a high OH^- migration through the CEM via the proposed backflow mechanism. This indicates that OH^- diffusion, eased by the highly hydrated membranes and the low thickness value of the membranes, could have facilitated the mentioned phenomenon. Hence, a concentrate with a neutral pH would minimize OH^- backflow into the diluate. In the present study, an alkaline pH had been chosen in order to prevent the formation of a protein fouling on the AEM defining the diluate compartment according to previous works [7].

3.2.2. Conductivity Variation of the Diluate and Concentrate Solutions. Conductivity values for the diluate solution were followed to indirectly describe the demineralization progress. As expected, the conductivity increase was higher than its respective decrease in the diluate solutions because the concentrate solution is also enriched by minerals migrating from the electrode rinsing solution. Conductivity values for the diluate solution showed that demineralization rates, calculated as the variation between the initial and the final conductivity readings, were similar for all Sicopion membranes ($35.94 \pm 3.53\%$, all membranes averaged). CMX-SB membranes, on the other hand, appeared to attain a higher demineralization rates ($45.54 \pm 2.79\%$), which was also confirmed by the faster conductivity increase of the concentrate solution (Figure 12). Although these demineralization rates are a good indicator of the overall process, they must be carefully interpreted, since OH^- influences the conductivity values [17]. Further analysis, such as cation migration, should be compared to conductivity changes in order to determine whether the demineralization rates reflected an accurate mineral depletion and not a combination of the latter with high pH variation (i.e., high OH^- variations).

3.2.3. Cation Migration. Cation migration evolution (K^+ , Na^+ , and Ca^{+2}) showed similar tendencies for all Sicopion membranes and confirmed the results obtained by solution-conductivity measurements. In all cases, a higher demineralization level of the diluate was found for CMX-SB membranes, with respect to Sicopion membranes (Figure 13), but equivalent mineralization levels of the concentrate streams for all membranes (Figure 13).

If cation demineralization is analyzed from the migrated charge perspective by calculating the equivalents of migrated mass, it is found that, once again, no significant differences are found between Sicopion membranes (Table 4). However,

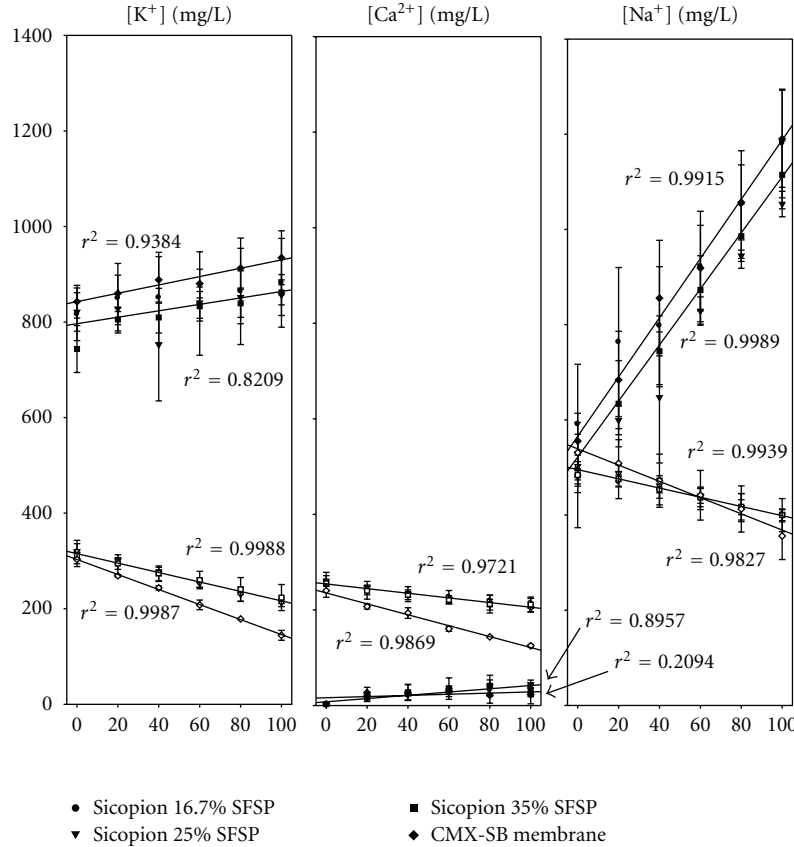


FIGURE 13: Cation concentration evolution in concentrate and diluate solutions (solid and empty symbols, resp.) treated by ED with CMX-SB or Sicopion membranes. Regressions are, according to the legend, for CMX-SB membranes and for all 3 Sicopion membranes.

TABLE 4: Total demineralization rates of the diluate solution in potassium, calcium, sodium, and total cations after 100-minute treatment, in milligrams per liter (mg/L) and milliequivalents per liter (mEq/L).

CEM membrane (of diluate compartment)	K		Ca		Na		Total mEq/L
	mg/L	mEq/L	mg/L	mEq/L	mg/L	mEq/L	
Sicopion 16.7% SFSP	100.85 ± 26.76	2.58 ± 0.68	45.92 ± 14.17	2.29 ± 0.71	96.38 ± 27.28	4.19 ± 1.19	9.06 ± 2.55
Sicopion 25.0% SFSP	108.00 ± 21.14	2.76 ± 0.54	57.48 ± 15.99	2.87 ± 0.80	104.23 ± 25.46	4.53 ± 1.11	10.17 ± 2.42
Sicopion 35.0% SFSP	87.42 ± 22.85	2.24 ± 0.58	44.03 ± 16.23	2.20 ± 0.81	84.47 ± 25.41	3.67 ± 1.11	8.11 ± 2.45
CMX-SB	158.66 ± 16.13	4.06 ± 0.41	115.40 ± 15.36	5.76 ± 0.77	175.20 ± 16.49	7.62 ± 0.72	17.44 ± 1.79

and in contrast to cation concentration evolutions, mineralization rates of the concentrate, expressed as net migrated milliequivalents, turned out to be equivalent for CMX-SB and Sicopion membranes (Table 5). On the other hand, demineralization rates of the diluate solution did show an important difference between the CMX-SB membrane and the Sicopion ones. Since the concentrate mineralization levels were equivalent and the demineralization rates were higher for the ED procedures where a CMX-SB was used, the balancing species mineralizing the concentrate would have come from the electrolyte solution. However, Na^+ concentrations are those with the higher migration rate towards the concentrate, confounding ions coming from the diluate and from the electrolyte solution into the concentrate compartment. According to the initial concentration of such ions

in the diluate, it is possible to say that they demonstrated to be the predominant cations for current flow. At the same time, the higher cation levels (K^+ , Na^+ , Ca^{2+}) present in the diluates demineralized with a Sicopion membrane would confirm what was explained in the pH evolution section of this paper. Cations migration was disfavoured by the enrichment in OH^- of the diluate, maintaining the electroneutrality of the solution as it compensated for the anions migrating through the AEM.

3.2.4. System Resistance. System resistance evolution was similar for all stacks equipped with Sicopion membranes (Figure 14). Towards the end of the demineralization procedures, resistance increased at a higher rate for CMX-SB membranes due to the lower conductivity of the diluate

TABLE 5: Total mineralization rates of the concentrate solution in potassium, calcium, sodium, and total cations after 100-minute treatment, in milligrams per liter (mg/L) and milliequivalents per liter (mEq/L).

CEM membrane (of diluate compartment)	K		Ca		Na		Total
	mg/L	mEq/L	mg/L	mEq/L	mg/L	mEq/L	mEq/L
Sicopion 16.7% SFSP	65.98 ± 37.96	1.69 ± 0.97	34.40 ± 5.08	1.72 ± 0.25	589.74 ± 53.05	25.65 ± 2.31	29.06 ± 3.52
Sicopion 25.0% SFSP	35.47 ± 8.09	0.91 ± 0.21	41.87 ± 8.48	2.09 ± 0.42	573.60 ± 14.27	24.95 ± 0.62	27.95 ± 1.09
Sicopion 35.0% SFSP	118.44 ± 71.45	3.03 ± 1.83	25.25 ± 10.90	1.26 ± 0.54	630.89 ± 49.81	27.44 ± 2.17	31.73 ± 4.33
CMX-SB	91.94 ± 26.72	2.35 ± 0.68	19.67 ± 19.23	0.98 ± 0.96	634.99 ± 43.82	27.62 ± 1.91	30.95 ± 1.60

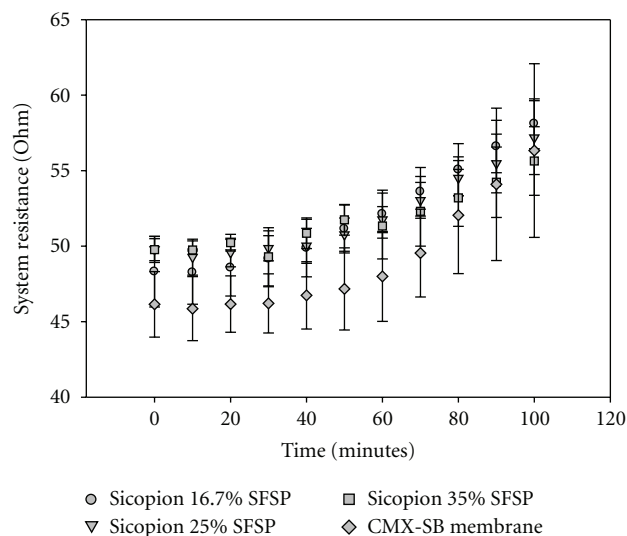


FIGURE 14: Resistance evolution of the ED stacks during the 100-minute demineralization procedure. Membranes specified in the legend indicate the CEM defining the diluate compartment.

solution, given by its higher demineralization level with respect to Sicopion membranes, as previously explained for conductivity variation. In addition, the stack resistance was found to be, in general, slightly higher ($\approx 5 \Omega$) when equipped with Sicopion membranes, with respect to the stack with CMX-SB (Figure 14). This could be explained by the OH^- traversing the CEM, partially hindering the current flow, since it was found that Sicopion membranes actually had a lower electrical resistance than CMX-SB membranes (Figure 5). This resistance difference seems normal, given the important thickness difference between the two types of membranes and to the fact that the materials they are made of have, in general, similar IEC values. Hence, the OH^- backflow could account for the global increased resistance of the system.

3.2.5. Energy Consumption. The results obtained showed a similar consumption for all membranes, Sicopion (1.47 ± 0.03 Wh) and CMX-SB (1.38 ± 0.08 Wh). Although CMX-SB membranes allowed a higher demineralization rate, total migration through Sicopion membranes was probably equivalent, given the high amount of OH^- transported through the latter. Such backflow would have consumed a

certain amount of energy, hence reducing the global demineralization rate of the diluate and increasing the energy consumption of the ED procedure.

4. Conclusion

In this study, it was shown that membrane conditioning actually leaches out the SFSP leaving a water-enriched microporous structure of SPEEK. Important variations were found only at the IEC level and water content of the membranes. These variations, however, did not show any significant effects on their practical electrodialytic characteristics for the demineralization conditions used in this particular work.

With respect to CMX-SB membranes, several differences were found for Sicopion membranes, but these were mainly due to the different nature of such membranes. The most important difference between both types of membranes was their OH^- permeability, being considerably higher for Sicopion membranes. Membrane composition and imaging supported the OH^- backflow hypothesis. The membrane cavities would contribute to higher water content of the membranes and, by creating microscopic pores, would increase the amount of OH^- backflow paths, as previously discussed. Although OH^- permeability of Sicopion membranes could offer a new perspective for some specific applications, like fruit juice deacidification [18], OH^- leakage could be reduced by increasing the membrane thickness, reducing the backflow and diffusion of OH^- . Sicopion membranes would then be an interesting option for procedures requiring relatively constant or acidic pH conditions. Indeed, according to previous studies [7], a neutral pH would minimize the risk of a CEM integrity alteration due to fouling during the demineralization of liquid foodstuffs containing proteins and divalent cations. In addition, the loss of SFSP during conditioning could be a way for manufacturing membranes with micro- or nanoscale pores that could be used in electrodialysis with filtration membrane. This new electromembrane technology separates bioactive molecules according to their charge (electric field as driving force) and size (molecular weight cutoff of the filtration membrane) [19]. Finally, one of the most attractive advantages of Sicopion membranes is their dry-to-hydrated dimensional stability which is of particular interest for industrial-scale ED stacks, since (as for CEM) it would allow a dry mounting process. This contrasts with the wet environment that must be maintained during the stack assembly for commercially available membranes.

Acknowledgments

The authors wish to thank Ms. Monica Araya-Farias from the Laval University, Ms. Diane Montpetit from the Agriculture and Agri-Food Canada, Mr. Pierre-Gilles Vaillancourt from the SiM Composite, and Ms. Isabelle Montplaisir from the Laboratory of Energy Technologies (LET) for their technical assistance. The support of the Hydro-Quebec Research Institute and access given to LET is also acknowledged. The authors recognized that there is no conflict of interests concerning the quality of results obtained.

References

- [1] M. St-Arnaud and P. Bebin, "Ion exchange composite material based on proton conductive silica particles dispersed in a polymer matrix," Patent, WO 03/083985 A2, 2003.
- [2] W. Richard Bowen, T. A. Doneva, and H. B. Yin, "Polysulfone—Sulfonated poly(ether ether) ketone blend membranes: systematic synthesis and characterisation," *Journal of Membrane Science*, vol. 181, no. 2, pp. 253–263, 2001.
- [3] V. Baglio, A. S. Aricò, V. Antonucci et al., "An NMR spectroscopic study of water and methanol transport properties in DMFC composite membranes: influence on the electrochemical behaviour," *Journal of Power Sources*, vol. 163, no. 1, pp. 52–55, 2006.
- [4] E. Ayala-Bribiesca, G. Pourcelly, and L. Bazinet, "Nature identification and morphology characterization of cation-exchange membrane fouling during conventional electrodialysis," *Journal of Colloid and Interface Science*, vol. 300, no. 2, pp. 663–672, 2006.
- [5] Association Française de Normalisation, Norme française homologuée pour les membranes polymères échangeuses d'ions NF X 45-200. France, 1995.
- [6] E. Räsänen, M. Nyström, J. Sahlstein, and O. Tossavainen, "Purification and regeneration of diluted caustic and acidic washing solutions by membrane filtration," *Desalination*, vol. 149, no. 1–3, pp. 185–190, 2002.
- [7] E. Ayala-Bribiesca, M. Araya-Farias, G. Pourcelly, and L. Bazinet, "Effect of concentrate solution pH and mineral composition of a whey protein diluate solution on membrane fouling formation during conventional electrodialysis," *Journal of Membrane Science*, vol. 280, no. 1–2, pp. 790–801, 2006.
- [8] D. A. Cowan and J. H. Brown, "Effect of turbulence on limiting current in electrodialysis cells," *Industrial & Engineering Chemistry*, vol. 51, no. 12, pp. 1445–1448, 1959.
- [9] L. Bazinet, F. Lamarche, R. Labrecque, and D. Ippersiel, "Effect of number of bipolar membranes and temperature on the performance of bipolar membrane electroacidification," *Journal of Agricultural and Food Chemistry*, vol. 45, no. 10, pp. 3788–3794, 1997.
- [10] L. Bazinet, D. Ippersiel, D. Montpetit, B. Mahdavi, J. Amiot, and F. Lamarche, "Effect of membrane permselectivity on the fouling of cationic membranes during skim milk electroacidification," *Journal of Membrane Science*, vol. 174, no. 1, pp. 97–110, 2000.
- [11] R. Jiang, H. R. Kunz, and J. M. Fenton, "Composite silica/Nafion membranes prepared by tetraethylorthosilicate sol-gel reaction and solution casting for direct methanol fuel cells," *Journal of Membrane Science*, vol. 272, no. 1–2, pp. 116–124, 2006.
- [12] L. Bazinet, D. Montpetit, D. Ippersiel, J. Amiot, and F. Lamarche, "Identification of skim milk electroacidification fouling: a microscopic approach," *Journal of Colloid and Interface Science*, vol. 237, no. 1, pp. 62–69, 2001.
- [13] L. Bazinet, D. Montpetit, D. Ippersiel, B. Mahdavi, J. Amiot, and F. Lamarche, "Neutralization of hydroxide generated during skim milk electroacidification and its effect on bipolar and cationic membrane integrity," *Journal of Membrane Science*, vol. 216, no. 1–2, pp. 229–239, 2003.
- [14] D. Seeliger, C. Hartnig, and E. Spohr, "Aqueous pore structure and proton dynamics in solvated Nafion membranes," *Electrochimica Acta*, vol. 50, no. 21, pp. 4234–4240, 2005.
- [15] S. Roualdes, N. Kourda, J. Durand, and G. Pourcelly, "Plasma-grafted PVDF polymers as anion exchange membranes for the electrotransport of Cr(VI)," *Desalination*, vol. 146, no. 1–3, pp. 273–278, 2002.
- [16] P. Piela and P. K. Wrona, "Some anion-transport properties of Nafion 117 from fuel cell hydrogen peroxide generation data," *Journal of Power Sources*, vol. 158, no. 2, pp. 1262–1269, 2006.
- [17] F. L. T. Shee, P. Angers, and L. Bazinet, "Relationship between electrical conductivity and demineralization rate during electroacidification of cheddar cheese whey," *Journal of Membrane Science*, vol. 262, no. 1–2, pp. 100–106, 2005.
- [18] E. Vera, J. Sandeaux, F. Persin, G. Pourcelly, M. Dornier, and J. Ruales, "Deacidification of clarified tropical fruit juices by electrodialysis—part I. Influence of operating conditions on the process performances," *Journal of Food Engineering*, vol. 78, no. 4, pp. 1427–1438, 2007.
- [19] L. Bazinet and L. Firdaous, "Membrane processes and devices for separation of bioactive peptides," *Recent Patents on Biotechnology*, vol. 3, no. 1, pp. 61–72, 2009.

Research Article

Hybrid Anion Exchange Hollow Fiber Membrane for Delivery of Ionic Drugs

Na Wang,¹ Mengbing Cui,¹ Cuiming Wu,² Yiyun Cheng,³ and Tongwen Xu¹

¹Laboratory of Functional Membranes, School of Chemistry and Material Science, University of Science and Technology of China, Hefei 230026, China

²School of Chemical Engineering, Hefei University of Technology, Hefei 230009, China

³School of Life Sciences, East China Normal University, Shanghai 200062, China

Correspondence should be addressed to Tongwen Xu, twxu@ustc.edu.cn

Received 30 October 2011; Revised 29 December 2011; Accepted 10 January 2012

Academic Editor: Victor V. Nikonenko

Copyright © 2012 Na Wang et al. This is an open access article distributed under the Creative Commons Attribution License, which permits unrestricted use, distribution, and reproduction in any medium, provided the original work is properly cited.

Hybrid anion exchange hollow fiber membranes (HAEHFMs) based on bromomethylated poly(2,6-dimethyl-1,4-phenylene oxide) (BPPO) are proposed as potential drug carriers for four anionic model drugs, including the sodium salts of benzoate (NaBS), salicylate (NaSA), meta-amino salicylate (NaMAS), and loxoprofen (NaLS). The results of the static loading and release experiments suggest that electrostatic interaction, hydrogen bonding, and hydrophobic interaction are the main interaction patterns between the membrane and the drugs. And they are directly influenced by the external phase conditions and the drug physicochemical characteristics, such as structure, molecular weight, dissociation (pKa), and hydrogen bonding capability. Among the four different drugs, NaSA and NaMAS appear to be the most suitable for controlled release by the HAEHFM due to their excellent adsorption/release behaviors.

1. Introduction

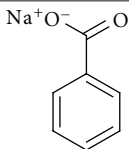
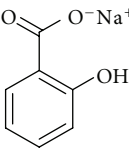
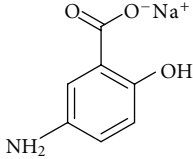
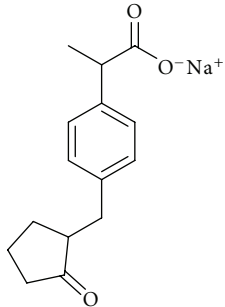
Controlled drug release has attracted increasing attention during recent decades because of its special advantages on providing a relatively steady blood level of drug, optimizing the drug therapeutics and improving patient compliance. The most significant pursuit of developing controlled release system is to prolong the retention of the drug and get a constancy of release rate. Membranes have been evaluated as one of the most promising drug delivery vehicles [1, 2]. In order to develop rate-limiting drug delivery membrane, ion transport and ion exchange mechanisms can be introduced through the use of ion exchange membranes (IEMs). The ion exchange groups of the IEMs can capture the ionized drugs through electrostatic interactions and thus provide a permselectivity for the therapeutic agents in the drug delivery profiles [3]. Up to date, many types of IEMs have been used directly or modified as drug vehicles such as Nafion [4], modified chitosan [1, 5–7], polypyrrole [8], poly(acrylic acid) grafted poly(vinylidene fluoride) (PAA-PVDF) [9, 10], and bromomethylated poly(2,6-dimethyl-1,4-phenylene

oxide) (BPPO) membranes [11]. The rate-limiting performance of the IEMs for ionic drugs mainly depends on the physical and chemical properties of the IEMs and the drugs, as well as the external solution conditions [12].

IEMs can be classified into ion exchange flat membranes and ion exchange hollow fiber membranes (IEHFMs) according to the physical configuration. IEHFMs, as a novel type of drug delivery vehicles, have been proved to be effective in rate-limiting drug release. Our research group has previously promoted a novel type of hybrid anion exchange hollow fiber membrane (HAEHFM) from brominated poly(2,6-dimethyl-1,4-phenylene oxide) (BPPO) and γ -methacryloxypropyl trimethoxysilane (γ -MPS) for controlled release of sodium salicylate (NaSA) [13]. The HAEHFM exhibits low toxicity, large effective surface area, and high ion exchange content (IEC), ensuring a high drug loading efficiency (28.4%) and a relatively low release rate (drug released in 7 days under physiological condition: 51.9%).

The present work is to extend our previous study and to investigate further the effect of the drug characteristics on the loading and release behaviors. As well known,

TABLE 1: Structures and physicochemical characteristics of the model drugs.

Compound	Structure	Mw	pKa ^{17–20}	HBD/HBA*
Sodium benzoate (NaBS)		144.1	4.17 (–COOH)	0/2
Sodium salicylate (NaSA)		160.1	2.98 (–COOH), 13.9 (–OH)	1/3
Sodium meta-amino salicylate (NaMAS)		175.1	2.74 (–COOH), 5.84 (–NH ₃ ⁺), 13.9 (–OH)	1/4
Loxoprofen sodium (NaLS)		268.3	4.20 (–COOH)	0/3

* Hydrogen bond donor (based on –OH groups)/hydrogen bond acceptor (based on O-atoms and N-atoms); it is assumed that carboxyl groups are ionized during the experiments.

the physicochemical properties of the drugs such as charge, molecular weight, dissociation (pKa), lipophilicity and hydrogen bonding can greatly affect the adsorption and release behaviors [12]. Previous researches are abundant regarding the effect of these drug properties on the controlled release behavior of ion exchange flat membranes, fibers, or resins [12, 14–16]. For example, Jaskari et al. and Hanninen et al., both, proved that lipophilic drugs tend to bond onto the weak base anion exchange fibers [15, 16]. However, few studies have been performed with IEHFM. For our IEHFMs, the interaction mechanisms with the drug might be even more complex, since there are both organic and inorganic components in the membrane matrix. The presence of –SiOH and ester groups from γ -MPS may influence the loading and release behaviors comprehensively.

Four model drugs are selected here, including the sodium salts of benzoate (NaBS), salicylate (NaSA), meta-amino salicylate (NaMAS), and loxoprofen (NaLS) (Table 1 [17–20]). Among these, salicylic acid (SA), meta-amino salicylate (MAS), and loxoprofen (LS) are widely used nonsteroidal anti-inflammatory drugs (NSAIDs). NaBS, a commonly used food preservative, is also used here for its structure similarity to the other drugs. The four drugs differ in physicochemical characteristics such as molecular weight, pKa, and hydrogen bonding capacity. Nevertheless, they all contain carboxyl groups, which produce negatively charged anions when

dissociated. The drug loading capacity and the drug release rate and extent from the HAEHFM in different external solutions are to be studied and compared. The mechanisms of drug binding into and release from the ion exchange drug carriers are to be discussed so as to provide guidance for the selection, optimization, and application of the drug vehicles.

2. Material and Methods

2.1. Materials. Brominated poly(2,6-dimethyl-1,4-phenylene oxide) (BPPO) hollow fiber membranes were kindly supplied by Tianwei Membrane Corporation Ltd. (Shandong, China) with 53% benzyl substitution ratio and 47% aryl substitution ratio. γ -methacryloxypropyl trimethoxysilane (γ -MPS) and triethylamine (TEA) were diluted with ethanol to 1.0 mol/L before use. Sodium salicylate (NaSA) and sodium meta-amino salicylate (NaMAS) were purchased from Tianjin Damao Chemical Reagent Factory (Tianjin, China) and Weihai Disu Pharmaceutical Co., Ltd. (Shandong, China), respectively. Sodium benzoate (NaBS), loxoprofen sodium (NaLS), and dialysis membrane (molecular weight cut-off, MWCO~3500 Da) were obtained from Bio Basic Inc. (BBI) (Shanghai, China). Bovine serum albumin (BSA) and glucose (Glc) were from Sinopharm Chemical Reagent Co., Ltd (Shanghai, China). The reagents were all of analytical grade and double-distilled water was used throughout.

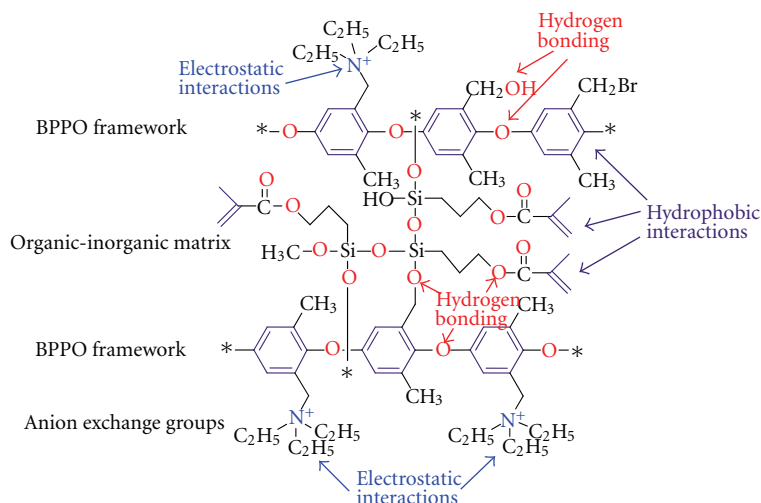


FIGURE 1: The structure of the HAEHFM and different interaction patterns between the HAEHFM and drugs.

Phosphate buffer solutions (PBSs) with pH values of 5.0, 7.4, and 9.0 were prepared by $\text{Na}_2\text{HPO}_4\text{-KH}_2\text{PO}_4$ with phosphate concentration of 0.2 mol/L. One simulated body fluid was prepared containing 0.2 mol/L PBS (pH = 7.4), 100 mg/dL glucose, and 70 mg/mL BSA. The simulated body fluid without BSA was also prepared.

2.2. Preparation and Characterizations of the Drug Carrier: The HAEHFM. The HAEHFM was prepared from BPPO hollow fiber membrane through three steps, as has been described in detail in our earlier study [21]: partial hydrolysis by KOH, in situ sol-gel process with γ -MPS, and quaternization by TEA. The main properties of the HAEHFM are as follows: inner and outer diameter of 0.70 mm and 1.06 mm, ion exchange capacity (IEC) of 1.76 mmol/g dry membrane, water content (W_R) of 62.9%, and dimensional change ratio (DCR) of 12.9% in water.

As illustrated in Figure 1, the BPPO frameworks are crosslinked by Si-O-Si network formed in the sol-gel process. According to the polymer structure, three main types of interaction patterns between the HAEHFM and drugs can be present: electrostatic interactions, hydrogen bonding, and hydrophilic interactions. The strong anion exchange groups (quaternary amino groups) on the backbone of the polymer provide sites for electrostatic binding. The oxygen atoms (from BPPO frameworks, ester bonding in γ -MPS, and the Si-O-Si bonding) and the hydroxyls groups (from BPPO and silanol groups) can form hydrogen bonds with drugs in water. Besides, hydrophilic interactions may exist between drugs and the benzene rings or methyl vinyls of the HAEHFM.

2.3. Drug Loading Studies. The HAEHFM was loaded with the model drugs through static adsorption. Dry membranes (0.05 g) were cut into pieces with length of 5–8 mm then added into 4 mL aqueous solutions of different drugs (from

TABLE 2: The UV test parameters of different drugs.

Drug	Wavelength (nm)	Test concentration ($\mu\text{mol/L}$)
NaBS	228	4–114
NaSA	295	27–266
NaMAS	330	27–11500
NaLS	225	12–132

0.05 to 100 mmol/L) and kept at 30°C for 24 h. Then the membrane was taken out and washed by water (with a total volume of 5 mL) to remove the drug adhered on the surface. The washing solutions and the adsorption solutions after drug loading were collected for concentration analysis.

For concentration determination, the drug solutions were diluted into proper concentrations and then tested using a UV-2550 UV-VIS spectrophotometer (Kyoto, Japan). The characteristic adsorption wavelength of each drug was found and listed in Table 2. Because there is a linear relationship between the absorbance and concentration when the absorbance is between 0.1–1.0, each sample was diluted to proper concentration before testing. The testing concentration ranges of the model drugs are also listed in Table 2. The drug loading content was calculated by the following equation:

$$S = \frac{V(c_0 - c)}{m} \times 10^{-3}, \quad (1)$$

where S (mmol/g dry membrane) is the total content of a model drug adsorbed by the HAEHFM; c_0 and c (mmol/L) are the concentrations of the model drug before and after drug loading. V (mL) means the volume of the adsorption solution, which is 4 mL in this study. m (g) means the weight of the testing membrane, which is 0.05 g in this study.

The curves of the loading contents versus original drug concentrations are fitted by the Langmuir isotherm mechanism [22]:

$$q = \frac{q_m K c_0}{1 + K c_0}, \quad (2)$$

where K is Langmuir equilibrium constant (mL/mg), q is the drug adsorption under a certain original drug concentration, and q_m is the maximum amount of drug adsorption. By curve fitting of the drug loading data under different drug concentrations, the value of q_m and K can be calculated.

2.4. Release Behaviors. Three different release experiments were performed for each model drug.

- (1) The release experiment in pure water. The HAEHFM (0.05 g) loaded with drugs were immersed into 50 mL of water and kept at 37°C for 12 h. 3 mL of the solution was sampled at each predetermined sampling time. Fresh water was added immediately after each sampling. The cumulative amount of drug released was determined by the UV absorbance.
- (2) The pH dependence. The procedures were the same as above in pure water, except that 0.2 mol/L PBSs with varied pH values (5.0, 7.4, and 9.0) were used.
- (3) Release behaviors under physiological condition. The HAEHFM loaded with the model drug was added into a dialysis bag containing 5 mL simulated body fluid medium. Then the dialysis bag was immediately immersed into the simulated body fluid without BSA (45 mL). 3 mL of the solutions out of the dialysis bag were sampled every 12 h and the experiments last for one week.

Diffusion coefficients D (cm²/s) can be obtained through fitting the release curves by the Higuchi equation [23]:

$$\frac{Q}{A} = 2C_0 \sqrt{\frac{Dt}{\pi}}, \quad (3)$$

where Q/A is the amount of drug released per unit area at the time t and C_0 is the initial concentration of a model drug in the HAEHFM. A is the membrane surface area and can be calculated from the inner, outer diameter, and the length of the membrane.

3. Results and Discussion

3.1. Binding of Different Drugs to the AEHFM. The data of the drug loading contents versus different original drug concentrations are fitted by Langmuir isotherm mechanism (2). Figure 2 suggests that the data of NaSA, NaMAS, and NaLS can fit the Langmuir isotherm mechanism well (the coefficient of determination (R^2) > 0.97). This indicates that the adsorption is congruous to the assumptions of the Langmuir isotherm mechanism: (1) the drug does not interact with itself; and (2) only one monolayer is formed at the maximum adsorption [22]. This way of adsorption is beneficial for slow and sustained drug release.

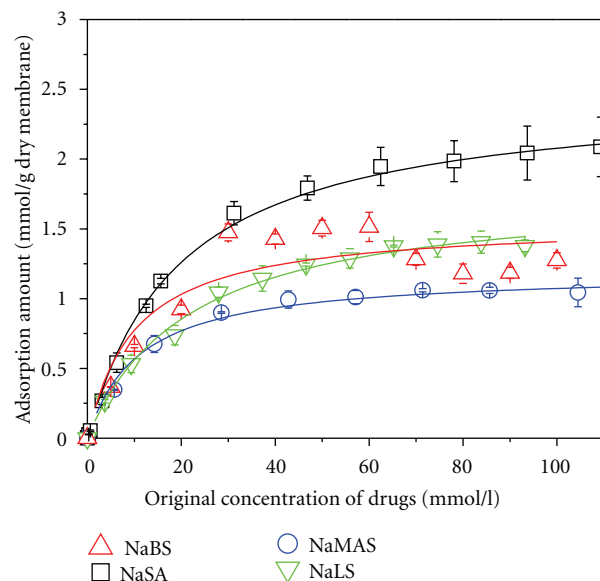


FIGURE 2: Loading contents of different drugs onto the HAEHFM as the original drug concentrations increase. Experimental conditions: 24 h at 30°C.

Nevertheless, the adsorption behaviour of NaBS does not agree well with the fitting result ($R^2 = 0.73$). The adsorption amount of NaBS increases first with the increase of NaBS concentration, then decreases somehow when NaBS concentration is in the range of 60–80 mmol/L, and finally increases again at NaBS concentration higher than 80 mmol/L. The abnormality of the NaBS adsorption behavior should be due to the peculiarity of the drug structure. As shown in Table 1, NaBS molecule possesses only one carboxyl group which is highly hydrophilic. The benzene ring, on the other hand, is highly hydrophobic. Hence phenyl stackings might be formed in aqueous solution through the parallel displaced or T-shaped arrangements [24] as shown in Figure 3. The possible explanation of the changing trend of the NaBS curve in Figure 2 can be presumed as follows. Under low concentration of NaBS, the drug adsorption amount onto the membrane increases with the NaBS concentration as the number of free drug molecules in the solution increases. However, when NaBS concentration is higher than 60 mmol/L, NaBS stackings begin to form, which decrease the number of free drug molecules and thereby the adsorption amount decreases. With further increase in NaBS concentration, the stackings grow in size and number and further formation of the stacking structure becomes more difficult. Therefore, the number of free drug molecules becomes increasing again, leading to an increase in drug adsorption amount.

The q_m values of the drugs are obtained from fitting the curves of the loading contents versus original drug concentrations by equation (2) and the results are illustrated in Figure 4. The q_m values are all over 1.2 mmol/g, relatively high as compared with some reported values [11, 25]. Meanwhile, the value of q_m/IEC , which indicates the ratio of maximal drug binding content and the ion exchange capacity of the membrane, is in the range of 68–141%. The q_m/IEC

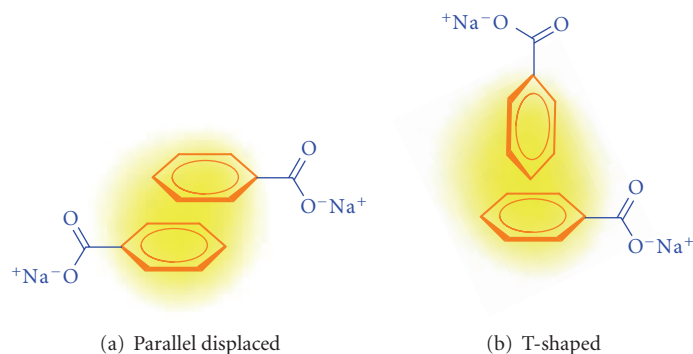
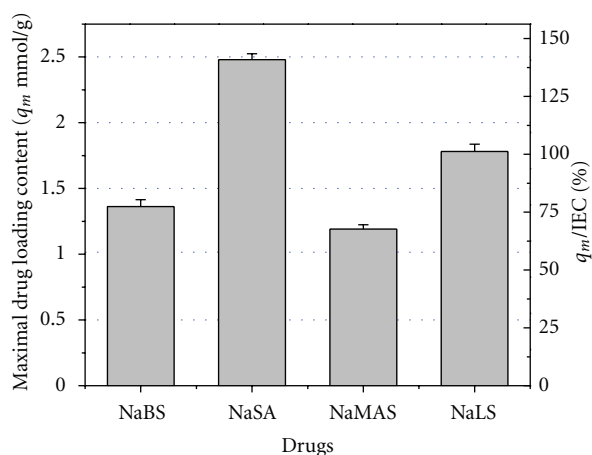


FIGURE 3: The supposed arrangements of the stackings formed in NaBS solution.

FIGURE 4: The maximal drug loading contents (q_m) and the values of q_m /IEC for different drugs onto the HAEHFM.

values of NaSA and NaLS are over 100%, indicating that some other interactions besides the electrostatic interaction are present.

The q_m values of the drugs can be arranged as NaSA > NaLS > NaBS > NaMAS. The reason should be attributed to the difference of the drug structures, as explained in the following.

- (1) Compared with NaBS and NaLS, salicylate (NaSA and NaMAS) possesses an extra phenolic hydroxyl group (Ph-OH). The Ph-OH group can partly dissociate into phenol anion (Ph-O⁻) and form hydrogen bonding with the drugs, both of which are beneficial for the affinity of the drug to the membrane. And the pKa values of NaSA and NaMAS are 2.98 and 2.74 (-COOH), much lower than the other two drugs (Table 1). Therefore, the high q_m value of NaSA can be well understood.
- (2) Nevertheless, NaMAS contains an amino group, which might be protonated into -NH₃⁺ group. Hence, neutral intrinsic molecular salts can be formed in NaMAS solution [12, 26], decreasing the adsorption of NaMAS to the membrane. Therefore, the q_m value of NaMAS is the lowest.

- (3) NaLS possesses one more carbonyl and one five-membered ring as compared with NaBS. The O-atom from the carbonyl can act as the hydrogen bonding acceptor, and the five-membered ring increases the hydrophobicity of NaLS. Hence the hydrogen bonding and hydrophobic interactions between NaLS and the membrane are increased, leading to higher q_m value of NaLS than NaBS.

3.2. Release of Different Drugs from the AEHFM

3.2.1. Release Behaviors of Different Drugs in Pure Water. The release behavior of the model drugs from the HAEHFM in pure water was examined and the result is shown in Figure 5. Only 0.85–7.24% of the entrapped drugs are released during the period of 12 h. The diffusion coefficients (D) of the drugs are calculated to be 4.7×10^{-7} – 3.5×10^{-5} cm²/s according to Higuchi equation (3), as listed in Table 3. The D values of NaSA and NaMAS are relatively low as compared with some reported values [12, 27], indicating the high potential of NaSA and NaMAS for controlled release by HAEHFM. As for NaBS, the D value is higher than some reported values. For instance, the D value of NaBS from liquid crystalline gels was 0.12×10^{-7} cm²/s, and the release percentage within 24 h was 25.2% [28]. The significant difference is mainly due to the difference of materials properties and the drug loading content. The release behaviour of NaLS has been rarely reported in the literature and hence the data here can give clues for its future research.

The release rates of the different model drugs (see Figure 5 or Table 3) decrease according to the following sequence: NaLS > NaBS > NaSA > NaMAS. Possible reasons for the change trend can be explained as follows.

- (1) The D values of salicylates (NaSA and NaMAS) are much lower than the other two drugs. This should be mainly due to their higher affinity to the membrane, since phenolic hydroxyl group (Ph-OH) can provide additional electrostatic interaction and hydrogen bonding.
- (2) The D value of NaMAS is the lowest among all the drugs. As discussed in Section 3.1, intrinsic molecular salts can be formed in NaMAS solution because

TABLE 3: Diffusion coefficients ($D/\times 10^{-6} \text{ cm}^2/\text{s}$) of different drugs from BPPO- γ -MPS(+) hollow fiber membrane at 37°C under different outer phase conditions, calculated by the Higuchi equation (3).

Outer phase conditions	NaBS	NaSA	NaMAS	NaLS
Pure water	16.79	1.456	0.4714	35.44
PBS at pH 5.0	1483	218.8	100.8	1598
PBS at pH 7.4	1327	123.9	77.42	4531
PBS at pH 9.0	1429	39.36	345.0	3803
PBS with 100 mg/dL Glc and 70 mg/mL BSA, pH 7.4	161.7	132.1	72.61	353.6

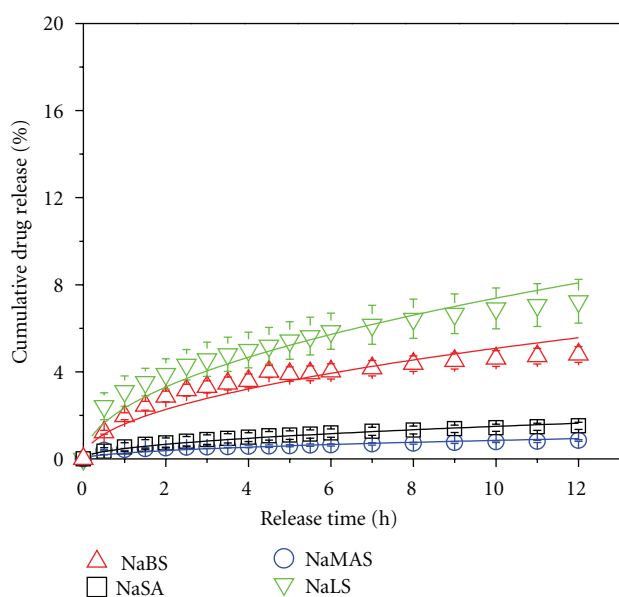


FIGURE 5: Release behaviors of different drugs from the HAEHFM in pure water at 37°C.

of the presence of $-\text{NH}_2$ groups. The electrostatic interaction with the membrane is diminished. On the other hand, the hydrogen bonding capacity of NaMAS is the strongest among all the drugs as illustrated in Table 1. Therefore, the low release rate of NaMAS should be mainly attributed to the hydrogen bonding by both $-\text{OH}$ group and $-\text{NH}_2$ groups.

- (3) NaLS shows the largest release rate in pure water, indicating the least stable association between NaLS and the membrane. As discussed in Section 3.1, NaLS contains five-membered ring and hence the hydrophobic interaction plays more important role for its affinity to the membrane. The hydrophobic interaction is relatively weak as compared with electrostatic and hydrogen bonding interactions. Besides, the five-membered ring increases the steric hindrance of NaLS. Therefore, the release rate of NaLS is the highest among all the drugs.

3.2.2. Release Behaviors of Different Drugs at Varied pH Values. Figure 6 illustrates the release behaviors of the model drugs in acidic (pH 5.0, Figure 6(a)), neutral (pH 7.4, Figure 6(b)), and basic (pH 9.0, Figure 6(c)) conditions. The D values are calculated and listed in Table 3. The D values are in the range of 3.9×10^{-5} – $4.5 \times 10^{-3} \text{ cm}^2/\text{s}$, much higher than the values in pure water. Hence, the increase of ion concentration in the external phase can lead to a significant increase in the drug release rate [13, 29]. As promoted by Haninen, the Donnan potential is decreased, and the molar amounts of counterions, as well as the concentration gradient, are increased when salty solutions are used [29]. Besides, the hydrogen bonding can also be disturbed by salty environment. All the changes can result into a higher release rate of the drugs.

At pH 5.0 and pH 7.4, the D values follow the same changing trend as in pure water: $\text{NaLS} > \text{NaBS} > \text{NaSA} > \text{NaMAS}$. Nevertheless, the D value of NaMAS is higher than that of NaSA at pH 9.0. This can be explained as follows. NaMAS contains additional $-\text{NH}_2$ groups and hence the hydrogen bonding plays important role in the affinity of NaMAS to the membrane. Hydrogen bonding tends to form at lower pH value, especially around the pK_a value of the drug [30]. In basic condition, the hydrogen bonding can be destroyed and hence the release rate is increased.

As for the influence of the pH values on the D values of each drug, interesting phenomena can be found from Table 3 as follows.

- (1) The D value of NaBS is not significantly affected by the pH value. NaBS has pK_a value of 4.17 and hence is negatively charged in different pH conditions (5.0, 7.4, and 9.0). The main interaction between NaBS and the membrane is electrostatic interaction. Thus the release behavior of NaBS is relatively stable when pH changes.
- (2) The D value of NaSA decreases gradually with the increase of the pH values. The reason for this changing trend has been discussed in our previous work [13]. Namely, the phenolic hydroxyls ($\text{Ph}-\text{OH}$) of NaSA can be partially deprotonated at higher pH condition. Therefore, the electrostatic interaction with the membrane is enhanced.
- (3) The D value of NaMAS at pH 9.0 is abnormally larger than that at the other pH conditions. This is due to the destruction of the hydrogen bonding, as discussed previously.
- (4) The D value of NaLS at pH 5.0 is relatively lower than the values at the other pH conditions. This should be due to the strengthening of the hydrogen bonding since pH 5.0 is near the pK_a value of NaLS (4.20) [30].

3.2.3. Release Behaviors of Different Drugs in a Simulated Body Fluid. As the HAEHFM is researched for the potential use of drug delivery to the focus in human body, the release behaviors of the drugs under physiological condition have been investigated. The curves in Figure 7 are fitted according to Higuchi equation (3) and the diffusion coefficients (D)

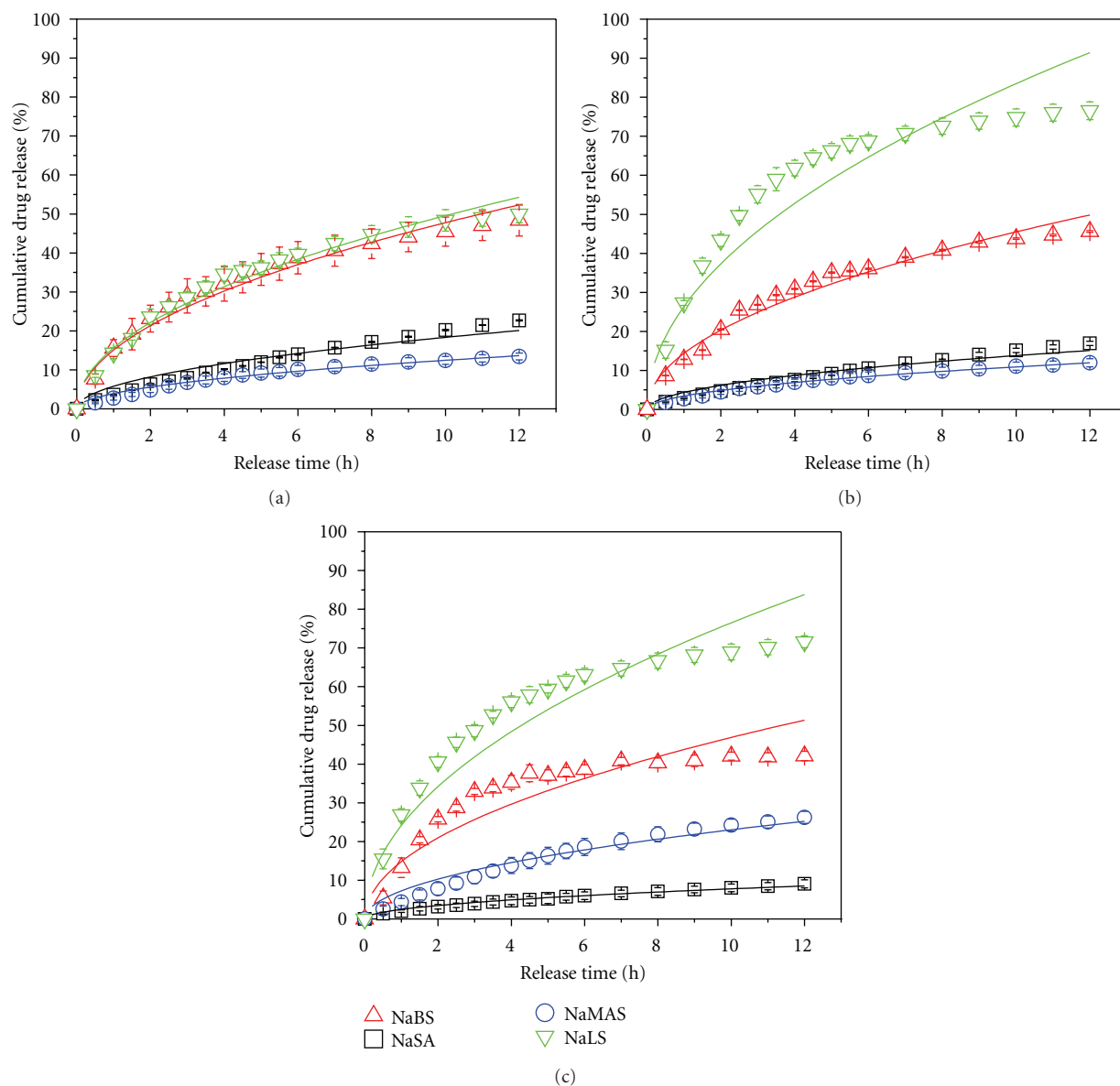


FIGURE 6: Release behaviors of different drugs from the HAEHFM at 37°C at (a) pH 5.0, (b) pH 7.4, and (c) pH 9.0.

are listed in Table 3. The release curves of NaSA and NaMAS can fit the equation well and the corresponding D values are similar to the values in PBS at pH 7.4. However, the curves of NaBS and NaLS in the simulated body fluid deviate from the Higuchi equation ($R^2 = 0.35$ and 0.74). This indicates that the release mechanisms of these two drugs do not accord with the assumptions of Higuchi equation. Three possible phenomena can be presented as the reasons: (i) there are protein and sugar in the solution, and hence the solubility of the drugs is decreased and the solution is not under a perfect dissolution condition; (ii) a constant diffusivity cannot be maintained as the viscosity of the solution is relatively high; (iii) the swelling of the polymer cannot be neglected. The size of NaLS molecule is the largest among all the drugs, and NaBS may form stackings due to the hydrophilic-hydrophobic interactions. Hence the three

possible phenomena, especially the former two, have more significant influence on their release behaviors, leading to the deviation from the Higuchi equation.

In Figure 7, the cumulative drug release of NaBS, NaSA, NaMAS, and NaLS after 7 days are 61.3%, 56.8%, 37.7%, and ~100% respectively. The changing trend of the D values in Table 3 follows the same order as in pure water: NaLS > NaBS > NaSA > NaMAS. Therefore, the salicylates (NaSA and NaMAS) are relatively more suitable for controlled release by the HAEHFM.

4. Conclusions

The model drugs including salicylates (NaSA and NaMAS) and aromatic monoacids with similar structures (NaBS and NaLS) can be effectively loaded onto the hybrid anion

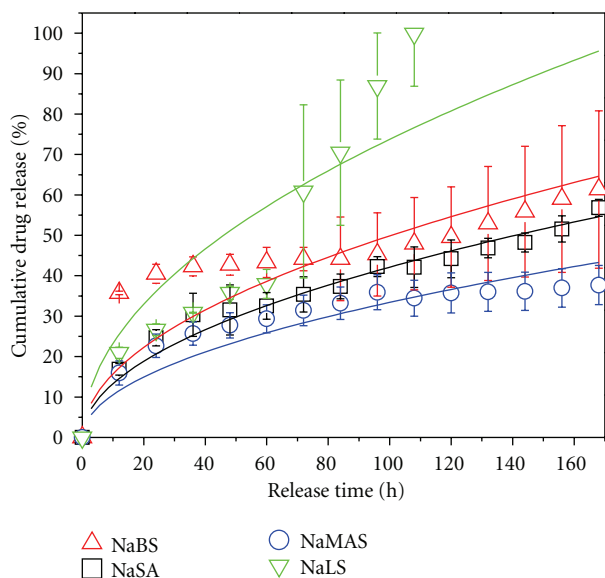


FIGURE 7: Release behaviors of different drugs from HAEHFM in a simulated body fluid at 37°C.

exchange hollow fiber membrane (HAEHFM) with the q_m value of 1.2–2.5 mmol/g dry membrane. The salicylates perform excellent release behavior (37.7% NaMAS and 56.8% NaSA released in simulated body fluid during 7 days). The physicochemical characteristics of drugs are crucial to the interaction patterns between the drugs and the membrane. Although the electrostatic interaction appears to play an important role between the anionic drugs and the anion exchange membrane, the nonelectrostatic interactions (hydrophobic interactions and hydrogen bonding) are also very significant to the drug release performances. Additionally, hydrogen bonding between the drugs and the membrane shows strong pH dependence. For example, the hydrogen bonding between NaMAS and the membrane can be disturbed in basic condition, resulting into an increase in the diffusion coefficient (D value) of NaMAS at pH 9.0. Thus, to optimize the release performance of the drug delivery system, the release environment, such as the salt concentrations and pH values, should be selected according to the physicochemical properties of the drug.

Acknowledgments

The authors gratefully acknowledge the financial support in part from the National Natural Science Foundation of China (Nos. 21025626 and 20974106), the National Basic Research Program of China (No. 2009CB623403), and the Natural Science Foundation of Anhui Province (No. 11040606M37).

References

- [1] M. M. Bonvin and M. M. de Bertorello, "In vitro drug release from chitosan membranes—study of the mechanisms of permeation," *Polymer Bulletin*, vol. 32, no. 1, pp. 69–75, 1994.

- [2] S. A. Burns, R. Hard, W. L. Hicks et al., "Determining the protein drug release characteristics and cell adhesion to a PLLA or PLGA biodegradable polymer membrane," *Journal of Biomedical Materials Research Part A*, vol. 94, no. 1, pp. 27–37, 2010.
- [3] S. P. Schwendeman, G. L. Amidon, M. E. Meyerhoff, and R. J. Levy, "Modulated drug release using iontophoresis through heterogeneous cation-exchange membranes: membrane preparation and influence of resin cross-linkage," *Macromolecules*, vol. 25, no. 9, pp. 2531–2540, 1992.
- [4] A. Narebska, S. Koter, and W. Kujawski, "Irreversible thermodynamics of transport across charged membranes. Part I: macroscopic resistance coefficients for a system with nafion 120 membrane," *Journal of Membrane Science*, vol. 25, no. 2, pp. 153–170, 1985.
- [5] Y. E. Fang, Q. Cheng, and X. B. Lu, "Kinetics of *in vitro* drug release from chitosan/gelatin hybrid membranes," *Journal of Applied Polymer Science*, vol. 68, no. 11, pp. 1751–1758, 1998.
- [6] R. M. P. da Silva, S. G. Caridade, J. San Roman, J. F. Mano, and R. L. Reis, "Transport of small anionic and neutral solutes through chitosan membranes: dependence on cross-linking and chelation of divalent cations," *Biomacromolecules*, vol. 9, no. 8, pp. 2132–2138, 2008.
- [7] H. N. Pei, X. G. Chen, Y. Li, and Y. Z. Hui, "Characterization and ornidazole release *in vitro* of a novel composite film prepared with chitosan/poly(vinyl alcohol)/alginate," *Journal of Biomedical Materials Research Part A*, vol. 85, no. 2, pp. 566–572, 2008.
- [8] K. Kontturi, P. Pentti, and G. Sundholm, "Polypyrrole as a model membrane for drug delivery," *Journal of Electroanalytical Chemistry*, vol. 453, no. 1-2, pp. 231–238, 1998.
- [9] S. Akerman, K. Akerman, J. Karppi et al., "Adsorption of drugs onto a poly(acrylic acid) grafted cation-exchange membrane," *European Journal of Pharmaceutical Sciences*, vol. 9, no. 2, pp. 137–143, 1999.
- [10] S. Akerman, B. Svarfvar, K. Kontturi et al., "Influence of ionic strength on drug adsorption onto and release from a poly(acrylic acid) grafted poly(vinylidene fluoride) membrane," *International Journal of Pharmaceutics*, vol. 178, no. 1, pp. 67–75, 1999.
- [11] L. Zhang, T. W. Xu, and Z. Lin, "Controlled release of ionic drug through the positively charged temperature-responsive membranes," *Journal of Membrane Science*, vol. 281, no. 1-2, pp. 491–499, 2006.
- [12] K. Hanninen, A. M. Kaukonen, T. Kankkunen, and J. Hirvonen, "Rate and extent of ion-exchange process: the effect of physico-chemical characteristics of salicylate anions," *Journal of Controlled Release*, vol. 91, no. 3, pp. 449–463, 2003.
- [13] N. Wang, C. M. Wu, Y. Y. Cheng, and T. W. Xu, "Organic-inorganic hybrid anion exchange hollow fiber membranes: a novel device for drug delivery," *International Journal of Pharmaceutics*, vol. 408, no. 1-2, pp. 39–49, 2011.
- [14] T. Jaskari, M. Vuorio, K. Kontturi, A. Urtti, J. A. Manzaneres, and J. Hirvonen, "Controlled transdermal iontophoresis by ion-exchange fiber," *Journal of Controlled Release*, vol. 67, no. 2-3, pp. 179–190, 2000.
- [15] T. Jaskari, M. Vuorio, K. Kontturi, J. A. Manzaneres, and J. Hirvonen, "Ion-exchange fibers and drugs: an equilibrium study," *Journal of Controlled Release*, vol. 70, no. 1-2, pp. 219–229, 2001.
- [16] K. R. Hanninen, A. M. Kaukonen, L. S. Murtomaki, and J. T. Hirvonen, "Effect of ion-exchange fiber structure on the binding and release of model salicylates," *Journal of Pharmaceutical Sciences*, vol. 94, no. 8, pp. 1772–1781, 2005.

- [17] E. A. Braude and F. C. Nachod, *Determination of Organic Structures by Physical Methods*, Academic Press, New York, NY, USA, 1955.
- [18] I. Raskin, "Role of salicylic acid in plants," *Annual Review of Plant Physiology and Plant Molecular Biology*, vol. 43, no. 1, pp. 439–463, 1992.
- [19] W. Lund, *The Pharmaceutical Codex, Principles and Practice of Pharmaceutics*, The Pharmaceutical Press, London, UK, 25th edition, 1994.
- [20] R. W. Sabnis, *Handbook of Acid-Base Indicators*, Taylor & Francis Group, San Francisco, Calif, USA, 2008.
- [21] N. Wang, C. M. Wu, Y. H. Wu, and T. W. Xu, "Hybrid anion exchange hollow fiber membranes through sol-gel process of different organic silanes within BPPO matrix," *Journal of Membrane Science*, vol. 363, no. 1-2, pp. 128–139, 2010.
- [22] I. Langmuir, "The constitution and fundamental properties of solids and liquids. Part I. Solids," *The Journal of the American Chemical Society*, vol. 38, no. 2, pp. 2221–2295, 1916.
- [23] W. I. Higuchi, "Analysis of data on the medicament release from ointments," *Journal of Pharmaceutical Sciences*, vol. 51, pp. 802–804, 1962.
- [24] M. L. Glowka, D. Martynowski, and K. Kozłowska, "Stacking of six-membered aromatic rings in crystals," *Journal of Molecular Structure*, vol. 474, no. 1–3, pp. 81–89, 1999.
- [25] V. S. Sumi, R. Kala, R. S. Praveen, and T. P. Rao, "Imprinted polymers as drug delivery vehicles for metal-based anti-inflammatory drug," *International Journal of Pharmaceutics*, vol. 349, no. 1-2, pp. 30–37, 2008.
- [26] T. Kankkunen, I. Huupponen, K. Lahtinen et al., "Improved stability and release control of levodopa and metaraminol using ion-exchange fibers and transdermal iontophoresis," *European Journal of Pharmaceutical Sciences*, vol. 16, no. 4-5, pp. 273–280, 2002.
- [27] O. L. Sprockel, M. Sen, P. Shivanand, and W. Prapaitrakul, "A melt-extrusion process for manufacturing matrix drug delivery systems," *International Journal of Pharmaceutics*, vol. 155, no. 2, pp. 191–199, 1997.
- [28] D. Fitzpatrick and J. Corish, "Release characteristics of anionic drug compounds from liquid crystalline gels: I: passive release across non-rate-limiting membranes," *International Journal of Pharmaceutics*, vol. 301, no. 1-2, pp. 226–236, 2005.
- [29] K. Hanninen, A. M. Kaukonen, T. Kankkunen, and J. Hirvonen, "Rate and extent of ion-exchange process: the effect of physico-chemical characteristics of salicylate anions," *Journal of Controlled Release*, vol. 91, no. 3, pp. 449–463, 2003.
- [30] J. L. Wood, "pH-controlled hydrogen-bonding," *Biochemical Journal*, vol. 143, no. 3, pp. 775–777, 1974.